INVESTIGATING THE MODE OF ACTION OF INTRACELLULAR LOOP 1 PEPDUCINS AT THE CXCR4 RECEPTOR

Birgit Caspar (4260590)

University of Nottingham

School of Life Science

Supervisors:

Stephen J Hill

Stephen J Briddon

Barrie Kellam

Michael Stocks

July 2019

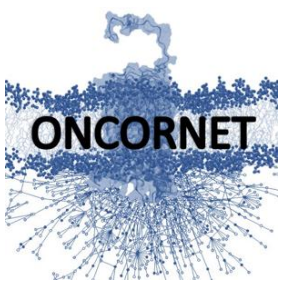

This thesis submitted for the degree of Doctor of Philosophy is entirely the candidate's own work. The experiments described in this thesis were performed by the author between September 2015 and August 2018 in the Cell Signalling Research Group, University of Nottingham, UK, Carsten Hoffmann's lab, University of Würzburg, Germany and at ALMAC Ltd., Edinburgh, UK. No part of the material has been submitted previously for a degree or any other qualification at any university.

Parts of this work have previously been published as conference abstracts:

B. Caspar, L.A. Stoddart, J. Goulding, S.J. Briddon, S.J. Hill (2017).

Functional and binding properties of CXCR4 intracellular loop 1 pepducins.

From the Pharmacology 2017 Meeting, Proceedings of the British Pharmacological Society

B. Caspar, L.A. Stoddart, J. Goulding, S.J. Briddon, S.J. Hill (2018).

Effect of intracellular loop 1 pepducins on ligand-receptor binding kinetics at the CXCR4 receptor.

From the Cell Signalling Meeting 2018, Proceedings of the British Pharmacological Society

Table of Contents

List of Abbreviations

7-TM	7 transmembrane
A_{2a}	adenosine A_{2a} receptor
AC	adenylyl cyclase
ACKR3	Atypical chemokine receptor 3
ATP	adenosine triphosphate
$ß_1$	$ß_1$ adrenergic receptor
$ß_2$	$ß_2$ adrenergic receptor
Boc	*tert*-butyloxycarbonyl
BRET	Bioluminescence Resonance Energy Transfer
BSA	Bovine Serum Albumin
cAMP	cyclic 3’5’-adenosine monophosphate
CCR5	C-C chemokine receptor type 5
CCL3	C-C chemokine ligand 3
CFP	cyan fluorescent protein
CMV	cyotomegalovirus
CXCL11	C-X-C chemokine ligand 11
CXCL12	C-X-C chemokine ligand 12
CXCR4	C-X-C chemokine receptor type 4
CXCR7	C-X-C chemokine receptor type 7
CD4	cluster of differentiation 4
Dde	$N_α$-Fmoc-$N_ε$-[1-(4,4-dimethyl-2,6-dioxocyclo-hexylidene)ethyl]
DIC	N,N’-Diisopropylcarbodiimide
DIEA	N,N-Diisopropylethylamine
DMF	Dimethylformamide
DMEM	Dulbecco’s modified Eagle’s medium
DMSO	Dimethyl sulfoxide
ECL	extracellular loop
EDT	1,2-ethanedithiol
EDTA	Ethylenediaminetetraacetic acid

EF1-alpha	elongation factor 1-alpha
e.g.	exempli gratia
FCS	Foetal Calf Serum
FDA	United States Food and Drug Administration
FlAsH	fluorescein arsenical hairpin binder
Fmoc	Fluorenylmethyloxycarbonyl
FRET	Förster Resonance Energy Transfer
FSK	Forskolin
G418	Geneticin
GC-content	guanine-cytosine content
GDP	guanosine-diphosphate
GPCR	G protein-coupled receptor
GRK2	G protein receptor kinase 2
GRK3	G protein receptor kinase 3
GRK6	G protein receptor kinase 6
GTP	guanosine-triphosphate
h	hour
HBSS	Hanks' Balanced Salt Solution
HEK293G	Human embryonic kidney 293-Glosensor™
HIV	human immunodeficiency virus
ICL	intracelullar loop
INT	Iodonitrotetrazolium
JAK	Janus kinases
LB	Lysogeny broth
LDH	Lactate Dehydrogenase
MAPK	mitogen activated protein kinase
min	minutes
Nluc	NanoLuc®
NK cells	Natural killer cells
PAR1	Protease activated receptor 1
PBS	phosphate buffered saline
PCR	Polymerase Chain Reaction

PI3K	phosphoinositide 3-kinase
PKC	Protein kinase C
PLC	phospholipase C
PTX	pertussis toxin
PyBOP	benzotriazol-1-yl-oxytripyrrolidinophosphonium-hexafluorophosphate
Rluc	Renilla-luciferin 2-monooxygenase
S	significant
SD	standard deviation
sec	seconds
SEM	standard error of the mean
STAT	signal transducer and activator of transcription proteins
TAMRA	5-Carboxytetramethylrhodamine
TFA	Trifluoracetic acid
TIS	Triisopropylsilane
WT	wild type
YFP	yellow fluorescent protein

Abstract

Background

Pepducins are lipid-peptides derived from the intracellular loop sequences of a G protein-coupled receptor and have been shown to act as allosteric modulators. Pepducins have been described for the chemokine receptor, CXCR4, which can exhibit agonist activity in the absence of the endogenous ligand C-X-C-Ligand 12 (CXCL12). To date, their precise mode of action is unclear. In this study, we investigated the mechanism of action of intracellular loop 1 pepducins at the CXCR4 receptor

Experimental Approach

Experiments were performed in HEK293 cells stably expressing the Glosensor™ cAMP sensor (HEK293G) and human CXCR4 tagged with (a) NanoLuc on its N-terminus (NL-CXCR4), (b) C-terminus (CXCR4-NL), (c) SNAP on its N-terminus (SNAP-CXCR4), (d) human CCR5 or (e) human CXCR4 with the first internal loop swapped for the CCR5 sequence (CXCR4_CCR5il1). The binding of fluorescently labelled CXCR4 ligands and their displacement was quantified with a NanoBRET assay using NL-CXCR4 or CXCR4-NL cells. Conformational changes caused by CXCL12 and pepducins were monitored with an intramolecular biosensor and a BRET assay looking at dimerisation. Moreover, cells were tested in functional assays looking at G protein activation, cAMP inhibition, ß-arrestin recruitment and internalisation after the addition of endogenous ligand CXCL12 or pepducin.

Results

The affinity of fluorescent CXCL12 (CXCL12-red) was determined through NanoBRET saturation binding. Competition binding experiments showed that CXCL12-red binding was inhibited by addition of small molecules or ATI-2341. Control pepducins with no lipid tail or modified sequences were unable to displace CXCL12-red

at concentrations up to 10 µM. ATI-2341f, a fluorescent version of ATI-2341, with an additional TAMRA tagged lysine on the N-terminal end of the sequence showed a displaceable increase in BRET ratio in CXCR4-NL, but only a small change in NL-CXCR4 membranes.

An intramolecular biosensor showed activation of CXCR4 by CXCL12 and ATI-2341. However, activation by ATI-2341 was delayed by 30 s. Dimers measured via BRET from one receptor to another showed an increase in BRET with CXCL12 and a decrease in BRET with ATI-2341.

Functional assays showed similar activation of CXCR4 by CXCL12 and ATI-2341. An ATI-2341 threonine to alanine mutant showed reduced potencies in all tested assays.

Key Conclusion

These data suggest that ATI-2341 follows the previously proposed interaction mechanism of pepducins.

In a first step, the lipid tail interacts with the membrane and the pepducin is flipped into the cell as supported by the 30 s activation delay observed with ATI-2341 in comparison to the endogenous ligand. Then, the interaction of ATI-2341 and CXCR4 takes place at the intracellular part of the receptor as suggested by the BRET binding studies. However, this interaction impacts the endogenous binding pocket of CXCL12. Furthermore, the functional activation of CXCR4 by CXCL12 is similar to the one observed with ATI-2341. The only difference can be observed in dimerisation and ß-arrestin recruitment experiments. Mutations of the pepducin identified the threonine as an important amino acid.

1 General

Introduction

Cancer is one of the major causes of death in today's modern society affecting all parts of the world. Analysis of the available data shows large geographical diversity in cancer occurrence and types within world regions. There are higher incidence rates in countries with high-income where the treatment at the same time is the best in the world. This is also related to the higher life expectancy in those countries. The probability of getting cancer is determined by different factors reaching from environment, personal behaviour to genetic background. In 2012, 14 million people were diagnosed with cancer and 8 million people died related to having cancer (Stewart and Wild, 2014). In 2018 this number rose to 18.1 million new cases and 9.6 million deaths (International Agency for Research on Cancer, 2018). This increase in cancer is caused by various factors including a growth in world population and ageing as well as the change in social and economic settings. Cancers observed in fast growing economies move from cancers related to poverty and infections to cancers connected to lifestyles typical of industrialized countries. Global data shows that 48.4 % of new cases worldwide occur in Asia, 5.8% in Africa, 21.0 % in the Americas and 23.4% in Europe (International Agency for Research on Cancer, 2018).

In order to provide better cancer treatment the fundamental processes leading to cancer and its progression and formation of metastasis need to be understood.

This project was part of the Marie Skłodowska-Curie Innovative Training Network "ONCORNET" with 15 PhD students in different laboratories around Europe with the focus to study different aspects of the two G protein-coupled receptors (GPCRs) C-X-C chemokine receptor type 4 (CXCR4) and atypical chemokine receptor 3 (ACKR3) in an oncogenic background. Projects ranged from compound design to pharmacological screens to *in vivo* studies. This project in particular concentrated on studying the mechanism of pepducins interacting with CXCR4. The following chapter will give the theoretical background in order to understand the obtained results and set these into the context of current knowledge.

1.1 G protein-coupled receptors

1.1.1 Structure and Function of G protein-coupled receptors

G protein-coupled receptors (GPCRs), also known as 7-transmembrane (7-TM) receptors, are the largest group of membrane proteins in the human genome. The receptors can be classed into 5 or 6 families based on their differences in sequence and their differences in structure caused by these variations in sequence.

These families are according to the GRAFS system: The glutamate family that is activated by glutamate, the rhodopsin family (historically the Class A family) with the largest amount of GPCRs, the adhesion family with very big extracellular domains, the frizzled/taste family and the secretin family that is regulated by peptide hormones from the glucagon hormone family (Fredrikson *et al.*, 2003; Bjarnadóttir *et al.*, 2006). Alternatively, the adhesion family is replaced by fungal mating pheromone receptors and cyclic AMP receptors.

All GPCR families share common structural motifs and also have motifs specific to only that family. The first structural insights into GPCRs were observed in two-dimensional crystal structures of rhodopsin in which a single layer of rhodopsin in lipid bilayers was measured (Schertler *et al.*, 1993; Krebs *et al.*, 1998). Later more detail was observed in three-dimensional crystal structures with the first human structure being the ß$_2$-adrenergic receptor (Rasmussen *et al.*, 2007). The crystal structures of CXCR4 and CC chemokine receptor type 5 (CCR5) are reviewed in detail in the subchapter **1.3.1 Crystal structure of CXCR4 and CCR5** (Wu *et al.*, 2010; Tan *et al.*, 2013).

In general the GPCR protein consists of one single peptide chain which was shown to fold into a typical barrel-like shape (**Figure 1-1**). The core of the GPCR is given by seven transmembrane α-helices connected by three extracellular loops (ECL1 – ECL3) and three intracellular loops (ICL1 - ICL3) that can differ immensely in size (**Figure 1-1 A**). The extracellular loops contain two conserved cysteines that form a disulphide bond. Due to the uneven number of

transmembrane domains the C- and N-terminal ends of the receptor are located at opposite sides of the cell membrane. The N-terminal end of the receptor, located at the outside of the cell, as well as the ECLs and easily accessible parts of the transmembrane regions are generally involved in the recognition of endogenous ligands. The C-terminal end of the receptor located inside the cell differs substantially between GPCRs, even within subfamilies, and is involved with the other accessible intracellular parts of the receptor in signal transduction. All GPCRs which have been structurally identified show a closed loop of the 7 TM domains in an anti-clockwise direction from TM 1 to TM 7 (**Figure 1-1 B**). The core structure is tightly packed and there is no evidence of GPCRs acting as tunnel structures (Ji *et al.*, 1998; Gether, 2000; Palczewski *et al.*, 2000; Bray *et al.*, 2010). The different classes of GPCRs can vary structurally significantly in particular with very big N- or C-terminal ends that are common within one class. As mentioned before GPCRs in the members of the adhesion family typically have large N-termini with cysteine rich sequences, however these long N-termini can also be found in members of the secretin, glutamate or frizzeld family (Fredrikson *et al.*, 2003).

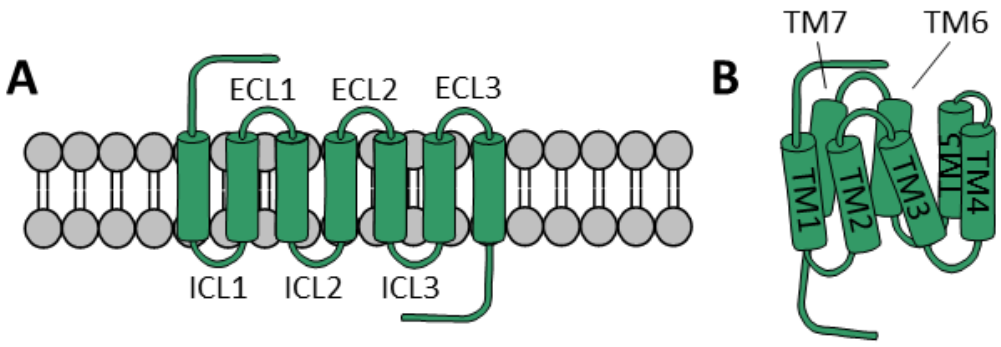

Figure 1-1: **GPCR representation.** (**A**) Schematic representation of a GPCR (green) with its 3 extracellular and 3 intracellular loops; (**B**) 3D arrangement of the 7 TM domains.

The main function of GPCRs is to transduce extracellular stimuli into signals inside the cell (Kroeze *et al.*, 2003). GPCRs are stimulated by a variety of activators, (e.g. hormones, neurotransmitters, ions,

photons, proteins, peptides, derivatives of amino acids or fatty acids) (Rosenbaum *et al.*, 2009) and accordingly are expressed throughout the body and show different functional properties ranging from metabolism, growth and cell adhesion to neuronal signalling and blood coagulation (Insel *et al.*, 2015). Consequently, GPCRs are implicated in a range of diseases from diabetes, cardiovascular diseases, infectious diseases and immunological disorders to cancer (Chin *et al.*, 2013) and serve as an important target for diseases and were already the target of 33% of approved drugs in 2016 in various illnesses (Santos *et al.*, 2016).

1.1.2 Signalling by GPCRs

GPCRs can be activated by photons or a ligand interacting with the GPCR by binding to the orthosteric endogenous ligand site or a different allosteric site. Ligands can activate the receptor or modulate the signal arising from the endogenous ligand positively or negatively. The distinction between orthosteric and allosteric site can sometimes be challenging as small molecule ligand binding pockets can partly overlap with the endogenous binding site (Christopoulos and Kenakin, 2002; Wootten *et al.*, 2013).

The binding of the ligand causes a conformational change of the receptor especially shifts in the transmembrane regions leading to a bigger intracellular surface allowing the interaction with signalling molecules (Farrens *et al.*, 1996; Lin and Sakmar, 1996; Dunham *et al.*, 1999; Kobilka, 2007).

It has been shown that ligands change the population distribution of conformations in favour of conformations sparsely populated in ligand free receptor to different extents. The activation of the receptor proceeds through a series of specific conformational intermediates eventually leading to a larger structural rearrangement near the transmembrane-intracellular region. The active state of the receptor becomes the dominant one once a signalling molecule is bound intracellularly (Venkatakrishnan *et al.*, 2013).

Once the ligand is bound extracellularly changes in the TM region occur. Common changes are a distortion of TM5, relocation of TM3 and TM7 and translation/rotation of TM5 and TM6. These changes are also connected by a rearrangement of a cluster of conserved hydrophobic and aromatic residues deeper in the receptor core resulting in a rearrangement of the TM3-TM5 interface and a formation of a new non-covalent contact at the TM5-TM6 interface. The changes especially in TM5 and TM6 are transmitted through the helix causing rearrangements at the cytoplasmic side opening the cleft needed for binding of signalling molecules (Standfuss *et al.*, 2011; Venkatakrishnan *et al.*, 2013).

Intracellular signalling via a GPCR may occur through a G protein-dependent or a G protein-independent (Azzi *et al.*, 2003; Shenoy *et al.*, 2006) pathway after activation of the receptor. The G protein can either be recruited or already be pre-coupled with the receptor (Nobles *et al.*, 2005). The conformational change of the receptor causes the heterotrimeric G protein located at the intracellular membrane to be activated. In the inactivated state of the heterotrimeric G protein, the α subunit is bound to guanosine-diphosphate (GDP). Upon activation of the GPCR a nucleotide exchange occurs releasing the GDP and allowing the binding of guanosine-triphosphate (GTP) to the Gα-subunit. This exchange leads to a dissociation of the G protein subunits into an α and a βγ unit moving along the cell membrane. The G protein is deactivated after some time by Gα-mediated hydrolysis of the GTP to GDP and returns to its inactive conformation (Bourne *et al.*, 1990; Simon *et al.*, 1990). G proteins are in general identified by their Gα subunits which are grouped in four families: $G\alpha_s$, $G\alpha_i$, $G\alpha_q$, and $G\alpha_{12}$. In these four families there are a total of 18 Gα proteins that are activated by different GPCRs and lead to different signalling pathways. Moreover, there are 5 Gβ and 12 Gγ variants (Syrovatkina *et al.*, 2016). The activated G protein can then interact with another target, a second messenger generating enzyme such as adenylyl cyclase and phospholipase C or ion channels, in the plasma membrane (Simon *et al.*, 1990; Lohse *et al.*, 2008).

Apart from signalling through second messengers from the cell surface, the activation of GPCRs also starts negative feedback mechanisms that can result in desensitization (homologoues or heterologous) of the receptor followed by internalisation of the receptor into the cells via endocytosis and finally recycling or degradation of the receptor (**Figure 1-2**).

Homologous desensitization is initiated by G protein-coupled receptor kinases' (GRKs) phosphorylation of serine, threonine or tyrosine residues of the third internal loop or C-terminal end upon continued stimulation by agonist at high concentration.

In contrast, heterologous desensitization is initiated by second messenger-regulated kinases (such as PKA) that phosphorylates not only the activated receptor but also inactive receptors containing the PKA consensus site. Afterwards, β-arrestins (Luttrell and Lefkowitz, 2002; Ma and Pei, 2007) can be recruited, which prevent further stimulation of G proteins and downstream signalling pathways by sterical hindrance (Krupnick and Benovic, 1998; Busillo and Benovic, 2007). Moreover, ß-arrestins contain motifs that serve as adapter proteins linking the GPCR to the clathrin dependent endocytosis machinery by binding towards clathrin and ß2-adaptin (Luttrell and Lefkowitz, 2002). Upon internalisation, the receptor can either be recycled or degraded at the lysosome.

Depending on the receptor, internalisation occurs either through the classical clathrin-coated vesicles pathway or non-coated vesicle pathway (Lefkowitz, 1998; Gainetdinov *et al.*, 2004; Magalhaes *et al.*, 2012).

On top of these negative regulatory effects there are also more and more reports showing signalling of the receptor after β-arrestin recruitment. Interactions with β-arrestin are able to activate or inhibit signalling pathways of GPCRs in a different way than G protein mediated signalling or can also modulate these G protein activated pathways (Cheng *et al.*, 2000). β-arrestins have been shown to be involved in an agonist dependent manner in the activation of ERK (Luttrell *et al.*, 2018) or act as a scaffold protein in the mitogen-

activated protein kinase (MAPK) pathway (Sun *et al.*, 2002; Reiter and Lefkowitz, 2006).

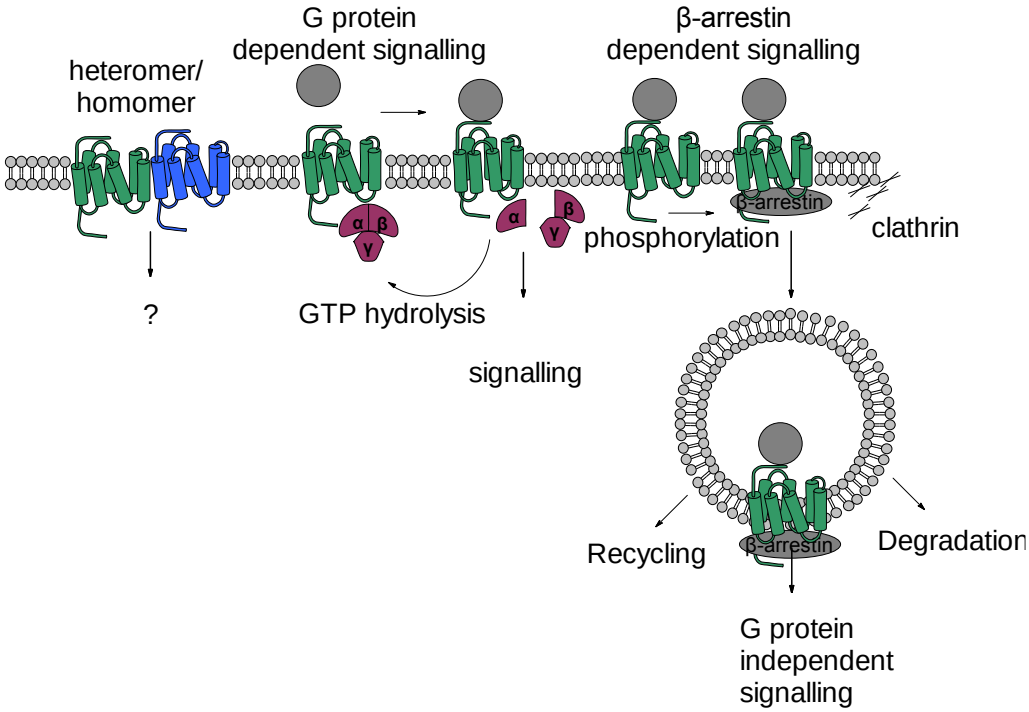

Figure 1-2: GPCR signalling. Signalling scheme for GPCRs including G protein-dependent and ß-arrestin dependent pathways.

GPCRs have been shown to exist in a monomeric, heteromeric or homomeric form (**Figure 1-2**) located within the cell membrane. The specific roles of dimers and oligomers in signalling pathways are still under investigation while homodimers have been reported for various GPCRs, e.g. CXCR4, beta-2 adrenoreceptor (β_2), adenosine A_{2a} receptor (A_{2a}) (Wang *et al.*, 2006; Wnorowski and Jozwiak, 2014; Felce *et al.*, 2017), heterodimers for $GABA_BR1$ and $GABA_BR2$ (Jones *et al.*, 1998; Kaupmann *et al.*, 1998) or oligomers for the dopamine D2 receptor (Guo *et al.*, 2008). Recent reports show that receptor dimerization can have an influence on various parameters such as cell surface expression, ligand binding, G protein coupling, signal transduction, internalisation and desensitization (Terrillon and Bouvier, 2004; Wnorowski and Jozwiak, 2014). Moreover, there are reports suggesting the importance of dimer dissociation and reassociation after activation and for signalling (Petersen *et al.*, 2017). These results demonstrate the importance of dimer

identification and understanding for drug discovery (Rozenfeld and Devi, 2010).

1.2 Chemokines and chemokine receptors

1.2.1 Chemokines

Chemokines are categorised into four classes dependent on the position and number of their conserved cysteine residues which stabilise the fold of the proteins by the formation of two (CXCL, CCL and CX3CL) or just one disulphide bridge in the case of XCL chemokines (**Figure 1-3**). CCL chemokines include two cysteines after each other in the amino acid sequence while the two cysteines in CXCL chemokines are separated by one amino acid or three amino acids in the case of CX3CL. Chemokines share 20-50% of their amino acid sequence with high values for chemokines within the same group (Bachelerie *et al.*, 2014).

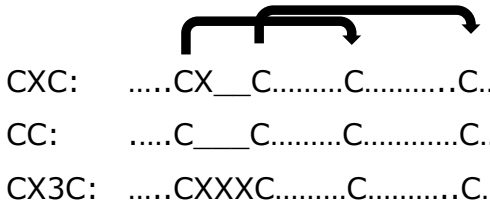

Figure 1-3: Nomenclature of chemokines. Name giving cysteines in CXC and CC chemokines where X can be any amino acid, disulphide bonds in the chemokine marked with arrows.

Most chemokines in the human body are classed into the two groups CXCL or CCL. In order to show representative differences the sequences of CXCL12, CXCL11 and CCL3 are shown in **Table 1-1**.

Table 1-1: Sequences of selected chemokines CXCL12, CXCL11 and CCL3 with cysteines in red and name giving C(X)C sequence underlined and bold

Chemokine	Sequence	Chemokine receptor
CXCL12 (SDF1α)	10 20 30 KPVSLSYR**CP C**REFFESHVAR ANVKHLKIN 40 50 60 TPNCALQIVA RLKNNNRQVC IDPKLKWIQE YLEKALNK	CXCR4 ACKR3 CXCR3
CXCL11 (I-TAC)	10 20 30 MSVKGMAIAL AVILCATVVQ GFPMFKRGR**C** 40 50 60 **LC**IGPGVKAV KVADIEKASI MYPSNNCDKI 70 80 90 EVIITLKENK GQRCLNPKSK QARLIIKKVE RKNF	CXCR3 ACKR3 CCR3 ACKR1
CCL3 (MIP-1α)	10 20 30 MQVSTAALAV LLCTMALCNQ FSASLAADTP 40 50 60 TA**CC**FSYTSR QIPQNFIADY FETSSQCSKP 70 80 90 GVIFLTKRSR QVCADPSEEW VQKYVSDLEL SA	CCR5 CCR1 ACKR2

These three selected chemokines show structural conserved motifs (**Figure 1-4**) that can be found in general across the chemokine subfamilies. The conserved disulphide bonds and other conserved residues are important for folding of the characteristic tertiary structure. The first and second cysteine are located close to the N-terminus of the chemokine and are followed by a flexible random coil region on the N-terminal site called the N-loop. The N-loop will interact with the receptor and undergo an induced fit conformational change. This N-terminal end and N-loop is followed by a single-turn helix and a three stranded β-strand in the case of CXCL12 which can be found in many chemokines. All three structures end with an α-Helix at the C-terminal end. These structures are connected by turns called 30s, 40s and 50s loop. The third and fourth cysteine are located within these 40s and 50s loops (Crump *et al.*, 1997; Dealwis *et al.*, 1998;

Czaplewski *et al.*, 1999; Fernandez and Lolis, 2002; Booth *et al.*, 2004).

Furthermore, in two of the crystal structures homodimers of the chemokines are shown which appear to be important for activity in vivo and in vitro (Laurence *et al.*, 2000; Proudfoot *et al.*, 2003; Jin *et al.*, 2007). The formation of dimers can be observed in many chemokines of the CXC and CC family. CC chemokine dimers are inactive due to the fact that CC chemokines use their N-terminal region to form a new antiparallel ß-sheet blocking their receptor interaction site (Jin *et al.*, 2007; Tan *et al.*, 2012). Interestingly, the interaction between chemokine and receptor results in the formation of a new antiparallel ß-sheet similar to the one in the chemokine-chemokine dimer (Kufareva *et al.*, 2017). In contrast to CC dimers, CXC dimers show activity as they dimerise at the existing ß-strands not impacting the N-terminal receptor binding site. Accordingly, trapped forms (unable to dissociate) of the chemokine dimers CXCL8 and CXCL12 show activation of their receptor which is comparable with the unmodified chemokines (Nasser *et al.*, 2009; Drury *et al.*, 2011). However, in order to make statements about interactions between dimeric chemokines with receptors, structures are needed. Predictions of the CXCL12-ACKR3 mode show a monomeric chemokine interacting with the receptor mimicking the dimer interface (Gustavsson *et al.*, 2017). Chemokines can also form higher order oligomers (Wang *et al.*, 2013) or heterodimers (Nesmelova *et al.*, 2005) that add complexity to the activation of chemokine receptors.

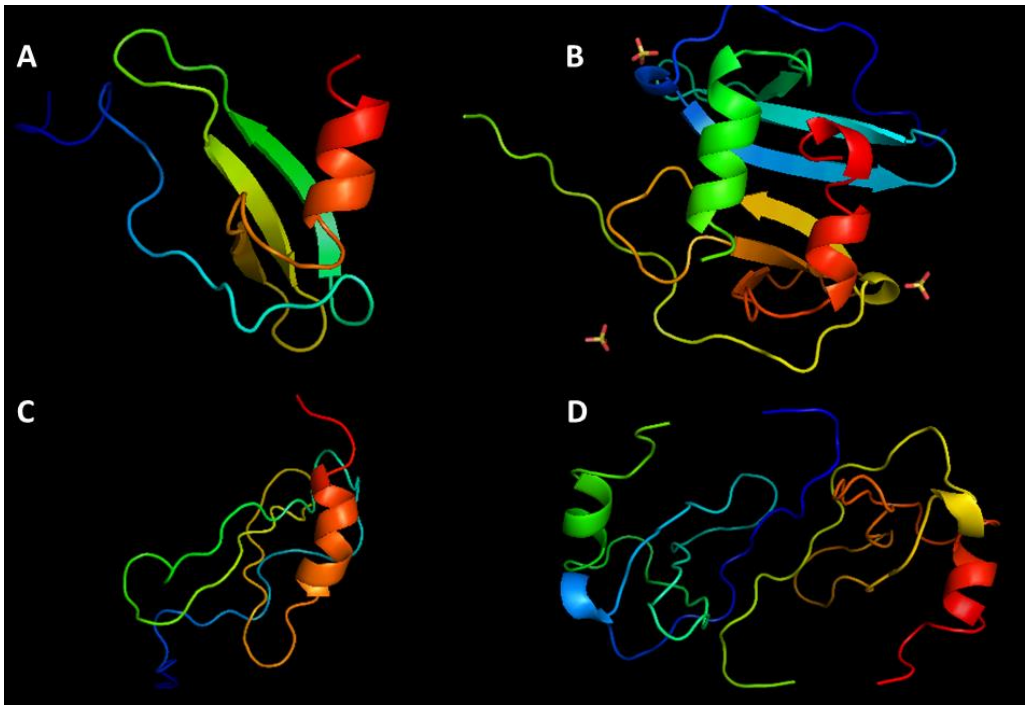

Figure 1-4: Tertiary structures of CXCL12, CXCL11 and CCL3 chemokines. (**A**) CXCL12 monomer NMR structure (Crump *et al.*, 1997), (**B**) CXCL12 dimer crystal structure (Dealwis *et al.*, 1998) (**C**) CXCL11 monomer NMR structure (Booth *et al.*, 2004) (**D**) CCL3 D26A dimer NMR structure (Czaplewski *et al.*, 1999); data from PDB exported with PyMOL; all structures follow the same colour transition starting on the N-terminal end with blue and ending in red on the C-terminal end.

Many chemokines are reported to exist in different variants due to truncation of either their C- or N-terminus in splicing variants or due to post-translational modifications (Stone *et al.*, 2017). CXCL12, the endogenous ligand of CXCR4, is reported to exist in six different splice variants with varying amino acid length named from α to θ in which CXCL12α and CXCL12β are the most common variants (Bachelerie *et al.*, 2014). In the case of CXCL12, CXCL12β has 4 more amino acids than CXCL12α at the C-terminus (Bray *et al.*, 2010; Sun *et al.*, 2010). During this work only the CXCL12α variant was used. Citrullination of CXCL12 (and CXCL11) has been shown to decrease receptor affinity (Loos *et al.*, 2008; Struyf *et al.*, 2009). Citrullination is one of the post-translational modifications common in chemokines in which arginine residues are converted to the amino acid citrulline in which one of the terminal nitrogen atoms of arginine is replaced by an oxygen (Loos *et al.*, 2008; Struyf *et al.*, 2009).

1.2.2 Chemokine receptors

Chemokine receptors belong to the biggest family of rhodopsin-like GPCRs. Mammalian genomes encode approximately 20 different chemokine receptors (**Table 1-2**) that share 25 – 80% of their amino acid identity (Murphy *et al.*, 2000). These chemokine receptors can be divided into two main groups. First G protein-coupled chemokine receptors like CXCR4 which activate G_i-type G proteins and secondly atypical chemokine receptors (ACKR) such as atypical chemokine receptor 3 (ACKR3) which seem to shape chemokine gradients and dampen inflammation by scavenging chemokines in a G protein-independent, β-arrestin dependent pathway (Bachelerie *et al.*, 2014; Stone *et al.*, 2017). ACKRs show poor conservation of the key structural motif "DRYLAIV" (Asp-Arg-Tyr-Leu-Ala-Ile-Val) at the intracellular end of TM3 which is conserved in most other GPCRs and chemokine receptors and is related to the interaction with G proteins.

Typical chemokine receptors are named after the class of their first identified endogenous chemokine ligand (CC, CXC or XC) and addition of an R for receptor and the next available number in the receptor subfamily (Bachelerie *et al.*, 2014; Arimont *et al.*, 2017; Stone *et al.*, 2017).

The chemokine receptors share structural motifs of all class A GPCRs; the seven transmembrane α-helices linked with three intracellular and extracellular loops as well as an extracellular N-terminal domain and an intracellular C-terminus (Gether, 2000). As most class A GPCRs, chemokine receptors incorporate two conserved cysteines in the extracellular loop 2 and top of TM3 forming a disulphide bond. In addition to those two cysteines, chemokine receptors contain two further cysteines forming a disulphide bond between the N-terminus and the ECL3 with the exception of CXCR6. Both disulphide bonds seem to be important for folding of the receptor as well as binding of ligands and their signalling. Moreover, crystal structures of the chemokine receptors CXCR4, CCR2, US28, CCR9 and CCR5 showed that the N-terminal end of TM7 is 1-2 helical turns longer than other class A GPCRs (Wu *et al.*, 2010; Tan *et al.*, 2013; Qin *et al.*, 2015;

Arimont *et al.*, 2017). The N-terminus and the extracellular loops are involved in ligand binding as observed in mutational experiments in which mutants showed significantly lower chemokine binding tested with radio ligand or Förster Resonance Energy Transfer (FRET) techniques (Blanpain *et al.*, 1999, 2003; Wescott *et al.*, 2016). Early binding models of the chemokine and its receptor show a two-site mechanism in which first the chemokine core interacts with the receptor N-terminus and the extracellular loops (chemokine recognition site 1 – CRS1) as highlighted in blue in **Figure 1-5**. The affinity of this first recognition site is increased by sulfation of the tyrosine residues (introduction of a sulfo group at the hydroxyl) in the N-terminus of the receptor. Once, the chemokine is bound to CRS1 the N terminus is orientated to allow binding to the second binding site (CRS2) located at the pocket of the receptor transmembrane helical domain as highlighted in yellow in **Figure 1-5** (Monteclaro and Charo, 1996; Crump *et al.*, 1997; Blanpain *et al.*, 2003).

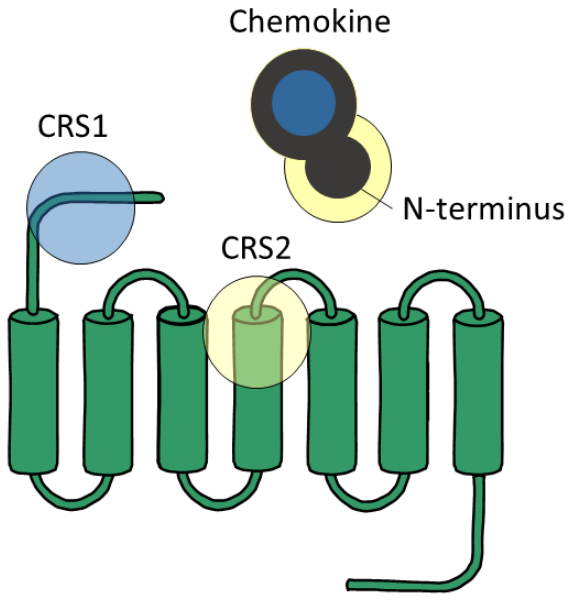

Figure 1-5: Chemokine interaction model. Chemokine interacting with receptor in two binding site model, the N-terminal end interacts with CRS2 (yellow) while the globular chore interacts with CRS1 (blue).

However, when considering the information given by the recent crystal structures of a chemokine and their receptor, the viral chemokine antagonist vMIP-II with CXCR4, CX3CL1 with the viral

chemokine receptor US28 and [5P7]CCL5 with CCR5 (Burg *et al.*, 2015; Qin *et al.*, 2015; Kufareva *et al.*, 2017; Zheng *et al.*, 2017), this model seems oversimplified. While all three structures showed the two chemokine recognition sites described before, structure density was missing for parts of the receptor N terminus. It seems like the crystal structures and modelling of the missing parts showed an interaction of CRS1 shows the chemokine receptor N-terminus interacting with the N loop/40s loop of the chemokine. The N-terminus of the chemokine interacts with the receptor transmembrane helical domain (CRS2). The observation of tight conserved packing lead to the definition of a CRS1.5 (Qin *et al.*, 2015; Kufareva *et al.*, 2017), between the two recognition sites CRS1 and CRS2 a conserved proline-cysteine motif of the receptor N-terminus is in close proximity with a conserved disulphide of the chemokines forming an antiparallel β-sheet similar to the chemokine dimer interface (Kufareva *et al.*, 2017).

Table 1-2: Human chemokine-receptor network; blue: agonist, red: antagonists, yellow: not specified or debatable; adapted from (Stone *et al.*, 2017); CCR5, CXCR4 and ACKR3 were used during this project

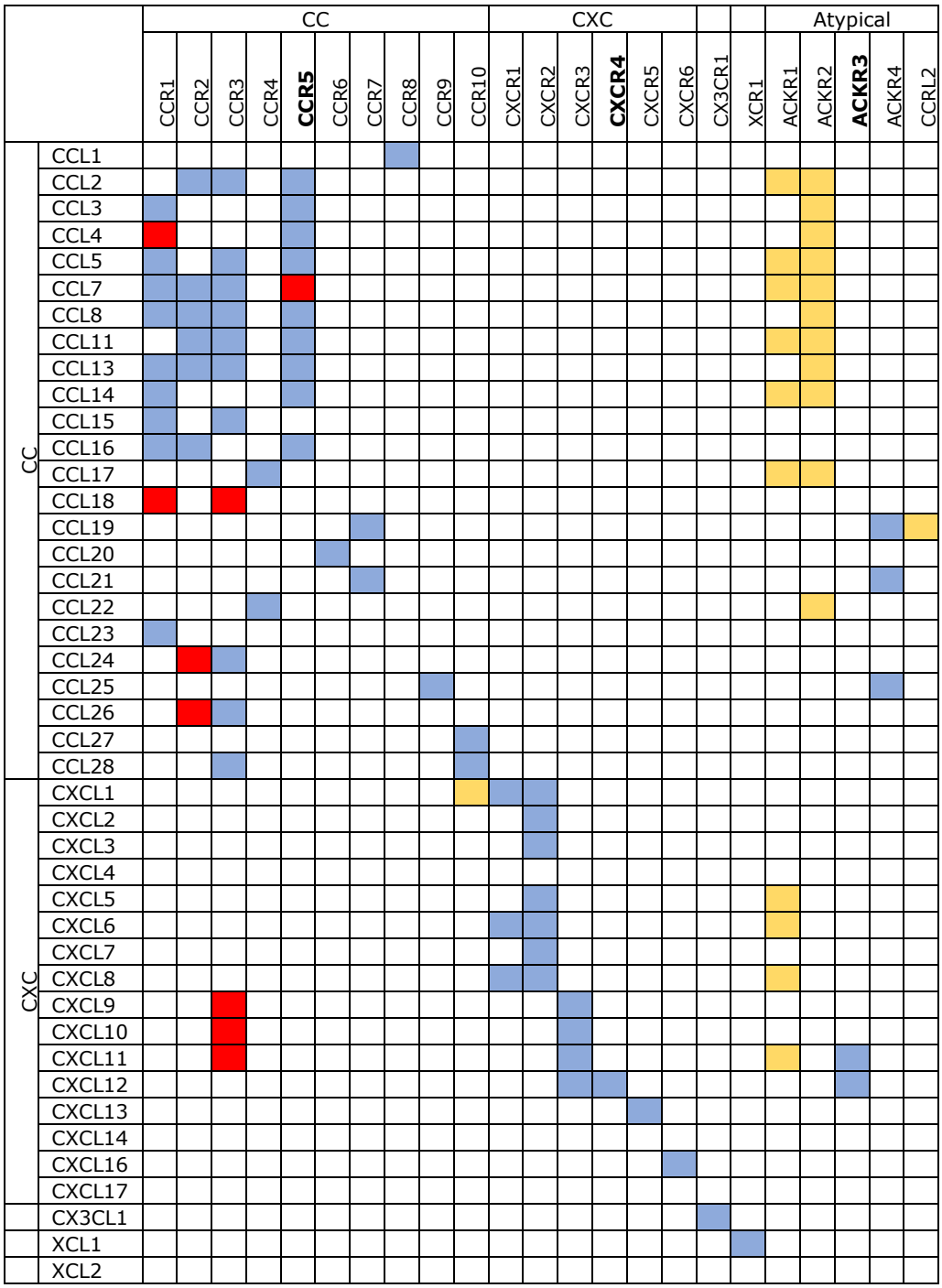

Dimerisation of receptors has been studied in detail in the past few years with some receptors showing robust evidence to dimerise while others showed contradicting results dependent on the study and

technique (Terrillon and Bouvier, 2004; Tan *et al.*, 2012; Felce *et al.*, 2017).

There have been multiple reports of chemokine receptors forming homo- and heterodimers with other chemokine receptors or GPCRs outside the chemokine family. The dimers form by parallel association of the transmembrane helices. In crystal structures, CXCR4 dimerises by association of TM5 and TM6 (Wu *et al.*, 2010) while the CCR5 homodimer interaction takes place between TM1 and TM7 (Tan *et al.*, 2013). The chemokine receptor dimers form in the membrane of the endoplasmic reticulum following their synthesis and folding. These dimers are then transported to the plasma membrane. For some dimers the presence of the second receptor has a positive or negative cooperative effect on the ligand binding of the other receptor potentially explained by differences in G protein coupling (Rodríguez-Frade *et al.*, 2001; Springael *et al.*, 2005; Muñoz *et al.*, 2012).

In the case of CCR2 the homodimer seems to be the functional entity (Rodriguez-Frade *et al.*, 1999).

1.2.3 Functional properties in health and disease

The majority of chemokines and their corresponding receptors such as CCL2 – CCL5 (see interacting receptors in **Table 1-2**) are involved in immune defence and inflammation by regulating the migration, activation and differentiation of leukocytes (Foxman *et al.*, 1997; Rossi and Zlotnik, 2002; Viola and Luster, 2008). Their expression is induced as a result of inflammation as constitutive levels are low and induction increases these levels dramatically (Nelson *et al.*, 2001; Zlotnik *et al.*, 2006). Chemokines expressed as a result of inflammation or trauma mobilise leukocytes to the site of infection by building chemokine concentration gradients that are essential for the movement of cells expressing the corresponding chemokine receptor (Maksym *et al.*, 2009). There are many publications reporting the increase of chemokine and chemokine receptor levels in diseased

tissues compared to healthy tissue (Fernandez and Lolis, 2002; Furusato *et al.*, 2010; Nagarsheth *et al.*, 2017) .

Apart from these chemokines which respond to inflammation there are also chemokines which are constitutively expressed regulating homeostatic cell migration such as CXCL12, CXCL13 or CCL21 (Zlotnik *et al.*, 2011; Teixidó *et al.*, 2018). Interestingly, constitutive expressed chemokines tend to be quite specific for their receptor, like CXCL12 and CXCR4 (Stone *et al.*, 2017). In addition there are chemokines that are classed as dual-function chemokines involved in both processes such as CCL11, CCL17 or CCL20 (Zlotnik and Yoshie, 2012). However, there are several inconsistencies in literature when looking at interacting chemokines and chemokine receptors suggesting a dependence on environment such as cell type, growth and assay conditions (Stone *et al.*, 2017).

Moreover, there is increasing evidence that chemokines are related to cancer progression and metastasis (Murphy *et al.*, 2000; Lappano and Maggiolini, 2012). Chemokines and their receptors are involved in three major aspects in cancer, the first being the influence on survival and growth, then the immune cell infiltration and last the influence on metastatic potential of the tumour cells. However, the chemokine network is used by the tumour environment in all stages and has direct anti-tumour as well as pro-tumour effects (Balkwill, 2004a, 2012; Chow and Luster, 2014; Nagarsheth *et al.*, 2017).

Chemokine receptor activation in tumour cells can activate pathways leading to the expression of growth-stimulating genes as well as shifting the balance between pro-apoptotic and antiapoptoctic proteins. For example, melanoma has been shown to express a number of chemokines implicated in tumour growth and progression (Payne and Cornelius, 2002). Moreover, the formation of blood vessels is important for the tumour's survival. Chemokines have been shown to be important for angiogenesis of tumours with CXCL12

being the most potent angiogenic chemokine (Chow and Luster, 2014).

Immune cells infiltrate tumours and are thereby responsible for the control of the growth or removal of the tumour. Chemokines play an important role in this process of infiltration in any tissue. Upon expression of chemokines in the tumour micro-environment a number of cells with antitumour effects are transported along the chemokine gradient to the tumour. These cells include $CD8^+$ T cells, T helper 1 cells, polyfunctional T_H17 cells and natural killer (NK) cells expressing different chemokine receptors (Balkwill, 2004a, 2012; Chow and Luster, 2014; Nagarsheth *et al.*, 2017).

The formation of metastatic tumours describes the spreading of a tumour from its primary site to distant sites in the body which makes targeting of the tumour more difficult. The expression of chemokine receptors on the tumour cell can cause those to follow chemokine gradients to specific anatomic sites which support the growth of metastatic tumour cells (Balkwill, 2004a; Zlotnik *et al.*, 2011; Chow and Luster, 2014). CXCR4 and CXCL12 have been reported to play an important role in metastasis as the blockage of the CXCR4/CXCL12 axis suppresses breast cancer metastasis to the lung (Müller *et al.*, 2001; Sun *et al.*, 2010).

Multiple chemokine receptors have been implicated in the entry of human immunodeficiency virus (HIV) into cells. HIV entry occurs by direct fusion of the viral and target cell membranes. This process is mediated by viral envelope glycoprotein gp120 binding to cluster of differentiation 4 (CD4) located on the cell surface of immune cells (Hendrickson *et al.*, 1998). However, the expression of CD4 is not enough to allow HIV cell entry leading to the conclusion that a co-receptor is needed for the process (Berger *et al.*, 1999). CCR5 (Dragic *et al.*, 1996) and CXCR4 (Bleul *et al.*, 1996; Feng *et al.*, 1996; Oberlin *et al.*, 1996) have been identified as the two major co-receptors with other chemokine receptors like CCR3, CCR8 or US28 also showing involvement (Berger *et al.*, 1999). The chemokine receptors engage also with the envelope glycoprotein, however this

also activates signalling pathways or supresses those activated by chemokines. It has been shown that the interaction of CCR5 or CXCR4 with glycoprotein induces tyrosine phosphorylation of the protein tyrosine kinase Pyk2 (Davis *et al.*, 1997), mobilises Ca^{2+} and activates ion channels (Liu *et al.*, 2000). On the other hand, gp120 shows to reduce CXCL12-mediated cell migration and proliferation (Wilcox and Hirshkowitz, 2005).

To date, solely two chemokine receptors are targeted by FDA approved drugs. CCR5 is targeted by maraviroc a HIV entry inhibitor that inhibits the interaction of receptor and virus and thereby stops the virus from entering the cell. CXCR4 is targeted by plerixafor (AMD3100) an immune stimulant to mobilize hematopoietic stem cells in cancer patients (Bachelerie *et al.*, 2014).

1.3 Chemokine receptors used in these studies

1.3.1 Crystal structure of CXCR4 and CCR5

CXCR4 was the first chemokine receptor for which highly diffracting co-crystal structures of a thermo-stabilized receptor version were available (**Figure 1-6**). Co-crystals are crystals composed of two or more interacting components such as receptors and ligands, antibodies or other interacting proteins - the binding of an interacting agent can stabilize the conformation of the receptor and is therefore easier to crystallise. This gives an insight into the structure of CXCR4 and offers improvements for modelling of other chemokine receptors. The co-crystals with IT1t (small molecule) and CVX15 (cyclic peptide with 16 amino acids) published in the same paper show that the main structural features are conserved in both crystal structures (Wu *et al.*, 2010). As expected, the structures show the seven transmembrane α-helices linked with three intracellular and extracellular loops as well as an extracellular N-terminal domain and an intracellular C-terminus. However, the structures show that CXCR4 helices reach further into the extra- and intracellular space than the helices of other known

GPCRs, e.g. rhodopsin (**Figure 1-6 B**) (Wu *et al.*, 2010). An additional cysteine bridge to the one connecting extracellular loop 2 and the top of TM3 is formed in the extracellular space in chemokine receptors between the N-terminus and the extracellular loop 3 as mentioned in **1.2.2 Chemokine receptors**. Both disulphide bonds are important for CXCL12 binding by shaping the entrance of the binding pocket. In general, the intracellular part of CXCR4 is more similar to other GPCRs than the extracellular, however many other GPCRs show a helix VIII at the C terminal end which is missing in CXCR4. Minor differences in the structures of CXCR4 with IT1t or CVX15 arise mainly at the N-terminal binding pocket due to the size of the ligands.

Furthermore, a third crystal structure of CXCR4 with a viral chemokine vMIP-II was published showing a very similar intracellular structure to the two crystal structures discussed above. However, the structure showed differences in the N-terminal binding pocket of the chemokine resulting in an outward shift of the transmembrane helices in the extracellular part of the receptor due to the bigger size of the chemokine compared to IT1t and CVX15 (Qin *et al.*, 2015).

Both publications show the formation of homodimers in all three crystal structures suggesting biological relevance (Wu *et al.*, 2010; Bachelerie *et al.*, 2014; Qin *et al.*, 2015). In addition there are also descriptions of CXCR4 forming heteromer structures with other GPCRs like CCR2, CCR5 or ACKR3 (Springael *et al.*, 2005; Levoye *et al.*, 2009; Wu *et al.*, 2010).

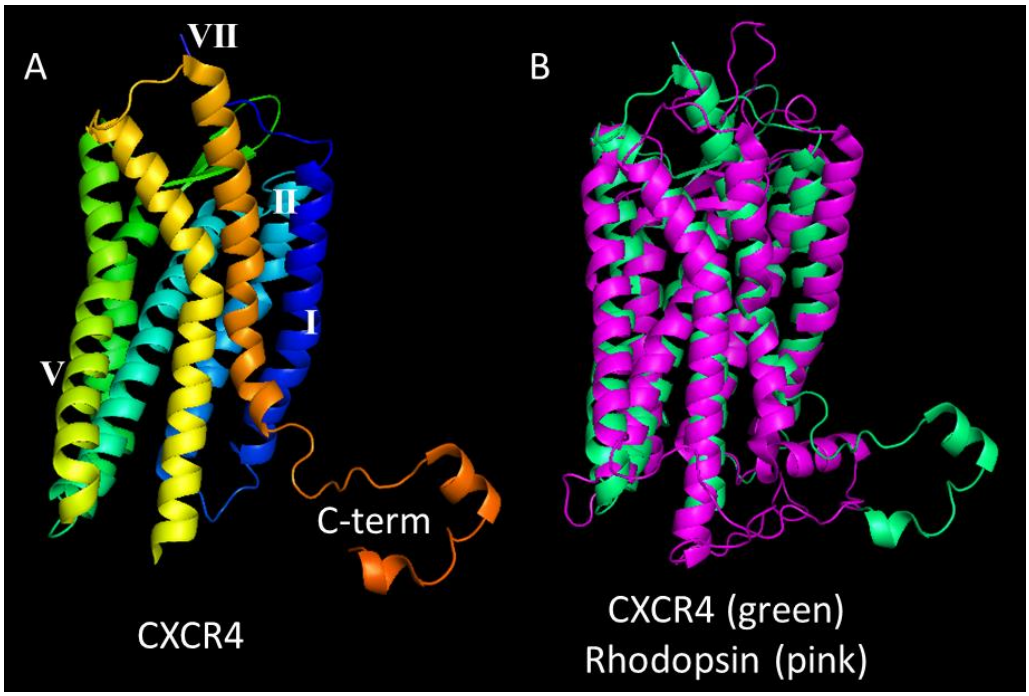

Figure 1-6: CXCR4 crystal structure. (**A**) Crystal structure of CXCR4 bound to small molecule antagonist IT1t (PDB ID: 3ODU) colouring from N-terminal end blue to C-terminal end orange; (**B**) Comparison of transmembrane helices of CXCR4 (green) with rhodopsin (PDB ID: 1U19; pink); (Okada *et al.*, 2004; Wu *et al.*, 2010)

Another chemokine receptor with two crystal structures available is CCR5. The first structure was solved with the FDA approved small molecule inverse agonist maraviroc bound (Tan *et al.*, 2013) and the second with the antagonistic chemokine [5P7]CCL5 (Gaertner *et al.*, 2008; Zheng *et al.*, 2017). The overall fold of CCR5 is similar in both crystal structures showing a similar architecture to other class A GPCRs and CXCR4 with 7TM helices connected by three extracellular and three intracellular loops. As expected, the extracellular region in the chemokine and maraviroc bound structures of CCR5 show differences due to spacing.

CCR5 and CXCR4 share a sequence identity of 34% and also show structural similarities (**Figure 1-7**). However, visible differences occur in the C-terminal end where CCR5 shows the presence of a helix VIII while CXCR4 has a disordered conformation probably due to changes in conserved sequences in CXCR4 needed for the formation of this helix VIII or differences in crystal packing interactions. Moreover, CCR5's helix IV is tilted by approximately 15° in

comparison to CXCR4, is 1.5 turns shorter at the intracellular part and forms a classical α helix in comparison to a distorted Π helix in CXCR4. The intracellular loop 2 of CXCR4 is unstructured while it contains a two-turn helix in CCR5 that is in parallel to the cell membrane due to a hydrophobic cluster of amino acids.

Comparing the ligand binding sites of IT1t with CXCR4 and maraviroc with CCR5 and the extracellular part of the receptor it is apparent that maraviroc binds deeper into the pocket and occupies a larger area with no contact to the extracellular loops showing a more open structure than the IT1t bound CXCR4. The CXCR4 binding pocket is partially covered by its N-terminus and extracellular loop 2. Because of these differences in the binding pocket, Helix VII is shifted outward by about 3 Å for CCR5 in comparison to CXCR4 as a corresponding shift in the N-terminal end of Helix VII is needed for binding of maraviroc (Wu *et al.*, 2010; Tan *et al.*, 2013). Moreover, there is a salt bridge in ECL2 of CXCR4 resulting in a 6 Å shift at the ß-hairpin tip of ECL2 toward the ligand-binding pocket compared with CCR5 with an absent salt bridge (Wu *et al.*, 2010; Tan *et al.*, 2013).

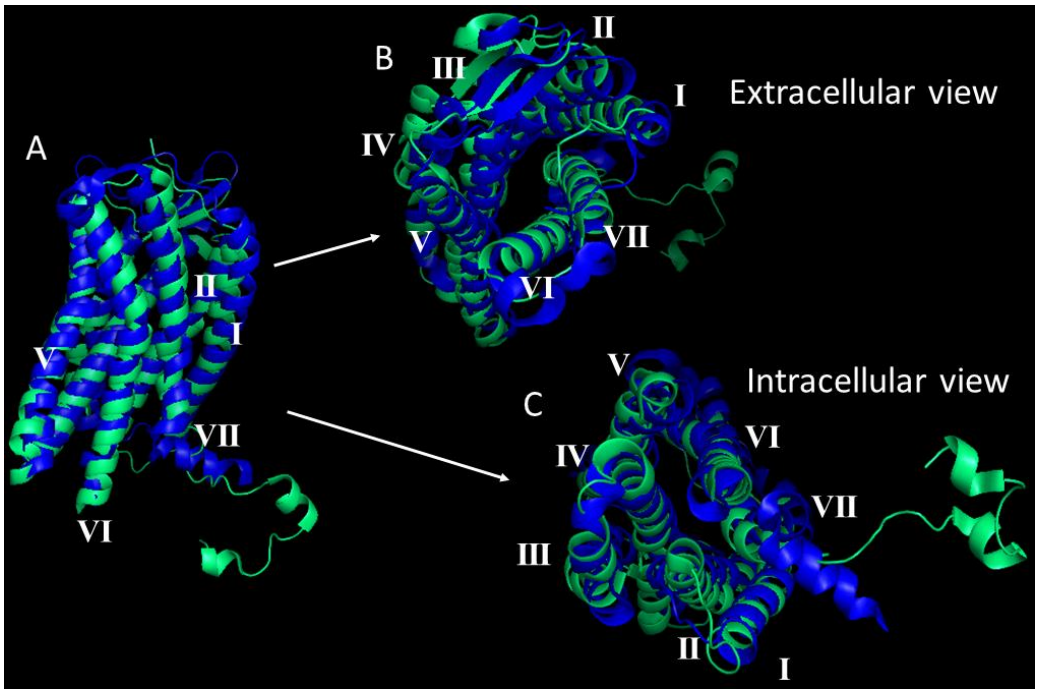

Figure 1-7: CXCR4 and CCR5 crystal structures in comparison. (**A**) Structure comparison of the overall fold of the CCR5-maraviroc complex (PDB ID:4MBS, blue) with CXCR4:IT1t (PDB ID: 3ODU, green) (**B**) Top view of the extracellular side of CCR5 and CXCR4; (**C**) bottom view of the intracellular side of CCR5 and CXCR4.

1.3.2 Function of CXCR4

CXCR4 is one of the most researched chemokine receptors due to its importance in mobilizing hematopoietic stem cells, its ability to mediate the metastasis of various cancers and role as a co-receptor for T-tropic (X4) HIV virus entry to $CD4^+$ T cells. Moreover, CXCR4 is one of only two chemokine receptors with an FDA approved small molecule ligand (AMD3100), an immune stimulant to mobilize hematopoietic stem cells in cancer patients. CXCL12 binds with high specificity to CXCR4 and initiates different signalling pathways that are typical for chemokine receptors, i.e. adhesion, chemotaxis, survival and proliferation (**Figure 1-8**). CXCR4 primarily couples to the G protein family $G\alpha_i$ and has been shown to couple in some cases to $G\alpha_{13}$ or G_q causing the activation of different signalling pathways. $G\alpha_i$ is known to inhibit the production of cAMP by inhibiting adenylyl cyclase which will be one of the focuses in the functional assays. CXCR4 activation causes the activation of the phosphoinositide 3-

kinase (PI3K) pathway, the activation of the tyrosine kinase Janus kinases (JAK) – signal transducer and activator of transcription proteins (STAT) pathway, the inhibition of the adenylyl cyclase (AC) pathway, the activation of the Ras - mitogen activated protein kinase (MAPK) pathway and the activation of the phospholipase C (PLC) pathway. Furthermore, CXCR4 can also signal through a β-arrestin pathway, after phosphorylation by GRKs, influencing G protein signalling, endocytosis, desensitization and chemotaxis (**Figure 1-8**) (Cheng *et al.*, 2000; Soede *et al.*, 2001; Tan *et al.*, 2006; Kleemann *et al.*, 2008; Quoyer *et al.*, 2013). A snake structure of CXCR4 with amino acids highlighted that are important in various aspects of ligand binding and signalling can be found in **Figure 1-9**. A rare mutation within humans occurring at R344 of CXCR4 causes an immunodefiency disease causing warts, hypogammaglobulinemia, infections, and myelokathexis (WHIM syndrome) (Hernandez *et al.*, 2003).

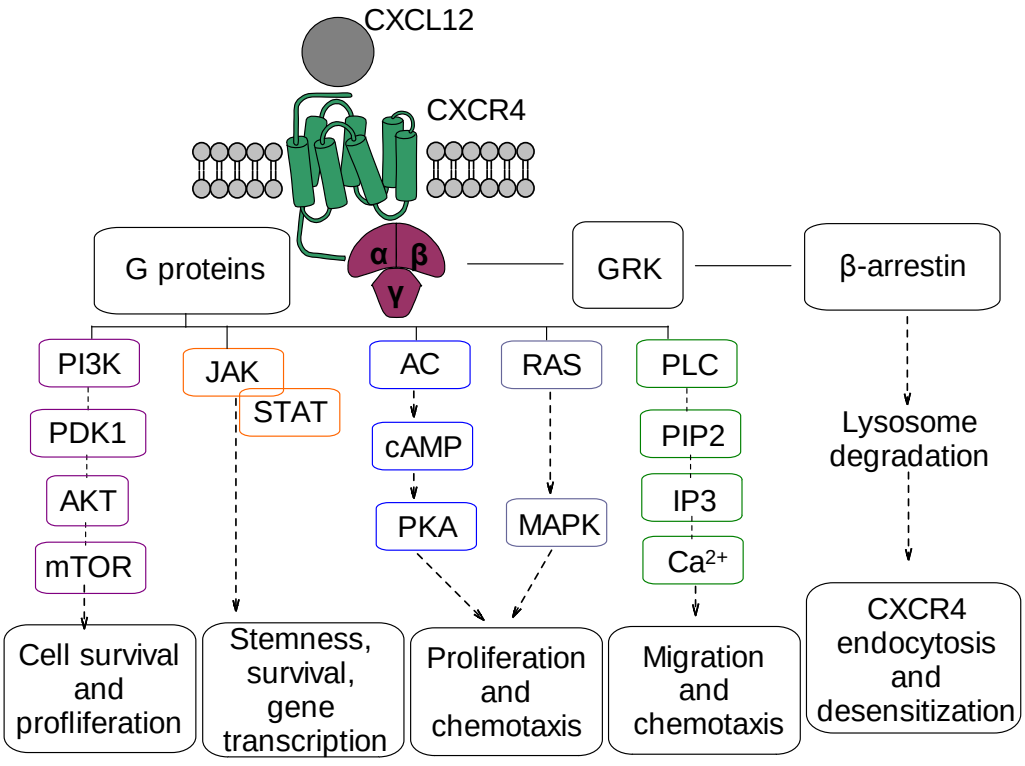

Figure 1-8: Signalling promoted by CXCR4 and CXCL12. G protein activation signals by activating PI3K-AKT-mTOR, Jak-STAT, Ras-MAPK and PLC pathways while blocking of adenylate cyclase and thereby cAMP production; adapted from (Teixidó *et al.*, 2018)

CXCL12 has constitutively high expression levels within bone marrow stromal cells, but is also expressed in other areas of the body and can be found in significant concentrations in neuronal cells, glandular cells, respiratory epithelial cells, cells in tubules, leydig cells, trophoblastic cells and epidermal cells (Bachelerie *et al.*, 2014; Uhlén *et al.*, 2015). CXCR4 can be activated by CXCL12 as the only chemokine and molecules that are released from damaged, stressed or inflamed cells like inflammatory cytokines and danger-associated molecular pattern molecules. These molecules include the pleotropic cytokine macrophage migration inhibitory factor, extracellular ubiquitin and high mobility group protein B1 (Bachelerie *et al.*, 2014). Furthermore, CXCR4 and CXCL12 play a major role in embryonic development and viability (Tachibana *et al.*, 1998; Zou *et al.*, 1998).

While the expression of CXCR4 in cancer cells is high and found in at least 23 types of human cancer, nearby healthy tissue has very low or no CXCR4 expression which may be a result of changes in the vasculature or in the O_2-carrying capacity of cells that lead to oxygen deficiency (Hirota and Semenza, 2006). Oxygen deficiency induces the activation of hypoxia-inducible factor-1 which may promote the expression of CXCR4 (Hirota and Semenza, 2006; Furusato *et al.*, 2010). The activation of CXCR4 promotes migration of cancer cells and increases their invasion through endothelial cells, bone marrow stromal cells and fibroblasts (Balkwill, 2004a; b). CXCR4 expression increases with tumour aggressiveness and CXCL12 concentration is higher in metastatic tumours in comparison to their primary tumour (Kato *et al.*, 2003; Furusato *et al.*, 2010). While tumour metastasis caused by CXCR4/CXCL12 seems to be a major focus in research, CXCR4 has also been shows to be involved in the blood vessel formation and survival of the tumour (Furusato *et al.*, 2010; Sun *et al.*, 2010; Teixidó *et al.*, 2018).

1.3.3 Function of ACKR3

Atypical chemokine receptor 3 (ACKR3), also known as C-X-C chemokine receptor type 7 (CXCR7) was first identified in 1990 in a dog cDNA library (Libert *et al.*, 1990) and was an orphan receptor for many years. ACKR3 is very similar in sequence and position on the human chromosome to other CXCR-type receptors and was named accordingly CXCR7 until it was renamed due to its signalling behaviour (Bachelerie *et al.*, 2014).

ACKR3 has been shown to be expressed in response to CXCL12-mediated chemotaxis on T lymphocytes. Furthermore ACKR3 is also connected to B cell development and differentiation as the ability of B cells to differentiate into plasma cells correlates with the expression of ACKR3 (Sun *et al.*, 2010). This suggests that ACKR3 is a marker for memory B cells which are able to develop into antibody secreting cells (Sun *et al.*, 2010).

It was initially proposed that ACKR3 may be a decoy receptor for CXCL12 as it had a 10-fold higher affinity towards CXCL12 than CXCR4 and seemed to show no signalling (Balabanian *et al.*, 2005; Naumann *et al.*, 2010; Bachelerie *et al.*, 2014). More recent signalling studies with ACKR3 are described below. Decoy receptors are non-signalling receptors that are able to recognize activating ligands of other receptors and bind them; thereby the effective concentration of available ligand for the signalling receptor is decreased. ACKR3 might be influencing CXCL12 gradients in various mechanisms like reperfusion (restoring blood flow to organs), inflammation and cell infiltration and migration (Maksym *et al.*, 2009). Apart from CXCL12, ACKR3 interacts with CXCL11 which was confirmed to compete with CXCL12 for binding to ACKR3 (Burns *et al.*, 2006).

The sequence of ACKR3 shows an important variation of the "DRYLAIV" motif mentioned before in **1.3.2 Chemokine receptors** to DRYLSIT which is crucial for the interaction with G proteins and normally found in the second intracellular loop of GPCRs (Maksym *et al.*, 2009; Ulvmar *et al.*, 2011; Bachelerie *et al.*, 2014). However, a ACKR3 mutant incorporating the DRYLAIV motif did still not activate

G proteins, mobilise intracellular Ca^{2+}, activate G protein-mediated extracellular signal-regulated kinase (ERK) phosphorylation or chemotaxis after activation by CXCL12 (Naumann *et al.*, 2010; Hoffmann *et al.*, 2012). Notably, the DRY part of the motif that often causes constitutive activity when mutated is conserved.

Nevertheless, there have been studies suggesting an interaction between G proteins and ACKR3. The first one showed an interaction between ACKR3-YFP and $G\alpha_{i1}$–Rluc in a Bioluminescence Resonance Energy Transfer (BRET) assay, but the receptor was unable to activate the G protein (Levoye *et al.*, 2009). The second study shows CXCL12 induced G protein activation via ACKR3 in primary astrocytes. CXCL12 and CXCL11 also induced ERK and Akt activation suggesting cell importance (Ödemis *et al.*, 2012).

ACKR3 recycles independently from ligands between the plasma membrane and endosomal regions. Truncation of the C-terminal end of the receptor or mutation of all serines and threonines traps ACKR3 on the cell surface (Naumann *et al.*, 2010; Ray *et al.*, 2012). However, this recycling is enhanced in the presence of CXCL12 which can be seen as an agonist driven response and therefore ACKR3 acting as a signalling receptor. CXCL12 causes deubiquitination of ACKR3 which is then followed by ß-arrestin recruitment (Canals *et al.*, 2012; Benredjem *et al.*, 2017) and internalisation. Moreover, it has been shown that ACKR3 promotes Akt and MAPK activity, ERK phosphorylation (Hattermann *et al.*, 2010; Rajagopal *et al.*, 2010; Décaillot *et al.*, 2011; Ödemis *et al.*, 2012; Torossian *et al.*, 2014) as well as activation of the JAK2/STAT3 pathway (Hao *et al.*, 2012). AMD3100, the CXCR4 antagonist, shows the ability to recruit ß-arrestin towards ACKR3 at high concentrations (Kalatskaya *et al.*, 2009). A snake structure of ACKR3 with amino acids and highlighted that are important in various aspects of ligand binding and signalling is shown in **Figure 1-10**.

In a similar way to CXCR4, ACKR3 has been shown to act as a co-receptor for HIV-1, HIV-2 and is likely to be involved in the formation of Kaposi sarcoma (a type of cancer connected to HIV that causes

patches of abnormal tissue). However, it is less understood and studied in that area than CXCR4 (Maksym *et al.*, 2009).

ACKR3 may promote expansion and metastasis of certain tumour types (Hattermann *et al.*, 2010; Balkwill, 2012). The expression level of ACKR3 is higher on neoplastically transformed cells than on their non-transformed analogue. In mouse models it was shown that prostate cancer cells overexpressing ACKR3 grow larger and better vascularized tumours (Maksym *et al.*, 2009). However, ACKR3's physiological role and molecular pathway are still unclear in most aspects.

1.3.4 Function of CCR5

CCR5 was the target of the first approved chemokine small molecule drug, maraviroc, which is a CCR5 allosteric modulator used in HIV infections as an entry inhibitor for HI-Viruses using CCR5 as entry into the cells (Garcia-Perez, Rueda, Staropoli, *et al.*, 2011; Lee *et al.*, 2017). The administration of maraviroc in monotherapy has been shown to drop the viral load by 1.6-log units (Fätkenheuer *et al.*, 2005). It has also been shown to reduce graft-versus-host disease in patients treated with allogeneic bone marrow transplantation for leukaemia (Moy *et al.*, 2017).

CCR5 has a broad expression pattern on the surface of T-cells (Bleul *et al.*, 1997; Brelot and Chakrabarti, 2018), hematopoietic cells (NK cells) (Khan *et al.*, 2006), ti-ssue-resident macrophage and microglial cells (He *et al.*, 1997), dendritic cells (Granelli-Piperno, 1996), Langerhans cells (Zaitseva *et al.*, 1997), and osteoclasts (Lee *et al.*, 2017). CCR5 can also be detected at the surface of non-hematopoietic cells such as vascular smooth muscle cells, endothelial cells, hepatic stellate cells, neurons, and glial cells (Brelot and Chakrabarti, 2018).

CCR5, as shown in **Table 1-2**, interacts with about 10 chemokines of the CCL family with CCL3L1 being the most potent CCR5 agonist (Menten *et al.*, 1999). The different chemokine ligands can lead to

biased activation of different pathways primarily involving the G proteins G_i and G_q (Mueller and Strange, 2004; Oppermann, 2004; Mueller *et al.*, 2006) as well as G protein-independent pathways involving arrestins, Janus kinases (JAK) or pyk2 kinases (Mueller and Strange, 2004; Del Corno *et al.*, 2011). A snake structure of CCR5 with amino acids highlighted that are important in ligand binding and implicated in HIV infection is shown in **Figure 1-11**.

CC-chemokines are expressed upon inflammation regulating the immune defence, therefore the main function of CCR5 is to enable leukocyte migration towards inflammation sites (Sorce *et al.*, 2011). Due to the wide range of expression CCR5 has also been reported in other functions than inflammation for example regulation of T-helper cells (Castellino *et al.*, 2006), recruitment of cells to the central nervous system (Sorce *et al.*, 2011), formation of atherosclerotic plaques (Jones *et al.*, 2011) and development of fibrosis (Seki *et al.*, 2009).

In cancer, CCR5 is expressed on various types of tumour cells and involved in tumour survival and migration (Nagarsheth *et al.*, 2017). Similar to CXCR4, a high expression of CCR5 correlates with poor patient prognosis. Therefore, CCR5 seems to be not only a good target for HIV infection but multiple other diseases.

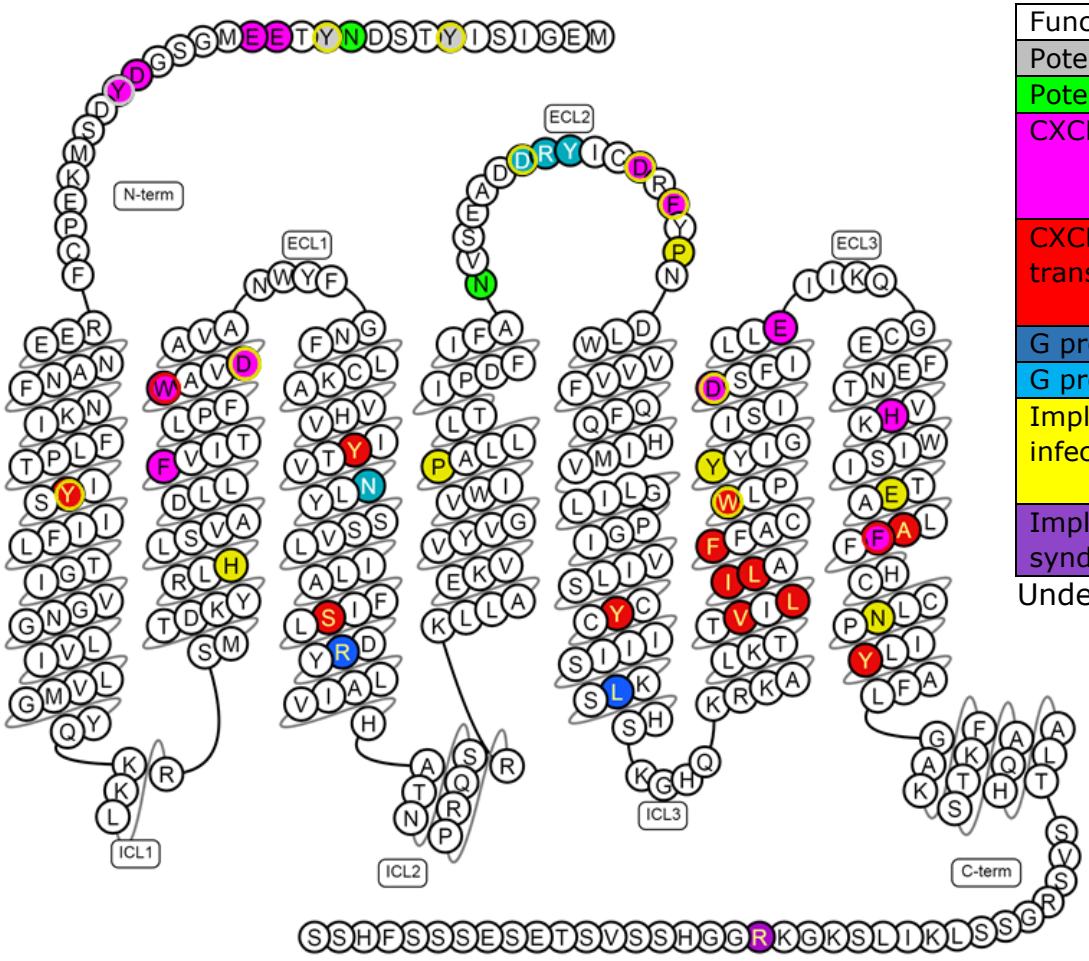

Function	Residue
Potential sulfation	Y7, Y12, Y21
Potential glycosylation	N11, N176
CXCL12 binding	E14, E15, D20, Y21, F87, W94, D97, D187, F189, D262, E268, H281, F292
CXCL12 signal transmission	Y45, W94, Y116, S131, Y219, V242, L244, I245, L246, F248, W252, A291, F292, Y302,
G protein recruitment	R134, L226
G protein signaling	N119, D182, R183, Y184
Implicated in HIV infection	Y7, Y12, Y45, H79, D97, P163, D182, D187, F189, P191, W252, Y255, D262, E288, N298
Implicated in WHIM syndrome	R334

Underlined residues are mentioned in two functions

Figure 1-9: CXCR4 snake structure. Schematic representation of the amino acid sequence of CXCR4 adapted from GPCRdb (Horn *et al.*, 2003) and key residues identified in (Brelot *et al.*, 2000; Tian *et al.*, 2005; Rapp *et al.*, 2013; Wescott *et al.*, 2016)

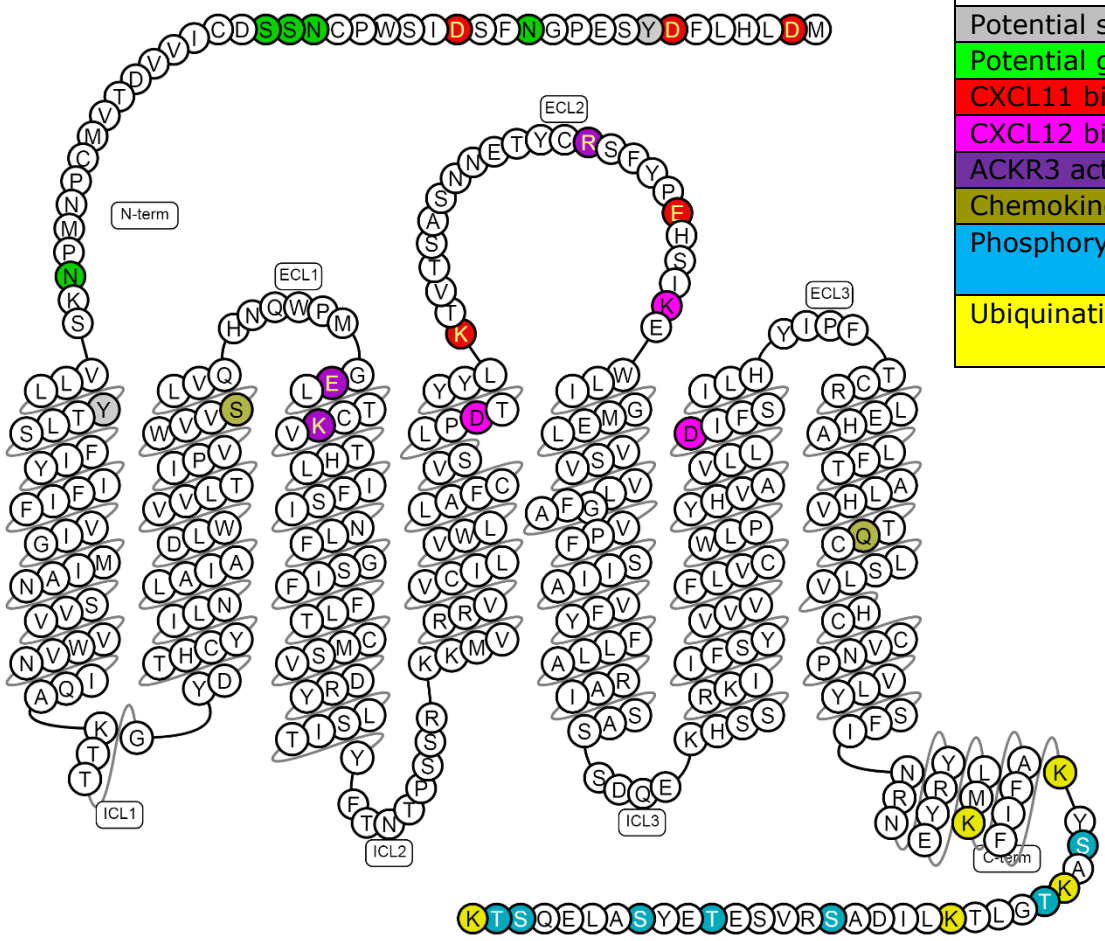

Function	Residue
Potential sulfation	Y8, Y45
Potential glycosylation	N13, N22, S23, S24, N39
CXCL11 binding	D2, D7, D16, K184, E202
CXCL12 binding	D179, K206, D275
ACKR3 activation	E114, K118, R197
Chemokine scavenging	S103, Q301
Phosphorylation sites	S335, T338, S347, T352, S355, S360, T361
Ubiquination sites	K328, K333, K337, K342, K362

Figure 1-10: ACKR3 snake structure. Schematic representation of the amino acid sequence of CXCR7/ACKR3 adapted from GPCRdb (Horn et al., 2003) and key residues identified in (Canals *et al.*, 2012; Benredjem *et al.*, 2017)

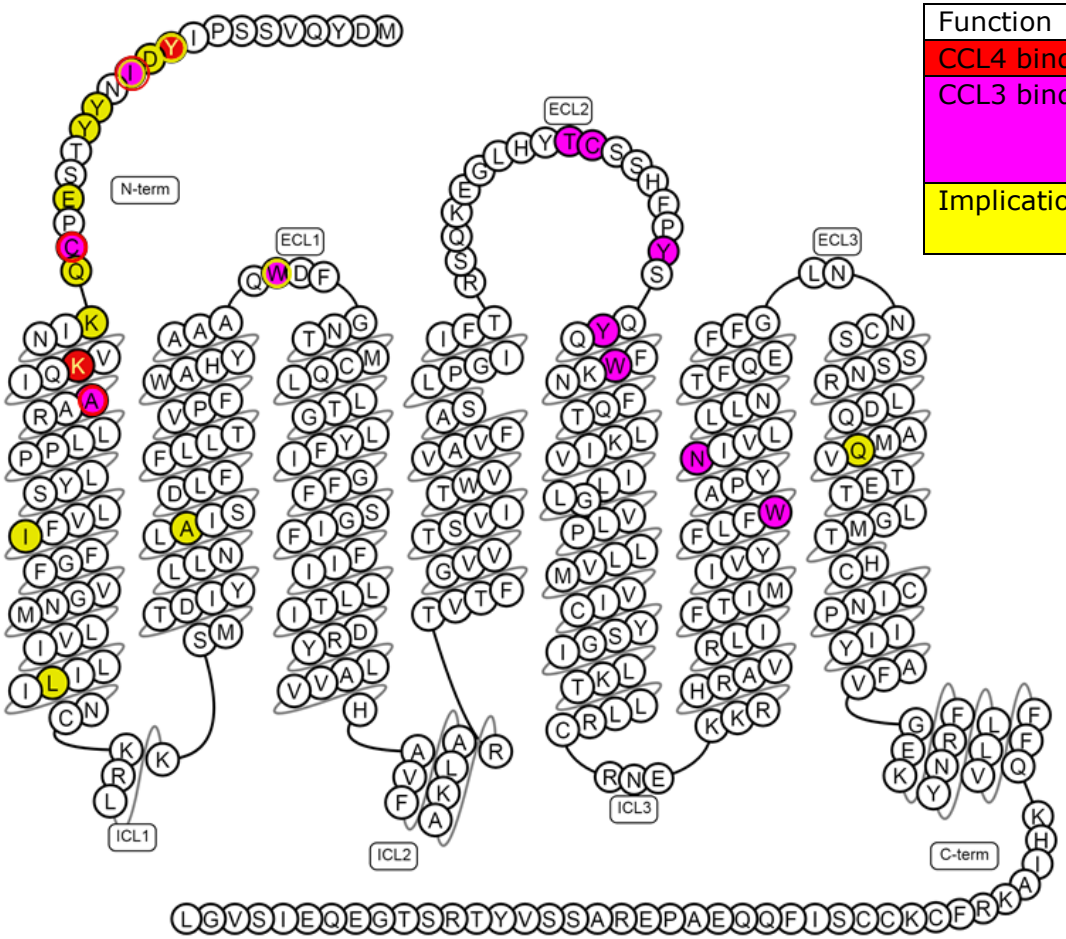

Function	Residue
CCL4 binding	Y10, I12, C20, K26, A29
CCL3 binding	I12, C20, A29, W94, T177, C178, Y184, Y187, W190, W248, N252
Implication in HIV infection	Y10, D11, Y14, Y15, E18, Q21, K22, I42, L55, A73, W94, Q280,

Figure 1-11: CCR5 snake structure. Schematic representation of the amino acid sequence of CCR5 adapted from GPCRdb (Horn et al., 2003) and key residues identified in (Farzan *et al.*, 1998; Howard *et al.*, 1999; Zhou *et al.*, 2000; Garcia-Perez, Rueda, Alcami, *et al.*, 2011)

1.4 Pepducins

1.4.1 Background

Pepducins, first described in 2002 (Covic *et al.*, 2002), are cell-penetrating lipidated peptides derived from the GPCR they are supposed to modulate. The sequence of the peptide part is derived from one of the internal loops of the GPCR and is typically 10-20 amino acids long, corresponding to 1,500 to 2,000 Daltons (Dimond *et al.*, 2011; O'Callaghan, Kuliopulos, *et al.*, 2012). The lipid component of the pepducin is usually composed of palmitate, myristate or lithocholic acid coupled to the peptide sequence via an amide bond (O'Callaghan, Kuliopulos, *et al.*, 2012).

Pepducins are highly specific modulators of GPCRs and are postulated to allow targeting of the intracellular site of the receptor (Covic *et al.*, 2002) in comparison to most small molecule drugs that target an allosteric extracellular ligand binding site or the orthosteric binding site in the transmembrane region of the receptor. However, there are recent reports of small molecule modulators also interacting with the intracellular part of the receptor, for example vercirnon at CCR9, CCR2-RA-[R] at CCR2 or cmpd15-PA at $ß_2$AR (Oswald *et al.*, 2016; Zheng *et al.*, 2016; Liu *et al.*, 2017; Chaturvedi *et al.*, 2018). The lipid tail of the pepducin is hypothesized to function as an anchor in the cell membrane and subsequently a flipping process occurs in which the pepducin enters the cell (Langel, 2011; O'Callaghan, Kuliopulos, *et al.*, 2012). Evidence for pepducins binding on the inside of the receptor is based on the finding that incubation of platelets or Rat1 fibroblasts with fluorescent pepducin for Protease activated receptor 1 (PAR1) followed by digestion of extracellular peptide with pronase results in cells with 5 times higher fluorescence as cells treated with unlipidated pepducin in flow cytometry (Covic *et al.*, 2002). Furthermore, it was shown in a FRET based assay using platelets that a PAR1 pepducin Rho-P1pal12 also quenched an intracellular marker (NBD-PS) as well as an extracellular marker (NBD-PC) while a control lipid analogue (Rho-PE) that does not cross the membrane was only able to quench the extracellular marker (Wielders *et al.*, 2007). However, both studies look at the location of

pepducins after receptor activation and these results might be explained by internalisation.

Pepducins can stabilize the receptor in an active or inactive conformation causing a positive or negative allosteric modulation, respectively (Covic *et al.*, 2002; Tchernychev *et al.*, 2010). Moreover, it has been shown that peptides from the C-terminal end of the $ß_2$AR directly activate purified G_s by mimicking the receptor without its presence (Strader *et al.*, 1994; Dimond *et al.*, 2011).

Other pepducins have been shown to act as either agonists (Tchernychev *et al.*, 2010) or antagonists (O'Callaghan, Kuliopulos, *et al.*, 2012). ATI-2341, an ICL1 pepducin for CXCR4, seemed to be biased towards G proteins over β-arrestin in BRET based recruitment assays (Quoyer *et al.*, 2013). Carr et al. (2014) investigated in depth a total of 51 pepducins derived from the $β_2$AR receptor in order to design G protein-biased pepducins. All pepducins included parts from one of the intracellular loops and some included adjacent transmembrane regions. It was shown that the pepducins, dependent on the region they are derived from, caused the activation of different signalling pathways in the cells, some even independently of the receptor itself. In total, four different classes of agonist pepducins were identified, the first one activating G_s and β-arrestin, the second one showing β-arrestin bias, the third receptor dependent G_s bias and the fourth receptor independent G_s bias. Pepducins derived from the internal loop 1 were in general β-arrestin biased agonists. However, one pepducin derived from the first internal loop (ICL1-15) showed activation of β-arrestin and G_s. Pepducins derived from internal loop 3, showed in general G_s biased signalling. It is suggested by the crystal structure of the $β_2$AR-G_s complex that the intracellular loop 3 is the key interactor between $β_2$AR and G_s (Carr *et al.*, 2014). However, due to the large number of pepducins screening was performed in only two assays, one for cAMP production and one for ß-arrestin engagement. Only those pepducins showing a prominent G protein bias in the two assays were then tested in more depth.

1.4.2 CXCR4 based pepducins

Pepducins offer a potential new therapeutic ligand class. Current studies mostly focus on their functional response while their exact mode of action is still unclear. Our focus was on CXCR4 pepducins (**Table 1-3**) and in particular ATI-2341 (**Figure 1-12**) a well-known pepducin based on the first internal loop of CXCR4 (Tchernychev *et al.*, 2010). ATI-2341 activates CXCR4-dependent signalling pathways similar to the endogenous agonist CXCL12.

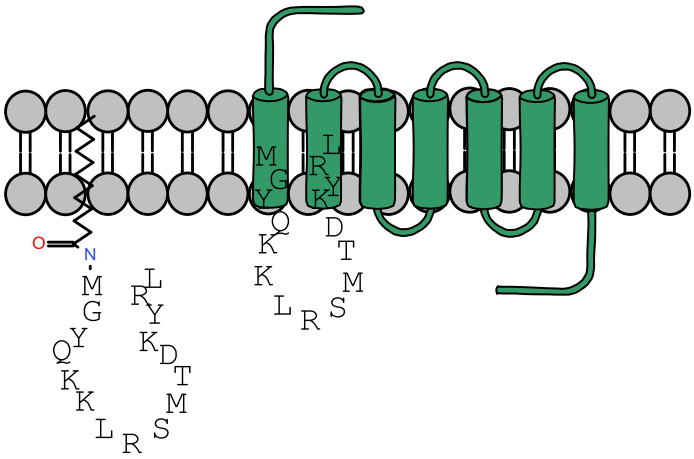

Figure 1-12: Pepducin representation. Schematic representation of pepducin ATI-2341 (left) in comparison with the sequence of the first internal loop of CXCR4 represented in green (right)

ATI-2341 has previously been shown to directly interact with CXCR4 in cross-linking experiments in which a fluorescent version of ATI-2341 (ATI-2766) is covalently attached to CXCR4 by activation of a photo-leucine with UV-light (Janz *et al.*, 2011). This activated photo-leucine incorporates an active carbine that reacts rapidly with atoms in close proximity. Interestingly, ATI-2766 also interacts with N-terminal truncated mutants of CXCR4. In cAMP assays these truncated mutants show a decreased potency of CXCL12, while the potency of ATI-2341 is not impacted. This suggests a different binding mode for CXCL12 and ATI-2341 in agreement with its postulated intracellular interaction (Janz *et al.*, 2011). The interaction of CXCR4 and ATI-2341 has also been modelled resulting in multiple possible binding modes of the pepducin in the extracellular and intracellular

region of the receptor (Planesas *et al.*, 2015). The extracellular region is located at the entrance of the main pocket of CXCR4 and delimited by the three ECL. The intracellular region included all three ICL in the interaction of ATI-2341 and CXCR4. However, the extracellular binding positions were fewer and not looked at in more detail.

ATI-2341 has previously been shown to cause inhibition of cAMP production (Tchernychev *et al.*, 2010; Dimond *et al.*, 2011), Ca^{2+} mobilization, polymorphonuclear neutrophil mobilization and in vitro and in vivo chemotaxis (Tchernychev *et al.*, 2010) as well as G protein recruitment and activation (Quoyer *et al.*, 2013).

CXCR4 internalisation has been observed in imaging techniques upon addition of ATI-2341 (Tchernychev *et al.*, 2010). However, it was also shown that ATI-2341 recruits β-arrestin only partially to CXCR4 in a BRET assay and is only a weak internalising agent compared to CXCL12 looking at cell surface expression in flow cytometry (Quoyer *et al.*, 2013). Obviously these two statements appear contradictory, however Quoyer et al. tested internalisation in two different ways, one showed no internalisation in HEK293T cells expressing tagged CXCR4 in flow cytometry and the other showed a significant loss in cell surface receptor expression in SUP-T1 cells after stimulation with ATI-2341 visualized with a fluorescent antibody and analysed via flow cytometry. The internalisation might not be dependent on the recruitment of β-arrestin as it has been shown for multiple receptors such as the m1, m3 and m4 subtypes of the muscarinic cholinergic receptor (Lee *et al.*, 1998). Moreover, the intracellular pepducin could interfere with the binding of the tagged ß-arrestin due to steric hindrance or the pepducins might act a lot slower than the endogenous ligand due to the mechanism involved in crossing the membrane and recruitment was only measured for up to 15 min. However, the timings for CXCL12 and ATI-2341 were similar to each other in G protein measurements.

Moreover, the ability of ATI-2341 to recruit G proteins ($G\alpha_i$, G13) has been investigated in the same BRET assay as the β-arrestin recruitment, with a C-terminal Rluc-tagged CXCR4 and an YFP-tagged

G protein or β-arrestin. These studies show a bias for G protein-dependent pathways favouring Gαi over G13. The recruitment of G proteins is sensitive to Pertussis toxin (PTX) (Quoyer *et al.*, 2013). ATI-2341 shows only a weak recruitment of β-arrestin in comparison to CXCl12 as mentioned above. This mechanism was further studied by looking at the activation of phosphorylation. G protein receptor kinase 6 (GRK6) and protein kinase C (PKC) both phosphorylates the activated form of CXCR4 and thereby initiate its deactivation. This phosphorylation is followed by the recruitment of ß-arrestin and finally internalisation. Ser-324 and Ser-325 are phosphorylated by PKC and GRK6 and Ser-330 is phosphorylated only by GRK6. ATI-2341 promoted PKC but not GRK6 phosphorylation as shown with antibody binding specific to the phosphorylated states. It was then further investigated if ATI-2341 recruits G protein receptor kinase 2 (GRK2) and 3 in a BRET assay which are also involved in the recruitment of β-arrestin. In agreement with the lower β-arrestin recruitment, ATI-2341 also recruits less GRK2 and 3 (Quoyer *et al.*, 2013).

Reported pepducin antagonists include the CXCR4 ligands x4pal-il1 (PZ-218) and x4pal-i3 (PZ-210) (O'Callaghan, Kuliopulos, *et al.*, 2012). x4pal-il1 also derived from the first internal loop of CXCR4 and x4pal-i3 derived from the third intracellular loop have been studied far less than ATI-2341, but show inhibition of calcium mobilization by CXCL12 in human neutrophils (Kaneider *et al.*, 2005; O'Callaghan, Lee, *et al.*, 2012), inhibition of ERK activation in Jurkat cells (O'Callaghan, Lee, *et al.*, 2012), and CXCL12-mediated chemotaxis of HEK, leukaemia and lymphoma cells as well as primary human B-CLL cells (Kaneider *et al.*, 2005; O'Callaghan, Lee, *et al.*, 2012).

Table 1-3: Pepducins published for CXCR4 modulation*

Pepducin	N-term	Sequence	Ref	Function
ATI-2341	Pal	MGYQKKLRSMTDKYRL	1, 2, 3	Biased Agonist; ICL1
ATI-2342	Pal	MGYQKKLRSMTDKYRLHL	1	Lower potency than ATI-2341
ATI-2346	Pal	KKLRSMTDKYRLH	3 SI	PAM
ATI-2347	Pal	KKLRSMTDKYRL	1	Lower potency than ATI-2341
ATI-2339 (PZ-217)	Pal	MGYQKKLRSMTDK	1, 2, 3, 4	No response
ATI-2504	NH_2	MGYQKKLRSMTDKYRL	1, 3	Non Palmitic control
ATI-2755	Pal	GGYQKKLRSATDKYRL	2	Parent ATI-2766 similar potency to ATI-2341
ATI-2756	Pal	GGYQKKLRpHTDKYRL	3 SI	ATI-2341 analogue with improved plasma stability
ATI-2766	shown below	GGYQKK-R_4-SATDKYRL	2	Fluorescent Pepducin
PZ-218 (x4pal-i1)	Pal	MGYQKKLRSMTD	4, 5	Antagonist; ICL1
PZ-210 (x4pal-i3)	Pal	SKLSHSKGHQKRKALK	4, 5	Antagonist; ICL3
PZ-253	NH_2	MGYQKKLRSMTD	4, 5	Non palmitic control
PZ-254	NH_2	SKLSHSKGHQKRKALK	4, 5	Non palmitic control

* The supporting information of (Tchernychev *et al.*, 2010) mentions further screening of 18 more intracellular loop 1 pepducins in a chemotaxis assay – all showed low potencies and sequences were not mentioned; the patent (US 9,096,646) (McMurry *et al.*, 2015) of CXCR4 pepducins mentions further pepducins from all 3 intracellular loops which partially were screened

ATI-2766:

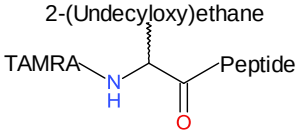

1. (Tchernychev *et al.*, 2010)
2. (Janz *et al.*, 2011)
3. (Quoyer *et al.*, 2013)
4. (O'Callaghan, Kuliopulos, *et al.*, 2012)
5. (Kaneider *et al.*, 2005)

1.5 Fluorescence and Luminescence

Many methods used during this work are based upon detecting light of specific wavelengths arising from the fluorescent tag of receptors, the luminescence caused by biosensors or emission caused by a ligand or protein tag that is excited by energy transfer. While luminescence describes the spontaneous emission of light due to chemical or biochemical reactions, fluorescent molecules have to be excited by light or other electromagnetic radiation from the outside in order to then emit light of a different, lower energy wavelength. This fluorescence or luminescence can either be detected as a brightness value or be visualized immediately on a microscope with good spatial and temporal resolution (Middleton and Kellam, 2005; Lohse *et al.*, 2012; Stoddart *et al.*, 2013).

The labelling of GPCRs and interacting proteins with fluorophores did not only enable research based on microscopy, but also allowed studies using two different labels looking at the interactions between the labelled sites, ligands or proteins via distance dependent energy transfer.

1.5.1 FRET and BRET

Förster Resonance Energy Transfer (FRET) is the radiation-less transfer of absorbed light between two chromophores in close proximity. A fluorophore is excited (donor) by a light source and then transfers its energy to an acceptor chromophore in close proximity if the two chromophores have a spectral overlap. This excited acceptor can then release the energy in form of light in a different wavelength (**Figure 1-13**). The efficiency of the transfer is dependent on the inverse sixth power of the distance, the orientation factor between the donor and acceptor as well as the degree of spectral overlap (Stryer, 1978; Lohse *et al.*, 2012).

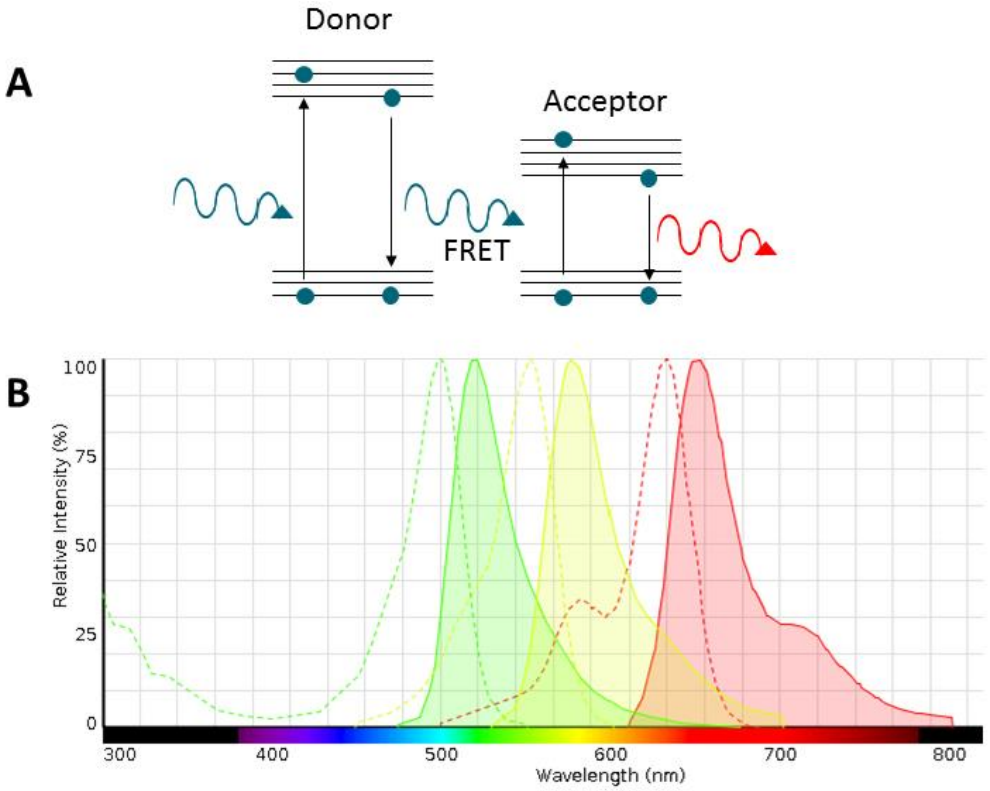

Figure 1-13: FRET. (**A**) Schematic representation of Förster Resonance Energy Transfer; (**B**) Spectral overlap of Alexa Fluor 488 (green), Alexa Fluor 633 (red) and TAMRA (yellow) showing excitation (dashed lines) and emission profiles; made with the ThermoFisher SpectraViewer

Bioluminescence Resonance Energy Transfer (BRET) is based on the same principles as FRET. However, bioluminescence is transferred from a donor to an acceptor without activating the donor with an energy source from the outside. Normally, bioluminescence is initiated by the addition of small luciferin like furimazine (for an Nluc-tag) or coelenterazine (for an Rluc-tag) that produces light when oxidized at the luciferase tag within the system. In practise there is only a good energy transfer when ligand and receptor are closer than 10 nm (Pfleger and Eidne, 2006; Machleidt *et al.*, 2015; Stoddart *et al.*, 2015).

BRET and FRET techniques have been applied to basically all steps in GPCR signalling, starting with monitoring the ligand binding using fluorescent versions of the ligand and a tagged receptor, to the activation of the GPCR using two internal receptor tags that change

their conformation to each other and thereby cause a change in energy transfer and finally constructs reporting the recruitment and activation of signalling proteins as G proteins or arrestins by a change in distance. One aspect to consider during these experiments is the size of the fluorescent tag in comparison to the protein or ligand of interest, the tags can be quite large and can change the behaviour of the protein considerably and should always be tested for functionality (Hoffmann *et al.*, 2005).

1.6 Aims

This project was part of the Marie Skłodowska-Curie Innovative Training Network "ONCORNET" as previously mentioned. All projects investigated different aspects of CXCR4 or ACKR3. This particular project concentrated on investigating the mode of action of pepducins in general and in particular for CXCR4 as a drug target in cancer. However, the mechanism of pepducins were not very well understood at the beginning of this study with most publications focusing on signalling effects caused by pepducins rather than mechanism.

The research questions we tried to answer in the following were:

I. Does ATI-2341 interact directly with CXCR4?
II. Does ATI-2341 bind intracellularly towards CXCR4?
III. Does ATI-2341 influence CXCL12 at CXCR4?
IV. Does ATI-2341 mediate downstream signalling of CXCR4?
V. What are the key residues causing the interaction of ATI-2341 and CXCR4?

Initially DNA constructs were made and peducins were synthesised in a cooperation with ALMAC (see **3. Preparation of DNA constructs and ligands**) using solid-phase peptide synthesis.

In order to study where ATI-2341 binds (intracellular or extracellular) and if it has an effect on CXCL12 binding an end point BRET assay was set up with C- and N-terminal tagged receptor. Moreover since the proposed binding mechanism of all pepducins involved a potentially time consuming process of the pepducin crossing the cell membrane a kinetic version of the BRET assay was developed (see **4. BRET studies to investigate the binding mode of pepdcuins**). In the next step the conformational as well as functional activation of CXCR4 by ATI-2341 was studied in more detail to identify differences between CXCL12 and ATI-2341 in the process of receptor activation. The activation of the receptor was monitored with an internal receptor FRET biosensor reacting to CXCL12. The effects of pepducins on receptor dimerisation as well as activation of a number of signalling pathways were tested, including G protein activation, cAMP inhibition, β-arrestin recruitment and receptor internalisation (see **5. Functional characterisation of CXCL12 and ATI-2341 at CXCR4**). In order to identify the key residues involved in binding of the receptor and pepducin, site directed mutagenesis as well as modified synthesis of pepducins was used and the mutated receptors and modified pepducins were studied in the existing assays (see **6. Studies to determine the location and mode of action of pepducins)**. Finally, the thesis is concluded with "**7. Discussion and Outlook**".

The following chapter will give the explanation of the methods used in the study in order to understand the experimental procedure and the obtained results.

2 Materials and Methods

In this chapter all methods used in this study are described starting with standard molecular biology and cell culture procedures. Next, binding and functional assays to study the interaction between CXCR4 and CXCL12 or pepducins will be described as well as imaging techniques. Finally, the analysis of all methods will be discussed.

A full list of the consumables used and their suppliers as well as buffer compositions can be found in **9.1 Appendix for Chapter 2**.

2.1 CXCR4 Ligands

The structures or amino acid sequences of agonists, antagonists and pepducins used in this study can be found in **Table 2-1**.

Table 2-1: CXCR4, ACKR3 and CCR5 agonists and antagonists used. Changes in the amino acid sequence of pepducins in comparison to ATI-2341 are marked in red. Carboxytetramethylrhodamine (TAMRA) is used as a fluorophore in one of the pepducins.

Agent	Structure/Sequence
CXCL12/SDF1-α (PeproTech, London, UK)	10 20 30 KPVSLSYRCP CREFFESHVAR ANVKHLKIN 40 50 60 TPNCALQIVA RLKNNNRQVC IDPKLKWIQE YLEKALNK
CXCL12-red/SDF1-α-red (ALMAC, Edinburgh, UK – sequence shown or Cisbio, Codolet, France – label location unknown)	10 20 30 KPVSLSYRCP CRFFESHVAR ANVKHLKILN 40 50 60 TPNCALQIVA RLKNNNRQVC IDPKLKWIQE YLEK(Alexa647®)ALN
CXCL12-green (ALMAC, Edinburgh, UK)	10 20 30 KPVSLSYRCP CRFFESHVAR ANVKHLKILN 40 50 60 TPNCALQIVA RLKNNNRQVC IDPKLKWIQE YLEK(Oregon Green® 488)ALN
CCL3//MIP-1α (PeproTech, London, UK)	10 20 30 ASLAADTPTA CCFSYTSRQI PQNFIADYFE 40 50 60 TSSQCSKPGV IFLTKRSRQV CADPSEEWVQ 70 KYVSDLELSA
ATI-2341	Pal-MGYQKKLRS MTDKYRL-NH_2
ATI-2755	Pal-GGYQKKLRS ATDKYRL-NH_2
ATI-2504	MGYQKKLRS MTDKYRL-NH_2
ATI-2339	Pal-MGYQKKLRS MTDK -NH_2
ATI-2346	Pal- KKLRSMTDK YRL-NH_2
ATI-2341TA	Pal-MGYQKKLRS MADKYRL-NH_2

ATI-2341f	Pal-K(TAMRA)-MGYQKKLR SMTDKYRL-NH_2
AMD3100 (Sigma Aldrich, Gillingham, UK)	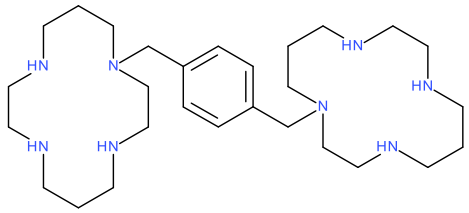
IT1t (Torcis bioscience, Bristol, UK)	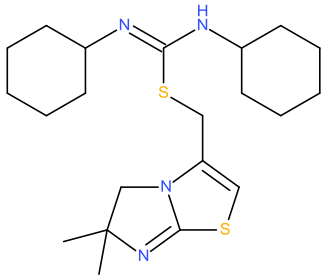
SD01-42 (provided as TFA salt, Sebastian Dekkers, CBS, University of Nottingham)	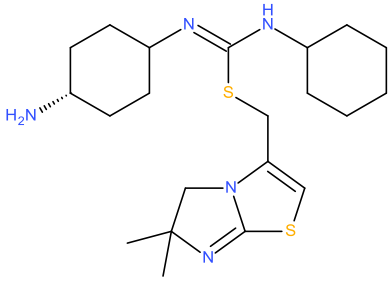
SD01-44 (provided as TFA salt, Sebastian Dekkers, CBS, University of Nottingham)	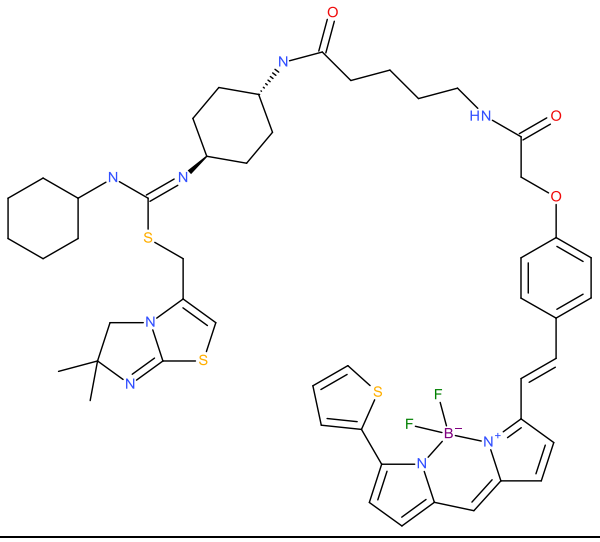

2.2 Molecular Biology

2.2.1 Parent-Vector

All constructs prepared during this work were cloned into pcDNA3.1(+) (map see **Figure 2-1**) with antibiotic resistances for ampicillin and neomycin.

The receptor DNA of WT CXCR4 and ACKR3 (Martine Smit, Vrije Universiteit Amsterdam) were supplied in a $pcDEF_3$ vector which is

similar to pcDNA3.1 with the exception that the CMV (cyotomegalovirus) promoter sequence is substituted for an EF1-alpha (elongation factor 1-alpha) promoter sequence.

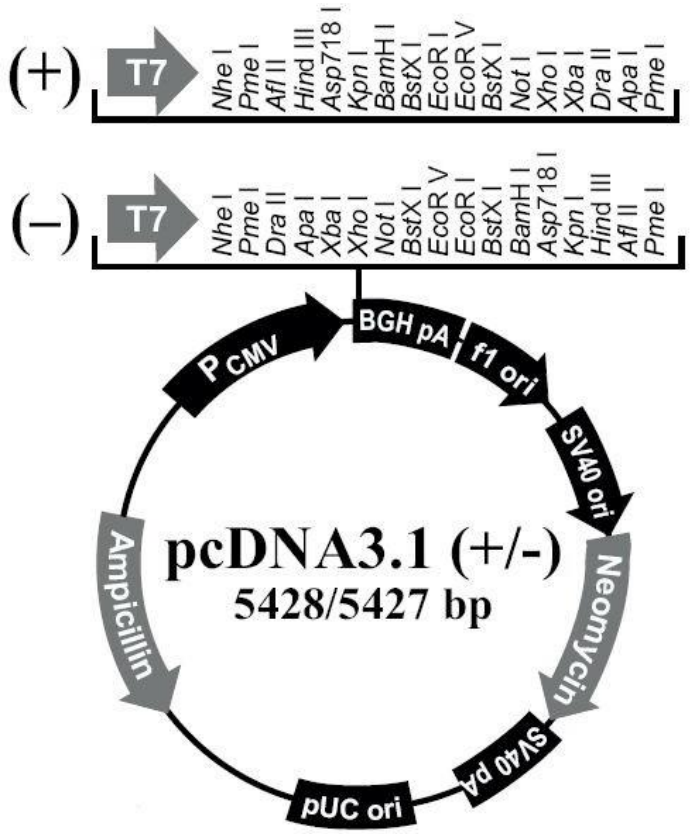

Figure 2-1: vector map of pcDNA3.1. pcDNA3.1 (+) and (-) with marked multi cloning site; Image taken from www.invitrogen.com

2.2.2 Restriction Enzymes

Restriction enzymes cut a DNA molecule specifically into two separate parts at a distinct base pair sequence producing either blunt (no overhang base pair) or sticky ends (overhang base pair). The map of pcDNA3.1 (**Figure 2-1**) shows the restriction sites present in the vector. The plasmid DNA can be digested with restriction enzymes and inserts with the complimentary overhang sequences can be introduced. The cutting sequence for all restriction enzymes used in these studies can be found in **Table 2-2**.

Table 2-2: Restriction Enzyme cutting sequences

Enzyme	Specific Sequence
KpnI	5′…GGTACC…3′ 3′…CCATGG…5′
BamHI	5′…GGATCC…3′ 3′…CCTAGG…5′
XhoI	5′…CTCGAG…3′ 3′…GAGCTC…5′
HindIII	5′…AAGCTT…3′ 3′…TTCGAA…5′
XbaI	5′…TCTAGA…3′ 3′…AGATCT…5′
DpnI (only cleaves when A methylated)	CH_3 5′…GA TC…3′ 3′…CT AG…5′ CH_3

2.2.3 Preparation of LB media

10 g of LB (Lysogeny broth) powder (Sigma Aldrich, Gilingham, UK) was added to 500 ml of double distilled water and autoclaved. LB media consists of 10 g/l Tryptone, 5 g/l Yeast Extract and 5 g/l NaCl.

2.2.4 Preparation of LB agar plates

7 g of LB agar (Sigma Aldrich, Gilingham, UK) was added to 200 ml of double distilled water and autoclaved. Each plate was prepared in Petri dishes (Thermo Scientific, Waltham, USA) using 20 ml LB agar in water with 50 µg/ml ampicillin (Sigma Aldrich, Gilingham, UK). The mixture was left to cool below 50°C after autoclaving to prevent inactivation of the antibiotic, then antibiotic was added and the mixture was poured still warm into the dishes to avoid solidifying before pouring. Dishes were then left to cool and solidify.

2.2.5 Transformation of E.coli cells

In order to transform *E. coli* cells, 25 µl of deep-frozen One Shot® TOP10 Chemically Competent *E. coli* cells (Invitrogen, Waltham, USA)

were thawed on ice (15 min) and mixed with the plasmid (1.5 µl – around 300 ng DNA for Minipreps less for mutations or ligations) by gentle stirring. Subsequently, the mixture was incubated for further 30 min on ice. The cells were heat shocked at 42°C for 30 seconds and again placed on ice for 3 min. Then, 250 µl of LB media was added to the cells and they were incubated at 37°C in the cell shaker at 220 rpm for 60 min. 200 µl of the liquid was plated out on LB ampicillin agar plates using a glass spreader and incubated overnight at 37°C. Colonies can be picked the next morning and transferred into LB media for further bacteria growth.

2.2.6 Plasmid DNA isolation

Plasmid DNA isolation was performed accordingly to the manual of the Maxiprep kit (GenElute™ HP Plasmid Maxiprep Kit, Sigma Aldrich, Gilingham, UK) or Miniprep kit (PureYield™ Plasmid Miniprep System, Promega, Southampton, UK) from transformed *E. coli* grown in different volumes of LB-medium overnight.

For a Miniprep purification constructs were grown overnight in 5 ml of LB media with 50 µg/ml ampicillin. Then, 1.5 ml of culture was centrifuged for 30 sec at 16,000 *g*. The supernatant was discarded and an additional 1.5 ml was centrifuged in the same way (3 ml total volume per pellet). The pellets of the overnight cultures were resuspended in 600 µl of double distilled water, then 100 µl of Cell Lysis Buffer was added and mixed by invertion of the tube in order to lyse bacteria. The alkaline lysate was neutralised by addition of 350 µl of neutralization solution resulting in a precipitate including cell debris, proteins, lipids, sodium dodecyl sulphate, and chromosomal DNA which was separated by centrifuging for 3 min at 16,000 *g*. The clear supernatant was transferred to a DNA column and loaded by centrifuging for 30 sec at 16,000 *g* and the flow through discarded. Subsequently, the column was washed in two steps with 200 µl of Endotoxin Removal Wash and then with 400 µl of Column Wash solution containing ethanol (centrifuging for 1 min at 16,000 *g*) in order to remove salt and protein contamination. The plasmid was

eluted by addition of elution buffer (10 mM Tris-HCl, 1 mM EDTA, pH approx. 8.0) and centrifuging for 15 sec at 16,000 *g*.

For a Maxiprep the different constructs transformed in competent *E. coli* cells were grown in 5 ml of LB-medium containing 50 µg/ml ampicillin during the day. They were then added overnight to a flask with 150 ml of LB-medium containing 50 µg/ml ampicillin and centrifuged the next morning for 10 min at 3,000 *g*. The pellets were then resuspended in 12 ml of Resuspension/RNase A solution, then 12 ml of lysis solution was added and mixed by inversion of the tube in order to produce a clear lysate. The alkaline lysate was neutralised by addition of 12 ml of neutralization solution resulting in a white precipitate which was separated by a filter syringes. The clear supernatant was loaded to a DNA silica column by centrifuging for 2 min at 3,000 *g* and the flow through discarded. Subsequently, the column was washed in two steps with 12 ml of Wash Solution 1 for endotoxin removal and Wash solution 2 containing ethanol or isopropanol (centrifuging for 3 or 5 min at 3,000 *g* respectively) in order to remove protein contamination. The plasmid was eluted by addition of 3 ml of 1x TE elution buffer or sterile deionized water and centrifuging for 5 min at 3,000 *g*.

2.2.7 Gel Electrophoresis

DNA products were analysed or purified via a 1% agarose gel prepared by adding 0.5 g of agarose (Sigma Aldrich Gilingham, UK) to 50 ml of 0.5x TBE (Tris/Borate/EDTA) buffer. The mixture was heated in a microwave until the solution was clear. The solution was allowed to cool for 5 min and subsequently 2 µl of ethidium bromide (Sigma Aldrich) was added. The mixture was poured into a mould and left for cooling. Meanwhile the samples were prepared by adding 5 µl of sample to 5 µl double distilled water and 2 µl of loading dye (0.4% orange G, 0.03% bromophenol blue, 0.03% xylene cyanol FF, 15% Ficoll® 400, 10mM Tris-HCl (pH 7.5) and 50mM EDTA (pH 8.0) - Promega, Southampton, UK) for analysis or 40 µl of sample with 7 µl

of loading dye for purification. Gels were run for 40 min at 100 V or 60 min at 90 V respectively. As a reference, 10 µl of a 1kB DNA ladder (Promega) diluted 1:1 with double distilled water was loaded to every gel.

2.2.8 Polymerase Chain Reaction

The Polymerase Chain Reaction (PCR) (Mülhardt, 2009) is a widely used technique for DNA amplification. The PCR thermocycler runs cycles of alternate temperatures leading to denaturation (**Figure 2-2** – Step 1), annealing (**Figure 2-2** –Step 2) and elongation (**Figure 2-2** – Step 3) of the DNA. 30 cycles were used for a PCR reaction with 1 min at 95°C for denaturation, 1 min at 60°C – 70°C for annealing and 3 min at 72°C for elongation. The annealing step was run as a gradient along the PCR thermocycler (Eppendorf, Stevenage, UK), one PCR tube always had the same annealing temperature but PCR tubes at another position in the machine had a different temperature.

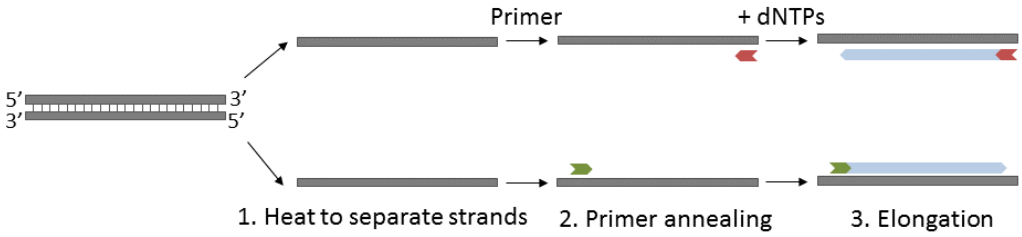

Figure 2-2: First cycle of a PCR reaction.

In order to amplify DNA, double distilled water was added to a PCR tube (Eppendorf, Hamburg, Germany) to add up to a total volume of 50 µl with 100 ng of plasmid DNA, 1 µl of 20 µM forward and reverse primer (Sigma Aldrich, Gillingham, UK), 5 µl of 1 mM dNTPs (dATP, dCTP, dGTP and dTTP each at 1mM in water), 1 µl of Pfu DNA Polymerase and 5 µl of Polymerase Buffer (all Promega, Southampton, UK).

2.2.9 Mutation of DNA

It is also possible to use the PCR thermocycler to mutate different base pairs within the DNA by the right choice of primers. For

mutations a complementary forward and reverse primer of the same sequence region are added to the starting DNA. The base pairs that will be mutated are placed at the centre of the primers with about 15 base pair with a high GC (guanine-cytosine) content on each side. In order to mutate the DNA of interest 50 ng of plasmid was added to a PCR tube with 5 µl reaction buffer, 1.3 µl of 10 µM forward and reverse primer, 2 µl of 1 mM dNTP solution, 1 µl Pfu DNA Polymerase and double distilled water for a total volume of 50 µl.

The mutation was performed in 15 cycles, with 30 sec at 95°C for denaturation, 2 min at 60°C – 70°C for annealing and 8 min at 68°C for elongation. The annealing step was run as a gradient along the PCR machine.

Subsequently, the parental DNA of the PCR was digested with the addition of 1 µl of DpnI to each tube for 1 h at 37°C. The product was then transformed into *E. coli* and plated on Agar plates as described before. DpnI only digests DNA that has been methylated at its recognition site (**Table 2-2**). DNA that is synthesised by bacteria is methylated while DNA generated in a PCR machine is not, resulting in DpnI selectively digesting the parental DNA instead of the newly generated mutated DNA.

2.2.10 TA Cloning

In order to insert a PCR product into its desired vector, the insert and vector have to be digested with two restriction enzyme suitable for the chosen vector. These restriction sites are introduced to the end of the insert with the primers of the PCR. Often, the direct digestion after a PCR fails as the restriction enzyme has to cut very close to the end of the insert (~ 5 base pairs) and is not able to interact with the DNA strand. This problem can be avoided by TA Cloning. The polymerase used for TA cloning is Taq-Polymerase, which adds an extra deoxyadenosine (A) to the 3’ end of the PCR product (**Figure 2-3**). This PCR product can then be ligated into a vector with overhang deoxythimodine (T). In the following step the insert can be digested

more easily placed within the TA cloning vector with the restriction enzymes suitable for the desired final vector.

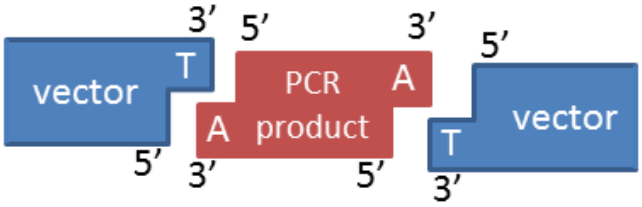

Figure 2-3: TA Cloning. Schematic representation of TA Cloning; vector with overhang T represented in blue and insert with overhang A in red

For TA cloning the PCR was performed as described before using a proofreading Pfu Polymerase. Subsequently the PCR product was purified using a gel electrophoresis, then 7 µl of this purified PCR product was added to 1 µl Taq DNA Polymerase Buffer, 0.2 mM dATP, 1 µl of Taq DNA Polymerase (Promega, Southampton, UK) and double distilled water to a total volume of 10 µl. This mixture was incubated for 20 min at 70°C. The insert was purified again via gel purification and subsequently ligated into a pcDNA2.1 vector using an Express T4 Ligase provided with the TA cloning kit (Invitrogen, Waltham, USA) as described below.

2.2.11 Cloning of DNA inserts into vectors

In order to prepare a DNA construct two cloning steps were needed. Firstly the cloning of the insert into the pcDNA2.1 TA cloning vector and then the second cloning into the final vector.

The inserts were prepared via PCR and visualized on a gel as described before. Positive PCR products were then ligated into the TA cloning vector pcDNA2.1 by adding 2 µl of 5x ligase buffer, 2 µl pcDNA2.1 vector, 1 µl of purified PCR product, 1 µl of ExpressLink™ T4 DNA Ligase and 4 µl of double distilled water (final volume 10 µl) and ligation performed for 15 min at RT. Subsequently, the ligation product was transformed into competent *E. coli* cells and prepared according to the miniprep protocol described before.

TA clones and empty pcDNA3.1 (Invitrogen, Waltham, USA) or pcDNA3.1 with NanoLuc (Promega, Southampton, UK) or SNAP tags (New England BioLabs, Ipswich, USA) were then digested for 2 h at 37°C with the appropriate restriction enzymes (all Promega) by adding 2 µl of TA clone or vector to 1 µl of each enzyme, 4 µl of the appropriate buffer (**Table 2-3**) and 32 µl of double distilled water.

Table 2-3: Appropriate Promega buffer choice for different enzyme combinations showing the cutting efficiency as a percentage of its highest performance

Enzyme	Buffer A	Buffer B	Buffer C	Buffer D	Buffer E	Buffer H
BamHI	75	75	75	50	100	50
XhoI	25	75	75	100	25	100
XbaI	50	75	75	100	100	100
HindIII	25	100	75	10	100	25

The digested products (inserts and vectors) were purified on a gel prepared as described before. The relevant bands were cut out of the gel and purified according to the GenElute™ Gel Extraction Kit (Sigma Aldrich, Gilingham, UK).

For ligation of the inserts and vectors 1 µl of T4 ligase was added to 1 µl of ligase buffer, 100 ng of vector and 120 ng of insert in a total volume of 10 µl. The mixture was ligated for 16 h at 16°C using a T4 DNA Ligase (Promega, Southampton, UK) and subsequently transformed into competent *E. coli*, plated and miniprep prepared according to the protocol before.

2.2.12 Sequencing

Sequencing was performed by the DNA sequencing laboratory at the School of Life Sciences, University of Nottingham. For sequencing DNA at a concentration of 100 ng/µl was provided and for pcDNA3.1 a T7 forward primer and a BGH reverse primer were used. TA clones in pcDNA2.1 were sequenced using M13 forward and reverse primers.

2.3 Cell culture

Cells used during this project were Human embryonic kidney 293-Glosensor™ (HEK293G; Promega, Southampton, UK) cells transfected with various constructs as described below. HEK293G cells stably express a biosensor based on a firefly luciferase activated in the simultaneous presence of GloSensor reagent and cAMP. In some experiments membranes made from these cells were used. For experiments performed in Carsten Hoffmann's group HEK293T (HEK293 cells transfected with a temperature sensitive mutated version of the Simian Vacuolating Virus 40 large T antigen) cells were used.

2.3.1 Passaging of cells

All cells were maintained in Dulbecco's modified Eagle's medium (DMEM/ Sigma Aldrich, Gilingham, UK) with addition of 10% Foetal Calf Serum (FCS, Sigma Aldrich, Gilingham, UK, complete DMEM) and incubated at 37°C in 5% CO_2. For the passaging of cells the media was aspirated off the cells using a glass Pasteur pipette attached to a vacuum pump. Subsequently, the cells were washed with Dulbecco's phosphate buffered saline (PBS/ Sigma Aldrich, Gilingham, UK) and then detached from their flask with 1 ml trypsin/EDTA (0.5 g/l trypsin, 0.2 g/l EDTA, ThermoFisher Scientific, Loughborough, UK) which digests adhesion proteins or chelates divalent cations, e.g. Calcium, respectively. Cells were then transferred into 10 ml of media and centrifuged at 1,000 rpm for 4 minutes. The resulting cell pellet was resuspended in media and seeded into 96-well plates (Greiner Bio-One, Stonehouse, UK) or plates for imaging, either 36 mm MaTek dishes (Ashland, MA, USA) or Nunc™ Lab-tek™ 8 well plates (Sigma Aldrich, Gillingham, UK) for experiments. In order to maintain a cell line cells were placed into a new T75 tissue culture flasks (ThermoFisher Scientific, Loughborough, UK).

2.3.2 Freezing of cells

Cells were frozen using a freezing mix consisting of 90 vol% FCS and 10 vol% DMSO (both Sigma Aldrich, Gilingham, UK) sterilised with a

0.2 µm syringe filter (Merck, Darmstadt, Germany). Cells were detached from T75 flasks as described above and collected by centrifugation. The cells were then resuspended in 2 ml freezing mix by gentle trituration of the freezing mix and 1 ml was put in each cryovial (ThermoFisher Scientific, Loughborough, UK). The cells were then slowly frozen at -80°C in an isopropanol insulated container which ensures a decreasing temperature of -1°C per minute. The cells were transferred to liquid nitrogen after 24 hours.

2.3.3 Defrosting of cells

Cells were rapidly defrosted at RT and then added to 10 ml of media. They were centrifuged for 4 min at 1,000 g to separate the freezing media from them and subsequently resuspended in 1 ml fresh media by trituration and placed in a T75 flask containing 20 ml of complete DMEM.

2.3.4 Generation of stable cell lines

Human embryonic kidney 293 (HEK293)-Glosensor™ (Promega, Southampton, UK) cells stably expressing human CXCR4 receptor (Cisbio, Codolet, France) containing an N-terminal SNAP-tag (Cisbio, Codolet, France) were created previously by Dr. Joëlle Goulding (Cell Signalling, University of Nottingham). All other stable cell lines were made during the project using the same native HEK293G cells as host. cDNA constructs were prepared as described in results **3.1 Preparation of DNA constructs**.

Native HEK293G cells were grown in complete DMEM in a T25 flask (ThermoFisher Scientific, Loughborough, UK) and transfected when 70 - 80% confluent. 26 µl of FuGENE® HD reagent (Promega, Southampton, UK) was added to a total volume of 414 µl of OptiMEM (ThermoFisher Scientific, Loughborough, UK) with 8.8 µg of DNA and incubated for 5 - 10 min at RT. Subsequently, the transfection mixture was added to the cells for 24 h. The transfection media was then replaced with media containing 1 mg/ml of the antibiotic geneticin (G418). Media was changed every two days until cell death had

plateaued, then the antibiotic concentration was lowered to 0.5 mg/ml. Cells were allowed to reach confluency and frozen.

These mixed population cell lines can be dilution cloned. Cells grown in complete DMEM in a T75 flask were trypsinised with 1 ml of trypsin/EDTA and centrifuged for 4 min at 1,000 g, the resulting cell pellet was diluted in 20 ml of complete DMEM. Cells were counted and diluted further to 0.25, 0.5, 1, 2 or 3 cells per 100 µl. For each dilution half of a 96-well plate was plated with 100 µl of cell suspension per well. After 48h all wells were checked for single colonies. Once identified, they were allowed to reach 50 % confluency then moved to a 24 well plate until 50% confluent and subsequently to a T25 flasks and frozen for later screening.

2.3.5 Generation of transiently transfected cells

Native HEK293G cells were plated at 10,000 cells/well into 96-well plates and incubated at 37 °C and 5% CO_2 overnight. For 10 wells 50 µl of transfection mix were prepared composed of 1.8 µl FuGENE® HD reagent and 10 ng/µl final concentration DNA and OptiMEM as medium. 5 µl of transfection mix were added to each well for 24h at 37 °C and 5% CO_2 before performing assays with the cells.

2.3.6 Preparation of cell membranes

Membranes were made from cells grown in complete DMEM in 500 cm^2 square trays (Corning 431110; NY, USA). Once the cells reached confluency the media was discarded and they were washed once with PBS. Subsequently, cells were scraped off the tray using a rubber spatula (manufactured for grouting tiles) with approximately 20 ml of PBS. The cells were spun down at 1500 rpm and then re-suspended in 15 ml of PBS. The cells were homogenised using an Ultra Turrax dispersing instrument which is a mechanical disruption device with rotating blades. Subsequently, unbroken cells were spun down at 1500 *g* for 20 min. The supernatant was transferred into an ultra-centrifuge tube and centrifuged at 41,415 *g* for 30 min. The resulting pellet was resuspended in 2 ml PBS and homogenised using

a motor driven pestle with a glass/Teflon homogenizer. The protein concentration was quantified using a BCA protein assay (ThermoFisher Scientific, Loughborough, UK) according to manufacturer's instructions.

2.4 Assays

For all experiments performed with poly-D-lysine coated 96 well plates, plates were coated by adding 50 µl/well of a 10 µg/ml poly-D-lysine (Sigma Aldrich, Gillingham, UK) solution in double distilled water. The plates were incubated for 45 min at RT and subsequently the liquid was aspirated. The plates were then washed with media for direct use or with PBS and stored for later.

All experiments were performed using Hanks' Balanced Salt Solution (HBSS) as a buffer system with addition of 0.2% BSA (Bovine Serum Albumin - Sigma Aldrich, Gillingham, UK). HBSS was composed of 2 mM Sodium Pyruvate, 145 mM NaCl, 10 mM D-Glucose, 5 mM KCl, 1 mM $MgSO_4 \cdot 7\ H_2O$, 10 mM HEPES, 1.3 mM $CaCl_2 \cdot 2\ H_2O$ and 1.5 mM $NaHCO_3$ at pH = 7.4.

2.4.1 NanoLuc assay

NanoLuc® (Nluc) is a genetically engineered natural luciferase isolated from deep sea shrimp. It is a relatively small luciferase (19kDa) that can be expressed on the N- or C-terminus of GPCRs and transported efficiently to the cell membrane (Hall *et al.*, 2012; Stoddart *et al.*, 2015).

The oxidation of furimazine (luciferin) is catalysed by the luciferase NanoLuc (**Figure 2-4**) resulting in an emission of light with a peak of 460 nm (Hall *et al.*, 2012).

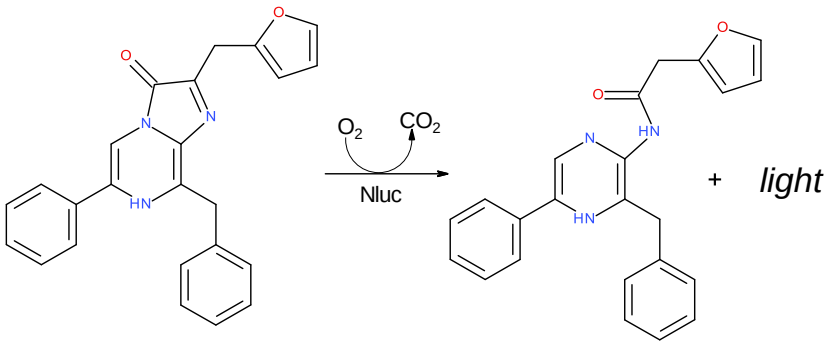

Figure 2-4: Reaction of furimazine with NanoLuc in the presence of oxygen.

A fluorescent ligand binding to the receptor and therefore being in close proximity to the Nluc-tag (<10 nm) can be excited by the light emitted by the oxidation of furimazine and emit light at a different wavelength (**Figure 2-5 step 1**). In order to measure the amount of non-specific emission or the influence of a ligand on the binding of the fluorescent compound the BRET transfer can be blocked by addition of unlabelled competing ligand causing the release of the bound fluorescent compound (**Figure 2-5 step 2**).

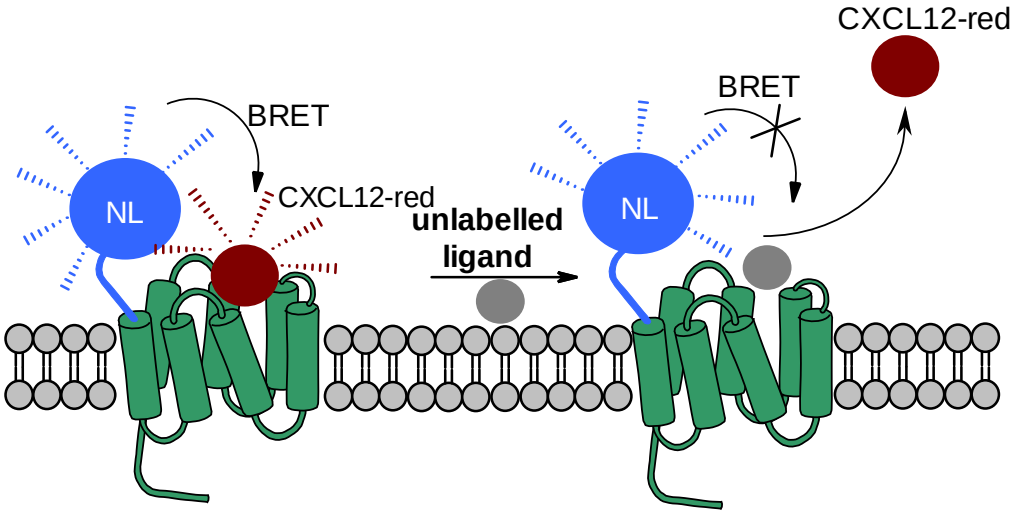

Figure 2-5: NanoBRET proximety assay. Schematic representation of NanoLuc binding assay; left side showing the BRET transfer between a NanoLuc tagged receptor and CXCL12-red; right side showing the displacement of CXCL12-red by an unlabelled compound that is not excited by the emitted light from the NanoLuc-tag

2.4.1.1 Saturation binding between a NanoLuc tagged receptor and a fluorescent ligand

HEK293G cells, stably transfected with Nluc tagged CXCR4 or ACKR3, were seeded into Poly-D-Lysine coated white clear bottom 96-well plates (Greiner Bio-One, Stonehouse, UK) 48h prior to the experiment (10,000 cells per well). On the day of the experiment the media was removed from the cells and 25 µl of HBSS buffer or HBSS containing unlabelled competing ligand was added. Subsequently, 25 µl of increasing concentrations of fluorescent ligand (CXCL12-red, CXCL12-green, SD44 or ATI-2341f) were added at 2x final concentration.

Alternatively, the saturation binding of fluorescent ligands was measured in membranes. Membranes were prepared as described in **2.3.6 Preparation of cell membranes**. 10,000 ng of protein were added to each well in 20 µl of PBS/HBSS buffer. Then 10 µl of HBSS (pH = 7.4) buffer or HBSS buffer containing unlabelled competing ligand were added as well as 20 µl of increasing concentration of fluorescent ligand.

The plate was covered with aluminium foil and incubated for 1.5 h at 37°C (no CO_2). Then, the Nluc substrate furimazine (Promega, Southampton, UK) was added to a final dilution of 1 : 400 (12.5 µM). The luminescence and fluorescence was then read on a PHERAstar FS plate reader (BMG Labtech) at RT. The raw BRET ratio was calculated by dividing the >610-nm emission (for red ligands), the >550-nm emission (for TAMRA tagged ligands) or the 535 nm emission (for green ligands) by the 460-nm emission (Nluc) (Stoddart *et al.*, 2015).

For kinetic experiments, furimazine was added in a final 1 : 200 dilution (25 µM) before any fluorescent ligand was added and incubated for 5 min in the PHERAstar at 37°C, the fluorescent ligand was then added and the NanoLuc and fluorophore emissions were monitored every minute for 1.5h.

Specific binding was defined by subtracting the raw BRET ratio of wells measuring the non-specific binding (wells containing fluorescent ligand and high concentrations of unlabelled competing ligand) from

the raw BRET ratio of wells measuring the total binding (wells only containing fluorescent ligand and buffer).

2.4.1.2 Competition binding between a fluorescent ligand and an unlabelled ligand targeting the same receptor

Competition assays were performed in cells or membranes prepared in the same way as for the saturation binding assays.

For cells, the media was removed and 25 µl of HBSS buffer or HBSS containing increasing concentrations of unlabelled compound were added. Subsequently, 25 µl of one concentration of fluorescent ligand was added.

For membranes, 10 µl of HBSS buffer containing increasing amounts of unlabelled ligand were added to the 20 µl membrane mixture as well as 20 µl of one concentration of fluorescent ligand.

The plates were covered with aluminium foil and left for incubation for 2h at 37°C (no CO_2). Furimazine (12.5 µM) was added and the plate read as described before for saturation binding assays (Stoddart *et al.*, 2015).

2.4.1.3 Receptor Dimerisation

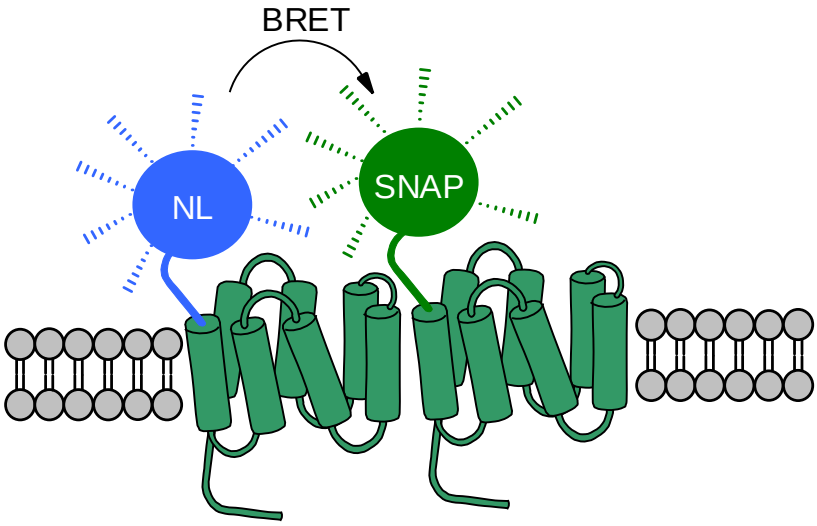

Figure 2-6: Receptor Dimerization. Schematic representation of the measurement of receptor dimerization – NanoLuc-tag luminescence transfer to AF488 labelled SNAP-tag

Dimerisation of receptors was studied in HEK293G cells which were transiently transfected with 50 ng/well Nluc- and increasing SNAP-tagged receptor as described in **2.3 Cell Culture**.

The medium was aspirated and cells incubated for 30 min at 37°C and 5% CO_2 in 100 µl/well complete DMEM containing 0.1 µM Cell surface SNAP Alexa Fluor 488 (Sigma Aldrich, Gillingham, UK). Subsequently, the media was removed and the cells were washed twice with HBSS buffer containing 0.2% BSA. 100 µl of HBSS buffer with 0.2% BSA was added for 1h at 37°C.

Then, the Nluc substrate furimazine was added to a final concentration of 12.5 µM. The luminescence and fluorescence was read on the PHERAstar FS plate reader (BMG Labtech) at RT. The raw BRET ratio is calculated by dividing the 535 nm emission (SNAP) by the 460-nm emission (Nluc).

For experiments investigating the change in dimers upon ligand treatment, cells were transfected with 50 ng/well Nluc- and 25 ng/well SNAP-tagged CXCR4, labelled and washed as described above. Then, the change in BRET ratio was monitored after the addition of furimazine and using the same filter set as above for 90 min every 6

seconds. After 5 initial cycles, 5 µl of either HBSS buffer or compound was added to the cells.

In order to quantify the amount of SNAP labelling in cells, cells were fixed, Höchst stained and visualized on the IX Micro Widefield Plate reader. The intensity of SNAP labelling was analysed with the MetaXpress 5.0 software using the multiwavelength cell scoring algorithm. The resulting integrated intensity values are a measure for the amount of SNAP-labelling in each site. This was done as a control to determine that transfection with more DNA leads to the expression of more receptor.

2.4.2 LDH Cytotoxicity Assay

In order to investigate whether high concentrations of pepducins cause cell membrane damage the amount of lactate hydrogenase (LDH) in media, which is only present in the buffer following cell damage, was measured using the Thermo Scientific™ Pierce™ LDH Cytotoxicity Assay Kit (Korzeniewski and Callewaert, 1983; Decker and Lohmann-Matthes, 1988).

Cells were seeded at 30,000 cells/well into clear 96-well plates 24h before the experiment and kept at 37 °C and 5% CO_2 overnight. On the following day increasing concentrations of pepducin were added to the cells for 2h at 37 °C and 5% CO_2. As a control, for the maximal LDH concentration, cells were lysed using the lysis buffer from the kit. 50 µl of media were than taken from each well and transferred into a flat bottom 96-well plate to which 50 µl of Reaction mix were added for 30 min at RT in which formazan dies are produced as shown in **Figure 2-7**. Subsequently, 50 µl Stop Solution was added and the absorbance of each well was measured at 490 nm and 680 nm using a CLARIOstar (BMG Labtech).

LDH catalyses the conversion of lactate to pyruvate in the presence of NAD^+. The Reaction Mix further contains colourless Iodonitrotetrazolium (INT) which reacts with the NADH produced resulting in the formation of violet iodonitrotetrazolium formazan

which can be quantified via the absorbance of the solution at 490 nm. The measurement at 680 nm serves as a control for the background signal from the plate reader.

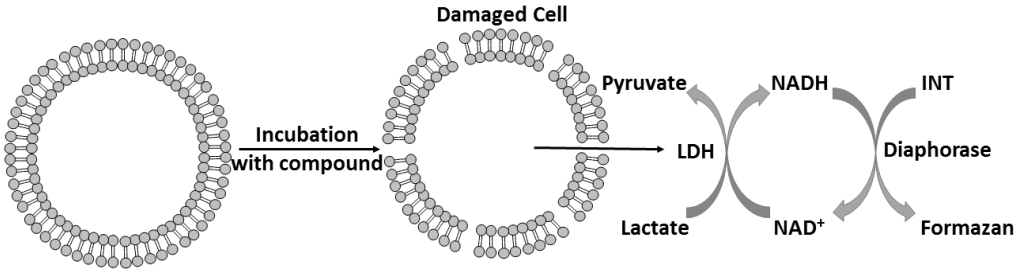

Figure 2-7: Schematic representation of LDH cytotoxicity assay.

2.4.3 G protein activation assay

This assay was performed in Carsten Hoffmann's group at the Julius-Maximilians-Universität Würzburg in cooperation with Cristina Perpiñá Viciano.

HEK293T cells (Martine Smit, Vrije Universiteit Amsterdam) were split into 10 cm round dishes and transiently transfected the following day at 60% confluency with 1.4 µg of untagged CXCR4 in $pcDEF_3$ and 3 µg of a FRET-based G protein sensor ($G\alpha_{i1}$, $G\alpha_{i2}$, $G\alpha_{i3}$ or G_q) in which all subdomains are on one vector. Upon activation of the G protein its α and βγ subdomains move apart resulting in a decreasing FRET signal between the Venus (on $ß_1$) and mTurquoise (on Gα) tags of the G protein subunits (Adjobo-Hermans *et al.*, 2011; Van Unen *et al.*, 2016; Adlere *et al.*, 2019). The following day, the cells were seeded into 96-well plates with 30,000 cells/well and kept at 37°C and 7% CO_2 overnight. Cells were excited using a 420/50 nm filter (420 ± 25 nm, 420 centre value and 50 nm bandpass, Biotek CFP-YFP filter; 1035013) and the FRET ratio was then calculated from measurements at 485/20 and 540/25 nm (Biotek CFP-YFP filter; 1035043) monitored on a Synergy Neo2 Multi-Mode Microplate Reader (Biotek) using the Gen5™ Data Analysis software. Fluorescence of the cells were measured at 37°C for an initial 5 min before adding different CXCR4 ligands or buffer to the wells and reading for another 20 min.

2.4.4 cAMP Assay

The GloSensor™ cAMP assay (Promega, Southampton, UK) monitors the changes in concentration of the intracellular second messenger cyclic 3'5'-adenosine monophosphate (cAMP). cAMP binds to a genetically encoded biosensor that consists of a split form of *Photinus pyralis* luciferase (firefly luciferse) fused to a cAMP binding domain B of protein kinase A (RIIβB) that is stably expressed by the HEK293G cells. The luciferase is split into two parts. In response to cAMP and GloSensor reagent binding a conformational change occurs which reconstitutes the luciferase enzyme and leads to bioluminescence (**Figure 2-8**). This change in bioluminescence is directly proportional to the amount of cAMP present between cAMP concentrations of 10 nM up to 10 µM and can be monitored in real-time on a luminescence plate reader (Wood *et al.*, 2008; Binkowski *et al.*, 2011; Goulding *et al.*, 2018).

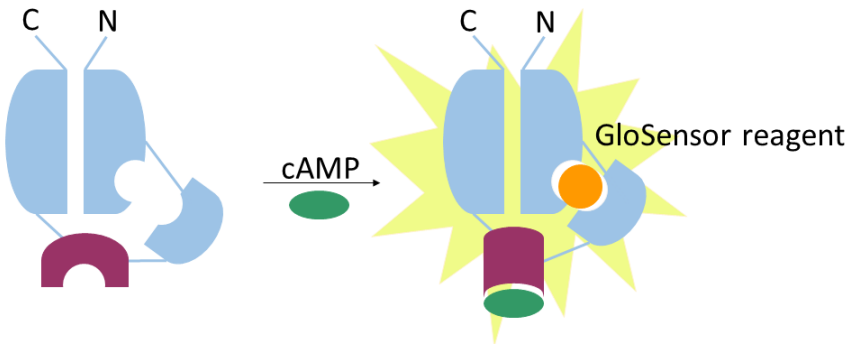

Figure 2-8: cAMP biosensor. Schematic representation of cAMP binding to biosensor fused to mutated Photinus pyralis luciferase occurring in GloSensor assay (Binkowski *et al.*, 2011)

The studies allow the investigation of $G\alpha_i$-coupled receptor activation or inverse agonist activity. In the assay forskolin (FSK, Tocris biosience, Bristol, UK) is added in order to activate adenylyl cyclase which produces cAMP from adenosine triphosphate (ATP). This production can be inhibited by CXCL12 activated CXCR4 and might be inhibited by the activation of ATI-2341 or other pepducins (**Figure 2-9**).

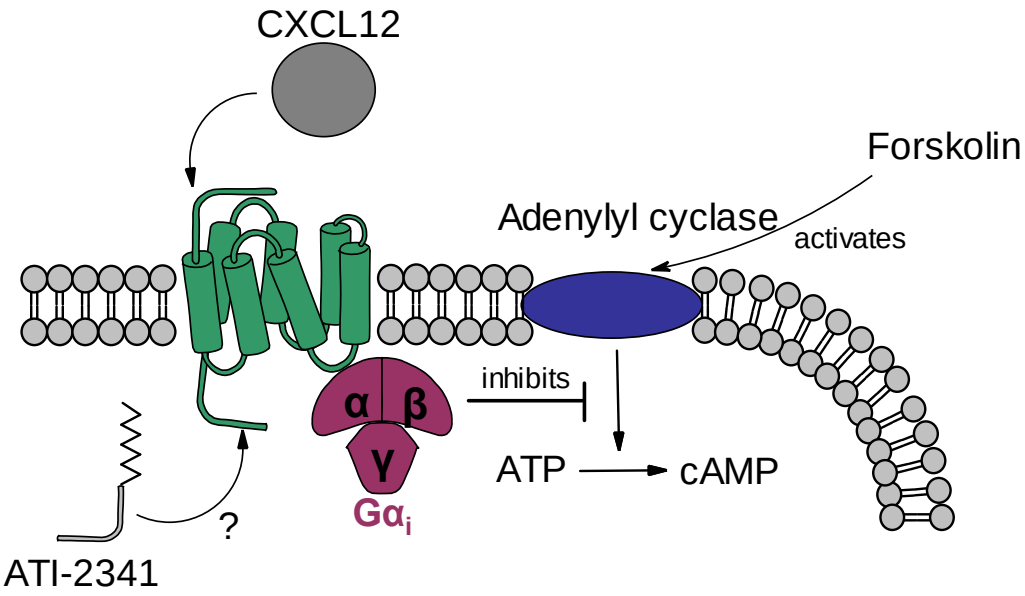

Figure 2-9: cAMP assay. Mechanistic representation of cAMP assay, CXCR4 is coupled to a $G_{\alpha i}$ unit after activation by the endogenous ligand CXCL12 and can inhibit FSK mediated cAMP production by adenylyl cyclase.

100,000 cells/well were seeded into white poly-D-lysine coated 96-well plates (Greiner Bio-One, Stonehouse, UK) to reach a high confluency at the next day and placed overnight into an incubator at 37°C and 5% CO_2.

When the cells reached a confluency of over 90% they were incubated for 2 hours at 37°C in HBSS buffer containing 0.2% BSA and 0.4 mg/ml GloSensor cAMP reagent (Promega, Southampton). Then, different compounds were added at the same time as 30 µM FSK. Luminescence was detected every 90 seconds with an EnVision® luminescence reader (PerkinElmer) for a 1 h time course at 37°C collecting emission from 400 – 700 nm. We later moved to a PHERAstar FS plate reader (BMG Labtech) using the same timings and collecting all luminescence (no filter).

2.4.5 β-arrestin recruitment assay

HEK293G cells were transiently transfected with 25 ng/well CXCR4-NanoLuc (C-terminal tag) and 10 ng/well VENUS/β-arrestin2 (White *et al.*, 2017) provided by Dr. Carl White (Harry Perkins Institute of

Medical Research, Australia) as previously described in **2.3 Cell culture**. VENUS is a yellow GFP variant first published in 2002 (Nagai *et al.*, 2002).

After 24h, cells were incubated at 37 °C for 30 min in HBSS containing 0.2% BSA. Afterwards, furimazine was added to a final concentration of 25 µM and the plate was read after 5 min for 5 cycles prior to adding compounds. Compounds were added and the recruitment of β-arrestin2 was monitored for 60 min every 28 seconds using a PHERAstar FS plate reader (BMG Labtech) at 37 °C. The raw BRET ratio is calculated by dividing the 535 nm emission (VENUS) by the 460-nm emission (Nluc).

2.5 Microscopic Techniques

2.5.1 SNAP-Label

Cell lines expressing CXCR4 fused with the SNAP-tag were generated and used in most techniques where CXCR4 was imaged. The SNAP-tag is a 19.4 kDa big protein based on the DNA repair enzyme, human O^6-alkylguanine-DNA-alkyltransferase and can be labelled covalently with O^6-benzylguanine derivatives (Cole, 2013). A thioether bond is formed between a reactive cysteine of the protein and the fluorescent dye (**Figure 2-10**). The SNAP-tag can be fused to the N- or C-terminal end of a protein without affecting its function (Keppler *et al.*, 2004; Srikun *et al.*, 2010). The advantage of the SNAP-tag is that it is a very specific label only labelling the target protein in a quantitative manner. Moreover there are multiple options in the colour and cell permeability of the fluorescent label (Cole, 2013).

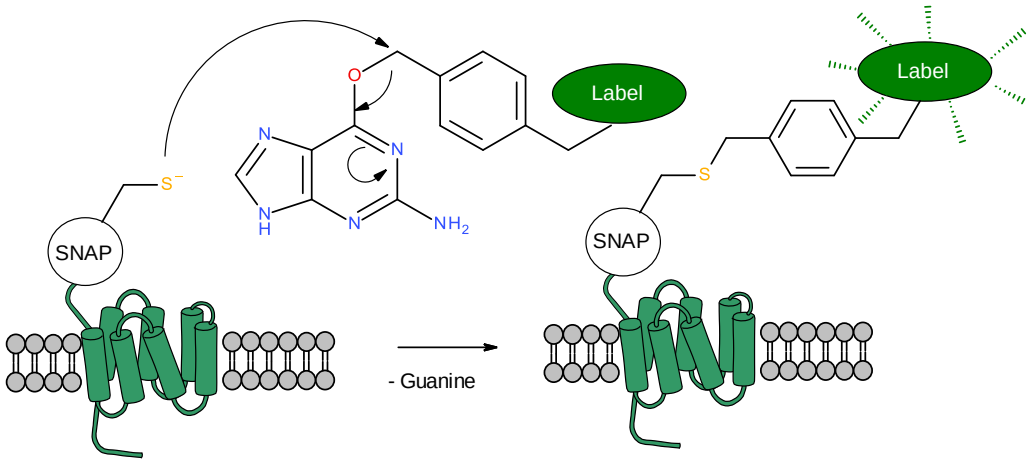

Figure 2-10: SNAP-labelling. A GPCR is fused to the SNAP-tag. The reaction of the SNAP-tag with O^6-benzylguanine (BG) derivatives results in the covalent attachment of the label to the active site cysteine

2.5.2 Internalisation Assay

In this internalisation assay the internalisation of SNAP labelled CXCR4 receptor was monitored in cells on a confocal plate reader in response to incubation with agonist and antagonists. Internalisation is the process of removal of the receptor from the cell surface due to continued stimulation (Dar *et al.*, 2005; Kilpatrick *et al.*, 2012; Magalhaes *et al.*, 2012).

The cells were grown to 70 % confluency on the inner 60 wells of a black Poly-D-Lysine coated 96-well plate (Greiner Bio-One, Stonehouse, UK). Subsequently, the medium was aspirated and cells incubated for 30 min at 37°C and 5% CO_2 in 100 µl complete DMEM containing 0.1 µM Cell surface SNAP Alexa Fluor 488 (NEB, Ipswich, MA, USA). The media was removed and the cells were washed once with HBSS buffer containing 0.2% BSA. If appropriate for the experiment, 100 µl of HBSS buffer with 0.2% BSA containing antagonists were added for 60 min at 37°C and then aspirated. Subsequently, 100 µl of HBSS buffer with 0.2% BSA and 5 µg/ml fluorescently labelled transferrin (568 nm, Invitrogen, Waltham, USA) was added to each well and at the same time 100 µl of HBSS buffer with 0.2% BSA with different agonist concentrations was added and incubated for 1 hour at 37°C. Afterwards the plates were washed with 100 µl HBSS per well and incubated in 100 µl of 4% paraformaldehyde

in PBS solution at RT for 15 minutes. The cells were washed with 100 µl PBS per well and 100 µl of a 0.1 mg/ml Höchst (H33342) stain (Sigma Aldrich, Gillingham, UK) in PBS was added per well for 15 min at RT. This was followed by a final washing step and the plate was stored overnight at 4°C in 100 µl PBS.

The plates were read on the ImageXpress Ultra-Confocal plate reader (Molecular Devices, Sunnyvale, USA) using a 40x Plan Fluor extra-long working distance (ELWD) objective with an NA of 0.6, a pinhole of 4 and using three detection channels: DAPI (405 nm, 30 % laser power), FITC (488 nm, 50 % laser power) and TexasRed (561 nm, 40 % laser power). Four central images with the size of 400 x 400 µm per well were acquired and analysed. Analysis was performed on MetaXpress 5.0 (Molecular Devices, Sunnyvale, USA) determining the average intensity of pixels co-localizing SNAP488 and transferrin (Kilpatrick *et al.*, 2012). Each plate was analysed individually, the minimum brightness value indicating a positive transferrin signal was set slightly higher than the plate background value and with the minimal and maximum area sizes indicated below. By this, a network of granules containing positive transferrin signals was built as seen in **Figure 2-11**. This network was then compared to the plane visualizing the tagged receptors. The brightness of SNAP label in the granules co-localizing SNAP and transferrin was analysed.

The analysis used the following settings:

Approximate width:	3 µm
Intensity above local background	(2,500)* to 30,000
Minimum area	10 μm^2
Maximum area	100 μm^2
Inner region distance in frame edge	0.5 µm

* varies from plate to plate

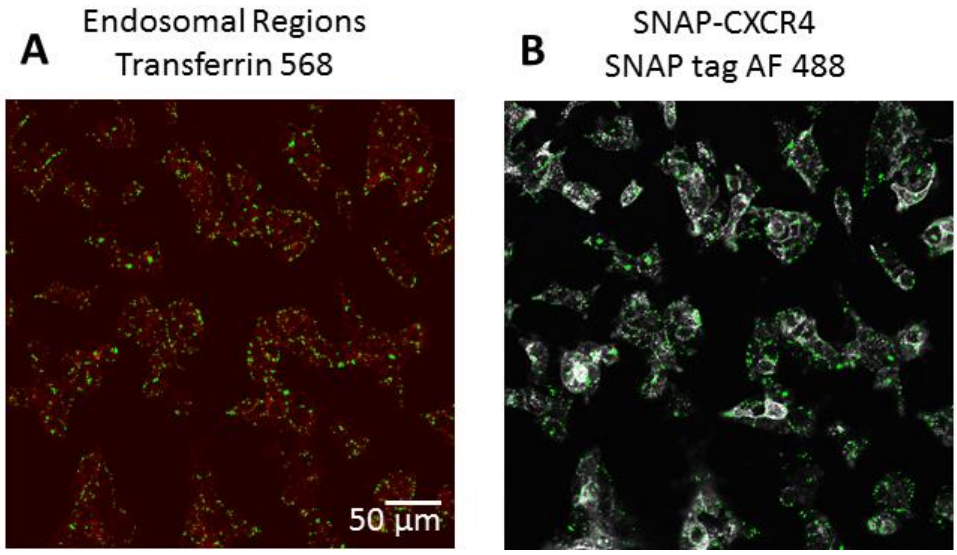

Figure 2-11: Analysis of Internalisation. (**A**) Network of granules containing transferrin with minimum brightness and size which is then used as a mask for (**B**) SNAP-tagged receptor and these are then analysed for their brightness

2.5.3 Single-Cell FRET Experiments

All single cell experiments were performed in Carsten Hoffmann's group at the Julius-Maximilians-Universität Würzburg in cooperation with Cristina Perpiñá Viciano (biosensor and method unpublished). Similar biosensors have been previously published for a number of receptors (Hoffmann *et al.*, 2005; Kauk and Hoffmann, 2018; Haider *et al.*, 2019).

HEK293T cells were seeded into poly-D-lysine coated 40 mm WillCo dishes (WillCo, Amsterdam, The Netherlands). 6h later, cells were transfected with 0.7 µg of 3HA-CXCR4-FlAsH228-CFP construct using Effectene (Qiagen, Hilden, Germany) according to the manufacturer's instructions. The media was changed after one day and experiments were performed 48h after transfection in measuring buffer (140 mM NaCl, 5.4 mM KCl, 2 mM $CaCl_2$, 1 mM $MgCl_2$, 10 mM HEPES, pH 7.3) plus 0.2% BSA.

The CXCR4 construct contains an N-terminal 3 HA tag, an internal cyan fluorescent protein on the C-terminal end (CFP) and a fluorescein arsenical hairpin (FlAsH) binder sequence. The sequence CCPGCC was introduced in the third intracellular loop between His228

and Ser229 and has to labeled prior to the experiment with FlAsH which is only fluorescent when bound to the amino acid sequence.

In the inactive receptor a laser can selectively excite the CFP tag and energy can be transferred via FRET from the CFP tag to the FlAsH tag. Upon activation of the receptor a conformational change will cause the CFP and FlAsH tag to move and will therefore cause a change in FRET (**Figure 2-12**). This change in FRET can be a decrease or increase dependent on the receptor.

In order to label cells with FlAsH, the transfected cells were washed twice with HBSS and then incubated at 37°C for with 500 nM FlAsH in HBSS containing 12.5 mM 1,2-ethanedithiol (EDT). After 1 h, cells were rinsed two more times with HBSS containing 0.2 % BSA, incubated for 10 min with HBSS containing 0.2 % BSA, 250 mM EDT and again rinsed twice with HBSS containing 0.2% BSA to reduce nonspecific labeling.

Single cell FRET measurements were performed on an inverted Zeiss Axiovert 200 microscope using an oil immersion 63x objective lens (NA=1.4) and a dual-emission photometric system (Till Photonics, Munich, Germany). A single cell was focused and excited at a 10 Hz frequency for 40 ms out of a total time of 100 ms with a polychrome IV (Till Photonics) in order to reduce photobleaching. Resulting emission of CFP (480 ± 20 nm) and FlAsH (535 ± 15 nm) were monitored at the same time and calculated into a FRET ratio. Emissions were detected with photodiodes, digitalized with an analogue-digital converter (Digidata 1440A, Axon Instruments, Union City, USA) and stored on Clompex 9.0 (Science Products GmbH).

During the measurements, cells were superfused with buffer, followed by a saturating concentration of CXCL12 or ATI-2341 using the Biopen® microfluidic pipette (Fluicell, Sweden). Kinetic profiles for a change in FRET ratio were monitored before and after addition of compound.

FRET ratios were calculated from the measured CFP and FlAsH responses. The acceptor emission (FlAsH) was corrected for bleed-through (from the donor) and direct excitation from the light source. FRET was normalized and corrected for photo-bleaching.

Data were analysed with Clampfit (Molecular Devices, Sunnyvale, USA) and then corrected and visualized with OriginPro 2016 (OriginLab Corporation, Northampton, MA) and GraphPad Prism version 6 (GraphPad Software, La Jolla, CA). The kinetics of receptor activation, reported as τ-values, upon ligand stimulation were determined by fitting the FRET change to a mono-exponential curve fit using Clampfit.

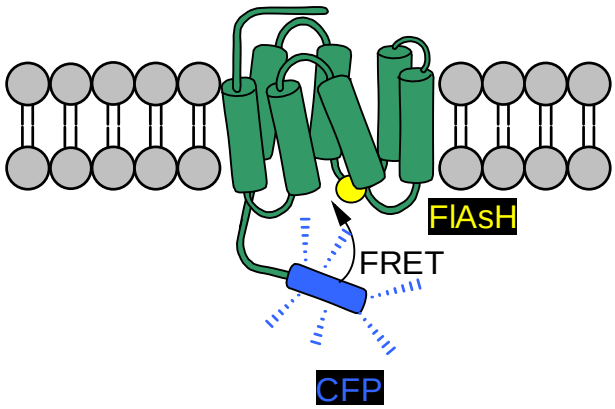

Figure 2-12: FRET biosensor. Schematic representation of the FRET biosensor with internal CFP on the C-terminal end of the receptor and a FlAsH binding sequence in the 3rd internal loop of CXCR4

2.5.4 Bioluminescence imaging

Cells were plated two days prior to the experiments in 36 mm MaTek dishes (Ashland, MA, USA) that are divided into 4 chambers at 20,000 cells/chamber and kept at 37 °C and 5% CO_2 for 48h in DMEM. The dishes were not coated with Poly-D-Lysine as the coating caused an increase in background luminescence.

On the day of the experiment the media was replaced with a total volume of 400 µl HBSS buffer and placed for 30 min into the heating chamber of the Olympus LV200 Wide field inverted microscope. ATI-2341f was added at 1 µM to one of the chambers for incubation

during the 30 min pre incubation period. Then, furimazine was added in 100 µl (final dilution 1 in 250, 20 µM) for 20 min before conducting experiments. Bioluminescence of the cells was recorded using a 60x oilimmersion objective with a 0.5 tube lens (1.42NA), a DAPI filter (414 - 462 nm, 5 sec exposure time) and the fluorescent ligand excited through the bioluminescence by the NanoLuc tag was monitored using the TAMRA filter (561 – 605 nm, 1 min exposure time). All images were acquired with gain set to 200 and an image size of 270 x 270 µm.

Regions of interest were drawn around the cells choosing the same regions for the Bioluminescence channel and the TAMRA channel analysing the Intensity with the Time Series Analyser V3 Plugin of Fiji ImageJ (Schindelin *et al.*, 2012). The brightness value from the TAMRA channel was divided by the NanoLuc emission giving a BRET ratio for each region of interest. If present, bright cells that reached detector saturation were excluded from this analysis. The observed BRET ratios were very reproducible from cell to cell within one experiment.

2.5.5 Confocal imaging

SNAP-CXCR4 HEK293G cells were imaged in Nunc™ Lab-tek™ 8 well plates (Sigma Aldrich, Gillingham, UK) or 36 mm MaTek dishes (Ashland, MA, USA) and seeded at a concentration of 30,000 or 80,000 cells per well respectively. After 2 days at 37°C and 5% CO_2 the cells were incubated for 30 min in 200 µl or 500 µl of 0.5 µM SNAP surface Alexa Fluor 488 tag in media at 37°C and 5% CO_2. Subsequently, the cells were washed 3 times with pre-warmed HBSS. A final volume of 200 µl or 500 µl HBSS in the presence and absence of antagonists was added for imaging.

Cells were imaged on a Zeiss 710 Confocal Microscope using a Zeiss 40 x 1.3 NA Plan-Fluar oil immersion lens (Zeiss, Cambridge, UK) using a pinhole of 1 Airy Unit (37 µm) to reduce any out of focus emission. Lasers used were the 488 nm argon laser (green) at 2.0%

power to visualize SNAP Alexa Fluor 488, the 633 nm HeNe laser (red) at 5.0% power for CXCL12-red and the 561 nm DPSS laser at 2.5% power for the TAMRA-tagged pepducin. Emission filters used were from 493 nm - 614 nm for the green channel 642 - 755 nm for the red channel and 566 – 685 nm for the TAMRA tag. Channels were recorded sequentially to allow for separation of each colour due to bleedtrough. The detector gain and offset were set with the built-in range indicator of the Zen 2012 software (Carl Zeiss, Jena, Germany). The stage was warmed during the experiments to 37°C.

2.6 Data Analysis

2.6.1 Statistical Analysis

All experiments were performed multiple times and the average value (eq. 1) was calculated in MS Excel by combining all individual values obtained from Graph Pad Prism 7.0 (GraphPad Software, La Jolla, CA, USA). For representation, figures show either one representative experiment or combined data.

$$\bar{x} = \frac{1}{n}\sum_{i=0}^{n} x_i \qquad \text{eq. 1}$$

$\bar{x}$ is the average value, x_i the individual value and n the number of experiments.

The data were normalised to control wells (GloSensor) or highest concentrations of agonists (internalisation, NanoBRET) which were set to 100%.

The Standard Error of the Mean (S.E.M) describes the precision of the mean. It is a measure of how far a sample mean is likely to be from the true average value (eq. 2). Where SEM is the standard error of the mean, SD the standard deviation, $\bar{x}$ is the average value, x_i is the individual value and N the sample size.

$$\mathrm{SEM} = \frac{\mathrm{SD}}{\sqrt{\mathrm{N}}} = \frac{\sqrt{\frac{1}{\mathrm{N}-1}\sum_{\mathrm{i}=1}^{\mathrm{N}}(\mathrm{x_i}-\bar{\mathrm{x}})^2}}{\sqrt{\mathrm{N}}}$$ eq. 2

The significant difference between two results was tested with a t-test using GraphPad Prism 7. The means of two groups of raw values obtained under different conditions were compared with an unpaired t test assuming a Gaussian distribution and non-equal SD values. The statistical significance was defined as $P < 0.05$.

If there were more than two groups of results to be compared an ANOVA (**An**alysis **o**f **Va**riance) test was used to analyse if the majority of the variance was in between the groups or within the group itself. This was followed by a Tukey's post hoc multiple comparison test. Statistical significance was again defined as $P < 0.05$.

2.6.2 Non-Linear regression with GraphPad Prism

All sigmoidal concentration response curves were fitted with the GraphPad Prism 7 option "log(agonist) vs response (3 parameters)". The equation sets a fixed Hill Slope of 1 and fits the data according to eq. 3. Where the top is given by the maximal response, the bottom by the basal response and the x value corresponds to the agonist concentration in log units (**Figure 2-13**).

$$\mathrm{f(x)} = \mathrm{Bottom} + \frac{(\mathrm{Top}-\mathrm{Bottom})}{1+10^{(\log \mathrm{EC_{50}}-\mathrm{x})}}$$ eq. 3

This can also be described in the more common equation 4. In which E_{max} is the maximal response of the system (Top-Bottom), [A] is the concentration of agonist used and EC_{50} is the concentration of agonist A that produces 50% of the maximal response.

$$\mathrm{Response} = \frac{E_{max} \times [A]}{[A]+\mathrm{EC_{50}}}$$ eq. 4

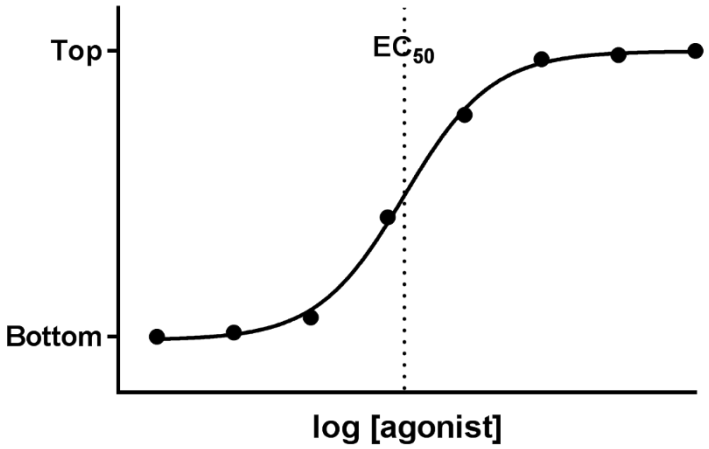

Figure 2-13: 3 parameter fit. Representation of GraphPad Prism fitted curve, 3 parameter log (agonist) vs response

2.6.3 Schild Analysis

In the case that an agonist and a reversible antagonist compete for the same binding site it is possible to characterise the affinity of the antagonist for the binding site by Schild analysis (Arunlakshana and Schild, 1959; Kenakin, 2014). Different concentrations of the antagonist were added to cells for at least 30 min before any agonist was added. The resulting concentration response curves show a shift of the agonist pEC_{50} value to lower potencies (**Figure 2-14**).

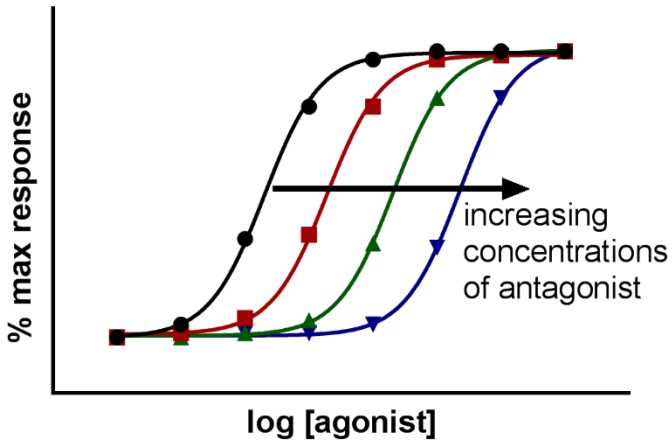

Figure 2-14: Schild analysis. Dose response curve of an agonist (black) antagonised by different concentrations of a competing agonist causing shifts of the response curves (Kenakin, 2014).

The affinity of the antagonist towards the receptor is described by a pK_b value (the negative logarithm of the equilibrium dissociation constant) which can be calculated from the shift of the agonist curve and the antagonist concentration (eq. 5). Where [A'] is the EC_{50} value with antagonist, [A] the EC_{50} value without antagonist, [B] the antagonist concentration and K_b the equilibrium dissociation constant for B, the antagonist.

$$\log\left(\frac{[\mathrm{A}']}{[\mathrm{A}]} - 1\right) = \log[\mathrm{B}] - \log(\mathrm{K_b}) \qquad \text{eq. 5}$$

If $\log\left(\frac{[A']}{[A]} - 1\right)$ is equal to 0 $\log[B]$ is equal to $\log(K_b)$. In order to find the value multiple concentrations of antagonist are measured and a linear regression is fitted through those (**Figure 2-15**). The pK_b value can then be found as the negative value of the x-intercept.

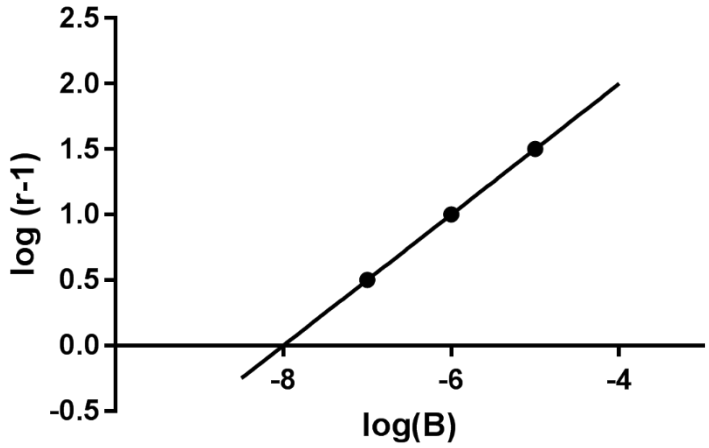

Figure 2-15: Schild plot. Determination of pK_b by linear regression of the values established by Schild Plot analysis

The Schild plot was fitted by GraphPad Prism 7 following the non-linear regression (eq. 3 and 4) from before with a variable Hill slop. The EC_{50} value, which is the concentration of agonist needed to produce 50% of the maximal response will shift with the presence of antagonist. The values are then plotted on a graph with the x-axis representing the antagonist concentration and the y-axis the change in EC_{50}-values and fitted with a simple liner regression. The Schild

slope should be 1 in the case of competitive binding and will vary in other binding modes.

2.6.4 Saturation binding

Saturation binding data obtained in the NanoBRET assay was fitted with GraphPad Prism fitting the specific and non-specific binding at the same time Figure **2-16**).

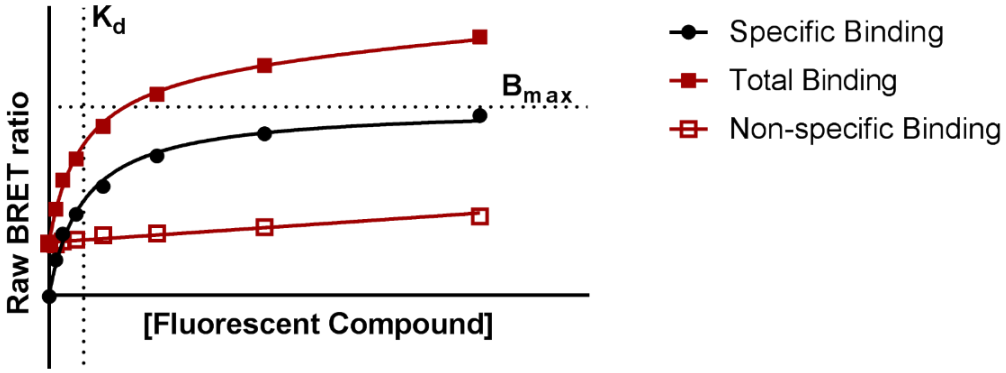

Figure 2-16: Saturation binding. Prism fit for specific and non-specific saturation binding simultaneously

Non-specific: $$y = mx + background$$ eq. 6

Specific: $$y = \frac{B_{max} * x}{x + K_d}$$ eq. 7

Total binding: $$y = \frac{B_{max} * x}{x + K_d} + (mx + background)$$ eq. 8

The non-specific binding was fitted with a linear-regression, m being the slope and "*background*" the y-intercept. The specific binding is fitted with B_{max} the maximum specific binding at high concentrations of ligand, K_d the equilibrium binding constant at which half of the receptors are occupied with the ligand.

2.6.5 K_i determination

The equilibrium dissociation constant K_i obtained from the competition of fluorescent CXCL12 in the NanoLuc assay was based on the measured IC_{50} value fitted with a normal non-linear regression, the concentration that inhibits half of the specific binding. The values were corrected (eq. 9) considering the used concentration [L] of CXCL12-red and the actual equilibrium binding constant K_d of the labelled ligand (eq. 3, 4 and 6 - 8).

Cheng-Prusoff equation:

$$K_i = \frac{IC_{50}}{1 + \frac{[L]}{K_D}} \qquad \text{eq. 9}$$

2.6.6 Fitting of Kinetic Data

Equations to analyse the binding of ligands were first described for radio ligand binding, but can also be used for our fluorescent ligands. These equations are based on the law's of mass action stating that the rate of a reaction is dependent on the concentration of the reagents, assuming one single interaction site (Kenakin, 2015). Based on these equations GraphPad Prism's fits the association for two or more ligand concentrations in a global fit in order to determine the equilibrium binding constant K_d of the compound (eq. 10, eq. 11 and **Figure 2-17**) with B_{max} the maximal signal observed with the added compound concentration, k_{on} the association rate constant, k_{off} the dissociation rate constant and $[Fluo_{nm}]$ the concentration of the fluorescent ligand in nM. The amount of non-specific binding was measured and subtracted from each curve by adding a displacing agent to the same amount of fluorescent compound.

Association: $y = B_{max} * (1 - e^{-1*((k_{on}*[Fluo_{nm}])+k_{off})*x})$ eq. 10

K_d: $K_d = \frac{k_{off}}{k_{on}}$ eq. 11

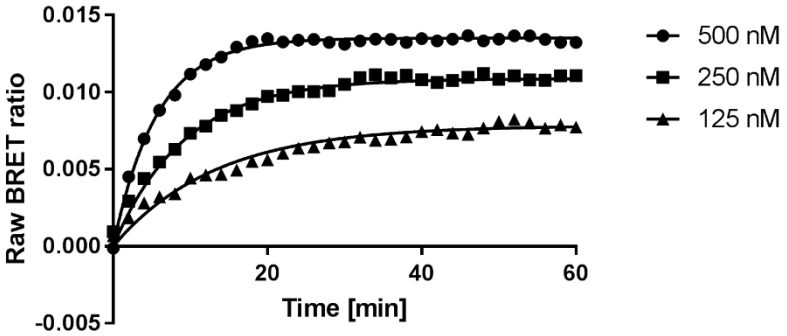

Figure 2-17: Kinetic binding. Prism fit for association kinetics for 2 or more fluorescent compound concentrations

In the case of addition of unlabelled compound an additional dissociation curve is fitted (eq. 12). In which t_0 marks the time of addition of unlabelled compound.

Association then Dissociation (eq. 12):

$$y = B_{max} * \frac{[Fluo_{nm}]}{[Fluo_{nm}] + K_d}\left(1 - e^{-1*([Fluo_{nm}]*k_{on})+k_{off})*t_0}\right) * e^{-1*k_{off}*(x-t_0)}$$

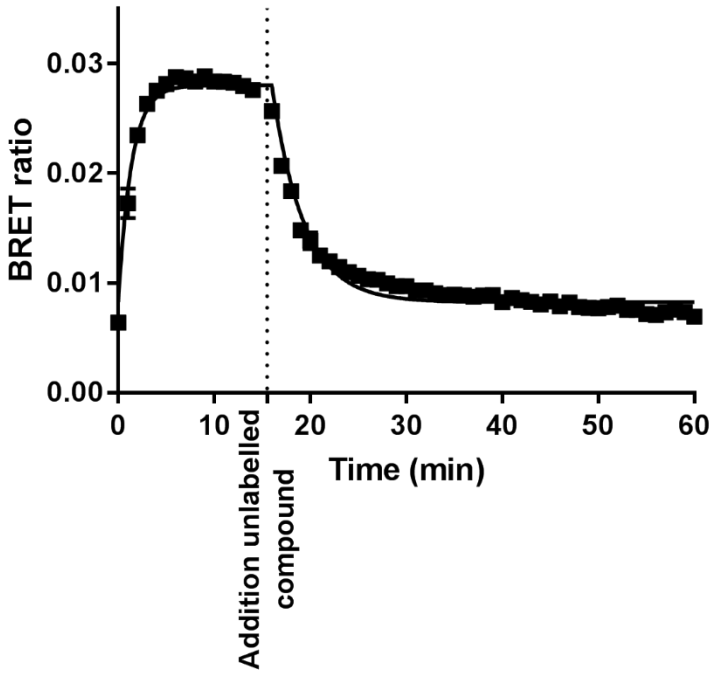

Figure 2-18: Prism fit for association and then dissociation kinetics for a fluorescent compound displaced by an unlabelled compound

Moreover, an "observed association rate constant" (k_{obs}) plot can be made from those kinetic association curves. In these plots, k_{obs} of one individual concentration which is equal to $k_{on}[Fluo_{nm}]+k_{off}$ and the concentration of the fluorophore are plotted against each other and should show a linear relationship with a positive slope if the kinetic association model fits for this receptor and ligand. k_{obs} of each individual concentration is calculated from a one component exponential fit (eq. 13) with B_{max} the maximal signal observed and K the rate constant which is equivalent to k_{obs} in our fits.

2.6.7 Fitting of Receptor activation

CXCR4 receptor activation measured with an intramolecular sensor and indicated by changes in FRET ratio were fitted using a one component exponential equation with B_{max} the maximal signal observed, K the rate constant which is reciprocal to τ. Moreover, ATI-2341 showed delays in its response. This latency was determined by hand, subtracting the time of compound addition from the time of first response where the exponential fit started.

$$f(x) = B_{max} * e^{-K*x} + background \qquad \text{eq. 13}$$

3 Preparation of DNA constructs and ligands

3.1 Preparation of DNA constructs

Experiments were performed using HEK293G cells stably expressing a biosensor for cAMP detection which only becomes detectable after incubation with the GloSensor substrate. In order to keep the cell background consistent, all cell lines were prepared from those cells. These cells were transfected with the DNA of the receptor of interest as described previously in **2.3.4. Generation of stable cell lines** or **2.3.5 Generation of transiently transfected cells**. In this chapter, the initial preparation of these DNA constructs and the synthesis of pepducins for the project will be discussed. The methods and materials used for this section can be found in detail in **2.1. Molecular Biology**.

3.1.1 Introduction

In order to investigate the binding and functional effects of pepducins on CXCR4 a number of tagged receptor construct were prepared for BRET experiments as a donor (NanoLuc-tag) and for visualisation of the receptor or as BRET acceptor (SNAP-tag). As pepducins are postulated to interact with the intracellular part of the receptor, both N- and C-terminal tagged CXCR4 constructs were prepared with a SNAP or a NanoLuc-tag. Moreover, the same constructs were prepared for ACKR3 as this project was part of a consortium concentrating on CXCR4 and ACKR3. In some cases the ACKR3 constructs were used as a control for effects seen with CXCR4.

Additionally, the interaction between CXCR4 and the pepducin ATI-2341 was studied with a range of receptor mutants. One of the initial theories was an interaction between the pepducin and the first internal loop of CXCR4. Because of this, a construct in which the first internal loop of CXCR4 was replaced by the sequence of the CCR5 receptor was provided by Thomas Sakmar, Rockefeller University, New York. A construct in which the first internal loop 1 of CCR5 was replaced by the CXCR4 sequence was created to investigate any effects seen in the reverse experiment. CXCR4 and CCR5 share eight amino acids in their first internal loop. These eight amino acids were

mutated in CXCR4 to alanine in eight separate constructs to study the effect of those shared amino acids on the interaction with ATI-2341.

3.1.2 Preparation of SNAP- and NanoLuc-tagged receptor

Initially, N- and C-terminal SNAP- and NanoLuc tagged CXCR4 and ACKR3 constructs were prepared. A number of DNA constructs in $pcDEF_3$ plasmids (WT CXCR4 and WT ACKR3 with and without triple His-tag) were provided by the ONCORNET consortium, Vrije Universiteit Amsterdam. All constructs were expanded by transformation into competent *E. coli* cells followed by a maxiprep and verified by DNA sequencing performed by the DNA sequencing laboratory at the School of Life Sciences, University of Nottingham as described previously.

CXCR4 and ACKR3 were N-terminal tagged with SNAP and NanoLuc. The sequence of these N-terminal tagged constructs starts with the kozak consensus sequence ensuring good translation (Kozak, 1986, 1987). This is followed by the start codon of the full constructs and a signalling sequence of 84 bases of which the first 75 bases are equivalent to the sequence of a ligand-gated ion channel membrane protein, the (mouse) 5-hydroxytryptamine (serotonin) 3A (5-HT_{3A}) receptor (Hargreaves *et al.*, 1994) ensuring a correct membrane insertion of the tagged receptor. This signalling sequence is fused to the SNAP or NanoLuc tag with the start codon of the tag changed to a Leucine from a Methionine (CTG instead of ATG) to allow a continuous expression of the construct starting with the signalling sequence of 5-HT_{3A} and then the tag. Finally, the receptor sequence of CXCR4 or ACKR3 is fused to the end of the tag sequence with the same start codon mutation from Methionine to Leucine. SNAP-β_1AR (Dr. Karolina Gherbi) and NanoLuc-$P2Y_2$ (Jackie Glenn, both Cell Signalling Group) in pcDNA3.1(+)-Neo were used as starting constructs. β_1AR and $P2Y_2$ were both cut from the vector using BamHI and XhoI restriction enzymes and discarded. Subsequently, CXCR4 or ACKR3 (**Figure 3-3**) were inserted between the BamHI and XhoI

restriction sites resulting in a two amino acid long linker determined by the BamHI sequence (Glycine, Serine) between tag and receptor. However, CXCR4 contains an internal BamHI restriction site (bp 482-487 of 1059 total bp) which was removed in the first step by a synonymous mutation keeping the coding amino acid isoleucine consistent (Primers **Table 3-1** and sequencing **Figure 3-1**).

Table 3-1: Primers designed for the mutation of the internal BamHI site of CXCR4

Primer	Sequence (5'-3')
CXCR4 no BamHI Fwd	GGC GTC TGG ATT CCT GCC CTC CTG C
CXCR4 no BamHI Rev	G CAG GAG GGC AGG AAT CCA GAC GCC

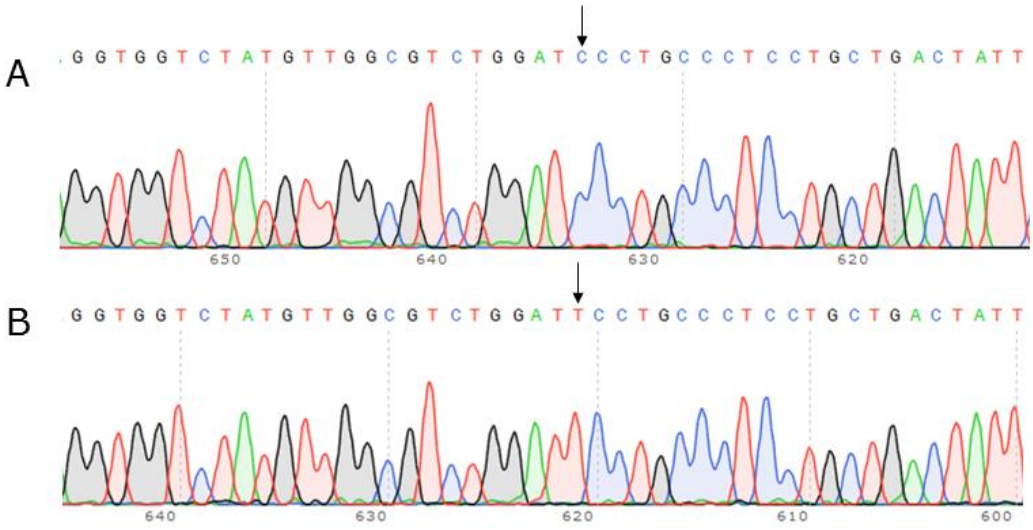

Figure 3-1: Mutation of internal BamHI site in CXCR4. Section of the sequencing chromatogram of (**A**) WT CXCR4 and (**B**) CXCR4 with a mutated internal BamHI restriction site (ATC to ATT both coding for isoleucine).

The restriction sites for inserting the receptor into the digested SNAP- and NanoLuc-tagged pcDNA3.1(+)-Neo vector were added to the C- and N-terminus of the CXCR4 and ACKR3 sequences via a PCR (Primers **Table 3-2**). In this step, the start codon of the CXCR4 sequence was also changed to a leucine (CTG instead of ATG) to avoid expression of the receptor without the tag, while the stop codon was kept. Overhang deoxyadenosines were added to the inserts prepared

via a PCR using an additional incubation step with Taq Polymerase and then ligated into a pcDNA2.1 vector with overhang deoxythimodine for an easier digestion with BamHI and XhoI restriction enzymes (also known as TA cloning see **2.2.10 TA Cloning**). In parallel to the receptor insert, the pcDNA3.1(+)-Neo vector incorporating a SNAP- or NanoLuc-tag was digested. The inserts and vectors were then purified via a gel and ligated using T4 ligase and finally transformed into competent *E. coli* cells and spread on LB Agar plates (see **2.2.11 Cloning of DNA inserts into vectors**). Colonies were then picked and the DNA constructs were initially prepared via minipreps and a small amount (2 µl) were digested with the BamHI and XhoI restriction enzymes and run to detect a correct sized insert on a gel (example gel **Figure 3-2**). Successful insertions were verified via sequencing. Finally, each constructs was bulked up by maxiprep and re-sequenced for confirmation.

Table 3-2: Primers designed for the PCR preparation of inserts for N-terminal tagged receptors

Primer	Sequence (5'-3')
CXCR4 Fwd (BamHI) no start	CCC/GGATCC/CTG GAG GGG ATC AGT ATA TAC
CXCR4 Rev (XhoI) stop	GGG/CTCGAG/TTA GCT GGA GTG AAA ACT TG
ACKR3 Fwd (BamHI) no start	CCC/GGATCC/CTG GAT CTG CAT CTC TTC G
ACKR3 Rev (Xhol) stop	GGG/CTCGAG/TCA TTT GGT GCT CTG CTC C

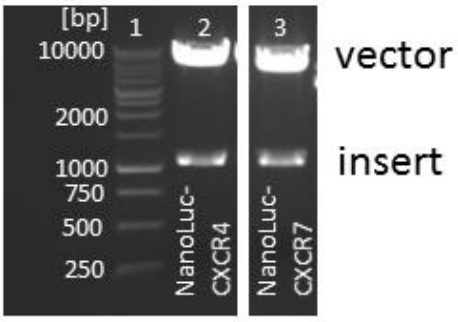

Figure 3-2: Agarose gel of digested DNA. Restriction enzyme digestion of pcDNA3.1(+)-Neo vector with NanoLuc-CXCR4 or NanoLuc- ACKR3 with BamHI and XhoI run on a 1% agarose gel, *lane 1* 1kb base pair ladder with 13 bands representing different DNA sizes of which some are marked in the figure (250, 500, 750, 1000, 1500, 2000, 2500, 3000, 4000, 5000, 6000, 8000 and 10000 bp), *lane 2* showing digestion of pcDNA3.1(+) NanoLuc-CXCR4 upper band vector with NanoLuc (6,128 bp) and lower band showing CXCR4 (1,059 bp), *lane 3* showing digestion of pcDNA3.1(+) NanoLuc-CXCR4 upper band vector with NanoLuc and lower band showing ACKR3 (1,085 bp).

The C-terminal tagged constructs were prepared in two steps with the SNAP- or NanoLuc-tag inserted between the restriction site XhoI and XbaI and the receptor between HindIII and XhoI for CXCR4 (using the WT CXCR4 instead of the mutated version) and BamHI and XhoI for ACKR3 (**Figure 3-3**) as no C-terminal tagged receptors were available in the group.

In the first step the CXCR4 and ACKR3 as well as the NanoLuc and SNAP inserts were prepared. In a PCR step the restriction sites were added to the C- and N-terminus of the sequences (Primers **Table 3-3**). The stop codon of the receptors was removed by removal of the last three base pairs to keep the receptor and tags in one reading frame, while the start codon was kept. The start codon of the SNAP and NanoLuc tag was changed to Leucine (CTG instead of ATG) to avoid expression of the tag without the receptor, while the stop codon was kept.

Next, the inserts (CXCR4 no stop, ACKR3 no stop, SNAP no start and NanoLuc no start) with additional overhang deoxyadenosines were ligated into pcDNA2.1 as previously described. Then the empty

pcDNA3.1(+)-Neo vector and inserts were digested with the appropriate restriction enzymes, followed by a first ligation step inserting SNAP or NanoLuc in the empty pcDNA3.1(+)-Neo vector in between the XhoI and XbaI restriction sites. These constructs were then transformed into competent *E. coli* cells, analysed via sequencing of a miniprep preparation as previously mentioned. Afterwards, a second digestion and ligation step inserting CXCR4 or ACKR3 in the same vector already containing the SNAP- or NanoLuc-tag was performed. The new constructs were transformed into competent *E. coli* cells and prepared via a miniprep. All constructs were checked for size and inserts on a gel and sequenced, before preparation by maxiprep and re-sequencing.

Table 3-3: Primers designed for the PCR preparation of inserts for C-terminal tagged receptors

Primer	Sequence (5'-3')
CXCR4 Fwd (HindIII) start	CCC/AAGCTT/CCACC/ATG GAG GGG ATC AGT ATA TAC
CXCR4 Rev (XhoI) no stop	GGG/CTCGAG/GCT GGA GTG AAA ACT TG
ACKR3 Fwd (Bam HI) start	CCC/GGATCC/CCACC/ATG GAT CTG CAT CTC TTC G
ACKR3 Rev (XhoI) no stop	GGG/CTCGAG/TTT GGT GCT CTG CTC C
NanoLuc Fwd (XhoI) no start	CCC/CTCGAG/CTG GTC TTC ACA CTC G
NanoLuc Rev (XbaI) stop	GGG/TCTAGA/TTA CGC CAG AAT GCG TTC GCA CAG C
SNAP Fwd (XhoI) no start	CCC/CTCGAG/CTG GAC AAA GAC TGC GAA ATG
SNAP Rev (XbaI) stop	GGG/TCTAGA/TTA AGC CCA GGC TTG CCC AGT

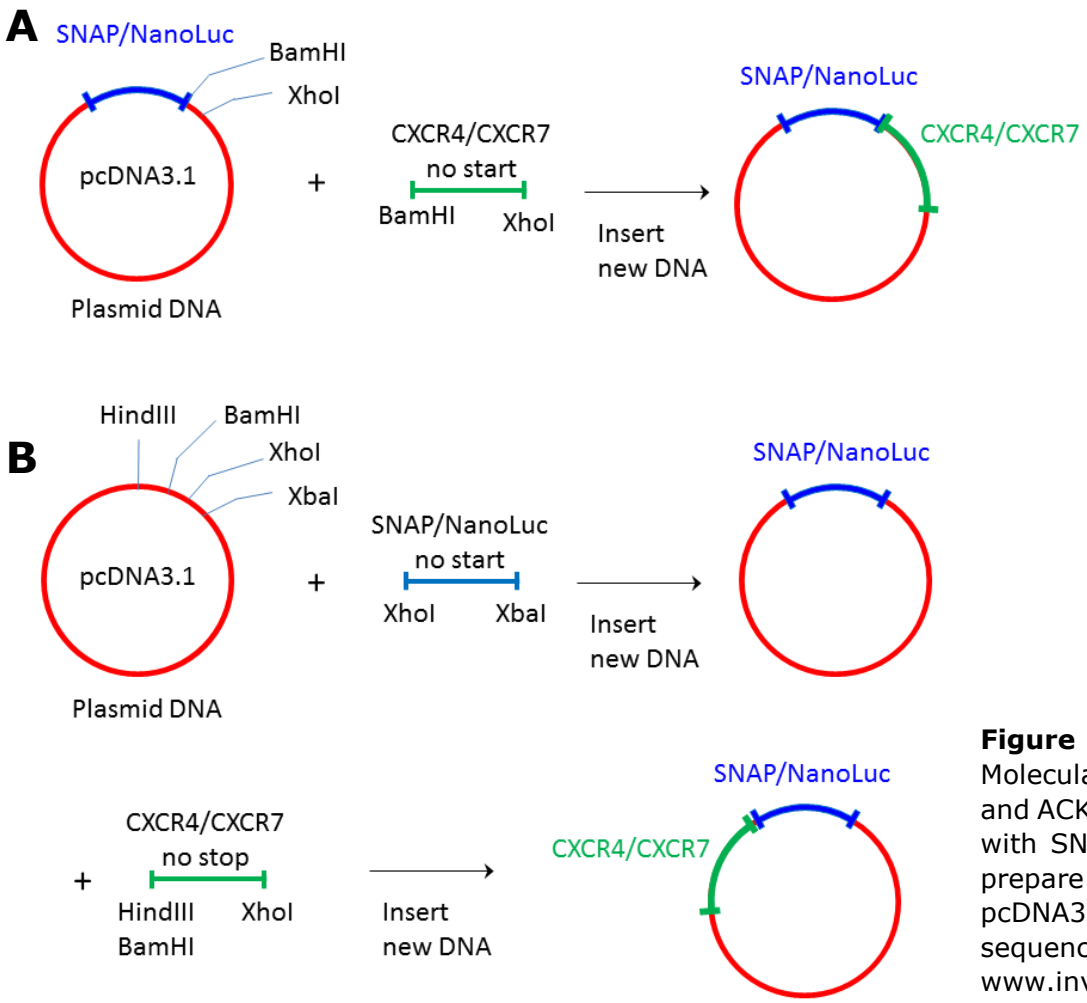

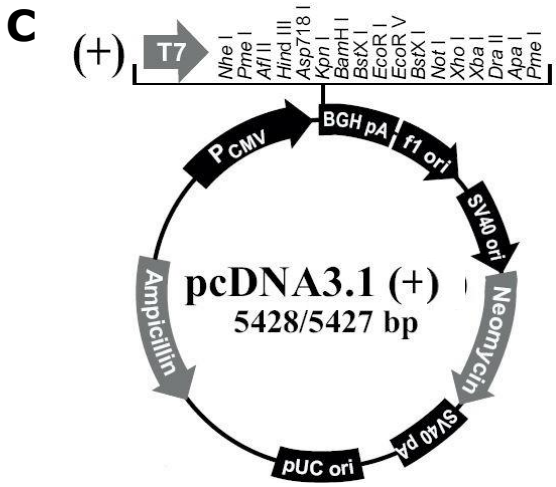

Figure 3-3: Molecular Biology strategy and vector. (**A**) Molecular Biology strategy to prepare N-terminal tagged CXCR4 and ACKR3 constructs from already existing pcDNa3.1. constructs with SNAP and NanoLuc tag; (**B**) Molecular Biology strategy to prepare C-terminal tagged CXCR4 and ACKR3 constructs in pcDNA3.1; (**C**) vector map of pcDNA3.1 (+) with CMV promoter sequence and multicloning region; Image taken from www.invitrogen.com

3.1.3 Preparation of mutations

A CXCR4 construct in which the first internal loop was exchanged for the first internal loop of CCR5 (CXCR4_ il1CCR5) in pcDNA3.1 was kindly provided by Professor Thomas Sakmar, Rockefeller University, New York.

This construct was modified to include an N-terminal SNAP- or NanoLuc-tag to study the properties of the chimeric receptor by replacing CXCR4 in the existing constructs (SNAP-CXCR4 and NanoLuc-CXCR4) with CXCR4_ il1CCR5 using the same techniques and primers as for WT CXCR4 including the mutation of the internal BamHI site and removal of the start codon (**Table 3-1** and **Table 3-2**).

A corresponding construct in which the first internal loop of CCR5 was replaced with the first internal loop of CXCR4 (CCR5_ il1CXCR4) was created (Primers and final sequencing see **Table 3-4** and **Figure 3-4**). This construct was not tagged with a SNAP- or NanoLuc-tag as all results with this construct were compared with HEK293G CCR5 cells previously made by Dr. Carolin Schwehm in the Cell Signalling group, University of Nottingham which also expressed an untagged CCR5 receptor (Schwehm *et al.*, 2017).

Table 3-4: Sequences of internal loop 1 in CXCR4, CCR5 and primers for the mutation strategy to transform loop1 of CCR5 to loop1 of CXCR4. Letters in red show the amino acids present in CCR5 while blue letters represent amino acids in CXCR4, in the primer sequence red letters show base pairs that are mutated in this step and blue letters show base pairs that have been mutated in the previous cycle

Name	Sequence loop 1	Primer Sequence (5'-3')
CCR5	LINCKRLKSMTDIYLL	
CCR5 M1	MINCKRLKSMTDIYLL	Fwd: G CTG GTC ATC CTC ATC ATG ATA AAC TGC AAA AGG
		Rev: CCT TTT GCA GTT TAT CAT GAT GAG GAT GAC CAG C
CCR5 M2	MGYCKRLKSMTDIYLL	Fwd: CTC ATC CTC ATC ATG GGA TAC TGC AAA AGG CTG AAG
		Rev: CTT CAG CCT TTT GCA GTA TCC CAT GAT GAG GAT GAG
CCR5 M3	MGYQKRLKSMTDIYLL	Fwd: CTC ATC ATG GGA TAC CAG AAA AGG CTG AAG AGC
		Rev: GCT CTT CAG CCT TTT CTG GTA TCC CAT GAT GAG
CCR5 M4	MGYQKKLKSMTDIYLL	Fwd: C ATG GGA TAC CAG AAA AAA CTG AAG AGC ATG ACT G
		Rev: C AGT CAT GCT CTT CAG TTT TTT CTG GTA TCC CAT G
CCR5 M5	MGYQKKLRSMTDIYLL	Fwd: TAC CAG AAA AAA CTG AGA AGC ATG ACT GAC ATC
		Rev: GAT GTC AGT CAT GCT TCT CAG TTT TTT CTG GTA
CCR5 M6	MGYQKKLRSMTDKYLL	Fwd: G AGA AGC ATG ACT GAC AAG TAC CTG CTC AAC CTG
		Rev: CAG GTT GAG CAG GTA CTT GTC AGT CAT GCT TCT C
CCR5 M7	MGYQKKLRSMTDKYRL	Fwd: GC ATG ACT GAC AAG TAC AGG CTC AAC CTG GCC ATC
		Rev: GAT GGC CAG GTT GAG CCT GTA CTT GTC AGT CAT GC
CXCR4	MGYQKKLRSMTDKYRL	

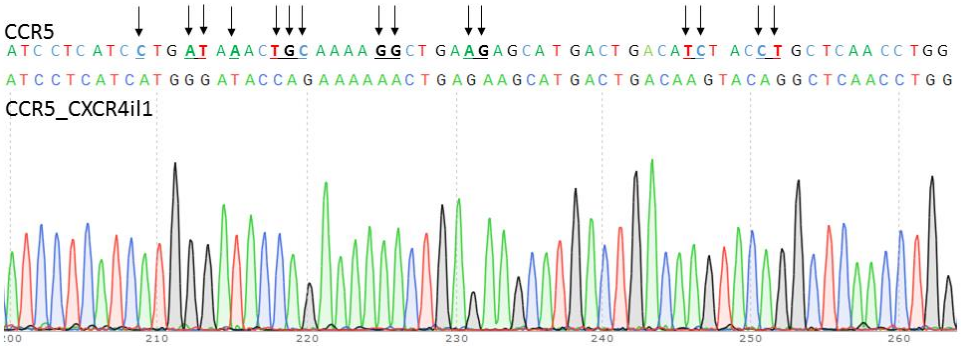

Figure 3-4: Mutations in CCR5. Sequencing of CCR5_CXCR4il1 showing all 14 base pair mutations in the full length CCR5 sequence

Afterwards, a series of point mutations was made in the full length construct of CXCR4 in which one of the eight amino acids that are equivalent in CXCR4 and CCR5 was mutated to Alanine (**Table 3-5** and sequencing **Figure 3-5**). These mutations were made in order to investigate the function of those amino acids common for both receptors in the interaction between CXCR4 and the pepducin.

Table 3-5: Sequences of internal loop 1 in CXCR4 or CCR5 and the alanine mutation series. Letters in red show the amino acids that are different in CCR5 and CXCR4, while the blue letters mark the amino acid common in both sequences that is mutated to alanine, in the primer sequences red letters show base pairs that are mutated in this construct.

Name	Sequence loop 1	Primer Sequence (5'-3')
CXCR4	MGYQKKLRSMTDKYRL	
CXCR4 K67A	MGYQAKLRSMTDKYRL	Fwd: GGT CAT GGG TTA CCA GGC CAA ACT GAG AAG CAT G
		Rev: C ATG CTT CTC AGT TTG GCC TGG TAA CCC ATG ACC
CXCR4 L69A	MGYQKKARSMTDKYRL	Fwd: GGG TTA CCA GAA GAA AGC CAG AAG CAT GAC GGA CAA G
		Rev: C TTG TCC GTC ATG CTT CTG GCT TTC TTC TGG TAA CCC
CXCR4 S71A	MGYQKKLRAMTDKYRL	Fwd: CAG AAG AAA CTG AGA GCC ATG ACG GAC AAG TAC AGG
		Rev: CCT GTA CTT GTC CGT CAT GGC TCT CAG TTT CTT CTG
CXCR4 M72A	MGYQKKLRSATDKYRL	Fwd: GAA ACT GAG AAG CGC CAC GGA CAA GTA CAG G
		Rev: C CTG TAC TTG TCC GTG GCG CTT CTC AGT TTC
CXCR4 T73A	MGYQKKLRSMADKYRL	Fwd: GAA ACT GAG AAG CAT GGC CGA CAA GTA CAG GCT G
		Rev: C AGC CTG TAC TTG TCG GCC ATG CTT CTC AGT TTC
CXCR4 D74A	MGYQKKLRSMTAKYRL	Fwd: CTG AGA AGC ATG ACG GCC AAG TAC AGG CTG CAC CTG
		Rev: CAG GTG CAG CCT GTA CTT GGC CGT CAT GCT TCT CAG
CXCR4 Y76A	MGYQKKLRSMTDKARL	Fwd: GCA TGA CGG ACA AGG CCA GGC TGC ACC TGT CAG
		Rev: CTG ACA GGT GCA GCC TGG CCT TGT CCG TCA TGC
CXCR4 L78A	MGYQKKLRSMTDKYRA	Fwd: GAC GGA CAA GTA CAG GGC GCA CCT GTC AGT GGC CG
		Rev: CG GCC ACT GAC AGG TGG GCC CTG TAC TTG TCC GTC
CCR5	LINCKRLKSMTDIYLL	

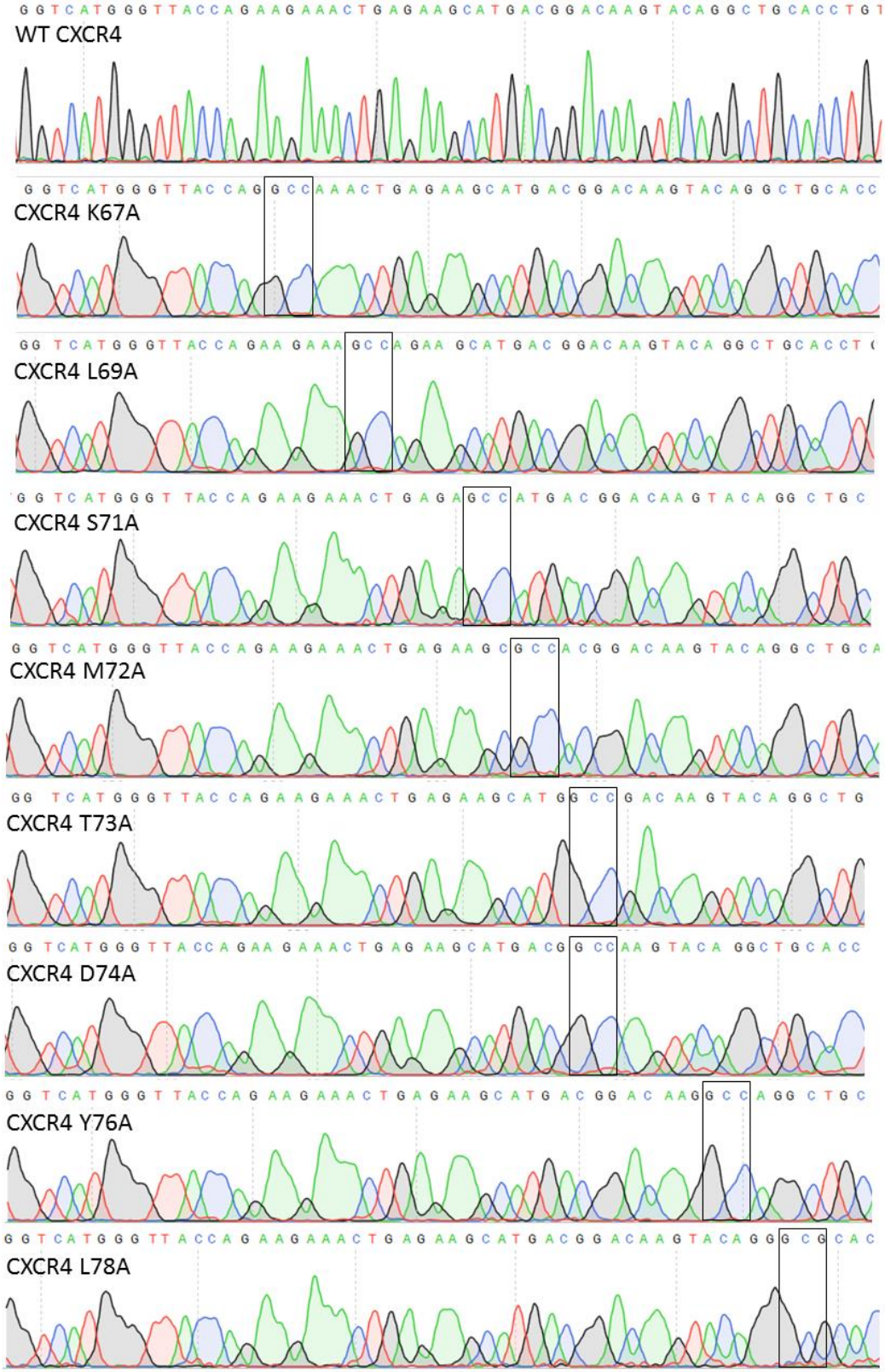

Figure 3-5: Alanine scan in CXCR4. Sequencing chromatograms of WT CXCR4 and all eight constructs with alanine point mutations in intracellular loop 1.

3.2 Pepducin synthesis

3.2.1 Introduction

Proteins and peptides are all built from the same 21 amino acids that change their properties when polymerized. The shape and chemical functionality of the protein is determined by its amino acid sequence. Because of this, great efforts have been made to be able to synthesise peptides and proteins systematically in order to study and understand them.

In order to synthesise peptides or proteins the carboxyl group of one amino acid reacts with the amine group of another in a condensation reaction to form an amide bond (also known as peptide bond - **Figure 3-6**).

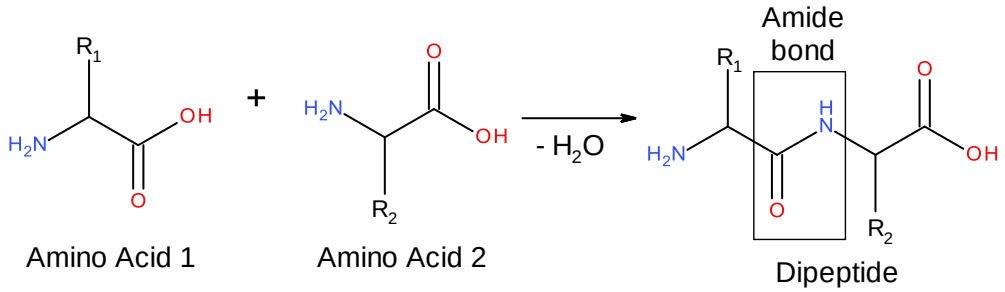

Figure 3-6: Formation of an amide bond between two amino acids.

However, each amino acid contains at least one carboxyl group and one amine group with additional potentially reactive groups in the side chains of the amino acids (**Figure 3-7**). Therefore the obvious challenge in peptide synthesis is selectively activating the right carboxyl and amine for reaction. This is achieved by the introduction of protecting groups that block the reaction of certain amines or carboxyl groups. These protecting groups can then be cleaved selectively from the peptide with the right conditions.

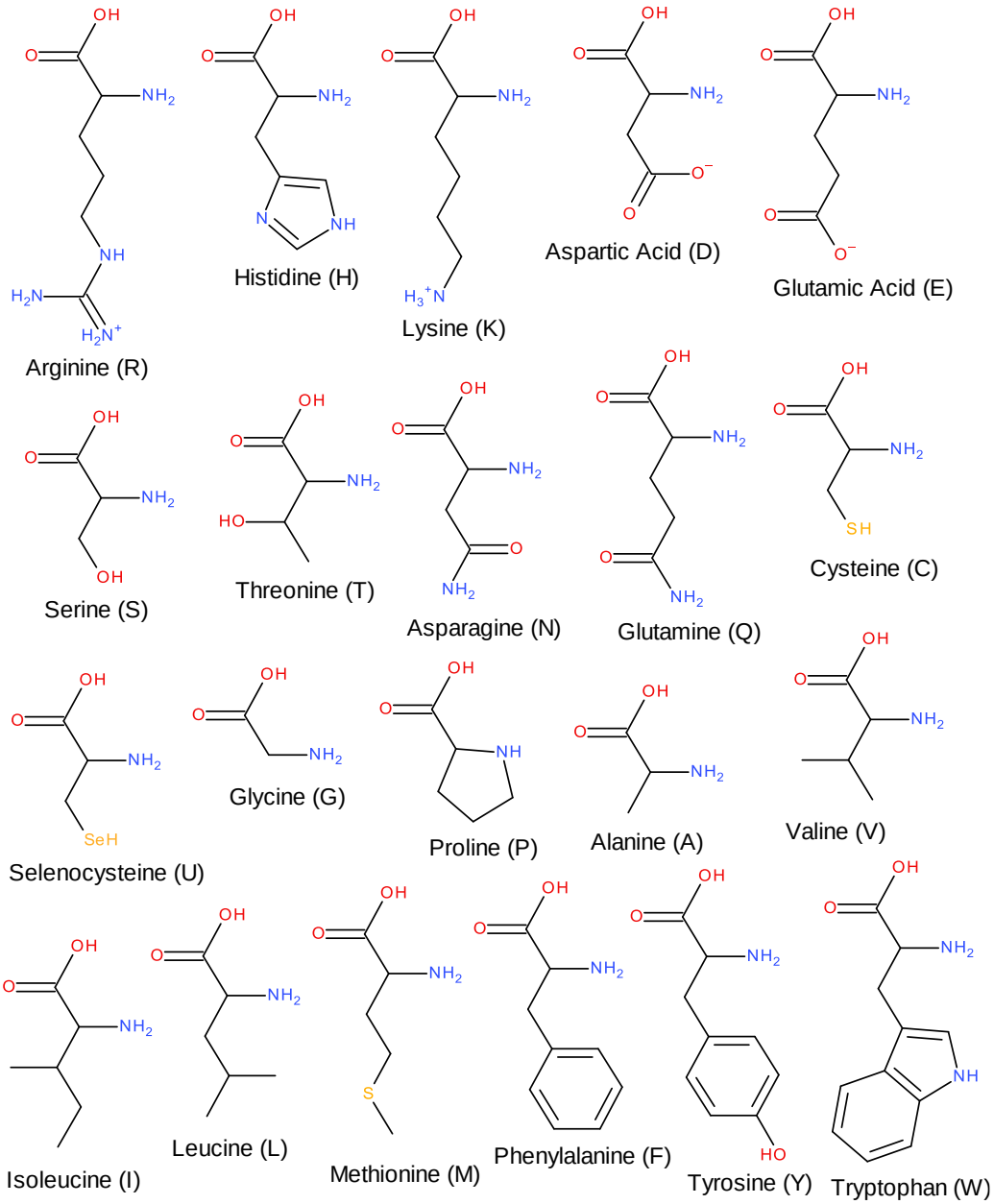

Figure 3-7: Natural amino acids. All 21 natural amino acids with side chains; with positive side chains for R, H and K; negative side chains for D and E; polar side chains for S, T, N and Q; hydrophobic side chains for V, I, L, M, F, Y and W.

By the 1950s liquid phase synthesis of small peptides, in which two amino acids are added to a solvent for reaction, was well established with the peptide product showing the same properties as their natural equivalents (Jaradat, 2018). In these liquid phase reactions side chains and the non-reacting carboxyl and amine were protected with protecting groups. Solid phase peptide synthesis based on these same

principle as its liquid counterpart was first described by Merrifield (Merrifield, 1963). The possible automation of the process with the introduction of washing and capping steps were the biggest advantages and enabled chemists to synthesis longer peptides with precise sequence. Before the introduction of these steps each intermediate product had to be purified for further reactions in order to remove any leftover reactants. In solid phase synthesise these are washed away. Furthermore, peptides that did not react with the next amino acid are capped by addition of acetic anhydride. Because of this wrong elongation of peptides is stopped and the product is easier to purify.

As an alternative to solid phase peptide synthesis, bacterial production of peptides in *E. coli* is often used for bigger, folded proteins as proteins synthesised with solid phase synthesis have to be folded afterwards using the right conditions which can be challenging (Stráner *et al.*, 2016). The synthesis of the proteins occurs at the ribosome which catalyses the formation of peptide bonds. The T7 RNA Polymerase gene is inserted into the chromosome of the bacteria and the transcription of the protein of interest is then induced by the addition of IPTG (iso-propyl- β-D-1-thiogalactopyranoside) acting on the lac operon (Terpe, 2006).

Peptides synthesised via all techniques are then purified using different column chromatography techniques.

Column chromatography techniques are based on packing a column with a resin (stationary phase) and running a liquid (mobile phase) through the resin. Both phases will interact differently with the peptides causing the peptides to separate dependent on their properties. Resins can for example interact with peptides dependent on size (Size Exclusion Chromatography), Affinity (Affinity Chromatography e.g. interactions with His-tags) or hydrophobicity (reversed phase chromatography) (Ettre, 1993).

In reversed phase chromatography a hydrophobic resin interacting with hydrophobic peptides is used. In contrast to this classic normal-

phase chromatography uses hydrophilic, unmodified silica as a stationary phase resulting in hydrophobic molecules to be eluted first.

In the reversed phase chromatography the column is first run with a polar solvent (water) and the percentage of an organic solvent (acetonitrile) dissolving the peptides is slowly increased separating the different peptides from each other. Eluted solvent is controlled by running it past a detector and measuring its absorbance at 280 nm indicating any presence of protein (Molnar and Horvath, 1976).

3.2.2 Synthesis strategy

Part of the pepducins were synthesised in cooperation with ALMAC (Edinburgh, UK) in a one month internship during January 2017. All chemical supplies for the synthesis were bought from Sigma Aldrich (Gillingham, UK). Initial pepducin stocks (ATI-2341, ATI-2755, ATI-2339 and ATI-2504) were available from Anchor Therapeutics (Cambridge, MA, USA) from a previous collaboration.

Peptides were synthesised via solid phase peptide synthesis (**Figure 3-8 A**; Merrifield, 1963) on a Symphony Multiple Synthesiser on a 0.1 mmol scale using 4-(2,4-dimethoxyphenyl-hydroxymethyl)-phenoxymethyl-polystyrene resin (commonly known as Rink resin; Rink, 1987) resulting in an amidated C-terminus upon cleavage, base instable fluorenylmethyloxycarbonyl (Fmoc) protected amino acids with acid instable *tert*-butyloxycarbonyl (Boc) protected side chains and Oxyma Pure (ethylcyanohydroxyiminoacetate)/N,N'-diisopropylcarbodiimide (DIC) coupling chemistry. The protected amino acids were prepared in 0.4 M Oxyma Pure solution (Oxyma Pure in DMF) and the activator base DIC was prepared in dimethylformamide (DMF). All amino acids were double coupled by addition of the next amino acid in the sequence, followed by a washing step and a second addition of the same amino acid in order to maximise yield. After each double coupling step a capping step using a wash with 0.5 M acetic anhydride in DMF was introduced to minimize unwanted peptide products by reacting with any uncoupled

peptide hence lowering the amount of wrong elongation products. Amino acids were deprotected with 20% piperidine/DMF (**Figure 3-8 B**). Palmitic acid was coupled to the last amino acid by addition of 1 mmol palmitic acid, 2 ml of 0.4 M Oxyma solution and 2 ml of 0.5 M DIC solution. The resin was mixed for 4 hours and subsequently washed with DMF and Ether.

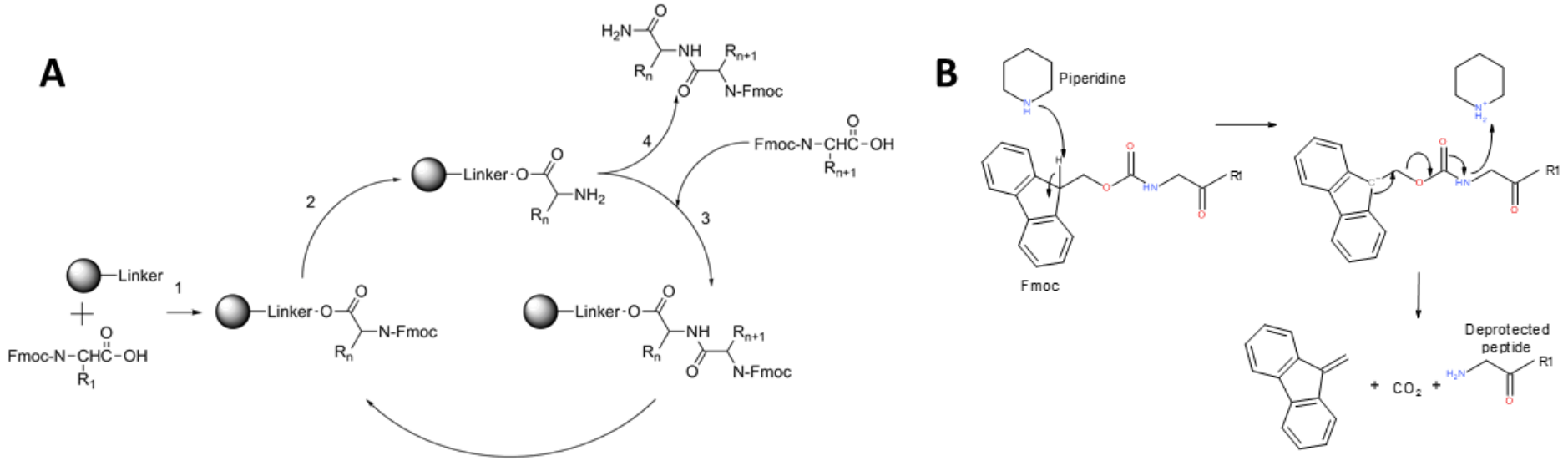

Figure 3-8: Mechanism of solid phase and Fmoc deprotection reactions. (**A**) Solid phase peptide synthesis using the Fmoc protection group strategy: 1) Attachment of a protected amino acid to the substrate; 2) Deprotection; 3) Elongation of the peptide chain; 4) Cleavage of the peptide polymer linker; (**B**) Deprotection of Fmoc protected amino acid with Piperidine.

The pepducins were cleaved from the resin by addition of 10 ml trifluoracetic acid (TFA) which also deprotected any Boc protected side chain (**Figure 3-9**), 500 µl water and 250 µl triisopropylsilane (TIS). In the presence of methionines in the peptide sequence, an additional 20 mg ammoniumiodide and 100 µl dimethylsulfide were added to avoid oxidation. The mixture was stirred for 4h at RT. Subsequently, the resin mixture was filtered through a filter syringe into cold ether where the pepducins precipitated. Pepducins were washed with ether and collected by centrifugation and dissolved in an acetonitrile/water mixture to freeze dry overnight.

Pepducins were purified on Äkta or Gilson purifier systems running a reversed phase chromatography (also known as hydrophobic chromatography) with an acetonitrile/water gradient on Luna HPLC columns.

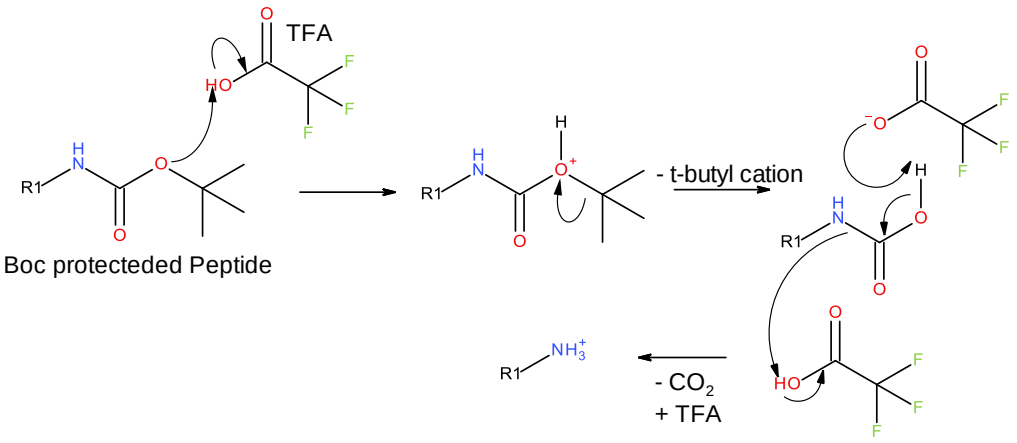

Figure 3-9: Boc deprotection. Deprotection of Boc protected side chains with TFA

In order to synthesise the fluorescently labelled pepducin the additional N-terminal lysine, to which Carboxytetramethylrhodamine (TAMRA) was attached, was coupled with a Dde protecting group (N_{α}-Fmoc-N_{ε}-[1-(4,4-dimethyl-2,6-dioxocyclo-hexylidene)ethyl]-L-lysine) instead of a Boc protecting group on its side chain. The Dde protecting group was then selectively cleaved by shaking the resin with a 3.85% hydrazinol in DMF solution. Afterwards the resin was washed and

dried overnight. The pepducin was then fluorescently labelled with the addition of 3 eq. of TAMRA and 3 eq. PyBOP (benzotriazol-1-yl-oxytripyrrolidinophosphonium hexafluoro-phosphate) and 6 eq. *N*,*N*-diisopropylethylamine (DIEA) in DMF by sonication for 3h (**Figure 3-10**). Afterwards the fluorescently labelled pepducin was detached from the resin as described before without the addition of ammonium iodide.

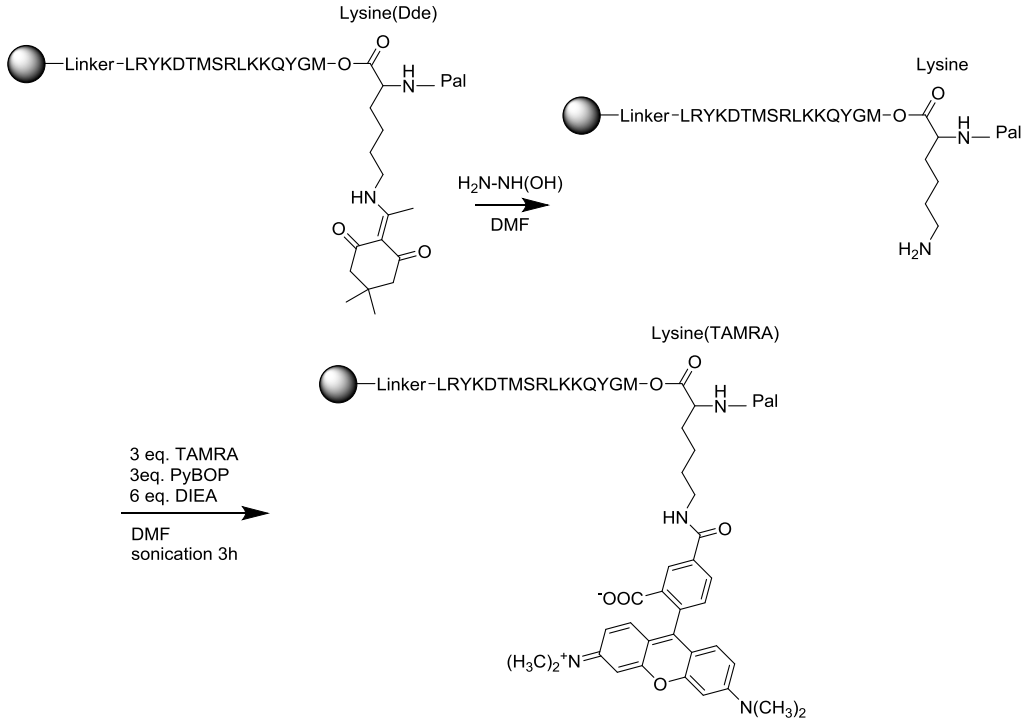

Figure 3-10: TAMRA labelling. Fluorescent labelling of pepducin; all other side chains are protected with a Boc protecting group

The pepducin's mass was analysed via Mass spectrometry and confirmed with the theoretical values (**Table 3-6**). The purity was confirmed via HPLC (see appendix for spectrograms and HPLC runs). All pepducins showed high purity >95%. Yields were calculated via absorbance measured at 280 nm accounting for the Tyrosines in the peptide sequence or at 550 nm for the TAMRA tagged pepducin.

Table 3-6: Analysis of synthesised pepducins

Pepducin	Sequence	Theoretical Mass	Mass in Mass Spectrometry	Purity (HPLC)	Yield
ATI-2341	Pal-MGYQKKLRSMTDKYRL-NH_2	2255.8	2255.35	98.56 %	5 mg
ATI-2341TA	Pal-MGYQKKLRSMADKYRL- NH_2	2225.8	2225.67	99.52 %	20 mg
ATI-2341f	Pal-K(TAMRA)-MGYQKKLRSMTDKYRL-NH_2	2796.5	2795.60	96.77 %	5.7 mg

4 BRET studies to investigate the binding mode of pepducins

4.1 Introduction

In this chapter a range of BRET binding studies were performed in order to understand the mechanism of binding of pepducins and their effects on the receptor conformation in more detail. The main questions of interest were to understand where the pepducin binds (extracellular or intracellular) and where in the cell the receptor and pepducin are located during this interaction, to see if the pepducin influences the binding of other CXCR4 ligands (CXCL12 and IT1t) and to study the kinetics involved in these binding processes as well as possible allosteric effects by the pepducin. Moreover, GTP was added to membrane preparations of CXCR4 expressing cells to activate the G protein and cause uncoupling from the receptor and thereby investigate which form of receptor is affected by the pepducin.

CXCL12, the endogenous ligand of CXCR4, has been shown to interact with the extracellular part of the receptor in particular with the N-terminus, the extracellular loops of the receptor, and also partly with the upper parts of the transmembrane regions (Crump *et al.*, 1997; Xu *et al.*, 2013; Wescott *et al.*, 2016). The binding model of CXCL12 based on simulation studies and mutations partly overlaps with the binding pocket found in the CXCR4 crystal structure for the small molecule IT1t which is bound to the transmembrane region of CXCR4 that is extracellularly accessible (Crump *et al.*, 1997; Wu *et al.*, 2010; Xu *et al.*, 2013; Wescott *et al.*, 2016).

CXCL12 binding has been tested previously using a radiolabelled version ^{125}I-CXCL12 in different settings with equilibrium binding constants ranging from 1.8 nM to 25 nM dependent on study and cell line (Crump *et al.*, 1997; Burns *et al.*, 2006; Drury *et al.*, 2011). However, radioligand binding does not give any information about the location of the interaction between receptor and ligand as signals are observed independently of the site of the ligand interaction. In order to investigate the location of the interaction with radioligand binding, receptor truncations or mutations have to be generated that can also impact the fold of the protein. Because of this, a BRET assay was developed to study the binding location of pepducins and CXCR4.

Moreover, pepducins show low potencies in functional assays (Tchernychev *et al.*, 2010; Quoyer *et al.*, 2013) which might be related to low binding affinities making radiolabelled pepducins unpractical due to safety reasons.

Recently, there has been a publication reporting the development of a NanoBRET assay for CXCR4 using an N-terminal tagged CXCR4 and a fluorescently tagged peptide antagonist TAMRA-Ac-TZ14011. The labelled antagonist was displaced with various unlabelled CXCR4 compounds including CXCL12 showing an IC_{50} of 3.2 nM (Sakyiamah *et al.*, 2019).

Pepducins have been postulated to interact with the intracellular site of their receptor as described in detail in **1.4 Pepducins**. Evidence suggesting that pepducins bind on the inside of the receptor are based primarily on two separate studies. In the first study, protease-activated receptor 1 (PAR1) expressing fibroblasts were incubated with the fluorescent pepducin Fluo-Pal-i3-19 which is based on IL3 of PAR1 and PAR2, this was followed by digestion of extracellular peptide and subsequent analysis of the fluorescence of the cells by flow cytometry showing increased fluorescence in comparison to cells treated with an unlipidated equivalent (Covic *et al.*, 2002). This effect can either be explained by an intracellular binding site of the pepducin or internalisation of the pepducin after activation of the receptor. The same study showed that an orthosteric small molecule antagonist binding at the extracellular site of PAR1 and competing with a PAR1 specific peptide SFLLRN was not able to stop the Ca^{2+} signal induced by the pepducin Pal-i3-19 (Covic *et al.*, 2002). The fact that an orthosteric ligand does not block pepducin induced Ca^{2+} signalling suggests two distinct binding pockets of the ligand and the pepducin, however both pockets could be extracellular. In the second study, Rho-P1-Pal-12 also targeting PAR1 was added to platelets incubated with a fluorescent extra- and intracellular marker. The fluorescent tag of the pepducin can quench the cellular markers if both, the marker and pepducin, are in close proximity. Rho-P1-Pal-12 quenched the extra- and intracellular marker while the unlipidated equivalent did

only quench the extracellular marker (Wielders *et al.*, 2007). However, while both studies give a good indication that pepducins bind intracellularly the results of the fluorescence measurements could also be obtained after extracellular interaction of the pepducin and receptor followed by internalisation of both.

ATI-2341 binding has been modelled showing possible binding modes in the extra- and intracellular part of the receptor (Planesas *et al.*, 2015). Furthermore, a fluorescent pepducin ATI-2766 based on ATI-2341 but incorporating an N-terminal TAMRA-tag and a photo-leucine, has been crosslinked to CXCR4 and two CXCR4 mutants with truncated N-termini using UV light (Janz *et al.*, 2011). Both truncated CXCR4 receptors showed reduced CXCL12 binding, but were still able to interact with ATI-2766 suggesting a different binding site for intracellular loop 1 pepducins and CXCL12 (Janz *et al.*, 2011).

Accordingly, the aims of this chapter were the investigation of the binding mode and working mechanism of ATI-2341 towards CXCR4 focussing on location in the cell and at the receptor and its influence on binding of extracellular ligands.

In order to study the binding of CXCR4 ligands to the receptor, the BRET binding assay was initially set up in an end point and a kinetic version using a fluorescent version of the endogenous CXCL12 (CXCL12-red or CXCL12-green) and an NLuc-tagged CXCR4. While the evidence suggested intracellular binding of the pepducin, an extracellular binding site was still possible. Therefore the BRET assay was tested with a fluorescent pepducin ATI-2341f and two separate cell lines expressing either an N- or C-terminal tagged CXCR4 in order to address the question of extracellular vs intracellular binding. These two cell lines were also imaged using bioluminescence microscopy in order to see differences in binding. Apart from bioluminescence imaging, the location of the interaction in the cell was also visualized using confocal imaging techniques. The potential intracellular binding site of the pepducin might have impacts on its kinetics which were tested next in binding assays monitoring the change in BRET in real time. Moreover, we wondered if the binding of ATI-2341 influences

the binding of the endogenous ligand CXCL12 or of IT1t either due to a direct competition or an allosteric effect caused by ATI-2341 that might be similar to the one caused by GTP binding.

4.2 Methods

Binding studies between CXCR4 and compounds were performed using saturation and competition binding BRET techniques in equilibrium and in a kinetic mode between an N- or C-terminal NanoLuc tagged receptor and a fluorescent version of CXCR4 ligands (CXCL12-red, ATI-2341f or SD44).

A BRET signal can only be observed if the NanoLuc tag of the receptor and the fluorescent ligand are within 10 nm distance from each other (Hall *et al.*, 2012; Stoddart *et al.*, 2015). The non-specific contributions to the increase of BRET signal were measured by the addition of high concentration of a specific, unlabelled CXCR4 ligand (10 µM AMD3100). AMD3100 is in direct competition to IT1t and CXCL12 binding while there was a lack of appropriate unlabelled ligand for the fluorescent pepducin. A more detailed introduction to the BRET technique can be found in the introduction (see **1.5 Fluorescence and Luminescence**) and in the method section (see **2.4.1 NanoLuc assay**) describing the theory behind the NanoLuc technique and the setup of the assay.

All experiments in this chapter were performed using cell lines stably expressing NanoLuc tagged receptors and were prepared as previously described in **2.2. Cell culture**. As the NanoLuc tagged constructs seemed to transfect very well, all cell lines were kept as mixed populations. Mixed population cell lines were generated by transfecting HEK293G cells with receptor DNA using FuGENE® HD reagent according to the manufactures instructions and then treating the cells with 1mg/ml G418 after 24h. Because of this, mixed populations are based on all cells that were transfected with the receptor DNA incorporating G418 resistance and the population shows a non-uniform receptor expression profile. Experiments were

performed at 37°C in agreement with body temperature and timings for the equilibrium measurements were chosen at 1.5 or 2h respectively due to the fact that the kinetic experiments showed constant BRET values only after about 70 min. Cell density and membrane concentrations were chosen to avoid saturation of the detector and have big signalling windows at the same time. Membrane concentrations are chosen to be very high as freeze thawing causes some of the membrane to precipitate at the bottom of the tube and initial measured membrane concentrations might not represent the actual ones after freeze thawing, however the concentration of membranes did not impact K_d values (see Appendix **Figure 9-1**).

4.3 Results

Initially, the influence of an N- or C-terminal tag on binding and signalling of CXCR4 was tested using a cAMP GloSensor assay in three cell lines stably expressing SNAP-CXCR4, NanoLuc-CXCR4 and CXCR4-NanoLuc which are used in the next three chapters.

The GloSensor assay reported the amount of cAMP present via a firefly luciferase based biosensor emitting light which is directly proportional to the cAMP amount in the presence of the GloSensor reagent. The production of luminescence can then be monitored on a plate reader in real time. Forskolin was added to the cells to activate adenylyl cyclase and produce cAMP from ATP. CXCR4 is known to couple to $G\alpha_i$ and hence its activation caused the inhibition of cAMP production. The assay is explained in more detail in **2.4.4 cAMP assay**. Further results and the kinetic profiles of the different ligands of this functional assay can be found in the next chapter (**5.5 Inhibition of cAMP production**) as it should serve here only as a control for the functionality of all used CXCR4 constructs.

In a first step, FSK, CXCL12 and ATI-2341 were added to the parental untransfected HEK293G cells in order to see the effect of CXCR4 ligands and test for the effect of endogenous CXCR4 on these cells.

Forskolin caused a 10-fold over basal increase in cAMP levels in untransfected HEK293G cells with a pEC_{50} of 6.39 ± 0.19 (n = 5). In contrast neither CXCL12 (up to 100 nM) nor ATI-2341 (up to 1 µM) caused a significant change in basal cAMP or were able to inhibit the response mediated by 30 µM FSK (**Figure 4-1**).

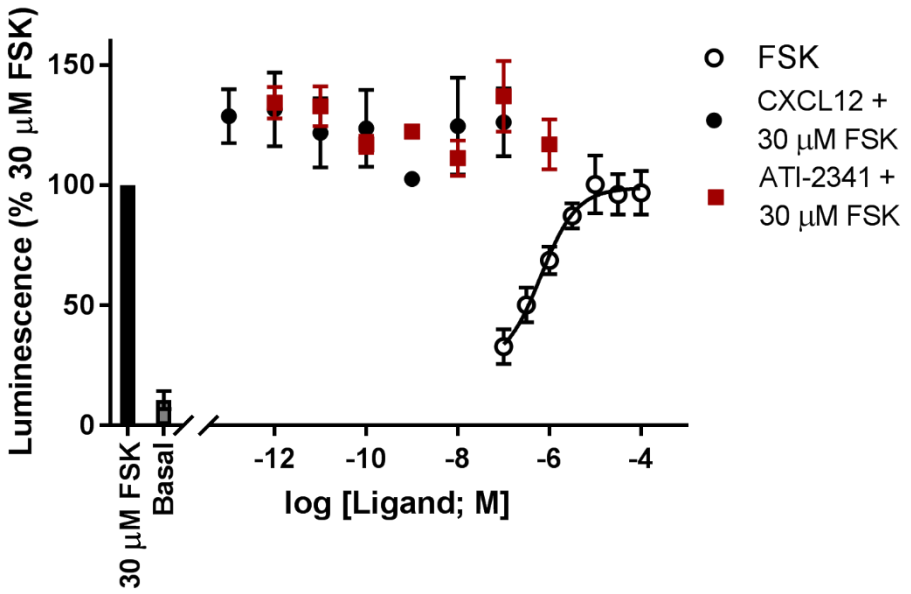

Figure 4-1: cAMP response in native HEK293G cells in response to forskolin and the effect of CXCL12 and ATI-2341. Native HEK293G cells were stimulated with the indicated concentrations of forskolin (FSK; O) or 30 µM FSK in the presence of CXCL12 (●) or ATI-2341 (■) in a GloSensor assay. Response measured as luminescence of the peak signal analysed from kinetic cAMP curves as described in the Methods section. Data are shown as mean ± S.E.M. of n= 5 (FSK), n=5 (CXCL12) and n=6 (ATI-2341) independent experiments, each performed in triplicate. Data were normalised to the response to 30 µM FSK. Luminescence was measured on an EnVision plate reader.

Next, the responses to CXCL12 and ATI-2341 were determined in the SNAP-CXCR4, NLuc-CXCR4 and CXCR4-NLuc-expressing cell lines to see the effect of the epitope tag on the CXCR4 response. Both, CXCL12 and ATI-2341 inhibited FSK mediated cAMP production with increasing concentration in all three cell lines. The maximal inhibition (efficacy) was the same for both compounds but the potencies of the two ligands were two orders of magnitude different from each other in all cell lines (**Figure 4-2** and values in **Table 4-1**). The potencies

of CXCL12 and ATI-2341 were not significantly different between cell lines ($P>0.05$, one-way ANOVA test). However, the maximal inhibitions showed differences between the different cell lines.

Moreover the selectivity of ATI-2341 was tested by trying to inhibit FSK mediated cAMP production in CCR5. While the endogenous ligand of CCR5, CCL3, showed an inhibitory effect on cAMP production, ATI-2341 did not have any effect in CCR5. These results are discussed in more detail in Chapter 6 (see **Figure 6-5**).

As mentioned before in **2.4.4 cAMP Assay** measurements were moved from the EnVision to the PheraStar at some point in the project. **Figure 4-1** and **Figure 4-2** are therefore measured on different plate readers. Potencies measured on different plate readers were compared and results can be found in the chapter discussing cAMP measurements (**5.5 Inhibition of cAMP production**).

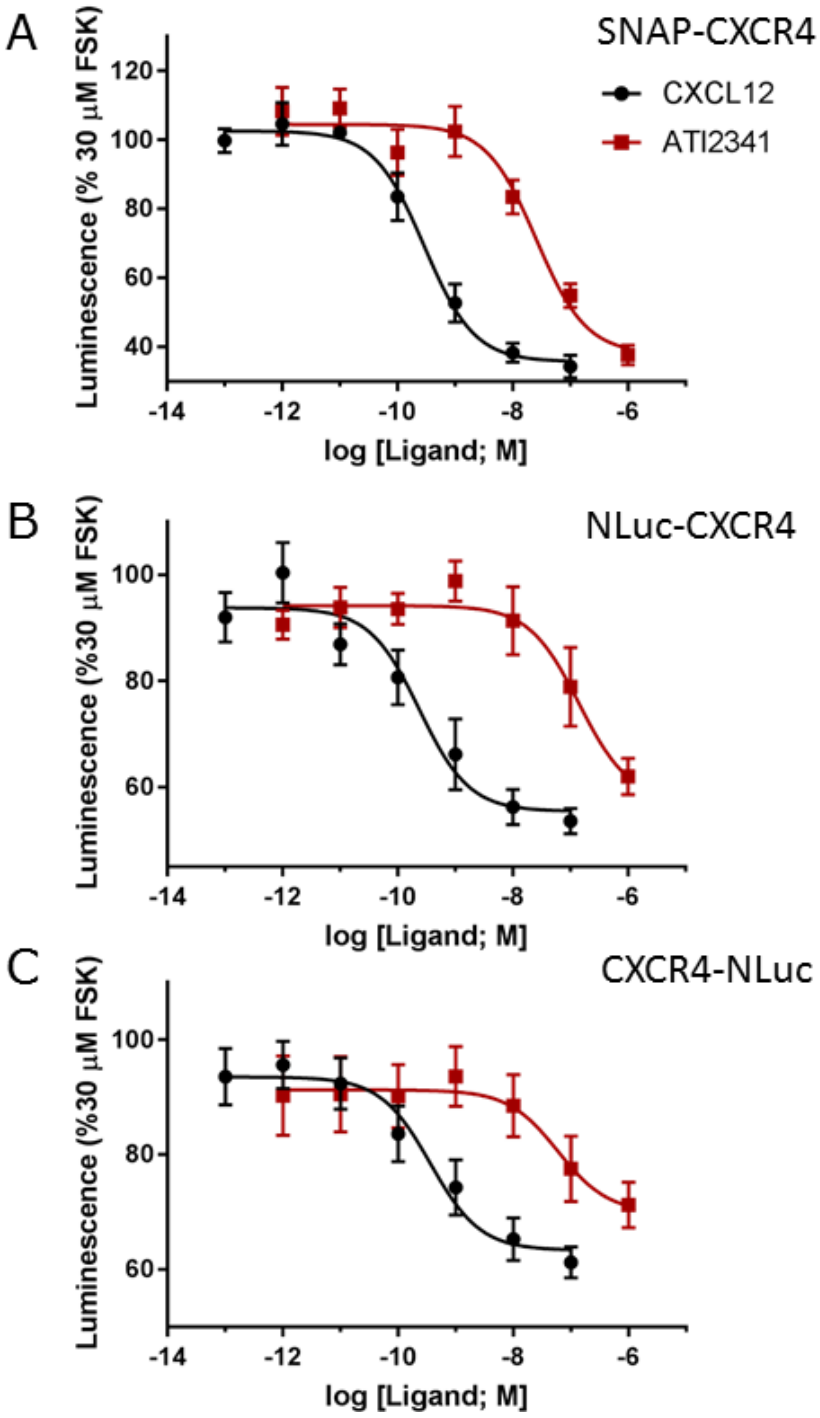

Figure 4-2: Effect of CXCL12 or ATI-2341 on FSK stimulated cAMP formation in HEK293G expressing differently tagged CXCR4 construct. HEK293G cells overexpressing different tagged versions of CXCR4 were stimulated with 30 μM FSK in the presence of CXCL12 (●) or ATI-2341 (■) in a GloSensor assay. Response measured as luminescence of the peak signal analysed from kinetic cAMP curves as described in the Methods section. Data are shown as mean ± S.E.M. of n = 5 in (**A**) HEK293G_SNAP-CXCR4, n = 7 in (**B**) HEK293G_NanoLuc-CXCR4 (N-terminal NLuc) or n = 9 in (**C**) HEK293G_CXCR4-NanoLuc (C-terminal NLuc) independent experiments, each performed in triplicate. Data were normalised to the response to 30 μM FSK. Luminescence was measured on a PheraStar plate reader.

Table 4-1: Potency and relative efficacy of CXCL12 and ATI-2341 in FSK mediated cAMP inhibition using the GloSensor assay in HEK293G-CXCR4 cell lines

Cell lines	CXCL12		ATI-2341	
	pEC_{50} (NS)	Percent inhibition of the response to 30 μM FSK	pEC_{50} (NS)	Percent inhibition of the response to 30 μM FSK
SNAP-CXCR4 (5)	9.57 ± 0.18	64.7 ± 3.1 (NS_1)	7.63 ± 0.27	64.1 ± 5.2 (NS_1)
NLuc-CXCR4 (7)	9.94 ± 0.15	46.6 ± 3.0 (NS_2)	7.55 ± 0.16	42.3 ± 2.9 (NS_2)
CXCR4-NLuc (9)	9.36 ± 0.30	38.8 ± 2.8 (NS_3)	8.24 ± 0.46	30.6 ± 4.7 (NS_3)

Potencies and efficacies are shown as mean ± S.E.M., n numbers are shown in brackets next to the cell line, potencies were shifted from CXCL12 to ATI-2341 but are not significantly (NS) different for one compound in different cell lines, efficacies differ from cell line to cell line but were NS different within one cell line using the two compounds.

4.3.1 Development of the CXCL12 NanoBRET assay

In a first step the NanoBRET binding assay was set up with fluorescent CXCL12 (CXCL12-red or CXCL12-green) in order to be able to measure ligand interactions with CXCR4 in equilibrium and determine equilibrium binding constants. The binding between CXCL12 and CXCR4 has previously been measured using a ^{125}I-CXCL12 radioligand, however this assay will allow us to test other CXCR4 ligands using higher concentrations than in radioligand binding assays and has further practical advantages over radioligands that have short shelf-lives and long signal acquisition times (Zwier *et al.*, 2010; Cottet *et al.*, 2013).

CXCL12-red and CXCL12-green are both labelled on their penultimate lysine with an Alexa Fluor 647® or Oregon Green® 488 respectively (ALMAC, Edinburgh UK). The CXCL12-CXCR4 interaction is highly dependent on the structure of the N-terminus of CXCL12, therefore the label was positioned on the C-terminus of CXCL12 (Xu *et al.*, 2013). However this positioning might have impacts on CXCL12-CXCL12 dimerisation.

Initially, the equilibrium binding constant of CXCL12-red in membranes made from cells stably expressing N-terminal NanoLuc tagged CXCR4 was determined using a saturation binding assay as described in **2.4 Assays** (**Figure 4-3 A**). In cells the interaction of receptor and ligand produce the activation of various signalling pathways with the interaction of other proteins or by internalisation (endocytosis) of the receptor into the cell potentially affecting the observed affinity. In membranes the receptor cannot internalise or signal, only interactions with membrane bound proteins are still possible. CXCL12-red was supplied by two different companies (Cisbio and ALMAC) over the course of the experiments. The affinity of both variants was tested in saturation binding experiments in HEK293G_NLuc-CXCR4 membranes and showed no significant difference in their affinities. CXCL12-red showed saturable high affinity binding over the concentration range tested in membranes with a pK_d of 7.61 ± 0.10 (27.4 nM, n=5) for Cisbio or a pK_d of 7.65 ±

0.07 (24.0 nM, n=5) for ALMAC. Non-specific binding was determined in the presence of 10 µM AMD3100. The non-specific binding component for CXCL12 was below 15 % in all cases.

Subsequently, the same technique was used to determine the equilibrium binding constant of CXCL12-red (Cisbio, Codolet, France) and CXCL12-green (ALMAC, Edinburgh, UK) in intact cells. CXCL12-red showed binding over the concentration range tested in cells with a pK_d of 7.15 ± 0.04 (K_d = 72.1 nM, n = 5, **Figure 4-3 B**). CXCL12-green showed a significantly different ($P < 0.05$) behaviour with a pK_d of 7.45 ± 0.06 (K_d = 36.2 nM, n = 5, **Figure 4-3 C**).

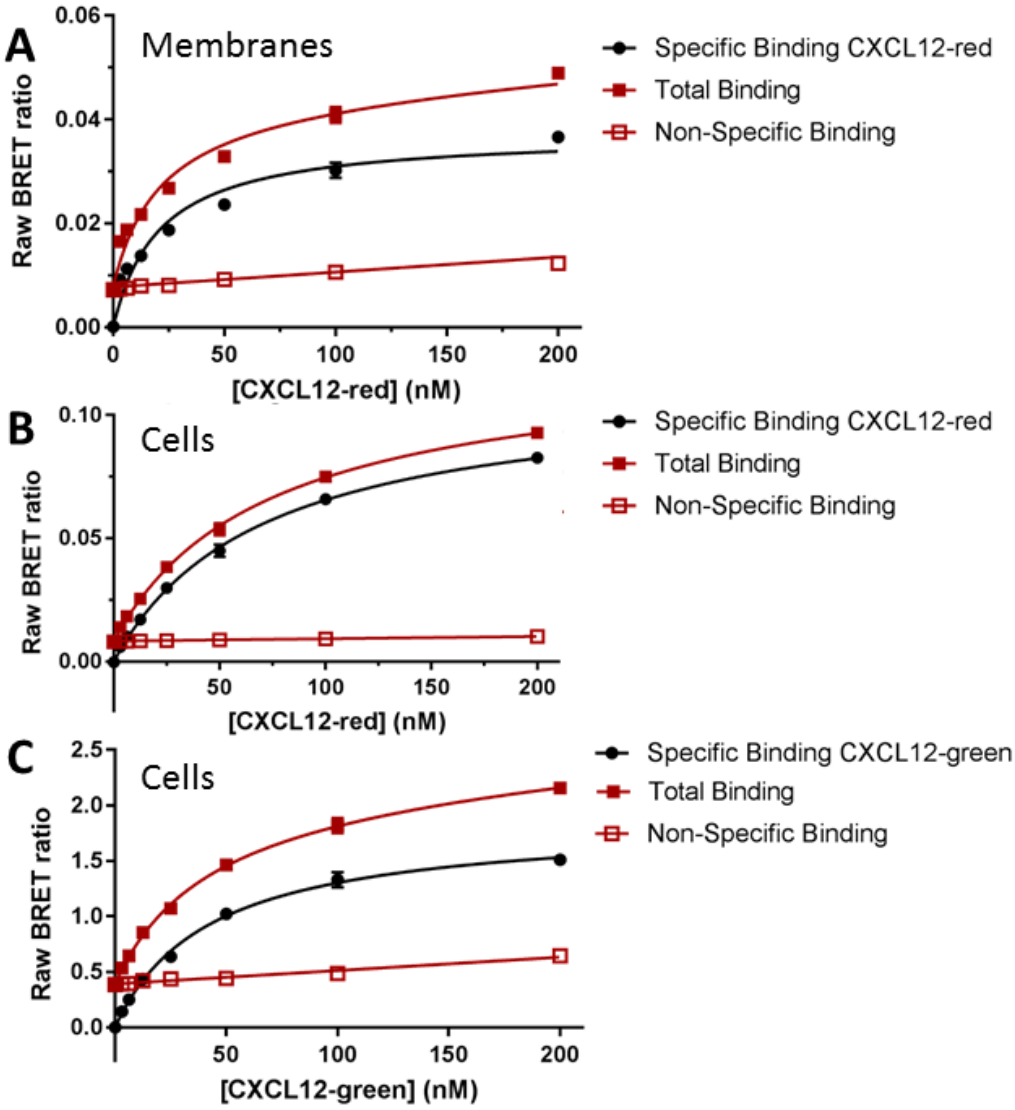

Figure 4-3: Saturation binding of CXCL12 variants in HEK293G_NLuc-CXCR4 membranes and cells. Membranes (**A**) or cells (**B, C**) were treated with different concentrations of CXCL12-red (**A, B**) or CXCL12-green (**C**) (■) or fluorescent CXCL12 and 10 µM AMD3100 (□) in a NanoBRET proximity assay, binding as Raw BRET ratio was calculated by dividing the emission of the fluorophore by the emission of the NLuc tag. Specific binding (●) was calculated by subtracting the non-specific binding from the total binding curve. Data are shown as mean ± S.E.M. of one individual experiment performed in triplicate. Similar data were obtained in four further independent experiments.

In a next step, CXCL12-red binding was studied in a kinetic binding assay in which the BRET values were read in real-time once every minute for 90 min using NanoLuc-CXCR4 cells and CXCL12-red as the ligand (**Figure 4-4**). The development of a kinetic version of the NanoBRET assay did not only allow us to investigate the kinetics of fluorescent ligands themselves but also study the influence of competing and allosteric ligands on the binding of the fluorescent ligand.

The profile for CXCL12-red binding to NLuc-CXCR4 cells shows a very rapid increase in BRET ratio followed by a slow decrease that lasts the full 90 min measuring window. Due to the decrease in BRET ratio it was not possible to fit the full 90 min measurement. Using only the first 20 min of association data, a pK_d can be obtained which was not significantly different to the one obtained with CXCL12-red in saturation binding (pK_d = 7.02 ± 0.08 (K_d = 104.8 nM, n = 7) (**Table 4-2**). Moreover, a k_{on} of 11.28 ± 1.74 x 10^6 M^{-1} min^{-1} and a k_{off} of 1.04 ± 0.11 min^{-1} was obtained. Since we were ultimately interested in the kinetics involved in pepducins interacting with whole cells (anchoring into the membrane and subsequent flipping) the kinetics in membranes were not measured.

Moreover a k_{obs} plot was generated from the observed association rate constants at each individual concentration. If the kinetic model is fitting for ligand and receptor the relationship should be linear. However, CXCL12 shows a behaviour that deviates from a linear relationship (**Figure 4-4 C**) probably due to internalisation effects or the observed multiple binding sites of chemokines.

The fitted equilibrium binding constants are shifted to significant higher affinities from cells to membranes (lower K_d, higher pK_d – see **Table 4-2**). The B_{max} values were significantly bigger in cells in comparison to membranes.

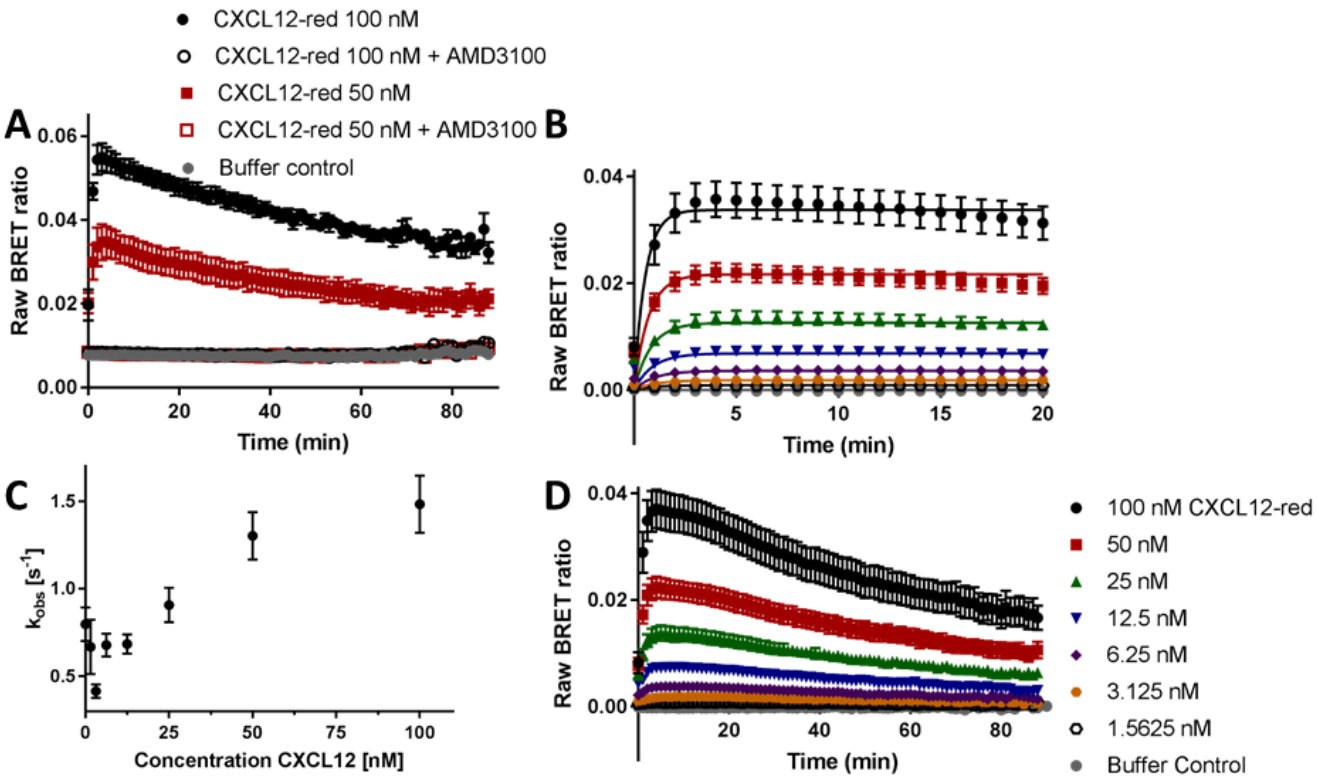

Figure 4-4: Kinetic binding of CXCL12-red to NLuc-CXCR4. HEK293G_NanolucCXCR4 cells were treated with different concentrations of CXCL12-red up to 100 nM or CXCL12-red and 10 µM AMD3100 in a NanoBRET assay. Binding shown as mean of the Raw BRET ratio ± S.E.M. Data are shown for (**A**) one individual experiment performed in triplicate showing the full 90 min measurement for CXCL12-red and CXCL12-red in the presence of AMD3100. Specific binding calculated by subtracting the non-specific binding with AMD3100 from the total binding of (**B**) the first 20 min or (**D**) the full 90 min measurement of n = 7 independent experiments, each performed in triplicates; (**C**) k_{obs} plot for the fitted first 20 min of the data.

Table 4-2: pK_d and B_{max} values obtained in CXCL12-red binding at NanoLuc-CXCR4 in cells and membranes

	pK_d (CXCL12-red)	**Maximal BRET ratio B_{max}**
Saturation in cells (5)	7.15 ± 0.04	0.112 ± 0.003 (200 nM)
Saturation in membranes (5)	7.61 ± 0.10 (CXCL12-red from Cisbio) 7.65 ± 0.07 (CXCL12-red from ALMAC)	0.035 ± 0.004 (200 nM)
Kinetic in cells (7)	7.02 ± 0.08	0.081 ± 0.012 (100 nM)

Equilibrium binding constants and B_{max} values of CXCL12 in cells and membranes shown as mean ± S.E.M., n numbers are shown in brackets next to the technique, equilibrium binding constant was shifted to significant higher affinities from cells to membranes (lower K_d, higher pK_d), B_{max} values were significantly bigger in cells

The third method in which the NanoBRET binding assay was used was to study the competition of unlabelled compounds with fluorescent ligands. These experiments were performed in order to determine if an unlabelled compound has a direct or indirect influence on the binding of the fluorescent ligand to its binding site. This assay was initially set up with CXCL12-red as the fluorescent ligand and CXCL12 and the two small molecules IT1t and AMD3100 as competing ligands in order to test if typical CXCR4 pharmacology was observed in the assay. According to literature all three compounds compete with CXCL12-red binding. The arising competition binding curves have a characteristic sigmoidal shape with decreased CXCL12-red binding at high concentrations of unlabelled compound (**Figure 4-5**). All unlabelled compounds displace CXCL12-red completely at high concentrations. The obtained equilibrium dissociation constants pK_i can be found in **Table 4-3**.

The maximal binding values for CXCL12-red in those experiments varied from plate to plate (from a raw BRET ratio of 0.018 to 0.047) and are therefore normalised as a percentage of the maximal response to CXCL12-red measured in each individual experiment.

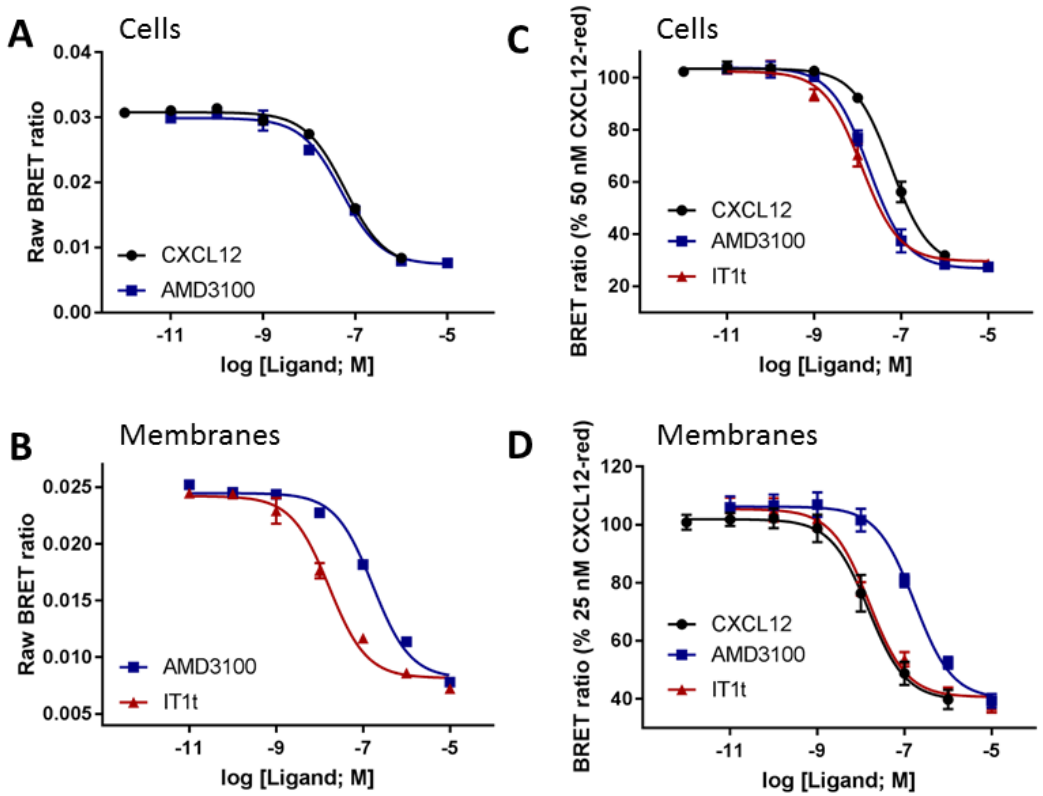

Figure 4-5: Competition binding of CXCL12-red with CXCL12, AMD3100 and IT1t. HEK293G_NLuc-CXCR4 cells (**A, C**) and membranes (**B, D**) were treated with 50 or 25 nM CXCL12-red respectively and increasing concentrations of CXCL12 (●), AMD3100 (■) or IT1t (▲) at the same time. Change in binding is expressed as a change in the normalized BRET ratio. Data are shown as mean ± S.E.M. of either one representative experiment performed in triplicate (**A, B**) or the combined data from 5 individual experiments, each performed in triplicates (**C, D**).

Table 4-3: pK_i values for competition binding of CXCL12-red and unlabelled compounds

Ligand	pK_i Membranes	Maximal BRET inhibition from total binding (% 25 nM CXCL12-red) in membranes (NS)	pK_i Cells	Maximal BRET inhibition from total binding (% 50 nM CXCL12-red) in cells (NS)
CXCL12	7.97 ± 0.07	60.4 ± 3.4 %	7.44 ± 0.09	72.4 ± 2.5%
AMD3100	7.00 ± 0.04	60.7 ± 2.4 %	8.08 ± 0.09	73.2 ± 1.9 %
IT1t	8.04 ± 0.01 (NS)	62.2 ± 2.5 %	8.16 ± 0.14 (NS)	70.5 ± 1.6%

pK_i values ± S.E.M. obtained in competition with CXCL12-red, all n = 5, maximal BRET inhibition was NS for different compounds within one system, pKi values are significantly different in cells and membranes for CXCL12 and AMD3100.

The pK_i values obtained in cells and membranes are close to each other for all compounds except AMD3100 which differs by a full log unit in potency. When measuring the binding of ligands towards receptors in membrane preparations half of the membranes will form vesicles that are flipped inside out blocking the access to the N-terminal side of the receptor (Creveling *et al.*, 1980). The different ligands could have different abilities to penetrate these flipped vesicles and are either able or unable to bind to half of the available receptors changing the actively measured concentrations needed to compete with CXCL12-red. The addition of saponin (Cohen *et al.*, 1996), a detergent causing permeabilization of membranes, should increase the amount of accessible receptor and thereby increase the B_{max} value for binding of the fluorescent ligand (**Figure 4-6**). Addition of saponin caused a significant increase in B_{max} of bound CXCL12-red (from 0.020 ± 0.004 to 0.038 ± 0.002, n=3, $P<0.05$) without causing a significant change in pK_d (from pK_d(CXCL12-red) = 7.56 ± 0.03 to pK_d(CXCL12-red + saponin) = 7.38 ± 0.12, n=3, $P>0.05$).

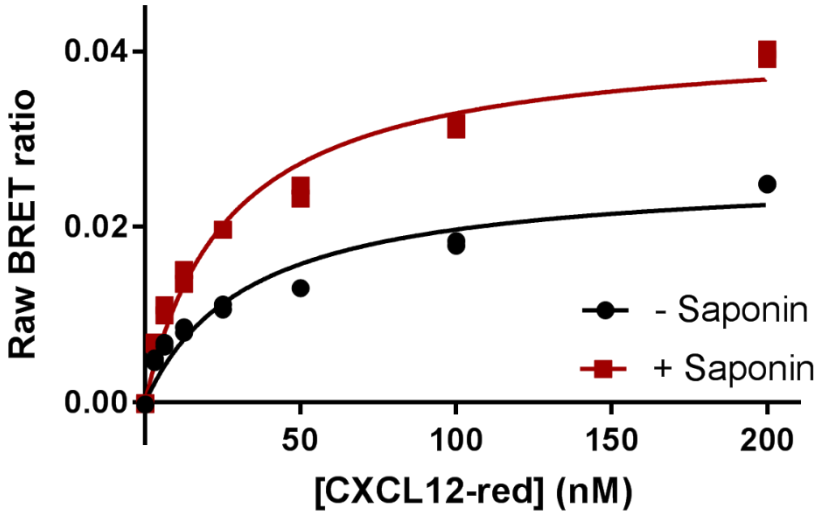

Figure 4-6: Binding of CXCL12-red to Nluc-CXCR4 in the presence and absence of saponin. Membranes were treated with different concentrations of CXCL12-red in a NanoBRET assay without saponin (●) or with with 0.25 mg/ml saponin (■), binding shown as specific binding portion of the Raw BRET ratio calculated by subtracting the response with 10 µM AMD3100 from the total binding. Data are shown as mean values from duplicate determinations of one individual experiment. Similar data were obtained in two more independent experiments.

Saponin was then added to membrane preparations in competition measurements of CXCL12-red and IT1t or AMD3100 to see if the membrane vesicles that are flipped inside have an influence on AMD3100 affinities (**Figure 4-7**). However, the addition of saponin did not shift the AMD3100 curve to its value observed in cells but to even lower affinities (pK_i(AMD3100, Membranes, Saponin)= 6.42 ± 0.01, n=3 in comparison to pK_i(AMD3100, Membranes)= 7.00 ± 0.04, n=5, significant and pK_i(IT1t , Membranes, Saponin)= 8.18 ± 0.02, n=3 in comparison to pK_i(IT1t , Membranes)= 8.04 ±0.01 n=5, not significant). Saponin was not added as a standard to membrane preparations as it did not seem to solve the reason for shifts in affinities and was only added when specifically mentioned. Moreover, detergents can have an influence on the fold of proteins and CXCL12 might be impacted.

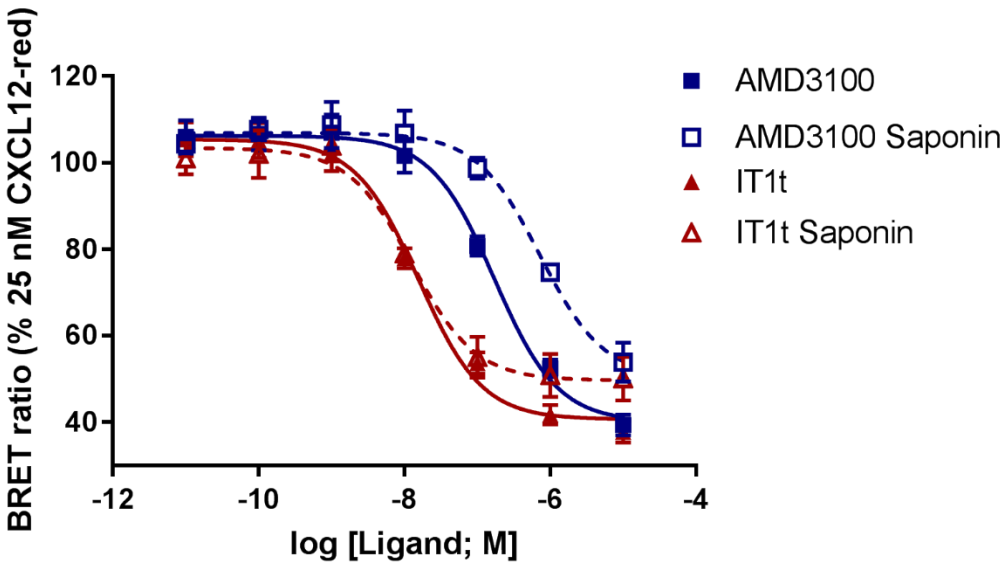

Figure 4-7: Competition binding of CXCL12-red with AMD3100 and IT1t with and without saponin. Membranes were treated with 25 nM CXCL12-red and increasing concentrations of AMD3100 (blue) or IT1t (red) at the same time in the absence (closed shapes) or presence (open shapes) of saponin. Inhibition of CXCL12-red binding as change of normalized BRET ratio, data are shown as mean ± S.E.M. of n=5 individual experiments performed in triplicates for experiments without and n=3 individual experiments performed in duplicate for experiments with saponin.

4.3.2 Binding of ATI-2341f

ATI-2341f is a fluorescent version of ATI-2341 which was designed and synthesised in a cooperation with ALMAC (Edinburgh, UK) as previously described in **3.2 Pepducin synthesis**.

The addition of a TAMRA tagged lysine to the peptide sequence increases the molecular weight of the compound by 540 g/mol which is about a quarter of its initial weight. Furthermore, at pH = 7 TAMRA is a polar molecule with a positively charged amine and a negatively charged acid. These changes in the molecule could have an influence on the binding properties and functional effects towards CXCR4. Because of this, the pepducin was tested for its ability to inhibit cAMP production in a GloSensor cAMP assay as described before (**Figure 4-8** and **Table 4-4**).

Increasing concentrations of pepducin inhibit cAMP production reaching a plateau at around 40% of the signal produced by 30 µM FSK. ATI-2341f showed an approximately 10-fold lower potency in comparison with the unlabelled ATI-2341 showing that the fluorescent version was still functionally active (**Table 4-4**). ATI-2341f did not seem to reach full saturation within the tested concentration range, the fitted potency was therefore only an estimation.

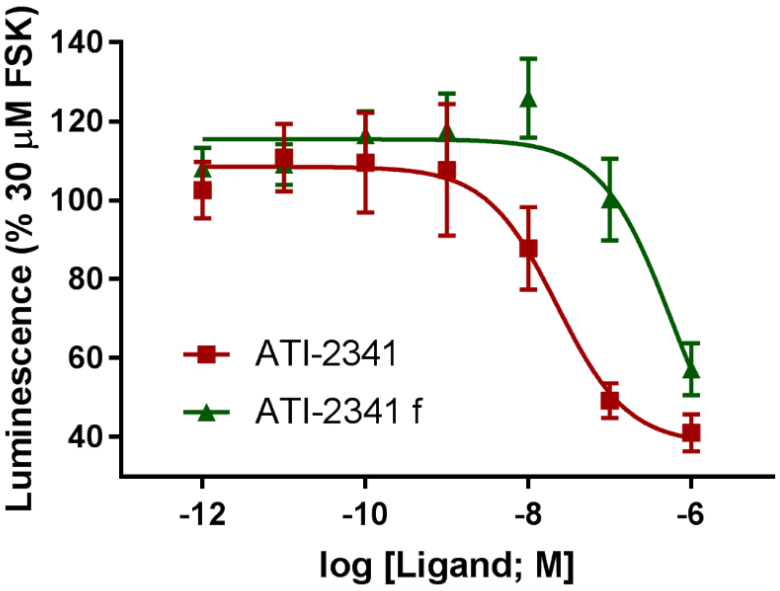

Figure 4-8: cAMP inhibition in HEK293G cells overexpressing CXCR4 in response to 30 µM and ATI-2341 or ATI-2341 f. Cells expressing SNAP-CXCR4 were stimulated with 30 µM FSK in the presence of ATI-2341 (■) or ATI-2341f (▲) in a GloSensor assay, response as luminescence read of the maximal signal as described in the Methods section. Data are shown as mean **±** S.E.M. of n = 5 independent experiments, each performed in triplicate. Data normalised to 30 µM FSK, measured on a PheraStar plate reader.

Table 4-4: GloSensor data for ATI-2341f in comparison to ATI-2341

	Peptide Sequence N-term: Pal C-term: NH_2	**pEC_{50} (GloSensor)**	**Maximal inhibition (% 30 µM FSK)**
ATI-2341	MGYQKKLRSMTDKYRL	7.63 ± 0.27	64.1 ± 5.2
ATI-2341f	K(TAMRA)-MGYQKKLRSMTDKYRL	6.64 ± 0.23	42.8 ± 6.6*

*not saturated

Pepducins are postulated to interact with the intracellular site of their receptor as described in detail in **1.4 Pepducins** and mentioned in the introduction of this chapter. Evidence of the binding mode of ATI-2341 has so far been based on modelling (Planesas *et al.*, 2015) and crosslinking a fluorescent pepducin ATI-2766 to CXCR4 and two mutants with a truncated N-terminus. These truncated CXCR4 receptors had reduced CXCL12 binding, but were still able to interact

with ATI-2766 suggesting a different binding site for ATI-2341 and CXCL12 (Janz *et al.*, 2011).

Because of the evidence suggesting intracellular binding two different cell lines were created, one with an N-terminal NanoLuc tag and one with a C-terminal NanoLuc tag in order to see where the pepducin positions itself in the cell membrane (**Figure 4-9**).

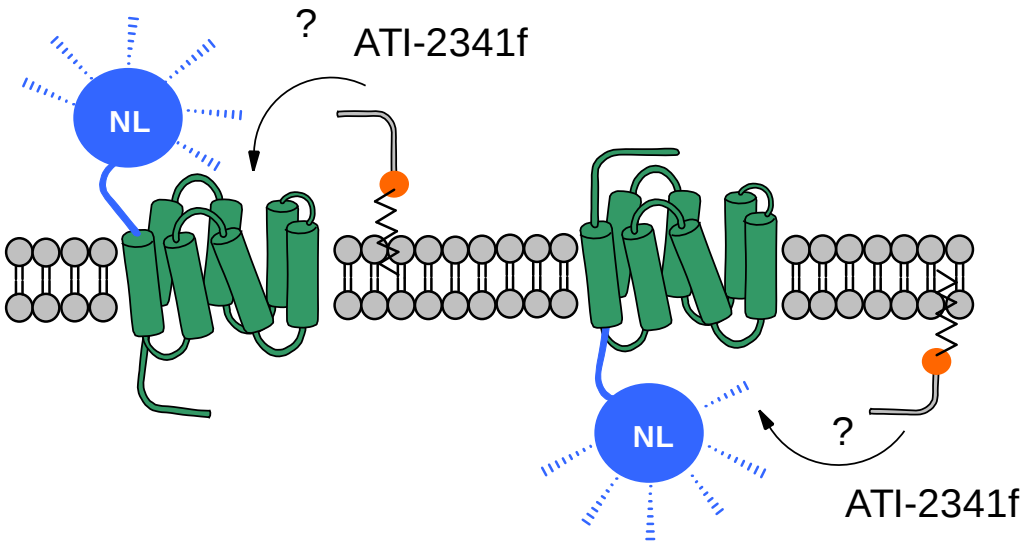

Figure 4-9: Potential ATI-2341f binding sites. Schematic representation of possible binding sites of ATI-2341f with CXCR4 observed in the NanoLuc proximity assay, represented in green and the N- and C-terminal NanoLuc-tag in blue.

ATI-2341f was added to membranes prepared from N-terminal and C-terminal tagged CXCR4 cells (**Figure 4-10**). Non-specific binding was determined by the addition of high concentrations of unlabelled ATI-2341 (30 µM). Both membrane preparations showed an increase in BRET ratio with increasing concentrations of ATI-2341f. However, while the N-terminal tagged CXCR4 shows a very small to no displaceable portion of BRET ratio dependent on repetition, the C-terminal tagged CXCR4 shows displaceable increase in BRET ratio by ATI-2341f suggesting an interaction specific to the C-terminal part

of the receptor. An equilibrium binding constant was not fitted due to the fact that no saturation was reached. Moreover, the raw donor and acceptor counts were plotted for all measurements. The N-terminal tagged CXCR4 cells show higher NanoLuc counts in comparison to the C-terminal tagged CXCR4 cells.

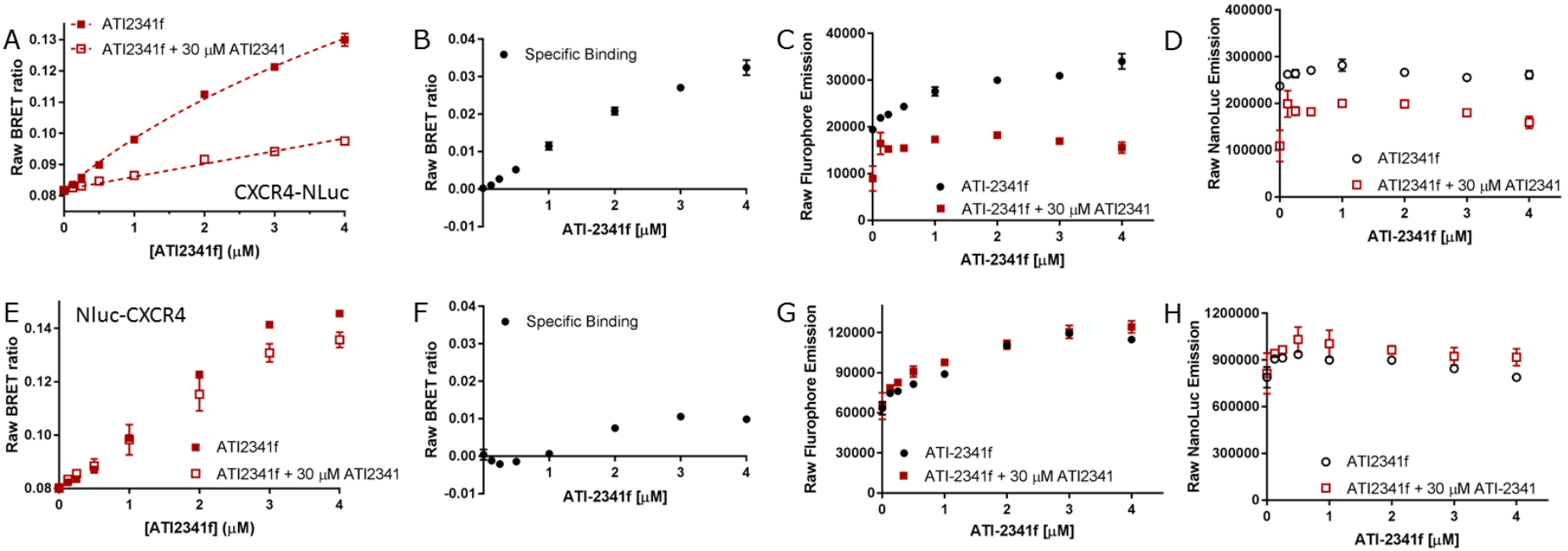

Figure 4-10: Saturation binding of ATI-2341f at CXCR4-NLuc and NLuc-CXCR4. (**A, E**) Membranes of CXCR4 cells were treated with different concentrations of ATI-2341f and buffer (■) or ATI-2341f and 30 µM ATI-2341 (□) in a NanoBRET assay, binding as Raw BRET ratio was calculated by dividing the emission of the fluorophore by the emission of the NLuc tag. (**B, F**) Specific Binding BRET (●) was calculated by subtracting the binding with 30 µM ATI-2341 from the total binding curve. Data are shown as mean ± S.E.M. of one individual experiment performed in triplicate. Similar results were obtained 4 more times for (**A, B, C, D**) HEK293G_CXCR4-NanoLuc and 3 more times for (**E, F, G, H**) HEK293G_NanoLuc-CXCR4. (**C, F**) showing the raw acceptor counts and (**D, H**) the raw donor counts for the experiments shown in A (C, D) and E (G, H).

In a next step we were interested to see if the localization of the pepducin ATI-2341f to the inner leaflet of the membrane was specific to membranes made from cells transfected with CXCR4. Because of this we used HEK293G cells stably transfected with NanoLuc-tagged ACKR3 constructs. CXCR4 and ACKR3 do not share a similar ICL1 sequence.

CXCR4-il1: MGYQKKLRSMTDKYRL

ACKR3-il1: NSVVVWVNIQAKTTGYDTHC

Interestingly, very similar data were obtained – both the N-terminal and C-terminal tagged cell membranes show an increase in BRET ratio with increasing ATI-2341f concentration. However, a clear displaceable BRET signal can only be measured with a C-terminal tagged receptor in membranes from HEK293G_ ACKR3-NanoLuc cells (**Figure 4-11**) while the N-terminal tagged cells show only a very small displaceable portion. Moreover, it is notable that the increase in BRET ratio at the N-terminal tagged ACKR3 is larger than the C-terminal BRET ratio or any of the CXCR4 signals. In the case of ACKR3 the C-terminal tagged cells show higher donor counts than the N-terminal tagged ones.

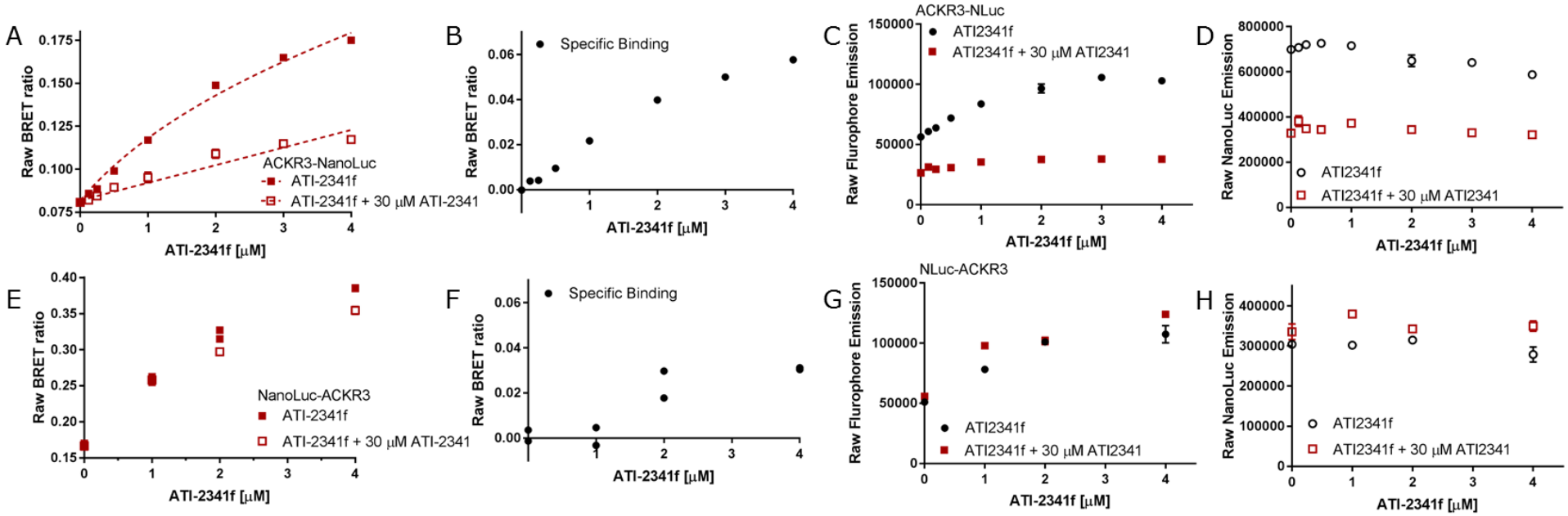

Figure 4-11: **Saturation binding of ATI-2341f at ACKR3-NLuc and NLuc-ACKR3.** (**A, E**) Membranes of ACKR3 cells were treated with different concentrations of ATI-2341 f and buffer (■) or ATI-2341f and 30 µM ATI-2341 (□) in a NanoBRET assay, binding as Raw BRET ratio was calculated by dividing the emission of the fluorophore by the emission of the NLuc tag. (**B, F**) Specific binding (●) was calculated by subtracting the binding with 30 µM ATI-2341 from the total binding curve. Data are shown as mean ± S.E.M. for ACKR3-NLuc (**A, B**) of one individual experiment performed in triplicate. For NLuc-ACKR3, data are shown as mean values from duplicate determinations of one individual experiment. Similar results were obtained four more times for (**A, B, C, D**) HEK293G_ACKR3-NanoLuc and three more times for (**E, F, G, H**) HEK293G_NanoLuc-ACKR3. (**C, F**) showing the raw acceptor counts and (**D, H**) the raw donor counts for the experiments shown in A (C, D) and E (G, H).

Subsequently, the binding of ATI-2341f was tested in whole cells expressing CXCR4-NLuc. The addition of 2 µM ATI-2341f showed a non-significant increase in raw BRET ratio. However, the addition of high concentrations of unlabelled ATI-2341 at the same time as fluorescent ATI-2341f showed an even bigger significant increase of raw BRET ratio instead of the expected decrease (**Figure 4-12 A**).

Pepducins interact with the cell membrane and therefore high concentrations might cause cell death or punctured membranes making the entry of the fluorescent version into the cell easier. Because of this, the disruption of cells was controlled after 2h of incubation with pepducin by measuring the Lactate dehydrogenase (LDH) concentration in media which is only released from the cell cytosol in case of cell damage. Cells treated with buffer served as a negative control and cells lysed with the cell lysis buffer included in the kit served as a positive control. Measurements showed a significant increase of LDH concentration in the buffer after 2h with 30 µM ATI-2341 therefore suggesting the disruption of membranes by pepducin at this time and concentration (**Figure 4-12 B**).

Therefore, experiments were repeated using cells pre-treated with 1 mg/ml saponin in order to permeablize the cells beforehand. After the treatment with saponin a significant larger increase was observed when adding 2 µM ATI-2341f. The addition of unlabelled ATI-2341 causes a non-significant decrease of raw BRET ratio in the combined data (**Figure 4-13**). However, in all individual experiments the decrease was significant. The saponin treated cells differ from membranes in the fact that they are plated as cells before the experiment and saponin was directly added to the wells instead of breaking up the cells mechanically and using a subsequent spinning, resolubilising, and freezing procedure.

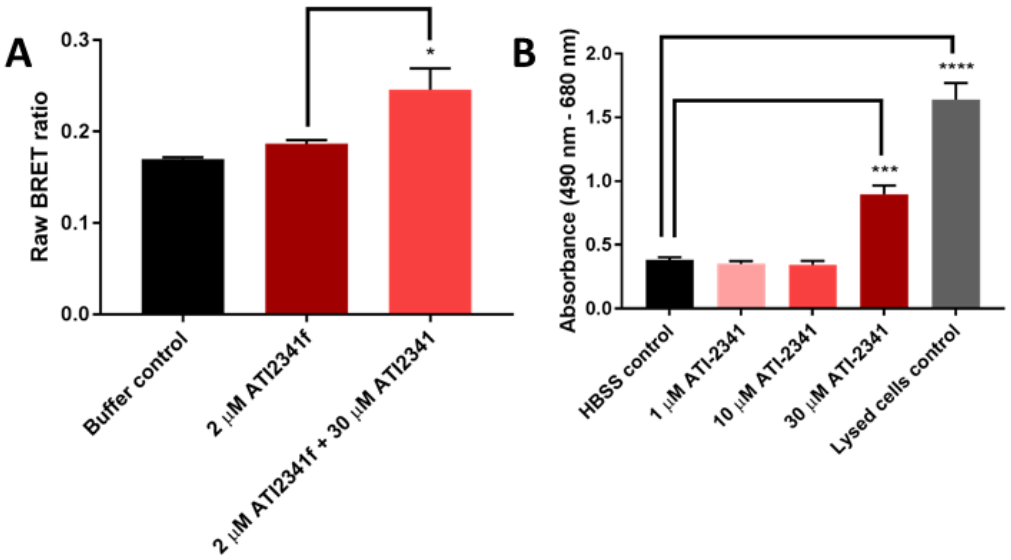

Figure 4-12: Binding of ATI-2341f at CXCR4-NLuc cells and LDH toxicity measurement. (**A**) HEK293G_CXCR4-NLuc cells were treated with 2 μM ATI-2341f and buffer or 2 μM ATI-2341f and 30 μM ATI-2341. Response as Raw BRET ratio, data shown as mean ± S.E.M. of n=5 independent experiments performed in triplicate. (**B**) HEK293G_CXCR4-NLuc cells were treated with 1, 10 or 30 μM ATI-2341 for 2h or lysed as a control. Response as absorbance proportional to LDH concentration, data are shown as mean ± S.E.M. of an n=5 individual experiment performed in triplicates. One-way ANOVA test followed by a Tukey's multiple comparisons test, number of stars showing significance between the measurements; P = 0.1234 (ns), P = 0.0322 (*), P = 0.0021 (**), P = 0.0002 (***), P<0.0001 (****)

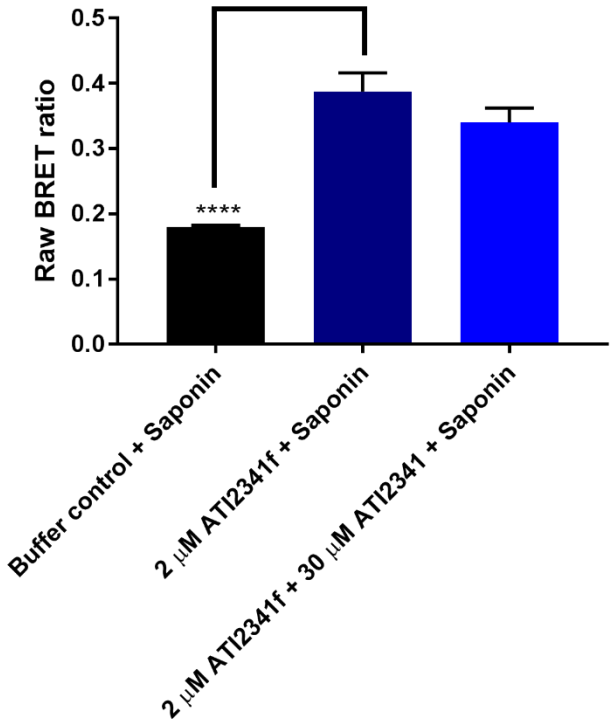

Figure 4-13: Binding of ATI-2341f at CXCR4-NLuc cells treated with saponin. HEK293G_CXCR4-NLuc cells were treated with 1 mg/ml saponin and 2 µM ATI-2341f or 2 µM ATI-2341f and 30 µM ATI-2341 at the same time. Response as Raw BRET ratio, data shown as mean ± S.E.M. of n=5 independent experiments performed in triplicate. One-way ANOVA test followed by a Tukey's multiple comparisons test, number of stars showing significance P = 0.1234 (ns), P = 0.0322 (*), P = 0.0021 (**), P = 0.0002 (***), P<0.0001 (****).

Next, various unlabelled ligands were tested in their ability to modulate the binding of ATI-2341f in order to see which compounds were able to compete directly with ATI-2341f or have an allosteric effect on the binding. However, modulating the binding of ATI-2341f seemed to be challenging. Increasing concentrations of unlabelled compounds were added to 2 µM ATI-2341f in HEK293G_CXCR4-NanoLuc membranes. CXCL12 (up to 1 µM), AMD3100 (up to 100 µM) and IT1t (up to 100 µM) were all unable to displace ATI-2341f at the tested concentrations. The only compounds displacing ATI-2341f were other pepducins (**Figure 4-14**). However, all tested pepducins had the same potency in interfering with ATI-2341f binding independent of their ability to activate CXCR4. In order to test pepducins with different properties ATI-2341, ATI-2346 and ATI-

2341TA were used. ATI-2346 has been published as a PAM for CXCR4 (Carlson *et al.*, 2012) and ATI-2341TA discussed in more detail as a pepducin variant in chapter 6 of this thesis showed a 10-fold lower potency towards CXCR4 in comparison to ATI-2341 in binding and cAMP assays. The observed decrease has a very steep slope and does not reach saturation (full sigmoidal curve shape) within the tested concentration range (up to 30 µM). This might be due to the influence of the pepducin on membrane vesicles. As a control palmitic acid was used, to see if a dilution effect or the increase in lipid caused the decrease in binding. Palmitic acid had no effect on ATI-2341f binding.

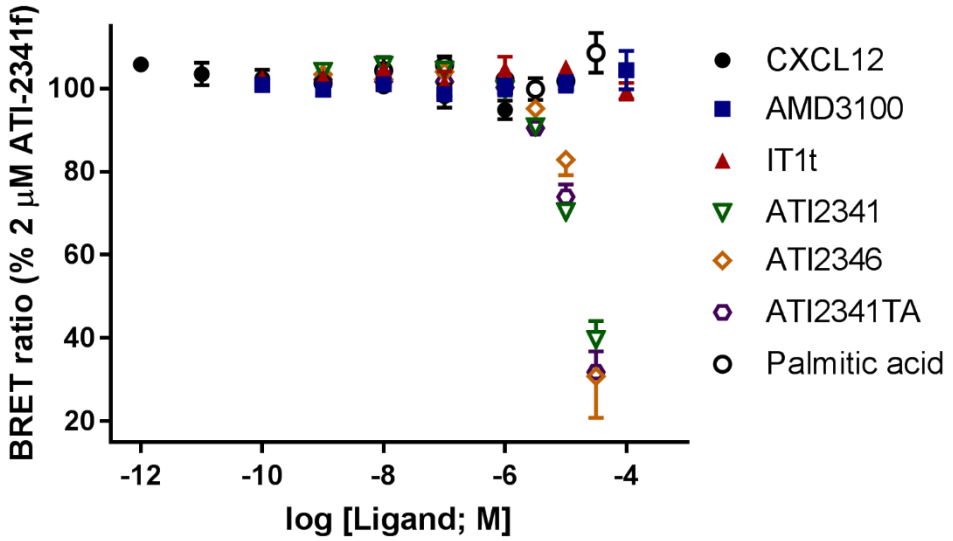

Pepducin	**Sequence**
ATI-2341	Pal-MGYQKKLRS MTDKYRL-NH_2
ATI-2346	Pal- KKLRSMTDK YRL-NH_2
ATI-2341TA	Pal-MGYQKKLRS MADKYRL-NH_2
ATI-2341f	Pal-K(TAMRA)-MGYQKKLR SMTDKYRL-NH_2

Figure 4-14: Competition binding assay of ATI-2341f with unlabelled CXCR4 ligands. HEK293G_CXCR4-NanoLuc cell membranes were treated with 2 µM ATI-2341f and increasing concentrations of unlabelled compounds at the same time in a BRET assay, binding as BRET ratio normalised to ATI-2341f. CXCL12 (●), AMD3100 (■), IT1t (▲) and Palmitic acid (○) did not interfere ATI-2341f binding, ATI-2341 (▽), ATI-2346 (◇) and ATI-2341 TA (⬡) did all interfere with ATI-2341f binding at high concentrations, all pepducins do not reach saturation and show a steep slope. Data are shown as mean ± S.E.M. of n = 3 independent experiments, each performed in triplicate.

Then, the kinetic binding of ATI-2341f to CXCR4 was monitored using HEK293G_CXCR4-NanoLuc cells treated with 1 mg/ml saponin measuring the BRET ratio once every minute as previously set up with CXCL12-red. The implied binding mechanism of the pepducin (Covic *et al.*, 2002; Kuliopulos and Covic, 2003) involves a multistep procedure of anchoring of the lipid tail into the cell membrane and subsequent flipping of the pepducin into the cell before interaction with the receptor can take place as explained in more detail in **1.4 Pepducins.** This suggests possible slow kinetics in comparison to extracellular ligands that were tested in this assay. The profile of ATI-2341f shows a much slower increase in Raw BRET ratio than CXCL12-red and reaches a plateau after about 15 min (**Figure 4-15**). It was not possible to subtract the amount of non-specific binding as there was no ligand available to fully displace ATI-2341f as seen in the competition binding measurements before. However, as a rough estimate the total binding subtracted by the buffer trace was fitted as a specific binding curve to obtain an equilibrium dissociation constant, association and dissociation rate resulting in a pK_d of 4.91 ± 0.17 (K_d = 17.29 µM, n=5), a k_{on} of 3.68 ± 1.46 x 10^4 M^{-1} min^{-1} and a k_{off} of 0.30 ± 0.05 min^{-1}. These apparent k_{on} and k_{off} rates are impacted by the permeabilization of the membrane as the multistep association mechanism might be impacted by this. Moreover, the k_{obs} plot shows that the kinetic model is not fitting for the interaction of pepducin and CXCR4 (**Figure 4-15 C**).

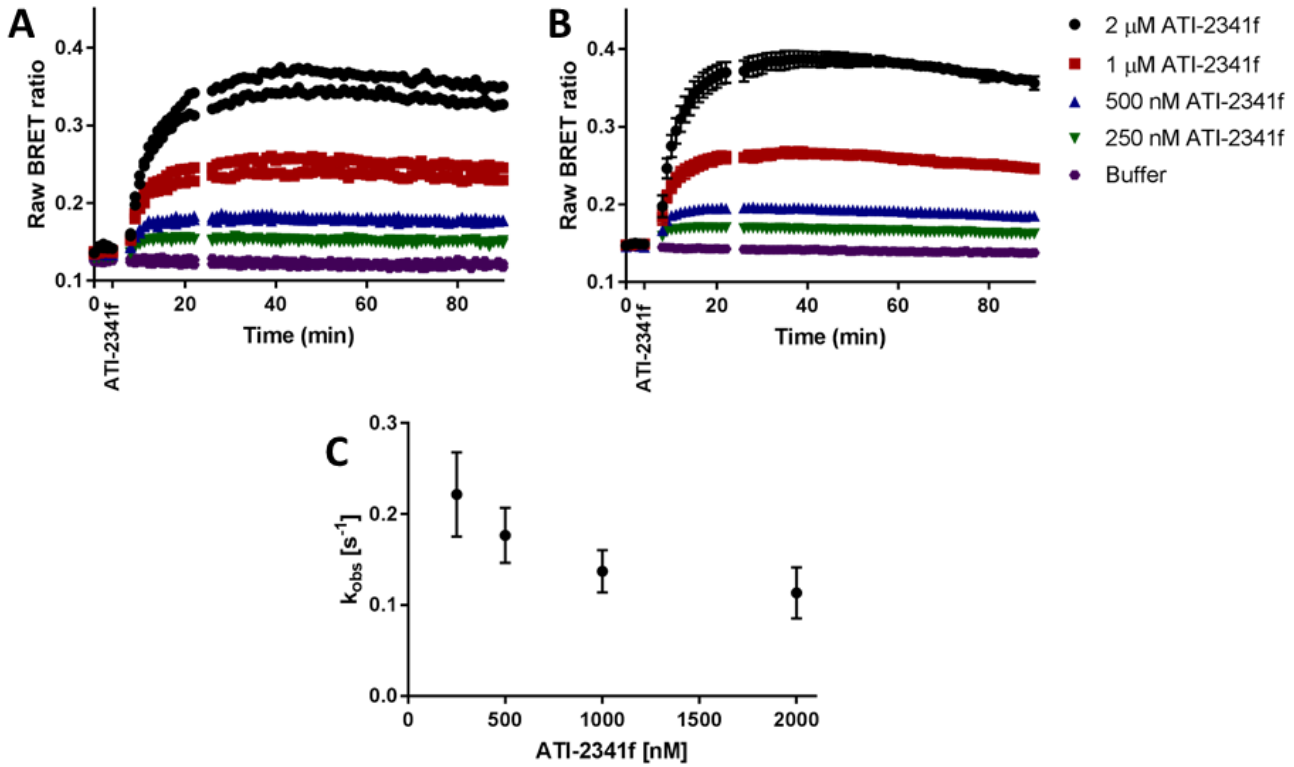

Figure 4-15: **Kinetic binding of ATI-2341f to CXCR4-NLuc.** HEK293G_CXCR4Nanoluc cells were treated with 1 mg/ml saponin and different concentrations of ATI-2341f up to 2 µM in a NanoBRET assay, binding as Raw BRET ratio. Data are shown for full 90 min for (**A**) one representative experiment showing the mean of duplicate determinations, (**B**) pooled data and (**C**) k_{obs} plot for association of ATI-2341f shown as mean ± S.E.M for n = 5 independent experiments, each performed in duplicates. Gaps in the time traces arise from the addition of compounds in other wells.

In a next step the kinetic findings and competition binding measurements were combined in a kinetic binding assay adding ATI-2341, CXCL12, AMD3100 or IT1t to the cells after 15 min of initial binding period of ATI-2341f (**Figure 4-16**). The extracellular compounds were added in order to see if any of them had an allosteric effect on the binding pocket of ATI-2341f. ATI-2341 was added as a competitor of ATI-2341f in order to see the kinetics involved of displacing already bound pepducin. There was no change in BRET ratio observable after the addition of CXCL12, IT1t or AMD3100. When using ATI-2341 to displace ATI-2341f the signal was decreased with a k_{off} = 0.013 ± 0.003 min^{-1} and reached a plateau of 69.7 ± 3.1 % of the signal of the untreated ATI-2341f within 15 min. The percentage of displaced ATI-2341f was consistent for all concentrations of fluorescent ligand with 2 µM ATI-2341f with 30 µM ATI-2341 reaching 70.4 ± 4.1 % of the 2 µM ATI-2341f signal, 1 µM ATI-2341f with 30 µM ATI-2341 reaching 68.8 ± 2.8 % of the 1 µM ATI-2341f signal and 0.5 µM ATI-2341f with 30 µM ATI-2341 reaching 69.7 ± 3.0 % of the 0.5 µM ATI-2341f signal.

The k_{off} determined for ATI-2341f in this experiment is 20x smaller than the one determined with ATI-2341 association kinetics (**Figure 4-15**). This is probably due to the fact that not enough ATI-2341 was used to compete ATI-2341f binding completely and prevent rebinding of ATI-2341f resulting in incomplete dissociation.

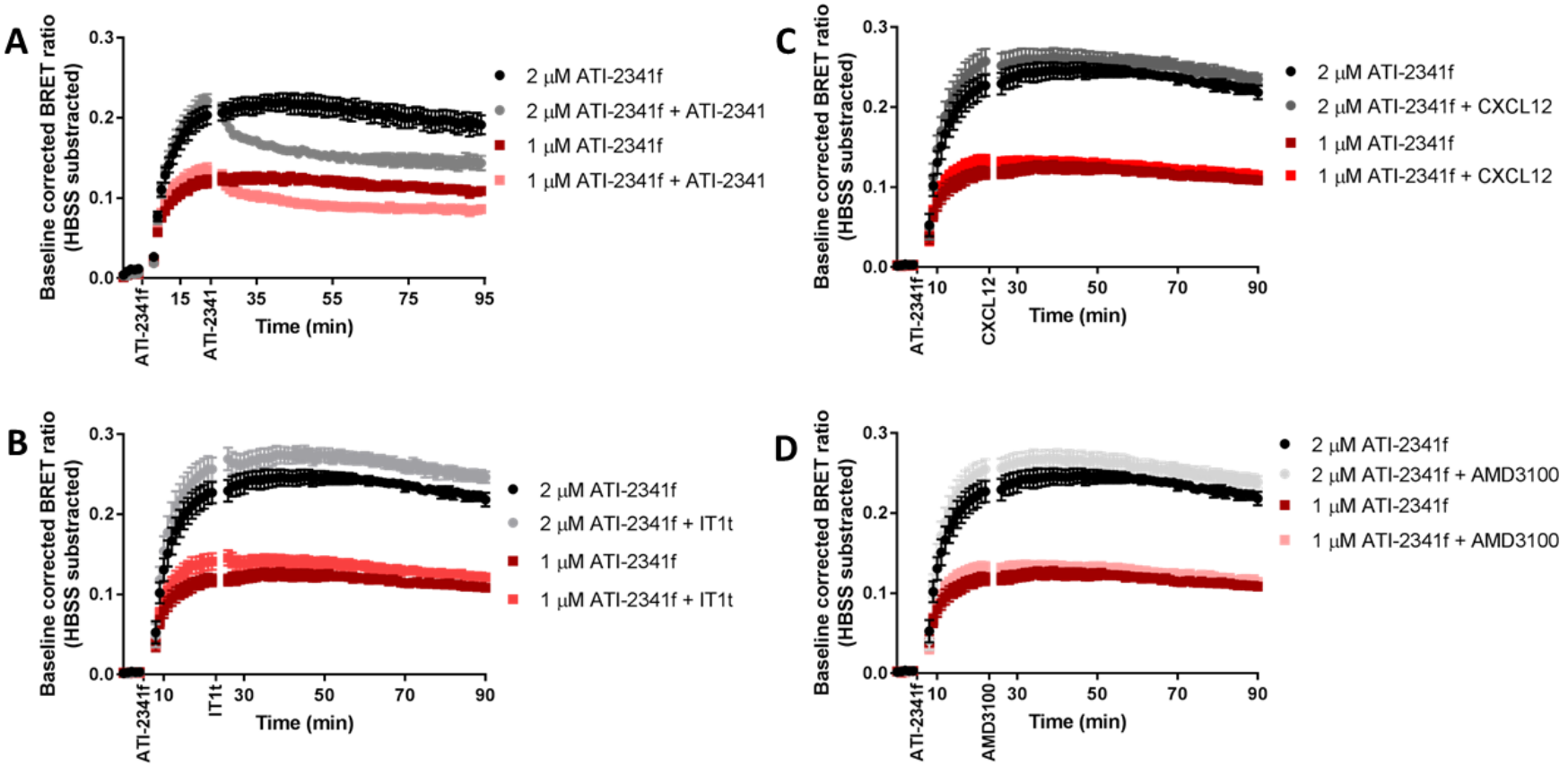

Figure 4-16: Kinetic binding of fixed concentrations of ATI-2341f to CXCR4-NLuc with addition of unlabelled compounds after 15 min. HEK293G_CXCR4-NanoLuc cells were treated with 1 mg/ml saponin and two concentrations of ATI-2341f (1 or 2 µM) in a NanoBRET assay, after 15 min (**A**) 30 µM ATI-2341, (**B**) 10 µM CXCL12, (**C**) 100 µM IT1t or (**D**) 100 µM AMD3100 were added. Binding is shown as a change in raw BRET ratio. Data are shown as mean ± S.E.M. for n = 5 independent experiments, each performed in duplicate.

4.3.3 Cell Imaging

After measuring the binding of CXCL12-red and ATI-2341f to CXCR4 in a BRET assay, the binding of the fluorescent pepducin and colocalization with the receptor was visualised using both bioluminescence imaging and fluorescent confocal microscopy in order to see where the colocalization of ligands and receptor occurs (on the cell membrane or intracellularly), as the BRET assay gives no information about the location in the cell of the interaction.

4.3.3.1 Bioluminescence Imaging

NanoLuc-CXCR4 and CXCR4-NanoLuc cells were imaged live using a Olympus LV200 bioluminescence microscope 20 min after the addition of furimazine (20 µM final concentration) in the absence and presence of 1 µM ATI-2341f pre-incubated for 30 min (**Figure 4-17**) at 37 °C as described in **2.5.2. Bioluminescence imaging**.

In the plate-based BRET assays a displaceable BRET ratio was only observable for the C-terminal tagged CXCR4 therefore we were interested to see if there are differences visible in the image-based technique. The TAMRA channel monitors emissions from 550 nm which is close to the NanoLuc emission peak of 460 nm. This results in an observable signal in the TAMRA channel caused by bleed through of the bioluminescence before adding any compound. When adding the ligand ATI-2341f to the cells both cell lines (transfected with C- and N-terminal tagged CXCR4 versions) showed a significant increase in BRET ratio (**Figure 4-18**) when analysing with Fiji ImageJ as described previously in **2.5.3. Bioluminescence Imaging** by drawing regions of interest and analysing their brightness values excluding any cells that reached the maximum detection level. The increase in BRET was not immediately apparent from the imaging. The increase in BRET at the N-terminal tagged receptor was bigger than the C-terminal tag.

High concentrations of pepducin cause changes in the cell membranes as seen in the LDH assay in **4.2.1 Binding of ATI-2341f**. Because of this, analysing image based techniques with high concentrations of

pepducin was difficult and the displacement with high concentrations of unlabelled pepducin was not measured.

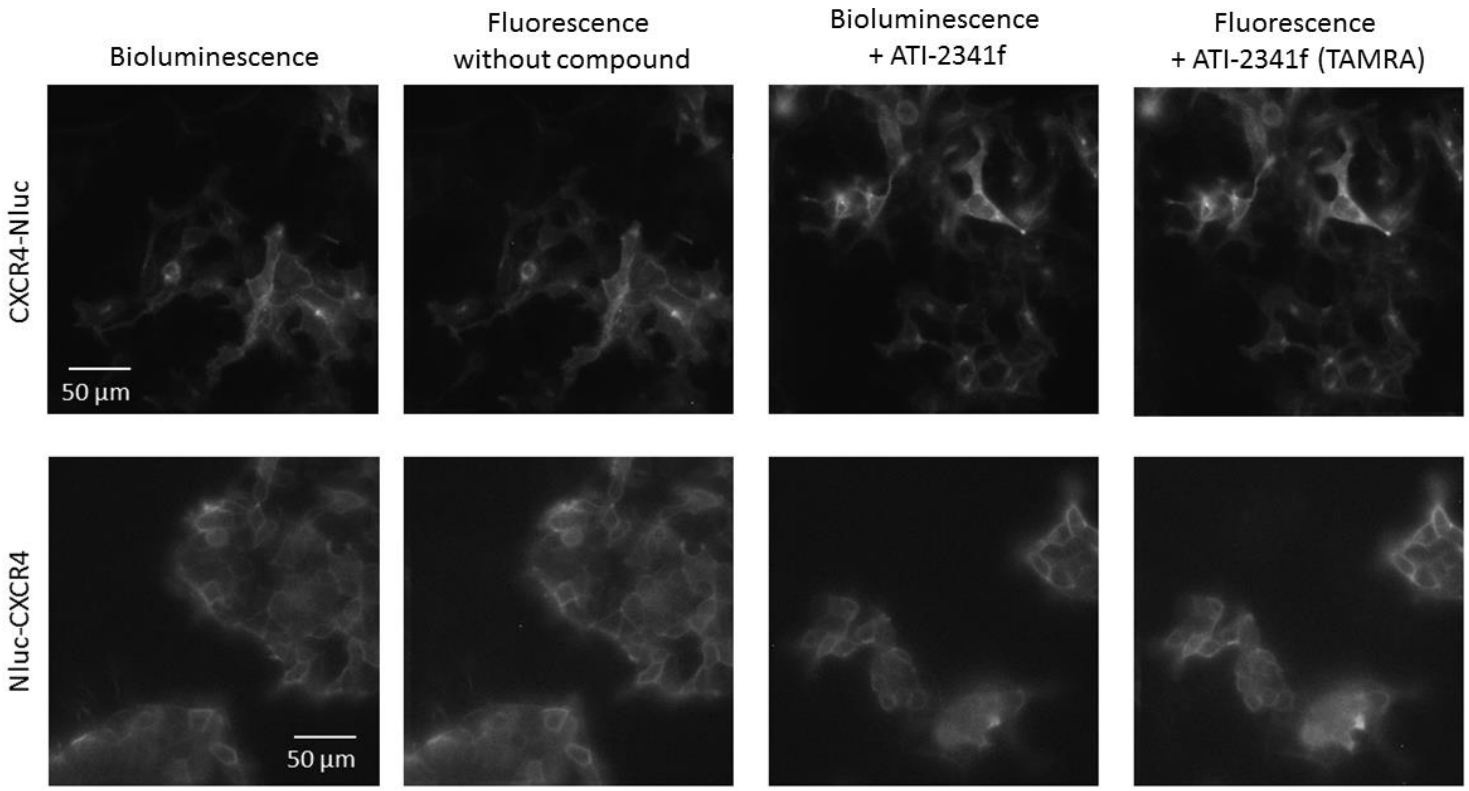

Figure 4-17: **Bioluminescence imaging of CXCR4 and ATI-2341f.** HEK293G-CXCR4-NanoLuc or HEK293G_NanoLuc-CXCR4 cells were imaged using an Olympus LV200 microscope 20 min after addition of furimazine and optional 30 min pre incubation with 1 µM ATI-2341 at 37 °C. Bioluminescence of the cells was monitored through an emission DAPI filter (row 1 and 3), the TAMRA tagged fluorophore was then excited by the bioluminescence of the NLuc-tag and monitored (row 4), however also in the absence of ligand a signal can be observed in the fluorophore channel (row 2). Data are shown as one representative image, similar images were obtained 3 more times for CXCR4-NanoLuc and 2 more times for NanoLuc-CXCR4 cells.

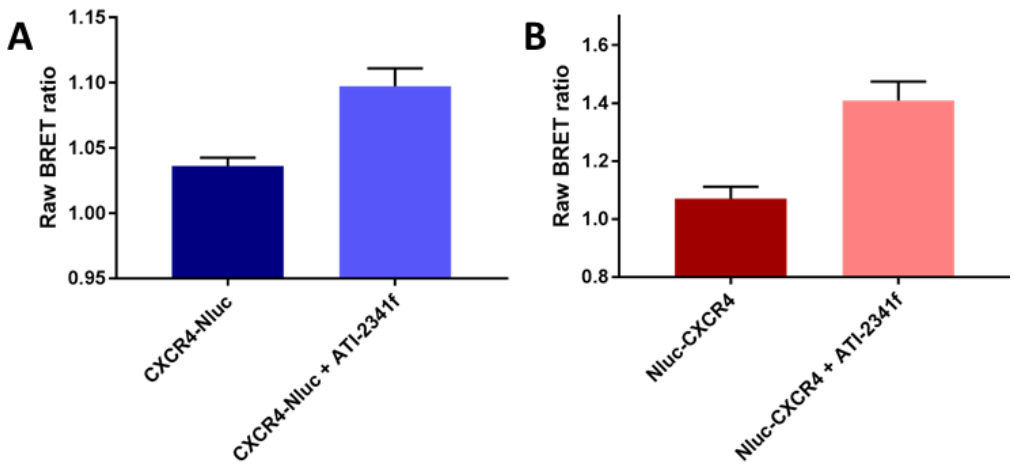

Figure 4-18: Quantification of Bioluminescence imaging of CXCR4 and ATI-2341f. HEK293G_CXCR4-NanoLuc cells (**A**) and HEK293G_NanoLuc-CXCR4 (**B**) cells were imaged with an Olympus LV200 microscope before and after addition of 1 µM ATI-2341f. BRET ratios were quantified via image analysis as described in the Methods section by dividing the fluorophore emission by the bioluminescence emission. Data are shown as mean ± S.E.M. for n = 4 (CXCR4-NLuc) or n = 3 (NLuc-CXCR4) independent experiments.

4.3.3.2 Fluorescent Confocal Microscopy

All confocal imaging was performed as described in **2.5.3 Confocal imaging** on a Zeiss 710 Confocal Microscope with HEK293G cells stably expressing CXCR4 with an N-terminal SNAP-tag which was labelled beforehand for 30 min with 0.5 µM SNAP-Surface-Alexa Fluor 488.

Our confocal experiments show that as expected CXCR4 was constitutively predominantly located in the cell membrane (**Figure 4-19** – first row). The addition of ligands can impact this localisation, CXCL12-red causes CXCR4 to internalise upon binding as visualized in the confocal imaging. CXCR4 can be found intracellularly after 30 min incubation with CXCL12-red. The agonist CXCL12-red seemed to internalise with the receptor and colocalise with it not only in the outer cell membrane but also inside the cell (**Figure 4-19** – second row). The subsequent addition of AMD3100 can displace binding of CXCL12-red from the cells (**Figure 4-20**) but does not bring the already internalised CXCR4 back to the cell surface.

ATI-2341f was observed to localize into the cell membrane of the HEK293G_SNAP-CXCR4 cells (**Figure 4-21**). However, it seemed like the pepducin anchors itself in all cells independent of expression levels of SNAP-CXCR4. Moreover, the orientation of the peptide in the pepducin was unclear as it could either localise at the inner or outer leaflet of the membrane. Apart from the cell membranes the pepducin also seemed to cover any glass or plastic surfaces.

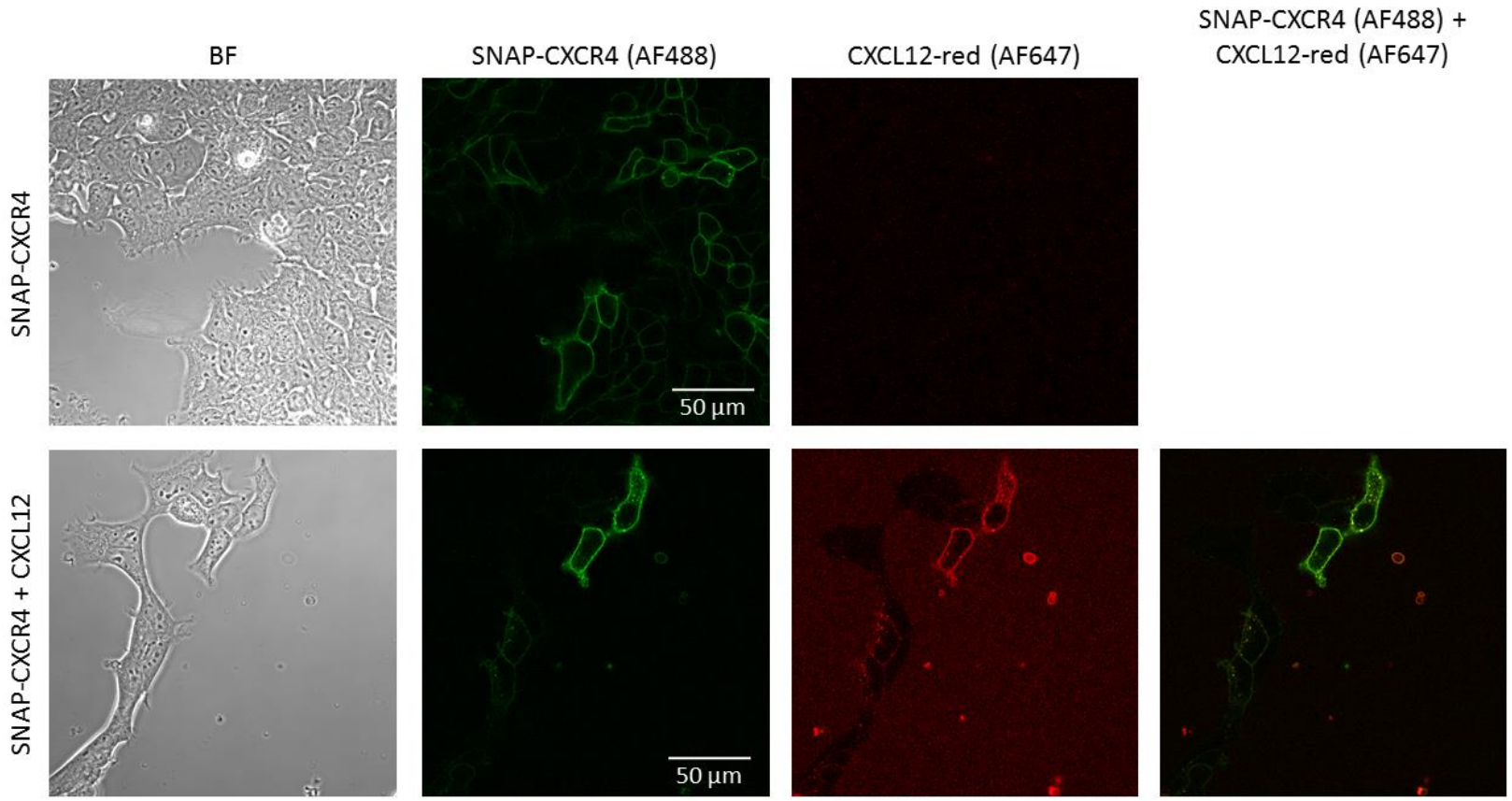

Figure 4-19: **Confocal Imaging of SNAP-CXCR4 with CXCL12-red.** HEK293G_SNAP-CXCR4 cells were imaged after SNAP labelling (first row) and after 30 min incubation with 25 nM CXCL12-red (second row) as described in the Methods section. The first column showing the Bright field image, the second the SNAP-tagged receptor, the third Alexa Fluor 647 tagged CXCL12 and the last the combined images of Alexa Fluor 488 and 647. Data are shown as one representative image, similar images were obtained 6 more times for both conditions.

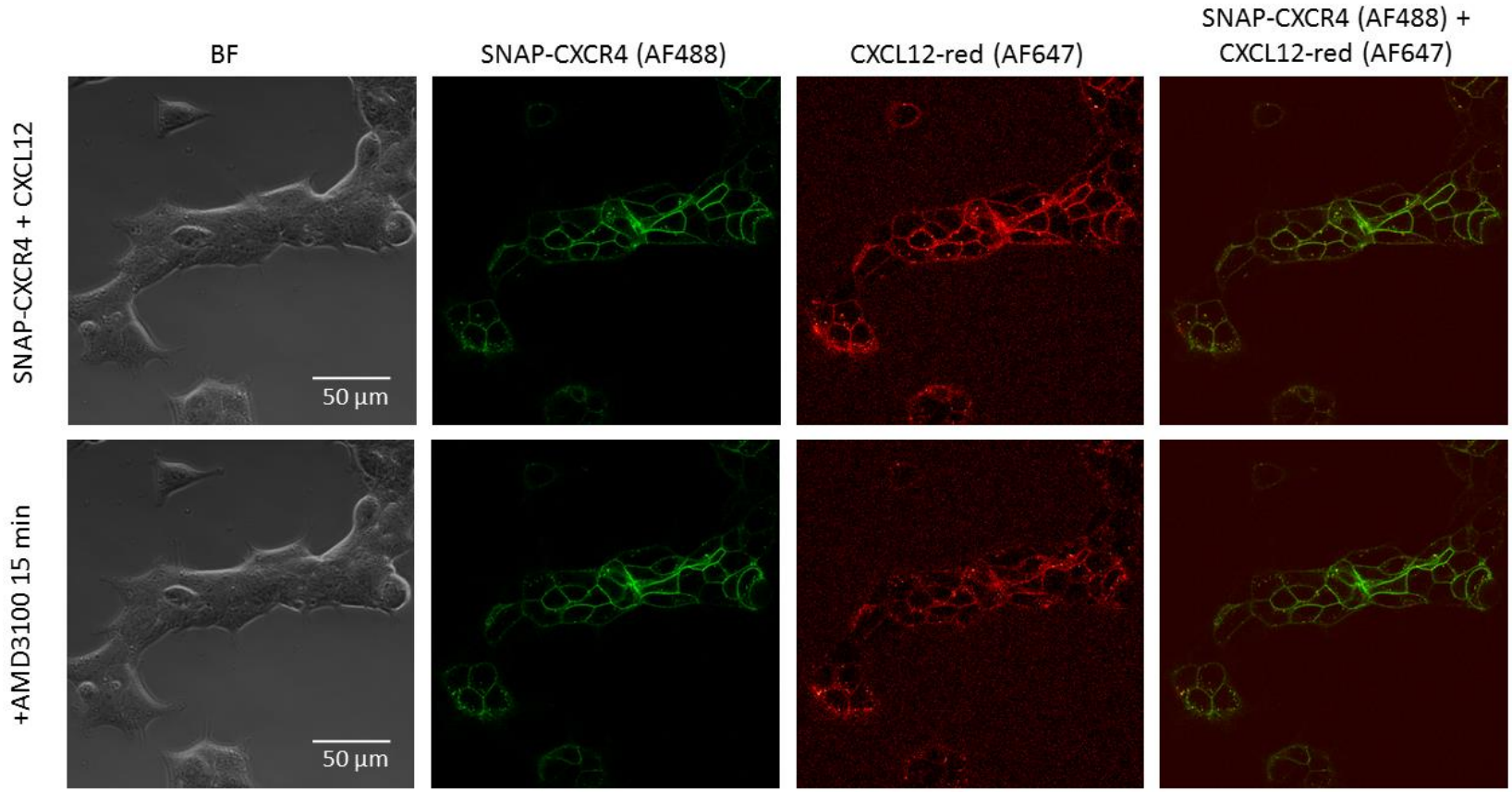

Figure 4-20: Confocal Imaging of SNAP-CXCR4 with CXCL12-red and AMD3100. HEK293G_SNAP-CXCR4 cells were imaged after SNAP labelling and 30 min incubation with 25 nM CXCL12-red (first row) and subsequent addition of AMD3100 for 15 min (second row) as described in the Methods section. The first column showing the Bright field image, the second the SNAP-tagged receptor, the third Alexa Fluor 647 tagged CXCL12 and the last the combined images of Alexa Fluor 488 and 647. Data are shown as one representative image, similar images were obtained 6 more times for both conditions.

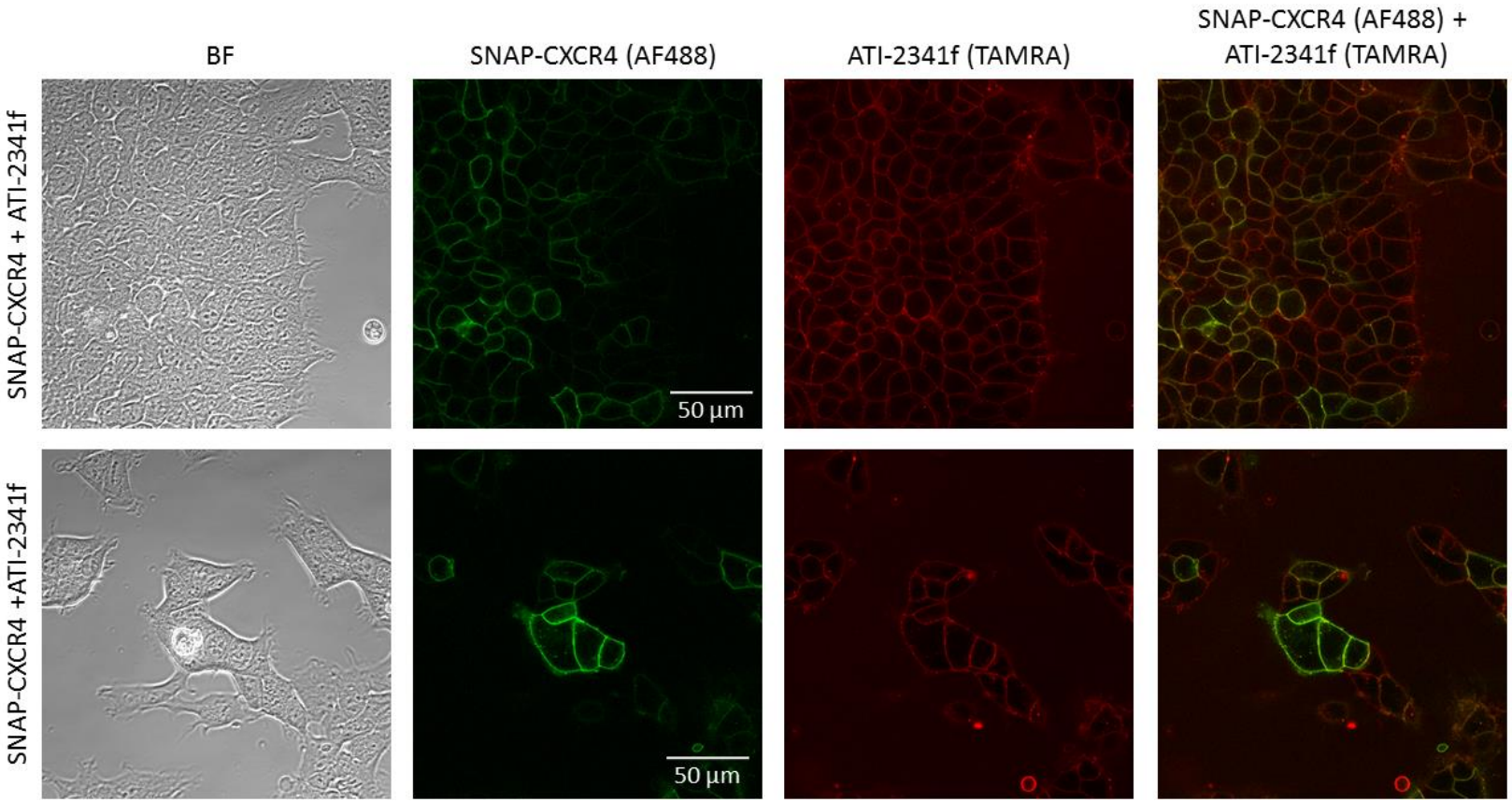

Figure 4-21: **Confocal Imaging of SNAP-CXCR4 with ATI-2341f.** HEK293G_SNAP-CXCR4 cells were imaged after SNAP labelling and 45 min incubation with 250 nM ATI-2341f as described in the Methods section. The first column showing the Bright field image, the second the SNAP-tagged receptor, the third TAMRA tagged ATI-2341f and the last the combined images of Alexa Fluor 488 and TAMRA. Data are shown as two representative image panels, similar images were obtained 5 more times.

4.3.4 Effect of ATI-2341 on CXCL12 binding

In the next step, competition binding experiments were performed with CXCL12-red or CXCL12-green and ATI-2341 in equilibrium in order to study if the pepducin influences CXCL12 binding (**Figure 4-22**) through an allosteric effect on the CXCL12 binding pocket. Moreover, the fluorescent pepducin ATI-2341f was tested for its ability to interfere with CXCL12-green binding to CXCR4 in order to see the effect of the fluorescent tag on binding. CXCL12-green was tagged with Oregon Green® 488 at the penultimate lysine of CXCL12 just as CXCL12-red and used because of the overlapping spectra of CXCL12-red and TAMRA.

IT1t showed full displacement of CXCL12-red and CXCL12-green in membranes and cells. The pK_i values for it were comparable with CXCL12-green and CXCL12-red as shown in **Table 4-5**. The pepducin ATI-2341 as well as ATI-2341f were able to displace CXCL12-red or CXCL12-green with increasing concentrations but did not reach full displacement within the tested concentrations (10 or 3 µM respectively). The potencies of ATI-2341f and ATI-2341 are comparable (**Figure 4-22 C**). However, the observed slope of ATI-2341f displacing CXCL12-green was steeper than the one of ATI-2341 (**Figure 4-22 C**).

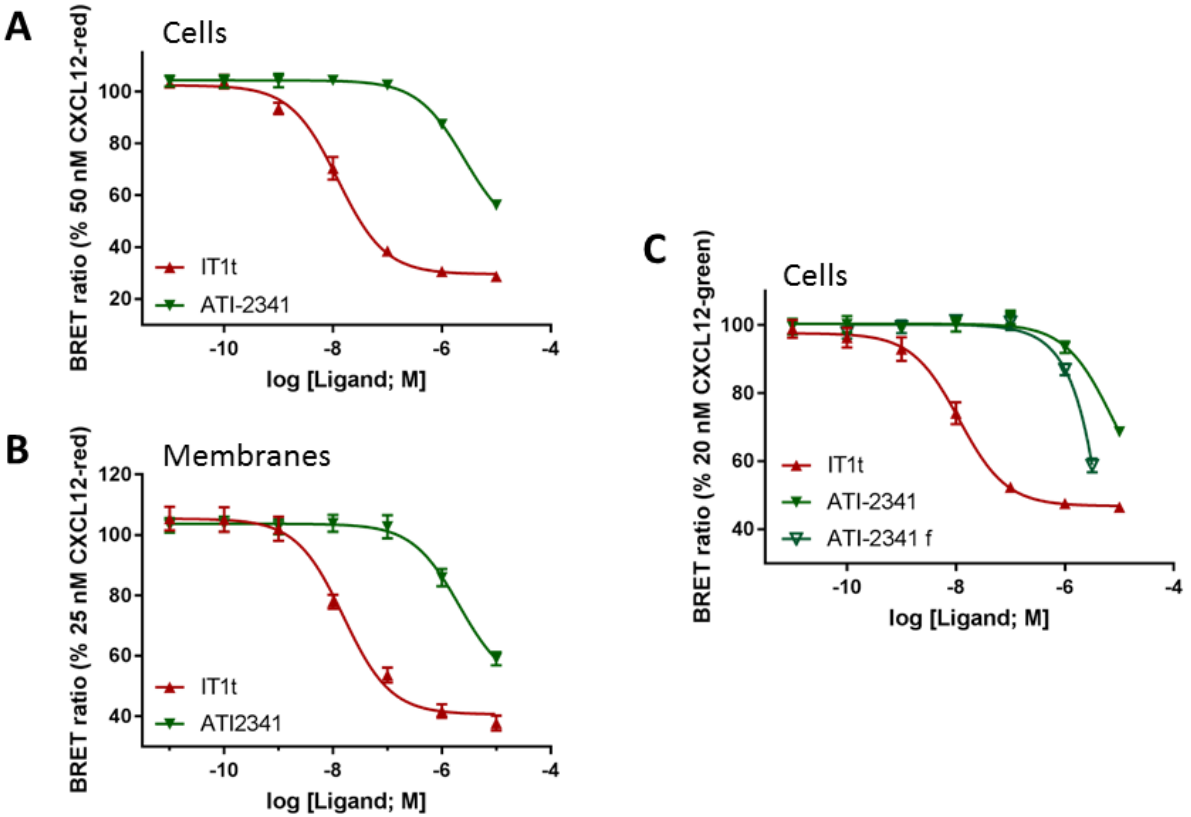

Figure 4-22: **Competition binding of CXCL12-red and CXCL12-green with ATI-2341, ATI-2341f and IT1t.** HEK293G_NLuc-CXCR4 cells (**A**) and membranes (**B, C**) were treated with 50, 25 or 20 nM CXCL12-red and increasing concentrations of ATI-2341 (▼), ATI-23412f (▽) or IT1t (▲) at the same time. Change in fluorescent CXCL12 binding as change of normalized BRET ratio. Data are shown as mean ± S.E.M. of n=5 individual experiments performed in triplicates.

Table 4-5: pK_i and maximal inhibition values ± S.E.M. obtained in competition with CXCL12-red or CXCL12-green, all n = 5

	IT1t		ATI-2341		ATI-2341f	
	pK_i	Maximal BRET inhibition from total binding (%CXCL12-red)	pK_i	Maximal BRET inhibition from total binding (%CXCL12-red)	pK_i	Maximal BRET inhibition from total binding (%CXCL12-red)
CXCL12-red (Cells)	8.16 ± 0.14	70.5 ± 1.6%	<6	56.3 ± 4.4%*	ND	ND
CXCL12-red (Membranes)	8.04 ± 0.01	62.2 ± 2.5 %	<6	41.7 ± 2.2%*	ND	ND
CXCL12-green (Membranes)	8.16 ± 0.12	53.5 ± 1.0 %	<6	31.4 ± 1.4%*	<6	41.2 ± 2.0%*

*Maximal inhibition at 10 µM for ATI-2341 and 3 µM for ATI-2341f, both did not reach saturation; ND = not determined

In the first chapter **4.3.1 Development of the CXCL12 NanoBRET assay** we saw that CXCL12 as well as the small compounds IT1t and AMD3100 displace CXCL12-red completely at high concentrations. ATI-2341 was also able to interfere with CXCL12-red binding but did not reach saturation within the tested concentration range up to 10 µM. In order to verify that the displacement of CXCL12-red by ATI-2341 was specific to this pepducin, two control pepducins were tested for their ability to interfere with CXCL12-red binding in cells and membranes. In a first step the importance of the lipid tail was controlled with a peptide equivalent, ATI-2504, which has the same peptide structure of ATI-2341, but is missing the lipid tail. ATI-2504 did not show any ability to interfere with CXCL12-red binding (up to 10 µM – **Figure 4-23**). Next, the importance of the specific peptide sequence was tested with a pepducin ATI-2339 that is missing the last three C-terminal amino acids of ATI-2341. ATI-2339 did also not show any ability to block CXCL12-red binding (up to 10 µM - **Figure 4-23**).

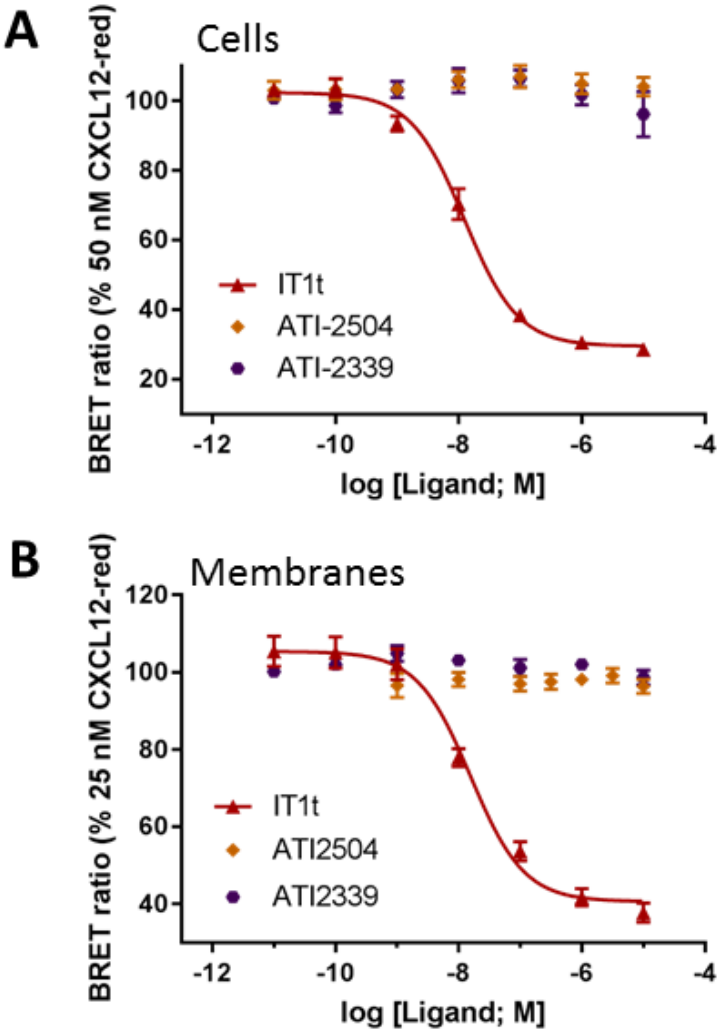

Pepducin	**Sequence**
ATI-2504	MGYQKKLRS MTDKYRL-NH_2
ATI-2339	Pal-MGYQKKLRS MTDK -NH_2

Figure 4-23: Competition binding of CXCL12-red and IT1t, ATI-2504 and ATI-2339. HEK293G_NLuc-CXCR4 cells (**A**) and membranes (**B**) were treated with 50 or 25 nM CXCL12-red respectively and increasing concentrations of IT1t (▲), ATI-2504 (◆), or ATI-2339 (⬣) at the same time. Change in CXCL12-red binding as change of normalized BRET ratio. Data are sown as mean ± S.E.M. of n=5 individual experiments performed in triplicates.

Potential explanations for the activity of pepducins is the direct interaction with G proteins or the direct interaction with the receptor pushing the conformation of the receptor into its active form similar to the conformation occurring when the GDP of the G protein is swapped for GTP. The addition of GTP allows a GTP-GDP exchange at the G protein resulting in the dissociation of the G protein from the receptor. Addition of GTP normally uncouples the receptor from G protein and creates a lower affinity conformation for agonists.

Because of this, the saturation binding of CXCL12-red was measured again in the presence and absence of GTP in NanoLuc-CXCR4 membranes. As expected, the addition of GTP caused a reduced CXCL12-red binding with a shift to lower K_d values and a raw BRET ratio of 0.018 ± 0.001 at 200 nM CXCL12-red instead of 0.024 ± 0.001 (**Figure 4-24 A**). When adding ATI-2341 to the membranes a similar behaviour of reduced binding was observed with a raw BRET ratio of 0.015 ± 0.002 at 200 nM CXCL12-red. When adding both, GTP and ATI-2341 a decreased raw BRET ratio of 0.012 ± 0.002 was observed. The saturation binding curve of CXCL12-red with ATI-2341 was not significantly different from the binding curve of CXCL12-red with ATI-2341 and GTP. The actual fits of the reduced saturation binding curves are only estimates due to the fact that none of them reach saturation, however all showed shifted K_d values with the values in the order of just CXCL12-red, CXCL12-red and GTP, CXCL12-red and ATI-2341 and then CXCL12-red with GTP and ATI-2341 at the same time, similar to the change in raw BRET ratio (**Figure 4-24**).

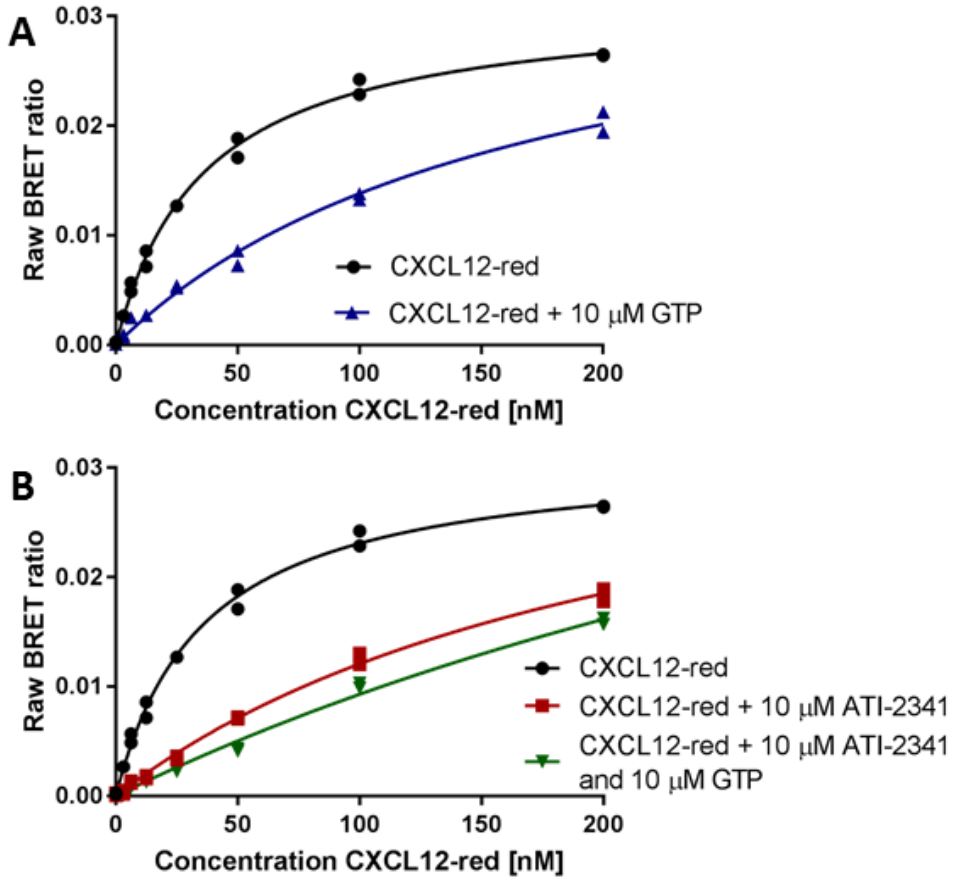

Figure 4-24: Saturation binding of CXCL12-red in presence of GTP and ATI-2341. Membranes from HEK293G_NanoLucCXCR4 cells were treated with CXCL12-red (●) and buffer with 0.25 mg/ml saponin with subtracted non-specific binding measured with the addition of 10 µM AMD3100 (**A**) treated with 10 µM GTP (▲) (**B**) treated with 10 µM ATI-2341 (■), or 10 µM ATI-2341 and 10 µM GTP at the same time (▼). Specific binding as change in raw BRET ratio, data are shown as mean values from duplicate determinations of one individual experiment, similar results were obtained two more times.

The previous results indicate that pepducins interact with the target receptor from the inside of the cell as demonstrated by the use of fluorescent ATI-2341f and CXCR4-NLuc in BRET experiments. This interaction has been suggested to follow a process of anchoring of the lipid into the cell membrane, flipping inside of the peptide and then interaction of the peptide with the receptor (Covic *et al.*, 2002; Wielders *et al.*, 2007). Because of this multistep process for interaction, the kinetics might be slower than for a ligand interacting with the extracellular part of the receptor. Therefore, the kinetics of the interference or displacement of CXCL12-red binding by ATI-2341 were measured in a kinetic binding assay. This kinetic information would give us a more detailed information about the time frame in which a mechanism takes place. As previously described CXCL12-red showed a rapid increase in binding indicated by an increase in BRET ratio which was followed by a continuous slow decrease. When adding 10 µM ATI-2341 at the same time as CXCL12-red, the B_{max} achieved in the presence of CXCL12-red and ATI-2341 was smaller than the one achieved in the presence of CXCL12-red alone while the shape of the curve stays similar. However, when trying to fit kinetic binding curves to the association curve of CXCL12-red added at the same time as ATI-2341 most fits fail resulting in ambiguous solutions (**Figure 4-25 A and C**). When adding 10 µM ATI-2341 after 15 min of initial binding period the bound CXCL12-red was displaced within 15 min reaching a plateau of 53.5 ± 1.0% of the total binding with a k_{off} = 0.43 ± 0.04 min^{-1} (**Figure 4-25 B and D**). The percentage of the reached plateau was consistent for all three analysed concentrations of CXCL12-red. The plateau reached were 50.7 ± 0.6% for 100 nM, 55.1 ± 1.3% for 50 nM and 54.5 ± 1.4% for 25 nM from the non-treated CXCL12-red curves.

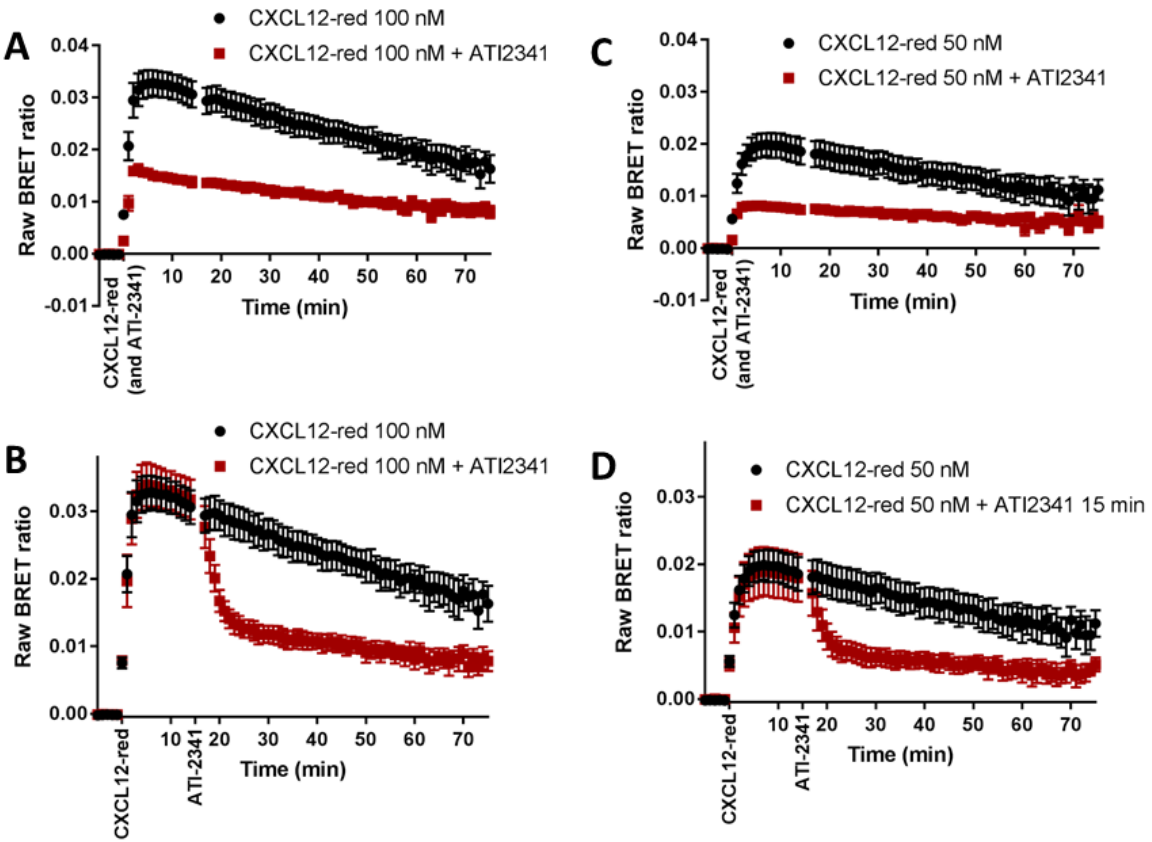

Figure 4-25: Kinetic binding of CXCL12-red in presence of ATI-2341. HEK293G_NanolucCXCR4 cells were treated with 100 nM (**A** and **B**) or 50 nM (**C** and **D**) of CXCL12-red (●) and 10 µM ATI-2341 (■) were either added at the same time (**A** and **C**) or 10 µM ATI-2341 were added after 15 min (**B** or **D**). Change in binding as change of Raw BRET ratio with subtracted baseline. Data are shown as mean ± S.E.M. of n=5 individual experiments performed in duplicates.

4.3.5 Interactions of CXCR4 and SD44 (a fluorescent It1t derivative)

In a second PhD project which was run in parallel to this project, fluorescent small molecules for CXCR4 based on already known compounds targeting the TM binding pocket were developed. These compounds were synthesised by Sebastian Dekkers and then characterized with the assays setup by us. SD44 (**Figure 4-26**) is a fluorescent version of IT1t with SD42 as a parent compound without the fluorophore (see **Table 2-1** in the material and method section for structures). IT1t has been shown to be an antagonist for CXCR4 and has been co-crystallised with CXCR4 (Wu *et al.*, 2010). IT1t binds at the extracellular transmembrane part of CXCR4 sharing some binding interactions with CXCL12, however the binding pocket does not fully overlap with the one of CXCL12 and has fewer ligand-amino acid interactions because of compound size. Because of this, we were interested to see if ATI-2341 was still able to interfere with binding of this small molecule.

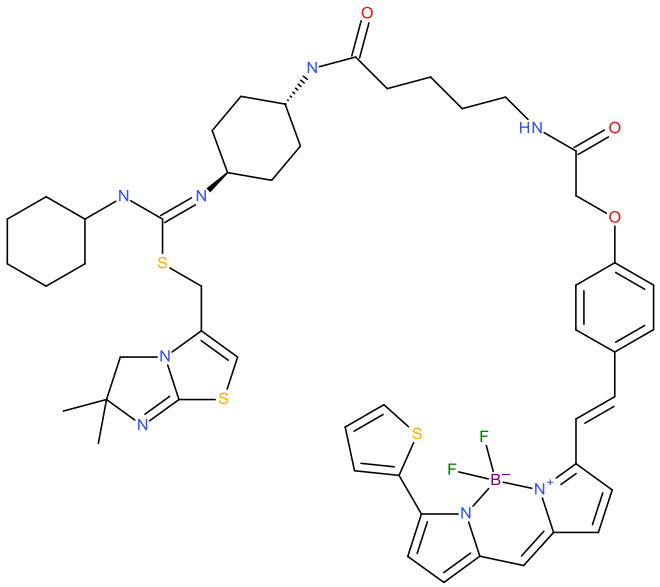

Figure 4-26: Structure of SD44.

The compound SD44 was tested in all assays described before in this chapter. First, the binding of the compound was tested with a saturation binding assay showing saturable binding with a pK_d of 7.04 ± 0.03, (K_d = 92nM), n = 4 - **Figure 4-27**).

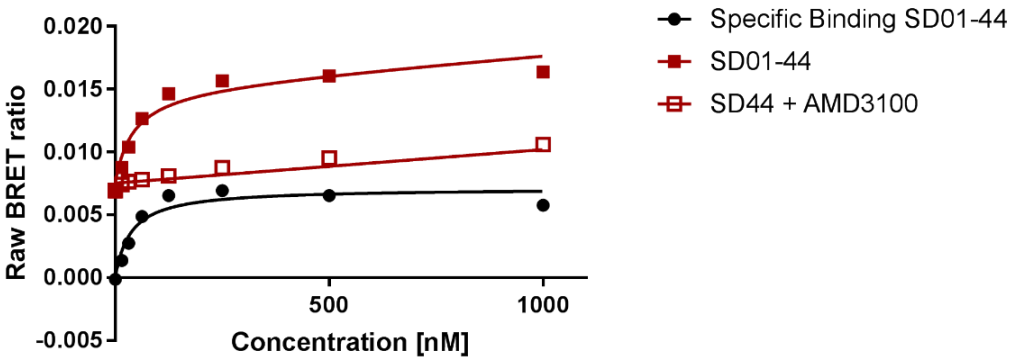

Figure 4-27: Saturation binding of SD44 in HEK293G_Nluc-CXCR4 membranes. Membranes were treated with different concentrations of SD44 and buffer (■) or SD44 and 10 µM AMD3100 (□) in a NanoBRET assay, binding as Raw BRET ratio by dividing the emission of the fluorophore by the emission of the NLuc tag. Specific binding (●) was calculated by subtracting the non-specific binding from the total binding curve. Data are shown as mean ± S.E.M. of one individual experiment performed in triplicate. Similar results were obtained 3 further independent experiments.

This binding affinity was also verified in cells using the kinetic binding assay (pK_d = 6.94 ± 0.07, K_d = 116.5 nM, n = 3 - **Figure 4-28**). Moreover, a k_{on} of 29.47 ± 6.46 x 10^4 M^{-1} min^{-1} and a k_{off} of 0.033 ± 0.007 min^{-1} was obtained. In comparison to CXCL12-red a slower increase in binding was observed. While CXCL12-red showed a consistent slow decrease in Raw BRET ratio, SD44 reached saturation and maintained the observed value within the 60 min measurement suggesting that receptor and antagonist do not move apart from each other. The k_{obs} plot of SD44 shows a linear relationship for high concentrations, at low concentrations the values deviate from the linear relationship.

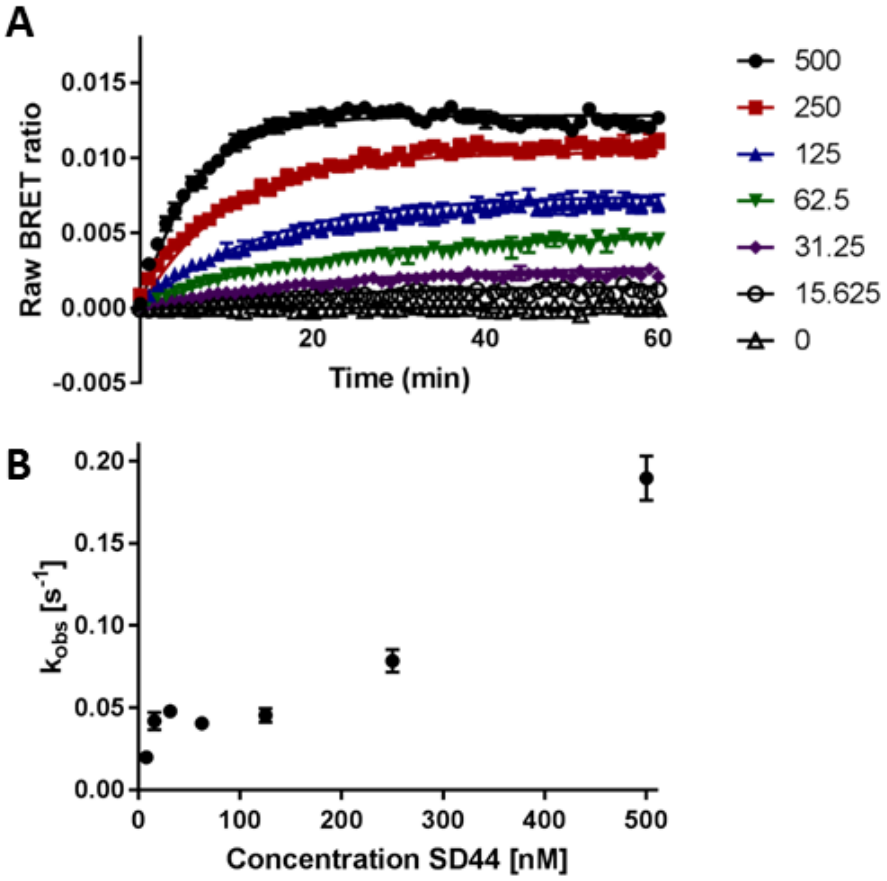

Figure 4-28: Kinetic saturation binding of SD44 to NLuc-CXCR4. (**A**) HEK293G_Nanoluc-CXCR4 cells were treated with different concentrations of SD44 up to 500 nM or SD44 and 10 µM AMD3100 in a NanoBRET assay, binding as Raw BRET ratio. Data are shown as specific binding curves by subtracting the non-specific binding with AMD3100 from the total binding and represented as mean ± S.E.M. of one individual experiment performed in duplicate, similar results were obtained in 2 more experiments. (**B**) k_{obs} plot of (A), showing an almost linear relationship between k_{obs} and concentration of SD44.

Competition binding experiments using SD-44 were carried out in membranes using CXCL12, small molecule antagonists and the pepducin ATI-2341 (**Figure 4-29**). The addition of the antagonists, including the parental compound SD42, showed full displacement of SD44 with the obtained pK_i values shown in **Table 4-6**. Interestingly, CXCL12 as well as ATI-2341 were not able to displace SD44.

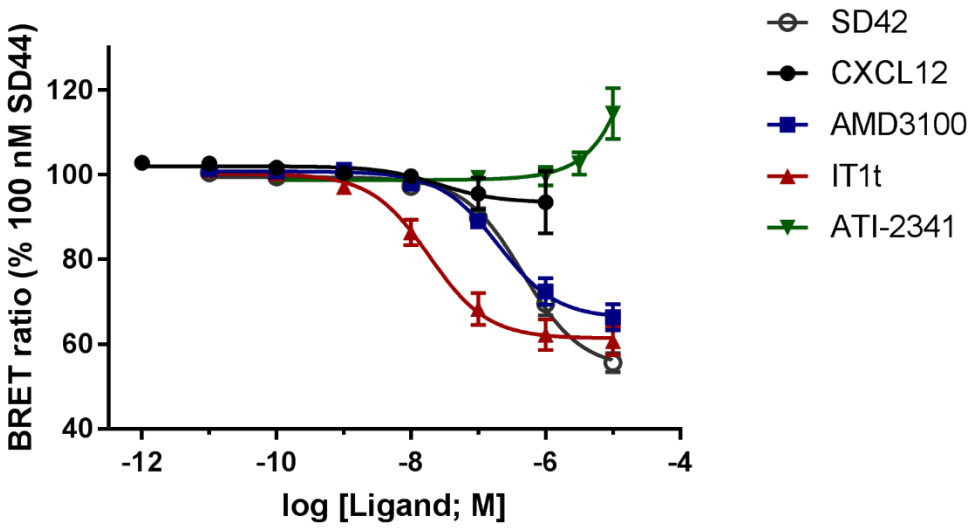

Figure 4-29: Competition binding assay of SD44 with unlabelled CXCR4 ligands. HEK293G_NanoLuc-CXCR4 cell membranes were treated with 100 nM SD44 and increasing concentrations of unlabelled compounds at the same time in a BRET assay, response as BRET ratio normalised to SD44 response. SD42 (○), AMD3100 (■) and IT1t (▲) did all compete for SD44 binding. CXCL12 (●) and ATI-2341 (▼) did not interfere with SD44 binding at high concentrations. Data are shown as mean ± S.E.M. of n = 4 independent experiments, each performed in triplicates.

Table 4-6: pK_i values for competition binding of SD44 and unlabelled compounds

Ligand	pK_i Membranes	Maximal BRET inhibition (% SD44) in membranes
SD42	6.60 ± 0.17	44.4 ± 2.3 %
CXCL12	ND	6.5 ±7.4 % (NS)
AMD3100	7.00 ± 0.07	39.3 ± 3.4 %
IT1t	8.03 ± 0.11	33.7 ±3.1 %
ATI-2341	ND	-14.5 ± 6.0 % (NS)

pKi values ± S.E.M., all n=5

4.4 Chapter summary and discussion

In this chapter the question of the binding position of the pepducin – extracellular vs intracellular and where in the cell the binding occurs was addressed. Moreover, the influence of pepducins on the binding of the extracellular ligands CXCL12 and SD44 was studied. Lastly, the experiments looked at the kinetic behaviour of different compounds for binding and displacement of those ligands in order to compare the binding of ATI-2341f which has to cross the cell membrane before binding. Fluorescent and unlabelled ligands were studied with NLuc tagged CXCR4 using a BRET proximity assay and in confocal and bioluminescence imaging.

First, all BRET assays were set up using CXCL12-red and CXCL12-green as fluorescent ligands which allowed comparison with literature values and a proof of concept of all our systems. Recent reports showed the development of a NanoBRET assay for CXCR4 using an N-terminal tagged CXCR4 and a fluorescently tagged peptide antagonist TAMRA-Ac-TZ14011 which showed to work in the same way as our assay (Sakyiamah *et al.*, 2019). CXCR4 is known to be localized in the cell membrane in lipid rafts (Mañes *et al.*, 2000) and the inside of cells in the absence of ligands or other stimulators (Busillo and Benovic, 2007). Upon activation more receptor is internalised (Marchese *et al.*, 2003; Wang *et al.*, 2006; Busillo and Benovic, 2007). Accordingly, SNAP-CXCR4 was primarily observed on the cell surface in the absence of any ligand as shown in confocal imaging. CXCL12-red was found colocalising with CXCR4 on the cell surface of SNAP-CXCR4 expressing cells as well as internalised with the receptor. The confocal images do not give any information about the interaction of the receptor and ligand. In the BRET binding studies CXCL12-red was shown to be in close proximity to the N-terminal tag of CXCR4 with a K_d of 36 nM for CXCL12-green in cells, 72 nM for CXCL12-red in cells and 25 nM for CXCL12-red in membranes. Binding affinities have been tested before using ^{125}I-CXCL12 in homologous displacement experiments. Breast tumour cells MCF-7 were shown to have an affinity of about 200 pM, however these cells seemed to not

mobilize calcium or migrate in response to CXCL12 (Burns *et al.*, 2006). A transformed T cell line CEM-NKr showed binding with an IC_{50} of 1.8 nM (Burns *et al.*, 2006). A CEM T cell line showed a K_d of 3.6 ± 1.6 nM (Crump *et al.*, 1997). Furthermore, dimeric and monomeric CXCL12 were tested for binding at CXCR4. K_d values for binding of WT CXCL12, a mutant that is mainly monomeric, and one that is dimeric were calculated as 25, 25, and 150 nM (Drury *et al.*, 2011). These literature values seem to be dependent on cell background but are comparable with the ones obtained in this study. When comparing these sets of data it should also be mentioned that our CXCR4 as well as our CXCL12 are modified by the introduction of tags which might impact binding values. The interaction of CXCL12-red and NLuc-CXCR4 was then also tested in a kinetic assay following the raw BRET ratio in real time. Upon addition of CXCL12-red the binding indicated by the raw BRET ratio showed a rapid increase with its maximum reached after only 5 min. Afterwards a consistent slow decrease in raw BRET ratio can be observed. This decrease can potentially be explained by internalisation of the receptor which is followed by dissociation of CXCL12-red and CXCR4.

The interaction between CXCL12-red and CXCR4 was fully blocked in the BRET binding assay by the simultaneous addition of high concentrations of unlabelled CXCL12 (pK_i of 7.97 ± 0.07 (membranes) or 7.44 ± 0.09 (cells)) as well as AMD3100 (pK_i of 7.00 ± 0.04 (membranes) or 8.08 ± 0.09 (cells)) and IT1t (pK_i of 8.04 ± 0.01 (membranes) or 8.16 ± 0.14 (cells)). AMD3100 was also shown to compete with CXCL12-red in confocal imaging and reduced its binding within 15 min. AMD3100 and IT1t have been shown to compete directly with CXCL12 binding due to a partly shared binding pocket and subsequent effects on the amino acids interacting with CXCL12 (Wu *et al.*, 2010; Planesas *et al.*, 2015). AMD3100 has been shown to displace ^{125}I-CXCL12 (pKi not published) in CEM-Nkr cells (Burns *et al.*, 2006). Moreover AMD3100 was shown to have a pK_i of 6.05 ± 0.11 in CXCR4 transfected COS-7 cells displacing the 12G5 antibody (Rosenkilde *et al.*, 2004). Furthermore ^{125}I-CXCL12 was

displaced in membranes by IT1t with a pIC_{50} of 8.0 ± 0.0, by AMD3100 with a pIC_{50} of 6.7 ± 0.1 and by CXCL12 with a pIC_{50} of 9.3 ± 0.1 (Adlere *et al.*, 2019). The values obtained for IT1t and AMD3100 are similar to the ones measured by us. The CXCL12 value measured with a radio ligand is shifted to higher affinities (comparing pK_i and pIC_{50}). The only difference in the membrane experiments between BRET and radioligand experiments are differences in the ligand (fluorescent tag vs radiolabel) and the temperature (37°C vs 25°C) at which measurements are performed and might influence binding.

In our studies, CXCL12 and IT1t behaved similarly in cells and membranes. However, AMD3100 showed a 10-fold lower potency in interfering with CXCL12-red binding in membranes compared to cells. One potential explanation of this effect could be the different abilities to penetrate membrane vesicles. Therefore the interference of CXCL12-red binding was measured with the addition of saponin, however this did not shift the AMD3100 curve towards the value obtained in cells. The difference between cells and membranes remained unclear. Other reasons might be the lack of interacting molecules and proteins in membranes that influence the binding of AMD3100.

After testing all assays with CXCL12-red, similar measurements were performed with ATI-2341f in order to determine binding location and provide insight into the binding kinetics.

It has previously been shown that a fluorescent pepducin ATI-2766 can be crosslinked to CXCR4 as well as to two mutants with a truncated N-terminus with a similar potency. Both mutants showed reduced CXCL12 binding in comparison to the WT CXCR4. These results suggested a different binding site for ATI-2341 to that of CXCL12 (Janz *et al.*, 2011). ATI-2766 is a fluorescent pepducin based on ATI-2341, both methionines are removed and replaced by one alanine and one glycine. It also has an N-terminal TAMRA-tag and a photo-leucine instead of a leucine which is able to be activated by UV light and form a covalent bond to an interacting protein. Apart from

this study there are no further publications looking at the binding mechanism of ATI-2341.

We found that ATI-2341f showed only a small displaceable to no increase in BRET ratio dependent on the individual experiment with an N-terminal NanoLuc tagged CXCR4, but did show a displaceable increase with a C-terminal NanoLuc tagged CXCR4 suggesting an interaction with the intracellular receptor side. When testing the increase of BRET ratio with NanoLuc tagged ACKR3 the exact same behaviour can be observed. While the N-terminal tagged ACKR3 showed an increase that is not displaceable, the C-terminal tagged ACKR3 showed only a small displaceable increase in BRET binding. Because of this, it is unclear if the localisation of ATI-2341f to the inner leaflet of the membrane is specific to the interaction with CXCR4. ATI-2341f might always orientate itself to the inner leaflet of the membrane before interacting with receptors. Notable was also that the increase in BRET ratio for the N-terminal tagged ACKR3 was a lot higher than for any other combination, potentially suggesting that more pepducin is in the extracellular part of the cell in the ACKR3 experiments. Interestingly, modelling efforts of the CXCR4 pepducins by the group of Charles Laughton (University of Nottingham) showed that ATI-2341 placed 2 nm above the cell membrane inserts itself into the cell membrane with the C-terminus attracted to the membrane bilayer without the presence of CXCR4 (unpublished). Moreover, it would be possible that ATI-2341f also interacts with ACKR3, even though the intracellular loops of CXCR4 and ACKR3 share no similarities. It could also be possible that the pepducin interacted with the endogenous CXCR4 in HEK293G cells and therefore was only observed at the intracellular site of the membrane in close proximity to ACKR3 receptors. ATI-2341f might be located at both sides of the membrane but the fluorophore of the pepducin could be positioned in a way that the energy transfer to the N-terminal tag of CXCR4 or ACKR3 is ineffective. The energy transfer is dependent on the distance of the tag and fluorophore and also the angle between the two.

In order to control the theories for ATI-2341f binding it would be useful to add a set of further control experiments, starting with measuring the expression levels of NLuc-CXCR4 and CXCR4-NLuc on the prepared membranes. The membrane concentrations could be changed according to the donor counts plotted in **Figure 4-10** and **Figure 4-11**. Moreover, a set of BRET experiments in cells not expressing endogenous CXCR4 and using other receptors that do not interact with ATI-2341 should be added, e.g. CCR5. Additionally, a small amount of binding at early time points is not surprising as the initial interaction of the pepducin with the membrane occurs at the N-terminal membrane leaflet, however this effect might be altered in membranes in comparison to cells.

Moreover, since we saw some interaction with ACKR3, it would also be useful to follow this up with signalling experiments in order to see if ATI-2341 activates ACKR3.

In bioluminescence imaging both cell lines (C- and N-terminal tagged CXCR4) showed a significant increase in BRET, however the set up was not tested for displaceability as high concentrations of pepducin change the cell morphology. The N-terminal cell line showed a bigger increase in BRET ratio than the C-terminal one. This bigger increase of the N-terminal tagged receptor might be explained by the amount of pepducin that stays outside of the cell but does not activate the receptor. In confocal imaging the pepducin localized itself into the cell membrane but it is unclear if the peptide is located outside or inside of the cell. Moreover, the pepducin can be seen on surfaces of the imaging dish and around the cells. In general, it seems like the pepducin localizes itself away from the solvent to lipophilic spots in the environment which seems to be expected due to the palmitic acid.

We tried to inhibit binding of ATI-2341f by the simultaneous addition of various unlabelled compounds to see any direct competition or indirect effects on the binding pocket. None of the extracellular ligands CXCL12, IT1t or AMD3100 were able to inhibit binding in equilibrium or displace ATI-2341f in a kinetic binding assay in which ATI-2341f was added 15 min prior to the unlabelled compounds. All

tested intracellular loop 1 pepducins (ATI-2341, ATI-2346, ATI-2341TA) displaced the fluorescent ATI-2341f from CXCR4 in an equilibrium binding assay with the same low potency not reaching saturation which suggested that the increase of pepducin in the receptor environment is more important than the specific binding properties to the receptor. Moreover, the slope of the curve is very steep which might suggest influence on the membranes causing a lower BRET transfer from the fluorescent pepducin. Interestingly, palmitic acid did not have the same effect as the pepducins suggesting that the effect is not based on the increase of lipid in the membranes. In a kinetic assay ATI-2341 was able to displace some of the ATI-2341f reaching a plateau within 15 min.

Next, the binding of ATI-2341f was followed in a kinetic mode. The binding of ATI-2341f towards CXCR4 was slower than CXCL12-red binding, however the kinetics were comparable with the antagonist SD44. Fitting of the curve resulted in an equilibrium dissociation constant pK_d of 4.91 ± 0.17 (K_d = 17.29 µM, n=5), association rate k_{on} of 3.68 ± 1.46 x 10^4 M^{-1} $min^{-1}$and dissociation rate k_{off} of 0.30 ± 0.05 min^{-1}. However, these parameters were only rough estimates due to the fact that non-specific binding in the presence of a competing unlabelled ligand was not measured due to a lack of an appropriate ligand. Because of this the buffer measurement was used as non-specific binding and a good estimation would only be obtained by this if a very small amount of binding is non-specific as it is the case for example for CXCR4 and CXCL12-red.

The next question was to determine whether ATI-2341 had an influence on the binding of other ligands by an allosteric effect.

ATI-2341 and ATI-2341f were able to displace CXCL12-red or CXCL12-green in the BRET proximity assay after reaching equilibrium. ATI-2341 and ATI-2341f showed similar potencies. However, the slope of the displacement curve of ATI-2341f was very steep which might suggest that the fluorescently tagged version has a bigger toxic impact on the cells than ATI-2341. Unfortunately, the fluorophore of ATI-2341f interferes with the absorbance measurement of the LDH

assay and the pepducin was therefore not tested in the toxicity assay. ATI-2341 was then also tested in a kinetic assay and displaced CXCL12-red within 15 min even though pepducins seem to bind at the intracellular site of the receptor. This suggests that ATI-2341 changes the conformation of CXCR4, in particular the conformation of the CXCL12 binding pocket in a way that results in interference with CXCL12-red binding. The control pepducins ATI-2504 (no lipid) and ATI-2339 (altered C-terminus) were not able to interfere with the CXCL12-CXCR4 interaction thereby showing the importance of the lipid tail for the ATI-2341 mechanism and that the effect is specific to the ATI-2341 sequence and not any lipidated peptide.

SD44, an IT1t derivative, was shown to bind towards the N-terminal site of CXCR4 and was blocked completely by its unlabelled parent compound SD42, IT1t and AMD3100. CXCL12 showed a non-significant decrease of SD44 binding at 1 µM and ATI-2341 showed a non-significant increase in binding at 10 µM.

Finally, the influence of ATI-2341 and GTP on CXCL12-red binding was tested. GTP exchanges GDP in G proteins coupled to CXCR4 and thereby causing the G protein to dissociate from CXCR4 to change its conformation into a low affinity conformation. CXCL12-red showed a lower binding affinity to this receptor conformation. Using a more stable GTPγS could have been a good option as well in order to make this change into the active form irreversible. ATI-2341 has the same effect on CXCL12-red binding. Addition of ATI-2341 causes the receptor to change its conformation which is a lower affinity state for CXCL12-red. Interestingly, the effects of GTP and ATI-2341 are not additive. This suggests that GTP and ATI-2341 cause similar changes in the receptor as two separate effects should be additive.

In summary, ATI-2341 seems to interact with the intracellular part of membrane bound CXCR4. This interaction influences binding of the endogenous ligand CXCL12 by changing the conformation of the receptor into its active form similar to the conformation formed when GTP is bound to the G protein-coupled to CXCR4. The binding kinetics of ATI-2341 seem to be slightly slower than the ones of CXCL12 but

are comparable with the antagonist SD44 which does not cross the membrane before binding.

5 Functional characterisation of CXCL12 and ATI-2341 at CXCR4

5.1 Introduction

ATI-2341 has previously been shown to activate CXCR4 and cause downstream signalling in a similar way to the endogenous ligand CXCL12 (Tchernychev *et al.*, 2010; Janz *et al.*, 2011; Quoyer *et al.*, 2013). In order to get a better picture of the downstream signalling effects caused by the pepducin the binding and compare those with the endogenous ligand CXCL12 a functional screen was performed. In the previous chapter two mutually exclusive effects on binding were observed for CXCL12 and ATI-2341.

In general, CXCR4 can signal via G protein-dependent and G protein-independent pathways (Quoyer *et al.*, 2013). The coupling of CXCR4 to various G proteins seems to be complex and cell-dependent as well as depending on changes in the expression level of the receptor and G proteins, however some G proteins seem to interact with CXCR4 in all settings (Soede *et al.*, 2001; Tan *et al.*, 2006; Kleemann *et al.*, 2008; Quoyer *et al.*, 2013). CXCR4 mainly activates G proteins of the $G\alpha_i$ family as a range of functional responses are sensitive to pertussis toxin (PTX) (Tchernychev *et al.*, 2010). BRET studies have shown CXCR4 interacts with $G\alpha_{i1}$, $G\alpha_{i2}$ and $G\alpha_{i3}$ in HEK293T cells after CXCL12 stimulation (Quoyer *et al.*, 2013) with more efficient coupling towards $G\alpha_{i1}$ and $G\alpha_{i2}$ than to $G\alpha_{i3}$ and $G\alpha_o$ in Sf9 cells (Kleemann *et al.*, 2008). The activation of the receptor and these G proteins results in inhibition of adenylyl cyclase observed through decreased cAMP production as well as in the activation of the PI3K/AKT (phosphoinositide 3-kinase/protein kinase B) pathway promoting cell survival and migration. PI3K can be activated by either the $G_{\alpha i}$ or $G_{\beta\gamma}$ subunit. Some studies also suggest the interaction with $G\alpha_{13}$, which is involved in the migration of Jurkat T cells in response to CXCL12 (Tan *et al.*, 2006) and in the trafficking of CXCR4 into endosomes (Kumar *et al.*, 2011). Furthermore, CXCR4 can also lead to $G\alpha_q$ activation in native dendritic cells and granulocytes, but not in T and B cells (Soede *et al.*, 2001).

CXCR4 has also been shown to recruit β-arrestins (Cheng *et al.*, 2000; Quoyer *et al.*, 2013). In general β-arrestin is recruited to the receptor

after GRK phosphorylation and this is then followed by receptor internalisation through clathrin-coated pits (Cheng *et al.*, 2000; Quoyer *et al.*, 2013). It has been shown that co-expression of CXCR4 with β-arrestin-2 increases internalisation of CXCR4 upon CXCL12 stimulation (Cheng *et al.*, 2000). In contrast, β-arrestin-1 only increases CXCR4 internalisation when GRK2 is overexpressed as well (Cheng *et al.*, 2000). Since GRK2 phosphorylates CXCR4, this suggests that the interaction between CXCR4 and β-arrestin-1 is much more dependent on the phosphorylation state of CXCR4. The same study showed overexpression of CXCR4 and β-arrestins reduced cAMP inhibition by CXCL12 stimulation demonstrating the modulation of G protein signalling by β-arrestins (Cheng *et al.*, 2000). In agreement with this, lymphocytes isolated from β-arrestin-2 knock-out mice showed lower desensitization and increased G protein coupling to CXCR4 (Fong *et al.*, 2002). β-arrestin-2 is also involved in the CXCR4/CXCL12-mediated chemotaxis of HeLa cells through the p38-MAPK (mitogen-activated protein kinases) pathway (Sun *et al.*, 2002).

It has previously been shown that ATI-2341 inhibits cAMP production that can be reversed with the addition of PTX (Tchernychev *et al.*, 2010), suggesting it activates the receptor in a similar way to CXCL12 activating $G\alpha_i$ pathways. Results regarding the internalisation behaviour of CXCR4 after the activation by ATI-2341 are contradictory. CXCR4 internalisation has been observed after the addition of ATI-2341 in fixed HEK cells transiently transfected with CXCR4-eGFP (Tchernychev *et al.*, 2010). In contrast, a different study showed that ATI-2341 is only a weak internalising agent compared to CXCL12 in HEK cells looking at cell surface expression in flow cytometry and in agreement only partially recruits β-arrestin 1 and 2 to CXCR4 in a BRET assay (Quoyer *et al.*, 2013). However, looking at SUP-T1 cells in flow cytometry ATI-2341 does promote internalisation of endogenous CXCR4 with a receptor loss of 49 ± 6% in comparison to 87 ± 2% for CXCL12 (Quoyer *et al.*, 2013). Because of these

ambiguous results, both internalisation and β-arrestin recruitment will be studied again.

This chapter will start with a look at conformational changes in an internal CXCR4 biosensor and in dimers caused by ATI-2341 and CXCL12 in order to study in more detail whether ATI-2341 and CXCL12 activate the receptor in the same way. Then, we will look at G protein activation and the connected inhibition of cAMP. Finally, ß-arrestin recruitment and receptor internalisation will be measured. All functional effects caused by ATI-2341 will be compared with the responses caused by CXCL12.

5.2 Receptor activation

Initially, we compared the conformational change of CXCR4 in response to the activation by CXCL12 or the pepducin ATI-2341 in order to see the direct influence of the compound on the receptor. Due to their different binding positions and modes we were interested to see if the conformational changes occurring in the receptor were similar to each other. This was measured using an intramolecular CXCR4 FRET biosensor in which a fluorescein arsenical hairpin binder (FlAsH) tag is located within the third internal loop of CXCR4 between His228 and Ser229 and a CFP tag on its C-terminus (C. Hoffmann group, unpublished). If the conformation of CXCR4 changes in response to ligand binding or activation, the FlAsh and CFP tags move causing a change in FRET ratio that can be monitored live on single cells. The ligand-induced FRET changes were fitted to a one component exponential equation in order to obtain the kinetic parameter τ. In the program, the area in which the activation of the receptor occurs can be highlighted visually and this section is fitted subsequently.

The experiments were performed within the ONCORNET consortium in Carsten Hoffmann's group at the Julius-Maximilians-Universität Würzburg in cooperation with Cristina Perpiñá Viciano. Details of the

method of these measurements can be found in **2.5.1 Single Cell FRET Experiments**.

The effect of CXCL12 on the receptor was investigated previously (C. Hoffmann group, unpublished) showing an immediate increase in the FlAsH signal (acceptor) and a simultaneous immediate decrease in the CFP signal (donor) resulting in a 3% increase in FRET ratio after addition of 30 µM CXCl12 (time constant for receptor activation was τ = 590 ± 50 ms (n=17 cells measured on four independent experimental days) - **Figure 5-1**). τ is calculated from $t_{1/2}$, the time it takes to activate 50% of all available receptors. Superfusion of the cells with buffer after CXCL12 stimulation returned the FRET signal to baseline. The slow but continuous decrease in the FRET ratio is mostly caused by photo bleaching of the FlAsH fluorophore.

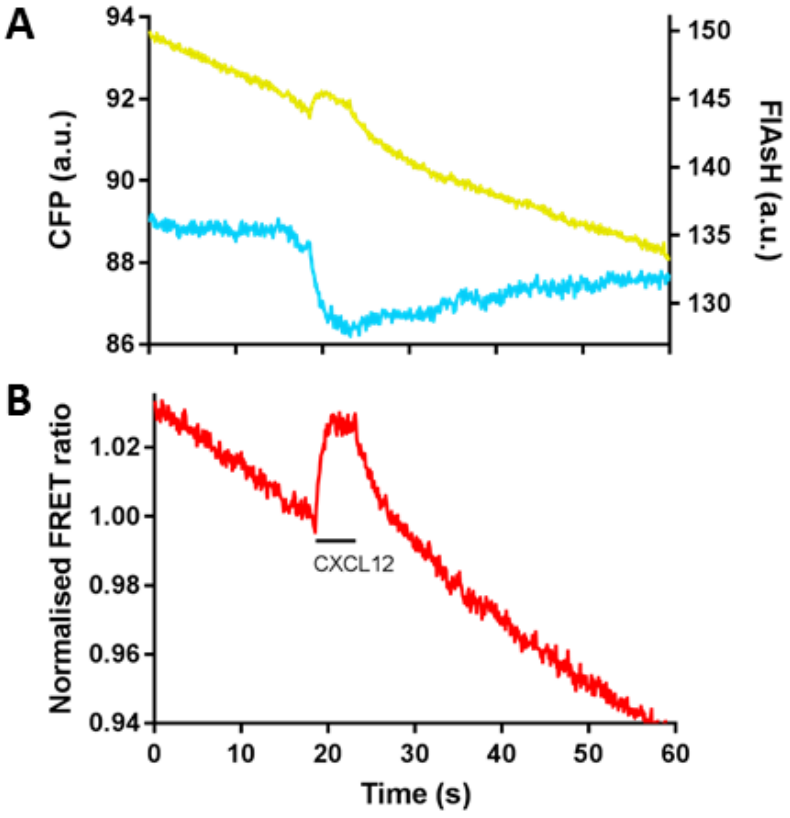

Figure 5-1: Activation of CXCR4 biosensor with CXCL12. HEK293T cells transiently transfected with 3HA-CXCR4-FlAsH228-CFP were treated with 1 µM CXCL12, the addition of CXCL12 is marked as bar in the graph and was followed by a washing step with buffer; showing the (**A**) individual CFP and FlAsH signals and (**B**) FRET ratio. Change in conformation as change in FRET ratio. Data are shown from one representative measurement performed by Cristina Perpiña Viciano (unpublished).

Similar experiments with ATI-2341 showed that addition of the pepducin also caused an increase in FlAsH and a decrease in CFP, indicating that ATI-2341 also caused a conformational change in CXCR4. However, in comparison to CXCL12 the addition of 10 μM ATI-2341 caused a slower (τ = 4339 ± 331 ms), but larger 8.0 ± 1.3 % increase in FRET ratio. A very interesting difference was that CXCL12 caused an immediate response in the biosensor while ATI-2341 had a response delay of 29.1 ± 3.8 seconds after addition (**Figure 5-2**). After the peak response the FRET response moved back to baseline.

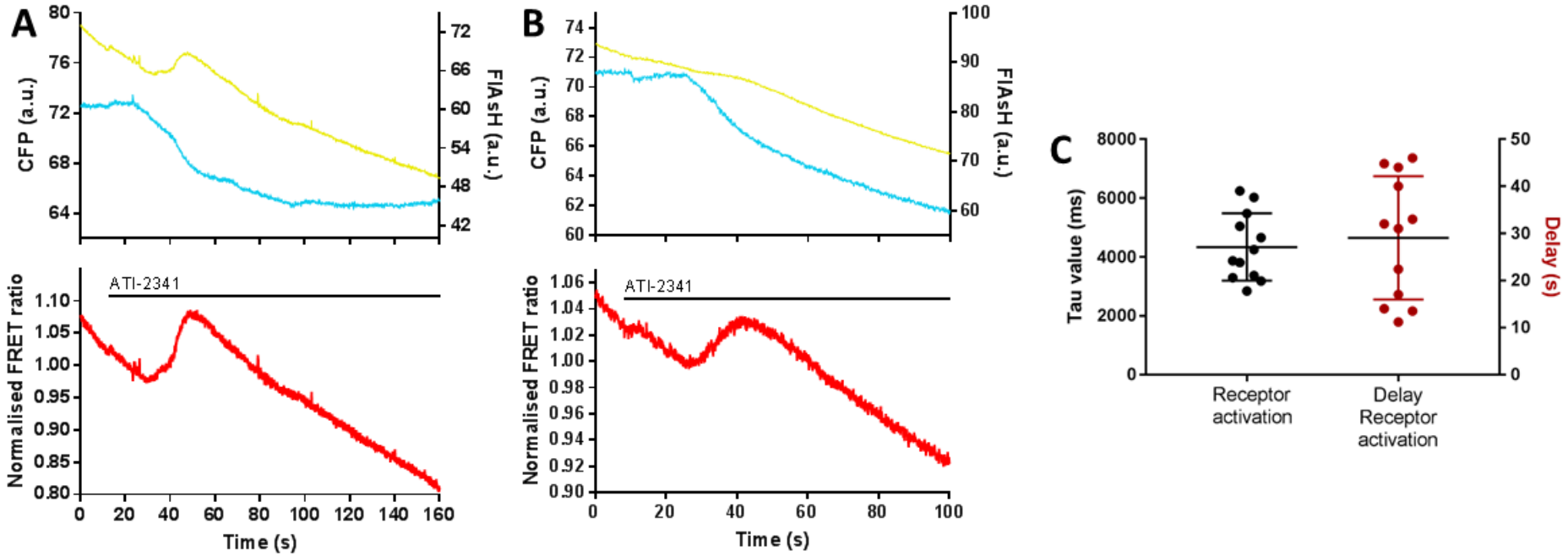

Figure 5-2: Activation of CXCR4 biosensor by ATI-2341. HEK293T cells transiently transfected with 3HA-CXCR4-FlAsH228-CFP were treated with 10 µM ATI-2341, the addition of ATI-2341 is marked as bar in the graph; showing the individual CFP (blue) and FlAsH (yellow) signals (first row) and FRET ratio (bottom panel in red). Change in conformation as change in FRET ratio. Data are shown from two representative single cells (**A + B**). (**D**) Showing all measured τ-values (receptor activation time) and delays (time from addition of ATI-2341 to response). Data are shown as mean ± S.E.M. of 12 individual cells from 3 independent experiments.

5.3 Oligomerization studies

5.3.1 Oligomerization of CXCR4 and ACKR3

The role of oligomeric receptors is still unclear with reports stating the importance of association and dissociation of the dimers and oligomers for signalling (Petersen *et al.*, 2017) with possible influences on ligand binding, cell surface expression, internalisation and desensitization (Terrillon and Bouvier, 2004).

CXCR4 has been observed to form dimers or oligomers in crystal structures, FRET or BRET measurements and single molecule imaging in a number of cell types including cells only expressing endogenous CXCR4 (Vila-Coro *et al.*, 1999; Babcock *et al.*, 2003; Percherancier *et al.*, 2005; Wang *et al.*, 2006; Wu *et al.*, 2010; Ge *et al.*, 2017). Furthermore, CXCR4 and ACKR3 have also been reported to form heterodimers (Levoye *et al.*, 2009; Décaillot *et al.*, 2011).

One of the initial hypothesis of the mechanism of action of pepducins was that they influence dimers or oligomers by mimicking or interfering with the receptor-receptor interaction interface. In this section, we therefore used a BRET-based approach to show the existence of CXCR4 oligomers in our cell lines to later investigate whether their formation is regulated by agonists, antagonists and pepducins.

First, the homooligomerisation of CXCR4 was studied (**Figure 5-3 A, C**). HEK293G cells were transiently transfected with 50 ng/well of NLuc-CXCR4 and increasing concentrations of SNAP-CXCR4. SNAP tagged receptor was then labelled using a SNAP Alexa Fluor 488 surface label. The transfer of energy from the furimazine oxidized at the NanoLuc-tag to the SNAP-tag was monitored by calculating the BRET ratio. A saturable increase in BRET ratio with a linear increase in receptor expression suggests an interaction between the two receptors, while a linear increase of BRET ratio suggests no interaction but a representation of the increasing fluorescence in the well. The BRET transfer does not give any information about stoichiometry of the receptor oligomers.

CXCR4 homooligmerisation experiments showed a saturable increase in BRET ratio (**Figure 5-3 A**). It was also notable that the increase in BRET ratio was bigger in CXCR4 oligomers than in any other combination. In order to control that more transfected DNA of SNAP tagged receptor results in more expressed protein, the cells were fixed after the experiments and the amount of SNAP labelling was quantified as described in the methods section (**Figure 5-3 C**). While the increase of SNAP-tagged receptor is not perfectly linear, all experiments showed an increase when transfected with more DNA that was not saturable.

ACKR3 oligomerisation measured between a constant concentration of 50 ng/well NLuc-ACKR3 and increasing concentrations of SNAP-ACKR3 showed a similar behaviour to CXCR4 oligomerisation, however a smaller increase in BRET was observed (**Figure 5-3 B, D**).

Next, heterooligomerisation between CXCR4 and ACKR3 was tested. Both transfection combinations were tested (NLuc-CXCR4 with SNAP-ACKR3 or NLuc-ACKR3 with SNAP-CXCR4). Both transfection combination showed a linear increase in SNAP-tagged receptor expression. However, the change in BRET ratio behaved differently. When transfecting a stable amount of NLuc-ACKR3 with increasing amounts of SNAP-CXCR4 a saturable increase was visible, however with NLuc-CXCR4 and SNAP-ACKR3 the increase was linear with a smaller saturable component (**Figure 5-4**).

In conclusion, oligomers are observed for CXCR4-CXCR4, ACKR3-ACKR3 and NLuc-ACKR3-SNAP-CXCR4.

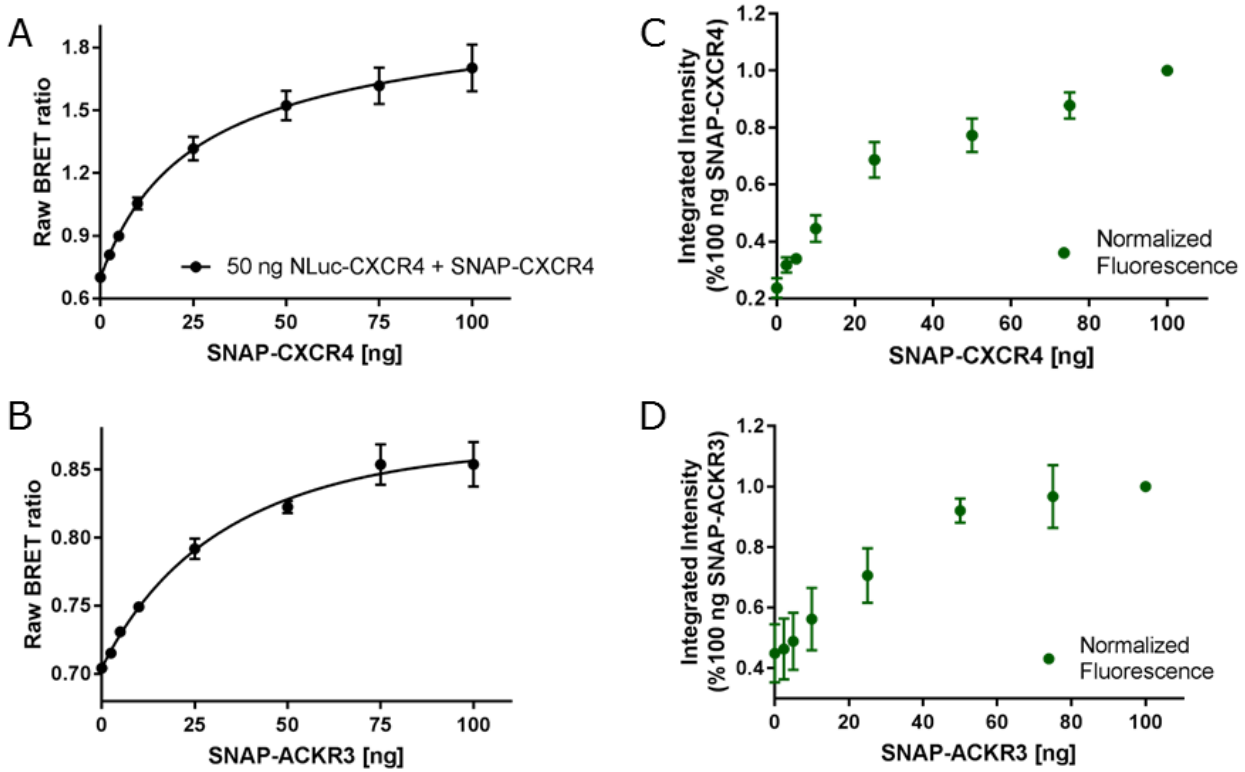

Figure 5-3: Homo-oligomerization of CXCR4 and ACKR3. Homo-oligomerisation of (**A**) CXCR4 and (**B**) ACKR3 by coexpression of a fixed concentration of Nluc- and increasing concentrations of SNAP-tagged receptor. Following transient transfection of SNAP-receptor, cells were labelled with SNAP-Surface-ALexaFluor488 for 30 min, before addition of furimazine and BRET ratio measurement. (**C**) and (**D**) cells were fixed after each individual experiment and the amount of SNAP-receptor was quantified on an ImageXpress Micro High Content plate reader. Data shown are mean ± S.E.M. of 4 independent experiments, each measured in triplicate.

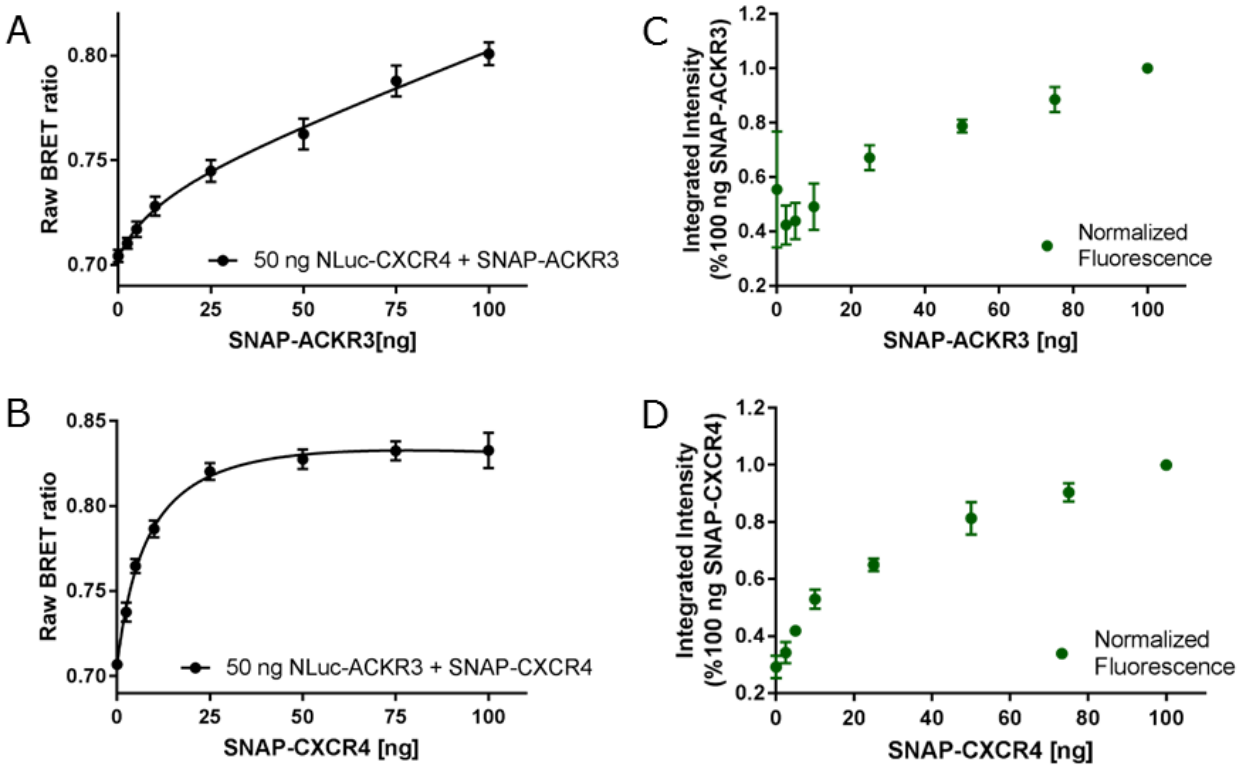

Figure 5-4: Hetero-oligomerization of CXCR4 and ACKR3. Hetero-oligomerization of CXCR4 and ACKR3 by coexpression of a fixed concentration of Nluc- and increasing concentrations of SNAP-tagged receptor (**A**) NLuc-CXCR4 and SNAP- ACKR3, (**B**) NLuc- ACKR3 and SNAP-CXCR4. Following transient transfection of SNAP-receptor, cells were labelled with SNAP-Surface-ALexaFluor488 for 30 min, before addition of furimazine and BRET ratio measurement. (**C**) and (**D**) cells were fixed after each individual experiment and the amount of SNAP-receptor was quantified on an ImageXpress Micro High Content plate reader. Data shown are mean ± S.E.M. of 4 (NLuc-CXCR4/SNAP-ACKR3) or 5 (NLuc-ACKR3/SNAP-CXCR4) independent experiments, each measured in triplicate

5.3.2 Ligand influence on Receptor Dimerization

After verifying that the BRET approach was able to monitor CXCR4 homooligomers, it was used to investigate whether oligomerisation was modulated by the addition of CXCL12 or ATI-2341. A change in BRET ratio could be caused by formation or parting of oligomers, but also because of conformational rearrangements in the oligomers.

In order to study the effect of ligands on dimers, a transfection of 50 ng/well Nluc-CXCR4 and 25 ng/well SNAP-CXCR4 was chosen in order to be able to see both increases and decreases in BRET ratio. Initially, BRET measurements were measured following a 2h incubation with a range of concentrations of IT1t, CXCL12 or ATI-2341 and no significant change in BRET ratio was observed, suggesting no change in dimer constitution (negative data shown in **9.4 Appendix for Chapter 5**).

To investigate whether changes could be observed at earlier time points, the change in BRET ratio was monitored in a kinetic mode every 9 s over a 2 h period (later the time frame was reduced to 1.5 h). Interestingly, a time-dependent change in BRET ratio was observed for all compounds. CXCL12 (1 – 0.01 μM) showed a concentration-dependent increase in BRET ratio with its peak response at approximately 8 min after addition of CXCL12. After the peak response the BRET signal observed from receptor-receptor interactions returned to its initial state (**Figure 5-5 A**). In contrast, ATI-2341 (10 μM) caused a significant decrease in BRET ratio that was slightly faster than the increase seen with CXCL12 with its negative peak at around 4 min. The amplitude of the decrease of ATI-2341 (-0.028 ± 0.003) was also a lot smaller than the increase in amplitude caused by CXCL12 (0.106 ± 0.016). IT1t, a small molecule antagonist, also showed a decrease of BRET ratio (-0.044 ± 0.011 after 5 min) suggesting the conformational change in the oligomers caused by IT1t and ATI-2341 are similar (**Figure 5-5 B**). Simultaneous addition of 1 μM CXCL12 and 10 μM ATI-2341 resulted in a curve similar to that of CXCL12 alone with a peak response of 0.089 ± 0.016 after 10 min. The peak values of all compounds

(CXCL12, IT1t, 10 µM ATI-2341 and CXCL12 + ATI-2341) except for the lower ATI-2341 concentration of 1 µM were significantly different from zero (one sample t test comparison to a theoretical value of zero, $P<0.05$).

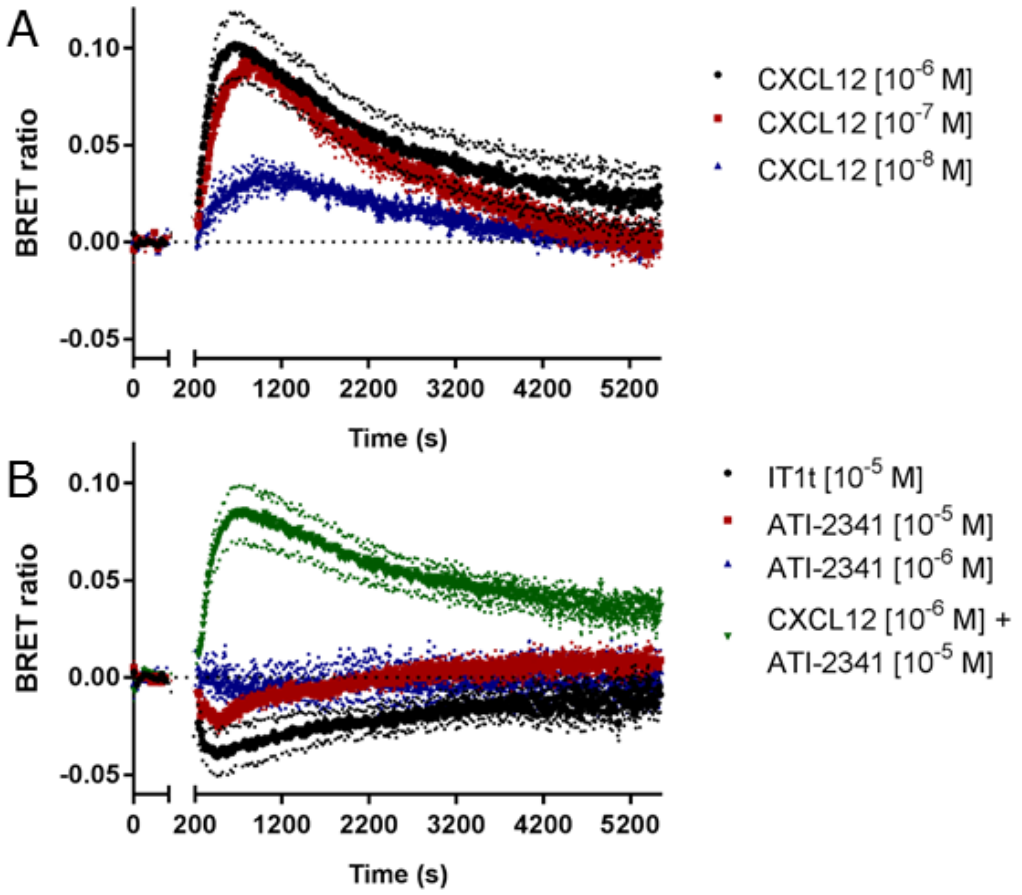

Figure 5-5: Influence of compounds on CXCR4 homo-oligomers. Change in oligomers as change in Raw BRET Ratio. HEK293G cells transfected with 25 ng/well SNAP-CXCR4 and 50 ng/well NanoLuc-CXCR4 in a kinetic BRET assay with subtracted HBSS trace, showing pooled data of (**A**) 10^{-6} M CXCL12 (n = 4), 10^{-7} M CXCL12 or 10^{-8} M CXCL12 (both n = 3) and (**B**) 10^{-5} M IT1t, 10^{-5} ATI-2341, 10^{-6} M CXCL12 + 10^{-5} M ATI-2341 (all n = 4) and 10^{-6} M ATI-2341 (n =3). Data are background subtracted (HBSS alone) and shown as mean ± S.E.M. as dotted lines around the signal of the indicated number of independent experiments, each performed in triplicate

5.4 G protein activation

In the next set of experiments the activation of G proteins by CXCR4 ligands was measured using G protein FRET sensors. These experiments were performed in order to investigate whether the pepducin activated the receptor and signalling pathways through the same initiating proteins as CXCL12. G proteins directly interact with the GPCR and are the canonical initiating protein for signalling pathways. HEK293T cells were transfected with untagged CXCR4 and a FRET-based G protein sensor ($G\alpha_{i1}$, $G\alpha_{i2}$, $G\alpha_{i3}$ or G_q) as described previously in **2.4.3 G protein activation assay**. The G proteins are tagged with an mTurqouise at their α-subunit and with a Venus at the β_1-subunit. Due to the plasmid the β_1- and γ_2-subunits are expressed in a 1:1 ratio and the expression of the α-subunit is approximately 1/3 lower (Adjobo-Hermans *et al.*, 2011; Goedhart *et al.*, 2011; Van Unen *et al.*, 2016).

The direct activation of $Gi\alpha_1$, $Gi\alpha_2$, $Gi\alpha_3$ and G_q by CXCL12, ATI-2341 and pepducin variants (ATI-2504, ATI-2339) as well as activation by ATI-2341 in cells without transfected CXCR4 was measured in a 96-well plate based assay using the G protein sensors from Carsten Hoffmann's group which show a decrease in FRET ratio upon activation due to the α and βγ subunits of the G protein moving apart from each other (Adjobo-Hermans *et al.*, 2011; Van Unen *et al.*, 2016). Cells were monitored for an initial 5 min before addition of compounds and then for a further 20 min. The decrease in FRET signal was then compared to the buffer control wells.

It was first tested if CXCL12 and ATI-2341 had the ability to activate G proteins via CXCR4 (**Figure 5-6** and **Table 5-1**). Both ligands caused a concentration-dependent decrease in FRET ratio indicative of activation of $Gi\alpha_1$, $Gi\alpha_2$ and $Gi\alpha_3$. For G_q, a significant response was observed only at the highest concentration. CXCL12 showed a 100-fold, significantly higher potency than ATI-2341 for activation of all three Gi family G proteins. In those three G proteins, no significant differences in potencies or in maximal response were seen within one compound, apart from ATI-2341 in $Gi\alpha_1$ and $Gi\alpha_2$ (**Table 5-1**). The

pepducin variant ATI-2504, without a lipid tail, and ATI-2339, missing the last three amino acids, show little activation of the G proteins and are significantly less potent than ATI-2341.

As another control, cells that were not transfected with CXCR4, but an empty pcDNA3.1, were treated with ATI-2341. For $Gi\alpha_2$ and $Gi\alpha_3$, only the highest concentration of ATI-2341 (10 µM) showed a response significantly different from 100 % in non-transfected cells. For $Gi\alpha_1$, the two highest concentration of ATI-2341 (10 and 1 µM) showed a response significantly different from 100 %. However, in all cases the responses were significantly smaller than the ones observed in transfected cells.

Table 5-1: pEC_{50} values obtained in G protein activation assay for CXCL12 or ATI-2341 with mTurquoise-$Gi\alpha_1$, $Gi\alpha_2$ and $Gi\alpha_3$; and Venus-Gß with co-expression of CXCR4. Data represented as mean ± S.E.M. from 5 independent experiments

G protein	**CXCL12**		**ATI-2341**	
	pEC_{50}	Max. FRET decrease	pEC_{50}	Max. FRET decrease
$Gi\alpha_1$	8.00 ± 0.25	98.3 ± 0.3 %	5.67 ± 0.14 (S)	97.0 ± 0.1 %
$Gi\alpha_2$	8.15 ± 0.25	96.5 ± 0.6 %	6.01 ± 0.19 (S)	93.9 ± 1.3 %
$Gi\alpha_3$	7.91 ± 0.17	97.2 ± 0.5 %	5.87 ± 0.14	95.6 ± 0.6 %

No significant differences in potencies or maximal FRET decreases between the different G proteins for one compound apart from $Gi\alpha_1$ and $Gi\alpha_2$ with ATI-2341 highlighted by (S)

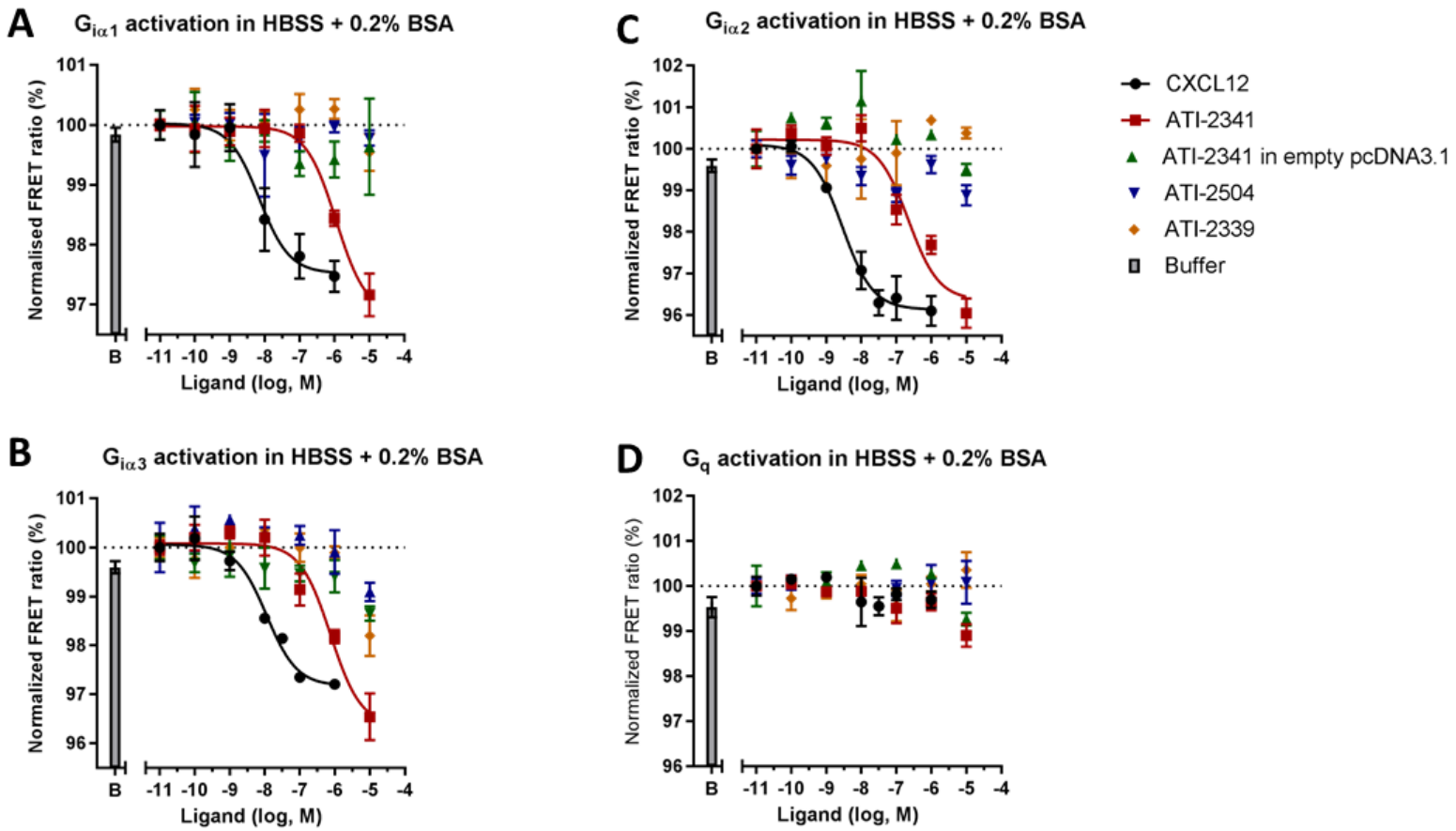

Figure 5-6: Change of normalized FRET ratio ± S.E.M. in HEK293T transiently transfected with WT CXCR4 or empty vector and (**A**) Giα$_1$, (**B**) Giα$_2$, (**C**) Giα$_3$ or (**D**) Gq treated with CXCL12 or ATI-2341, showing one representative experiment with 3 replicates for each concentration, similar data were obtained in 4 more experiments

5.5 Inhibition of cAMP production

The functional response of CXCR4 stimulation by the endogenous agonist CXCL12 and the pepducin ATI-2341 was studied in a GloSensor assay monitoring the inhibition of forskolin (FSK) mediated cAMP production. The activation of G_i family of G proteins through CXCR4 by CXCL12 and ATI-2341 was verified in the previous section **5.4 G protein activation**. As a next step the functional response of CXCR4 was measured in order to see if the pepducin has the same downstream signalling output as the endogenous ligand and was sensitive to antagonists. As shown in the previous chapter, native HEK293G cells did not show a measurable modulation of their FSK signal with the addition of CXCL12 or ATI-2341 (**Figure 4-1**).

FSK was added to the cells to stimulate adenylyl cyclase and increase cellular levels of cAMP. The activation of CXCR4 lead to the inhibition of the cAMP levels through coupling to $G_{i/o}$. The experiments were performed with HEK293G cells stably expressing the GloSensor biosensor, which becomes bioluminescent upon binding to cAMP, and CXCR4 containing an N-terminal SNAP-tag. FSK (30 μM) was added to each well at the same time as increasing concentrations of agonist or control ligands. Furthermore, the influence of the antagonist AMD3100 on the effects of CXCL12 and ATI-2341 was studied by pre-incubating the cells with the antagonist. The luminescence of each well, reflecting the amount of cAMP present, was then measured every 90 seconds for 1 hour.

The addition of FSK caused an increase in cAMP present, resulting in a fast increase of luminescence that reached its maximum within 5 min (**Figure 5-7A** and **B**) cAMP levels then decreased back to baseline levels within the next 30 min. The simultaneous addition of the agonists CXCL12 or ATI-2341 decreased the maximal response to FSK in a dose-dependent manner. The position of the maximum caused by FSK shifted to an earlier point in time with higher concentrations of both added CXCL12 and ATI-2341 (**Figure 5-7A and 5-7B**).

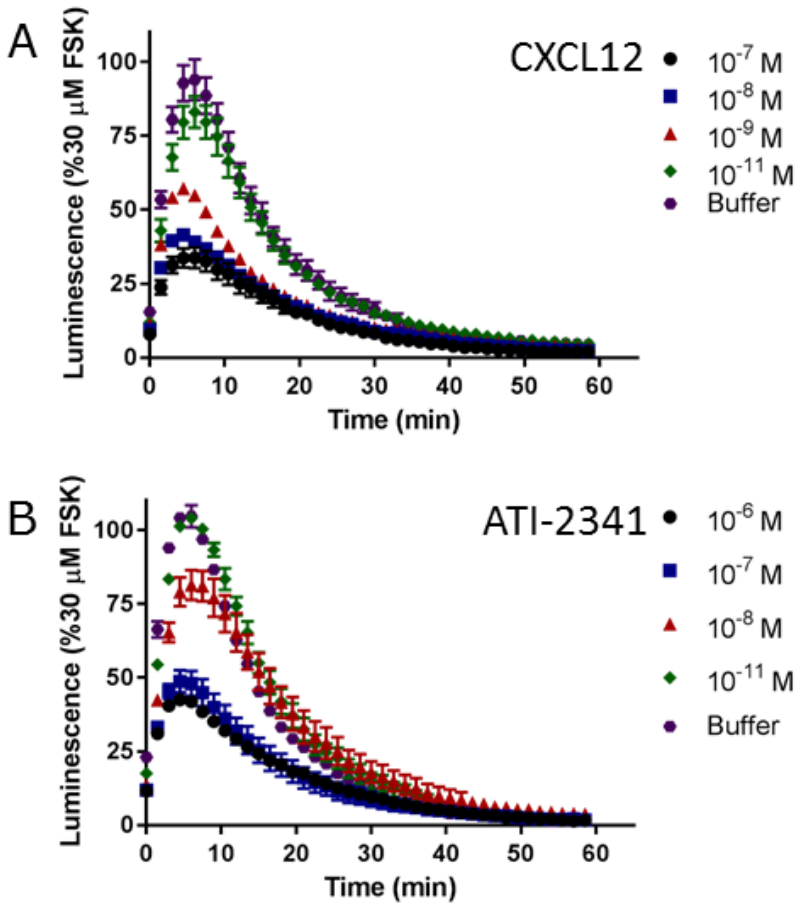

Figure 5-7: Time course of cAMP production. cAMP in HEK293G_SNAP-CXCR4 cells treated with 30 µM FSK and different concentrations of (**A**) CXCL12 or (**B**) ATI-2341. Data shown were normalized to 30 µM FSK, showing one representative individual experiment as mean ± S.E.M. of 4 replicates. Similar data were obtained in (**A**) 8 or (**B**) 12 individual experiments.

The acquired data was then evaluated by the height of the maximal response as described in **2.6 Data Analysis** and a dose response curves were fitted. The increase of cAMP caused by 30 µM of FSK was inhibited by the addition of the endogenous ligand CXCL12 or by the pepducin ATI-2341. With increasing concentrations of compound the obtained peak in luminescence was decreased. The resulting curve had a characteristic sigmoidal shape as shown in **Figure 5-8** from which pEC_{50} and E_{max} were calculated. CXCL12 was shown to inhibit 47.7 ± 3.3% of the signal caused by FSK with a pEC_{50} value of 9.73 ± 0.16 (n=9). In comparison ATI-2341, inhibited 54.5 ± 3.3% of the signal caused by FSK (NS different from CXCL12) with a pEC_{50} value

of 7.98 ± 0.09 (n=13). Initially, the data were also analysed by calculating the area under the curve instead of the height of the maximal response in order to compare analysis approaches, and compare the obtained values for pEC_{50} and E_{max} (**Figure 5-9**). Since there were no significant differences in the two approaches the height of the maximum was used in order to analyse the data for all future experiments.

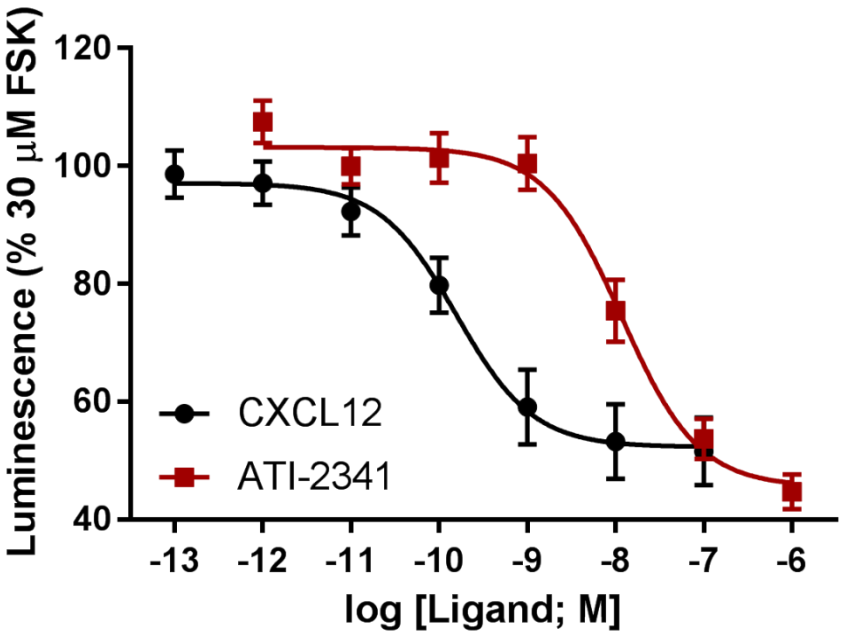

Figure 5-8: Effect of CXCL12 or ATI-2341 on FSK stimulated cAMP formation. HEK293G cells overexpressing CXCR4 were stimulated with 30 µM FSK in the presence of CXCL12 (●) or ATI-2341 (■) in a GloSensor assay. Response measured as luminescence of the peak signal analysed from kinetic cAMP curves as described in the Methods section. Data are shown as mean ± S.E.M. of n=9 (CXCL12) or n=13 (ATI-2341) independent experiments, each performed with 4 replicates. Data were normalised to 30 µM FSK (100%) and basal levels without FSK reached up to 5%. Luminescence was measured on an EnVision plate reader.

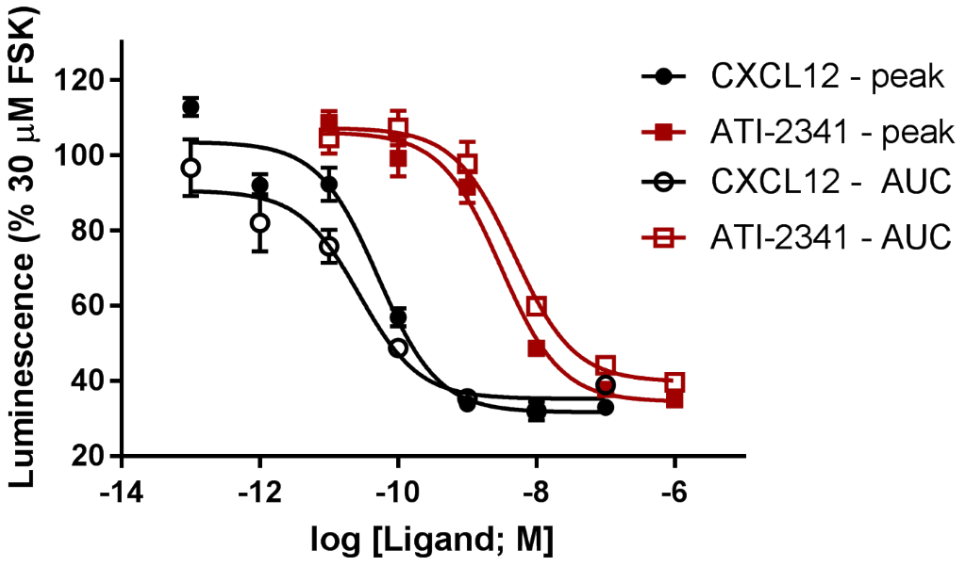

Figure 5-9: Comparison of analysis of the cAMP assay via area under the curve or height of the maximal signal. HEK293G cells overexpressing CXCR4 were stimulated with 30 μM FSK in the presence of CXCL12 (circles) or ATI-2341 (squares) in a GloSensor assay. Response measured as luminescence of the peak signal (closed symbols) or area under the curve (open symbols) analysed from kinetic cAMP curves as described in the Methods section. Data are shown as mean ± S.E.M. of one individual experiment performed with 4 replicates. Data were normalised to 30 μM FSK. Luminescence was measured on an EnVision plate reader.

In order to confirm that the decrease in cAMP production seen above is dependent on the activation of $G_{i/o}$, pertussis toxin which blocks the ability of $G_{i/o}$ to couple to a GPCR (Baker and Hill, 2007) was incubated with the cells overnight (**Figure 5-10**). While untreated cells show a concentration-dependent inhibition of cAMP production, cells treated with PTX show no inhibition after the addition of CXCL12 or ATI-2341 ($P > 0.05$, $n = 5$).

Initially an EnVision plate reader was used to monitor luminescence, however later in the project we changed to a PheraStar plate reader on which all curves seemed to shift to not significantly lower potencies with a larger inhibition window (**Table 5-2**).

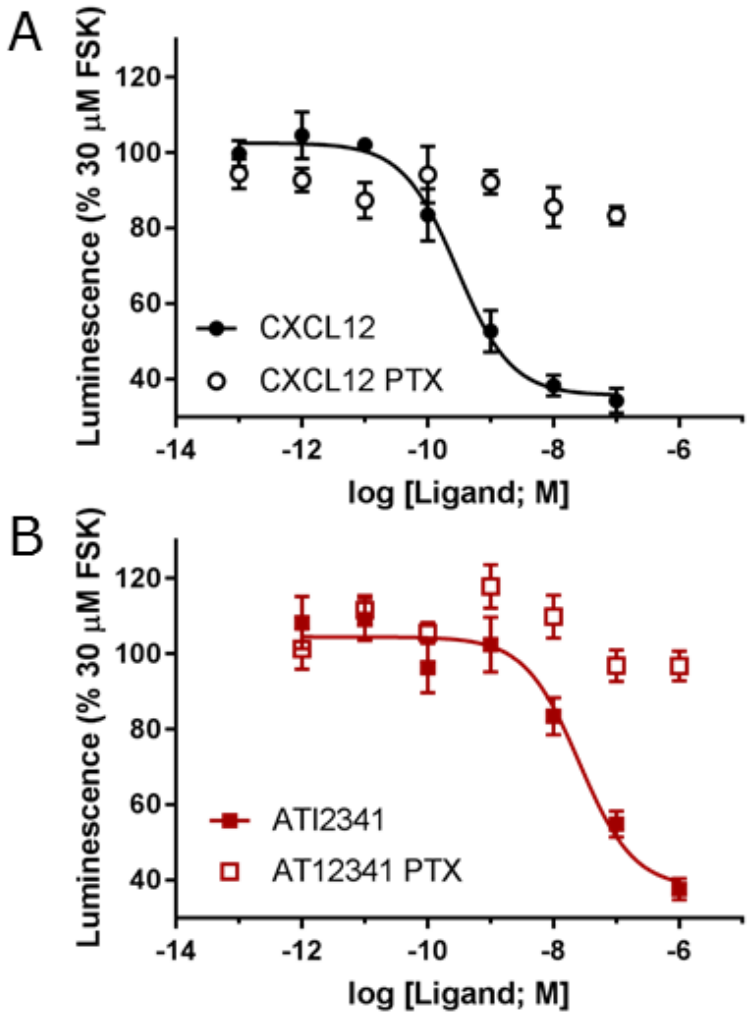

Figure 5-10: Effect of PTX on inhibition of FSK mediated cAMP production. HEK293G_SNAPCXCR4 cells were stimulated with 30 µM FSK in the presence of (**A**) CXCL12 or (**B**) ATI-2341 in a GloSensor assay. Cells were either untreated (closed symbols) or treated with 100 ng/ml PTX overnight (open symbols). Response measured as luminescence of the peak signal analysed as described in the Methods section. Data are shown as mean ± S.E.M. of n=5 individual experiments performed in triplicate for ATI-2341 and duplicate for CXCL12. Data were normalised to 30 µM FSK (100%) and basal levels without FSK reached up to 5%. Luminescence measured on a PheraStar plate reader.

Table 5-2: pEC_{50} and maximal inhibition values obtained from GloSensor cAMP assay for CXCL12 or ATI-2341 on EnVision and PheraStar plate reader in comparison

	EnVision		PheraStar	
	pEC_{50}	Maximal inhibition (% 30 µM FSK)	pEC_{50}	Maximal inhibition (% 30 µM FSK)
CXCL12	9.73 ± 0.16 (9)	47.6 ± 5.4 %	9.57 ± 0.18 (5)	64.7 ± 3.1 %
ATI-2341	7.98 ± 0.09 (13)	54.0 ± 2.8 %	7.63 ± 0.27 (5)	64.1 ± 5.2 %

Data represented as mean ± S.E.M. from n individual experiments. N numbers in brackets next to the pEC_{50} values. All data were NS different from another one the two different machines

Furthermore the effect of the antagonist AMD3100 on the CXCL12 and ATI-2341 response was determined to see whether the inhibition by pepducins can be antagonised by an antagonist that has been shown to compete with CXCL12. Cells were pre-incubated for 1h without or with 0.1 - 10 µM AMD3100. Inhibition curves of CXCL12 and ATI-2341 were shifted in parallel to the right when treated with AMD3100 and show the same maximal inhibition. A pA_2 value of 7.01 ± 0.23 with a Schild slope of 0.75 ± 0.05 (significantly different from 1, n=5) for AMD3100 on CXCL12 (**Figure 5-11 A, B**) and a pA_2 value of 7.37 ± 0.25 (n=10) with a Schild slope of 0.83 ± 0.08 (NS different from 1) for AMD3100 on ATI-2341 were obtained (**Figure 5-11 C, D**). The pA_2 and Schild values for AMD3100 on CXCL12 and AMD3100 on ATI-2341 are not significantly different from each other ($P > 0.05$). However, the relationship between AMD3100 on ATI-2341 might not be linear as the three concentrations could also be fitted with a curve and more concentrations would be needed for a better fit. AMD3100 seems to have an influence on the response obtained by FSK addition in the absence of any other ligand. This effect is potentially caused by the influence of AMD3100 on the constitutive active portion of CXCR4.

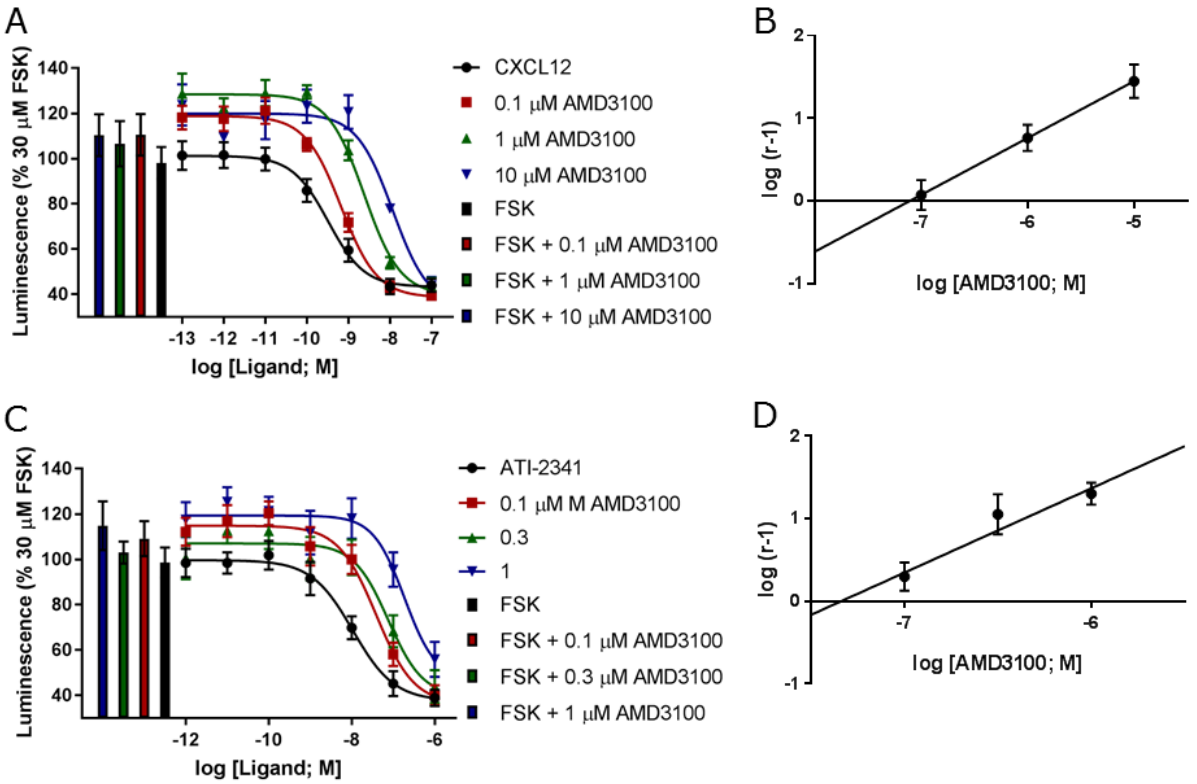

Figure 5-11: Effect of AMD3100 on inhibition of FSK mediated cAMP production by CXCL12 or ATI-2341. HEK293G_SNAPCXCR4 cells were pre-incubated with indicated concentrations of AMD3100 for 1h and then stimulated with 30 μM FSK and (**A**) CXCL12 or (**C**) ATI-2341 in a GloSensor assay. Corresponding Schild plots are shown in (**B**) and (**D**). Response measured as luminescence of the peak signal analysed as described in the Methods section. Data are shown as mean ± S.E.M. of n=5 (all CXCL12 curves) or n=10 (ATI-2341), n=9 (ATI-2341 with 0.1 and 1 μM AMD3100) and n=5 (ATI-2341 with 0.3 μM AMD3100) individual experiments performed in triplicates. Data were normalized to 30 μM FSK and basal levels without FSK reached up to 5%. Luminescence measured on an EnVision plate reader.

In a next step, control pepducins were measured in order to investigate the importance of the sequence of ATI-2341 (**Figure 5-12** and **Table 5-3**). ATI-2755 with the two methionines mutated to one glycine and one alanine showed a similar response to ATI-2341 with a pEC_{50} of 8.52 ± 0.34. While ATI-2339, missing the last three amino acids of the C-terminus of ATI-2341, and ATI-2504 (missing the lipid) showed a significant response but with significant lower potency, with maximum inhibition not being reached at concentrations up to 1 µM. ATI-2504 seemed to increase the baseline of the FSK response. ATI-2346, missing the first four amino acids of the N-terminus of ATI-2341, showed no response. This shows that the activity of the pepducin is heavily dependent on sequence and the lipid tail.

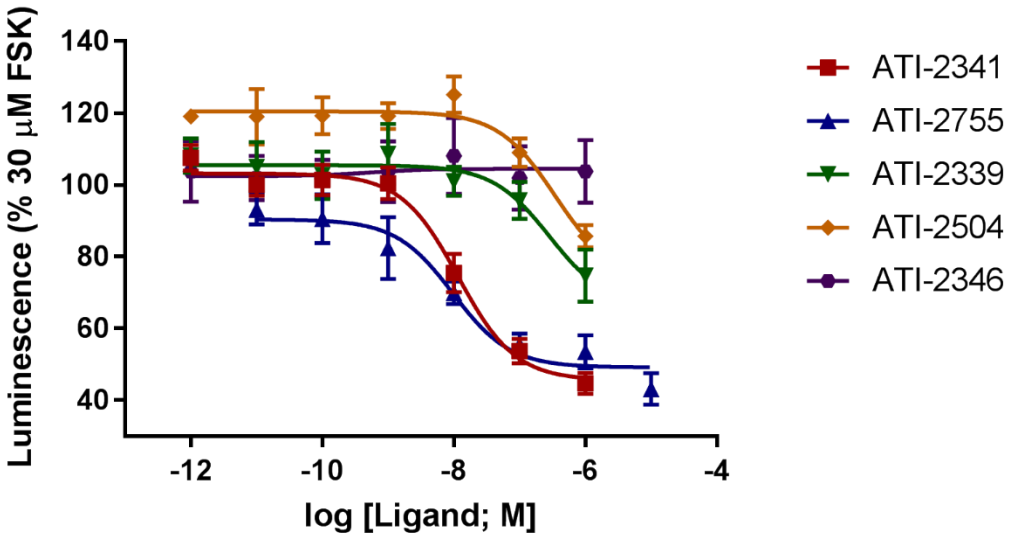

Pepducin	**Sequence**
ATI-2341	Pal-MGYQKKLRS MTDKYRL-NH_2
ATI-2755	Pal-GGYQKKLRS ATDKYRL-NH_2
ATI-2339	Pal-MGYQKKLRS MTDK -NH_2
ATI-2504	MGYQKKLRS MTDKYRL-NH_2
ATI-2346	Pal- KKLRSMTDK YRL-NH_2

Figure 5-12: **Effect of pepducin variants on FSK mediated cAMP production.** HEK293G_SNAPCXCR4 cells were stimulated with 30 µM FSK in the presence of various pepducin variants in a GloSensor assay. Response measured as luminescence of the peak signal analysed as described in the Methods section. Data are shown as mean ± S.E.M. of n=5 individual experiments performed in triplicate. Data were normalised to 30 µM FSK (100%) and basal levels without FSK reached up to 5%.

Table 5-3: pEC_{50} and maximal inhibition values obtained from GloSensor cAMP assay for pepducin varaints on EnVision or PheraStar plate reader; data represented ± S.E.M. from n separate experiments

Compound	pEC_{50}	Maximum inhibition/Inhibition at 1 µM
ATI-2755	8.52 ± 0.34	49.1 ± 3.4 % (max inhibition)
ATI-2504	<6	69.9 ± 23.6 % (at 1 µM)
ATI-2339	<6	63.1 ± 21.4 % (at 1 µM)
ATI-2346*	ND	104.5 ± 4.8 % (at 1 µM)

* measured on PheraStar, all other measurements on EnVision, all n=5

5.6 β-arrestin recruitment

It has previously been shown that ATI-2341 only recruits small amounts of β-arrestin2 and β-arrestin1 to CXCR4 in comparison to CXCL12 (Quoyer *et al.*, 2013). In order to verify these findings, the experiments were repeated using a BRET-based assay detecting the interaction between CXCR4-NanoLuc and β-arrestin2-VENUS (**Figure 5-13 A**). Furthermore, as this seemed to be one of the few functional responses where ATI-2341 did not activate the receptor in the same way as CXCL12, ATI-2341 was tested for its ability to inhibit β-arrestin2 recruitment by CXCL12. ATI-2341 was added 30 min prior to or at the same time as CXCL12 (**Figure 5-13 B**).

CXCL12 caused a rapid increase in BRET ratio reaching its peak signal at 10 min and then slowly decreasing not returning to baseline levels within the measured time frame. In contrast, ATI-2341 seemed to recruit β-arrestin2 more slowly with a significant signal different from zero seen only after 30 min. When adding ATI-2341 for 30 min before CXCL12, CXCL12 was still able to produce further β-arrestin2 recruitment to the level of CXCL12 alone. The peak responses of CXCL12 and CXCL12 pre-incubated with ATI-2341 were not significantly different from another showing that the effects of CXCL12 and ATI-2341 are not additive. The simultaneous addition of ATI-2341 and CXCL12 also causes a signal similar to the one observed with CXCL12 with maximal responses that are not significantly different from another.

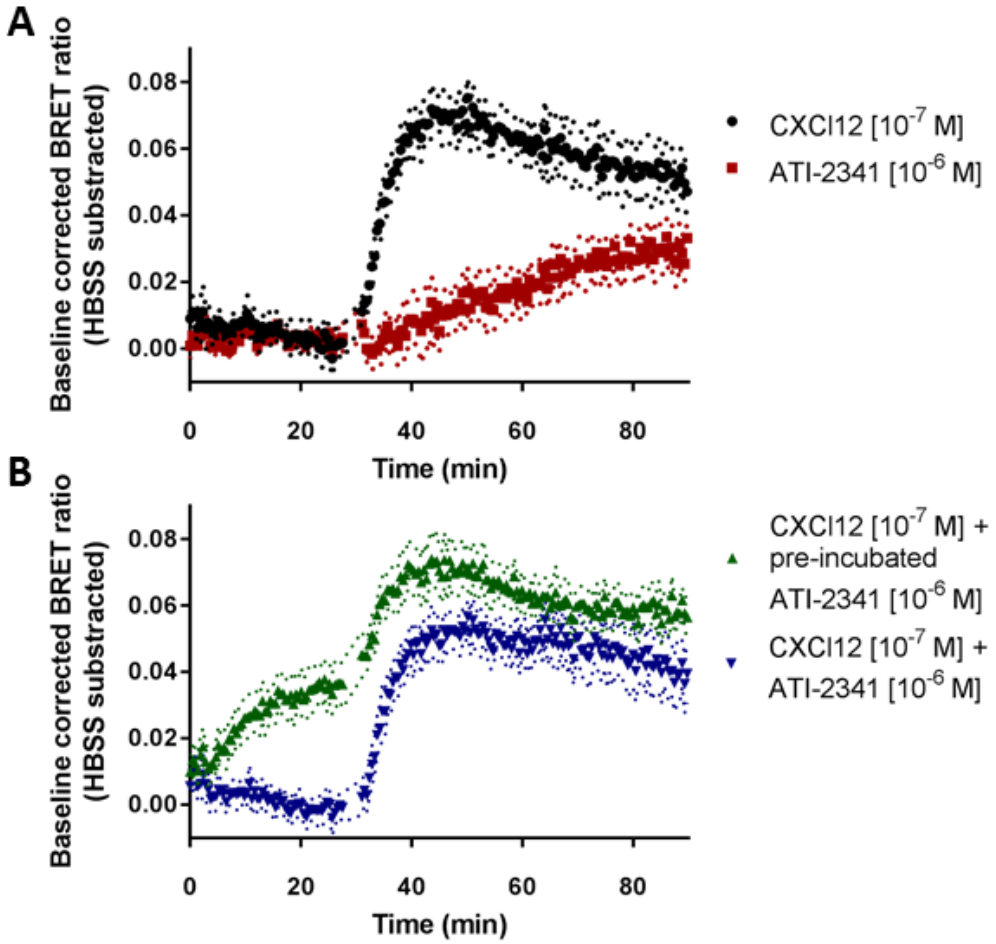

Figure 5-13: ß-arrestin recruitment to CXCR4. HEK293G cells were transiently transfected with 25 ng/well CXCR4_NLuc and 10 ng/well VENUS-β-arrestin. Recruitment as change in BRET ratio. Cells were treated with (**A**) one high concentration of CXCL12 or ATI-2341 or (**B**) CXCL12 and ATI-2341 either at the same time or with 30 min pre-incubation of ATI-2341. Data are shown as mean ± S.E.M. as dotted lines around the signal of n=6 independent experiments performed in triplicate.

5.7 Internalisation

In addition to the reports of ATI-2341 only recruiting β-arrestin to CXCR4, there were also contradictory reports regarding ATI-2341-mediated internalisation of CXCR4 based on confocal imaging or flow cytometry (Tchernychev *et al.*, 2010; Quoyer *et al.*, 2013). The internalisation of receptors is a process classically connected with β-arrestin. Interactions with β-arrestin are able to activate or inhibit signalling pathways of GPCRs in a different way than G protein mediated signalling. β-arrestin has the ability to link receptors to

clathrin coated pits for internalisation in an agonist-dependent manner (Sun *et al.*, 2002; Reiter and Lefkowitz, 2006).

In contrast to the previous measurements of β-arrestin, we saw slow recruitment by ATI-2341 and then measured internalisation in the same time frame. In order to quantify the internalisation of SNAP-tagged CXCR4 receptor we used a high content imaging approach using multiplex staining for the cell nucleus (Höchst 33342), SNAP-tagged CXCR4 receptor (SNAP-Surface Alexa Fluor 488) and endosomal regions were visualized using transferrin Alexa Fluor 568. The amount of internalisation in response to agonist was evaluated as described in the method section by the average intensity of SNAP-CXCR4 continuing-granules co-localizing with AF568-transferrin (**Figure 5-14**).

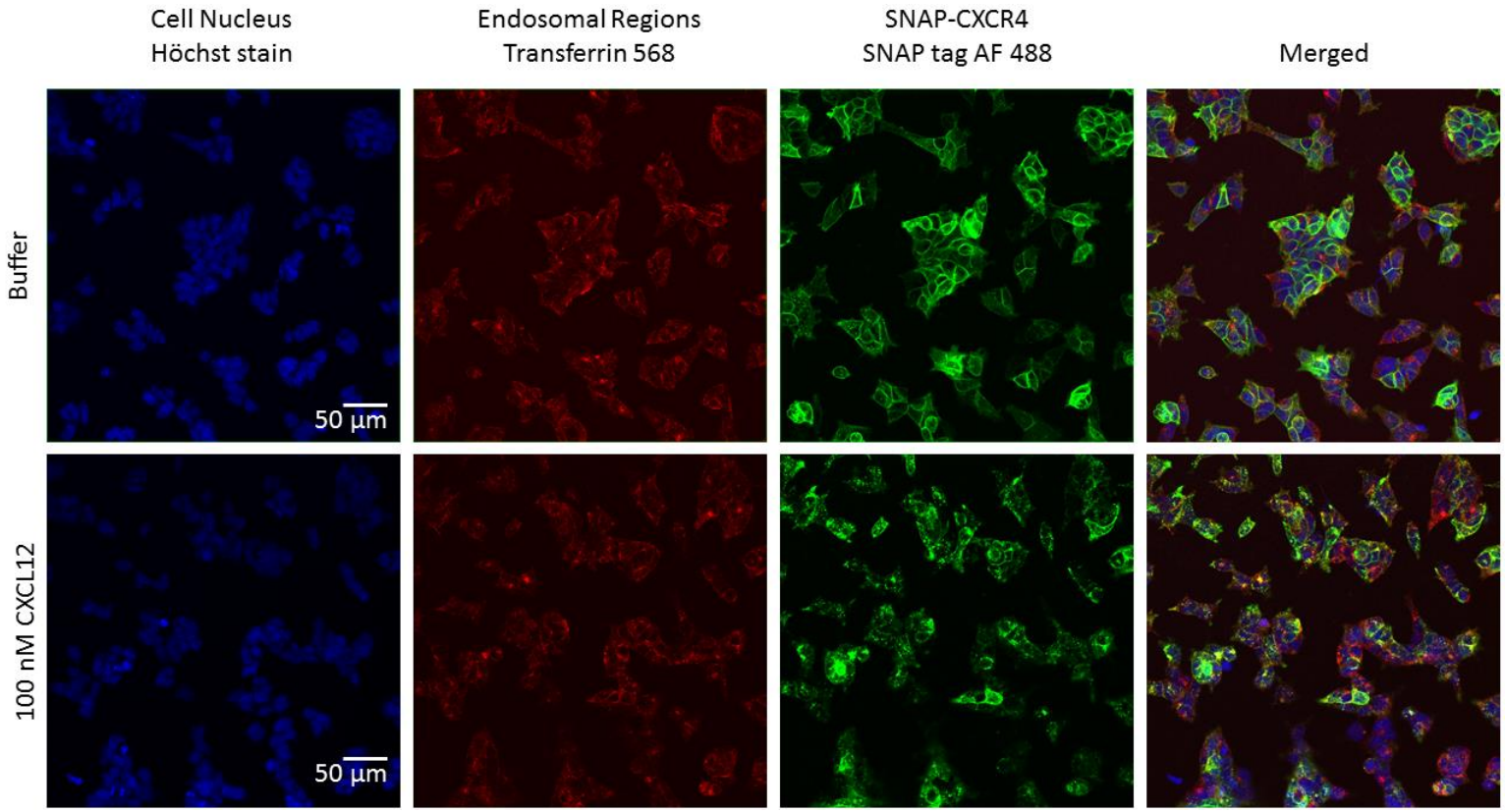

Figure 5-14: Confocal imaging showing internalisation of CXCR4. Representative images of HEK293G SNAP-CXCR4 cells stained with Hoechst stain (nuclei; blue), AF568-transferrin (endosomes; red) and SNAP Surface Alexa Fluor 488 (SNAP-CXCR4; green) in control (top) and after addition of 100 nM CXCL12 for 60 min at 37 °C (bottom); imaged on ImageXpress Ultra-Confocal plate reader with 40x magnification. Single image representative of 4 images obtained per well in triplicate from 7 independent experiments.

First, the ability of CXCL12 to promote internalisation was tested (**Figure 5-15 A**). Increasing concentrations of CXCL12 caused an increase in internalised SNAP-CXCR4 and the average brightness of co-localizing granules was increased with a pEC_{50} = 8.84 ± 0.83 (n=7). Furthermore, the ability of pre-incubated AMD3100 to antagonise the internalisation of CXCL12 was studied in the same set up. Cells showed less internalisation with the response curve of CXCL12 shifting in parallel to lower potencies to the initial sigmoidal response in the presence of AMD3100 (**Figure 5-15 B**). The obtained pA_2 for AMD3100 for CXCL12 was 6.23 ± 0.69 (n = 7).

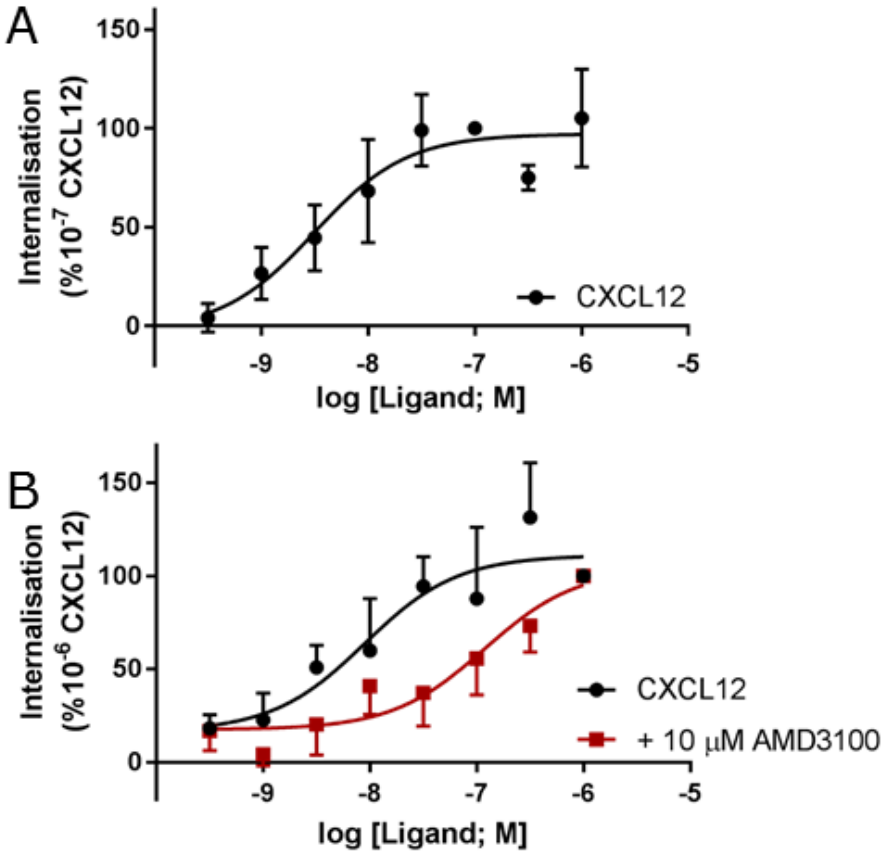

Figure 5-15: Internalisation of CXCR4 mediated by CXCL12. HEK293G_SNAP-CXCR4 cells were (**A**) treated with increasing concentration of CXCL12 or (**B**) pre-incubation with 10 µM AMD3100 for 1h and then increasing concentration of CXCL12. Response as increase in brightness of granules colocalising SNAP-label AF488 and AF568-treansferrin. Data are normalised to 1 µM or 100 nM CXCL12 respectively. Data in A was normalised to 100 nM in order to compare to other compounds which were measured with 100 nM CXCL12 normalisation wells. Data are shown as mean ± S.E.M. of n=7 independent experiments performed in triplicate.

After verifying that the assay shows internalisation promoted by CXCL12 and can be antagonised using the known CXCL12 antagonist AMD3100, the experiment was performed with ATI-2341. ATI-2341 caused a concentration-dependent increase in internalisation, similar to the sigmoidal response of CXCL12 with a 100-fold lower potency (**Figure 5-16 A**) with a pEC_{50} of 6.71 ± 0.14 and an E_{max} of 136.5 ± 17.7 % (NS different from CXCL12, n=7). Interestingly, AMD3100 was also able to antagonise the ATI-2341 response (**Figure 5-16 B**) with a pA_2 not significantly different from the one obtained with CXCL12 (pA_2 = 6.28 ± 0.25, n = 5).

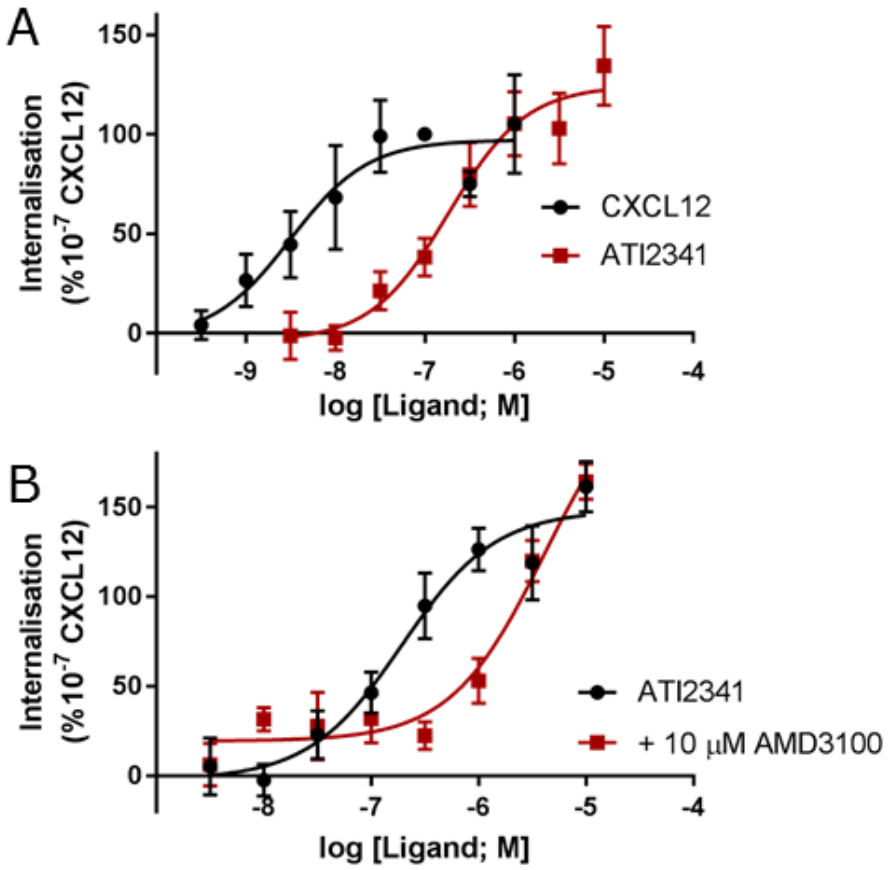

Figure 5-16: Internalisation of CXCR4 mediated by ATI-2341. HEK293G_SNAP-CXCR4 cells were (**A**) treated with increasing concentration of ATI-2341 or CXCL12 or (**B**) pre-incubation with 10 µM AMD3100 for 1h and then increasing concentration of ATI-2341. Response as increase in brightness of granules colocalising SNAP-label AF488 and AF568-treansferrin. Data are normalised to 100 nM CXCL12. Data are shown as mean ± S.E.M. of (**A**) n=7 or (**B**) n=5 independent experiments performed in triplicate.

In a last step, the importance of the lipid tail of the pepducin in stimulating internalisation was verified. The non-lipidated pepducin ATI-2504 was added to the cells and an E_{max} of 31.4 ± 4.6 % (at 10 µM, n = 4) (**Figure 5-17**) was reached which was significantly lower than the one observed for ATI-2341. Potencies differed from experiment to experiment from pEC_{50} values of 5 up to 14.

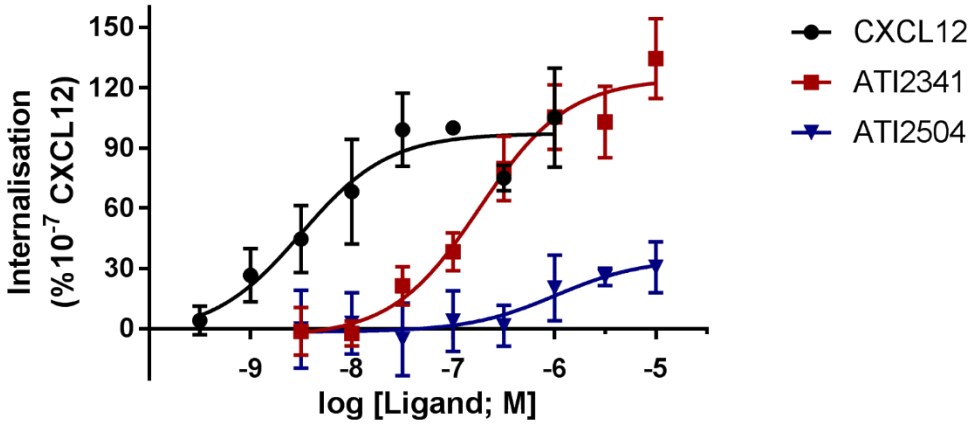

Figure 5-17: Internalisation of CXCR4 mediated by CXCL12, ATI-2341 or ATI-2504. HEK293G_SNAP-CXCR4 cells were treated with increasing concentration of CXCL12, ATI-2341 or ATI-2504. Response as increase in brightness of granules colocalising SNAP-label AF488 and AF568-treansferrin. Data are normalised to 100 nM CXCL12. Data are shown as mean ± S.E.M. of n=7 (CXCL12, ATI-2341) or n=4 (ATI-2504) independent experiments performed in triplicate.

5.8 Chapter Summary and Discussion

In this chapter the conformational change caused at CXCR4 as well as the functional signalling pathways mediated by ATI-2341 at CXCR4 were studied in comparison to CXCL12.

A CXCR4 biosensor was used to investigate the conformational change caused by CXCL12 and ATI-2341 in order to see any differences arising from the two distinct binding modes. Similar FRET and BRET biosensors have been described previously for about 20 other GPCRs (Hoffmann *et al.*, 2005; Lohse *et al.*, 2012; Kauk and Hoffmann, 2018). One major benefit of these is that receptor activation kinetics can be investigated within the membrane of a whole cell. However, the influence of the tags on the receptor

behaviour and signalling should always be taken into account. Initially, receptors were tagged with CFP and YFP (each about 28 kDa) which doubled the molecular mass of the receptor. By introduction of the FlAsH sequence (0.7 kDa) this influence was reduced significantly (Hoffmann *et al.*, 2005). These FRET and BRET sensors have been a very useful tool to investigate kinetics involved in the activation and signalling of GPCRs. The β_1-adrenoceptor, A_{2A} and α_{2A} receptors have been reported with conformational change and G protein interaction half-lives of 30 to 50 ms, while the activation of the G protein can take 10 times as long and the accumulation of cAMP taking place with a half-life of 20,000 to 50,000 ms (Lohse *et al.*, 2008; Jensen *et al.*, 2009). The activation of the internal biosensor in CXCR4 by CXCL12 and ATI-2341 verified the direct effect of the pepducin on CXCR4. ATI-2341 showed a slower ($\tau \approx 4300$ ms compared to 600 ms) but larger increase (8% in comparison to 3%) in FRET ratio with a delay in response of 30 seconds in comparison to CXCL12. The slower activation of the FRET biosensor suggest once the pepducin and the receptor interact the change in conformation is slower than with CXCL12. The 30 s delay between addition of pepducin and response can potentially be explained by the time it takes the pepducin to anchor into and cross the membrane and finally interact with CXCR4. In the previous chapter, looking at the kinetic signal in plates rather than single cells, this time delay was not as apparent as in single cells, however binding of CXCL12-red was faster than of ATI-2341f. Moreover, the unlipidated pepducin does not show any influence on binding of CXCL12-red to CXCR4 or potent mediation of downstream signalling. All of these data and the differences seen for BRET measurements with N- and C-terminal tagged receptor in **4.2.1. Binding of ATI-2341f** support the theory of intracellular interactions of pepducins and receptor. While the direction of the change in FRET remains the same (increase in FRET ratio) the timings of the increase are different suggesting the change in the receptor might be different too. This difference in conformational change might be related to a different impact on dimers which was tested next.

Following the receptor rearrangement we investigated the formation and arrangement of oligomers of CXCR4 and the influence of compounds on these. CXCR4 has been reported as a dimer multiple times (Vila-Coro *et al.*, 1999; Babcock *et al.*, 2003; Percherancier *et al.*, 2005; Wang *et al.*, 2006; Wu *et al.*, 2010; Ge *et al.*, 2017). CXCR4 and ACKR3 have also been reported to form heterodimers (Levoye *et al.*, 2009; Décaillot *et al.*, 2011). It has previously been observed in BRET based techniques that CXCL12 as well as AMD3100 cause ligand induced changes in CXCR4 homodimers that are caused by rearrangement of dimers rather than formation or breaking of them (Percherancier *et al.*, 2005). Both, CXCL12 and AMD3100 show an increase in BRET. In agreement we found the presence of oligomers in a BRET assay using a fixed concentration of NLuc-tagged CXCR4 and increasing concentrations of SNAP-tagged CXCR4. Interestingly, heterodimers were visible when using NLuc-ACKR3 and SNAP-CXCR4 but when swapping the tags a bigger linear portion in the BRET increase was observed. This might be due to the fact that ACKR3 is mostly expressed intracellularly (Luker *et al.*, 2010) and brought to the membrane more efficiently by the NanoLuc-tag than the SNAP-tag. The labelling with cell permeable SNAP label instead of SNAP surface did not change this observation. In contrast to previously published data we saw an influence of pepducins on CXCR4 homodimers. The previously published data (Quoyer *et al.*, 2013) used 1 µM ATI-2341 and 500 nM CXCL12 compared to our highest concentrations of 10 µM ATI-2341 and 1 µM CXCL12. These smaller concentrations caused only very small responses in our system. Furthermore, the change in receptor oligomerisation was previously measured in an endpoint assay after 20 min. In our assay we saw a clear time dependence as the dimers go back to their initial state and 20 min might have been too late to observe any changes. Within the time frame receptors might have mediated any downstream signalling, internalise and dissociate from the ligand. While CXCL12 caused an increase in BRET ratio in our system, we observed a decrease in BRET ratio for ATI-2341 and IT1t suggesting ATI-2341 caused oligomer rearrangements similar to the one by IT1t and

different from CXCL12. However, the functional signalling mediated by ATI-2341 is equivalent to an agonist. In a next step, full concentration curves for the rearrangement of dimers should be measured for all compounds at the time of their peak value.

It has previously been shown that ATI-2341 causes downstream signalling via CXCR4 in a similar way to the endogenous ligand CXCL12 (Tchernychev *et al.*, 2010; Quoyer *et al.*, 2013). In agreement with these studies we found ATI-2341 caused G protein activation ($G\alpha_{i1}$, $G\alpha_{i2}$ and $G\alpha_{i3}$ but not G_q), inhibits cAMP production in a PTX sensitive manner and causes internalisation of the receptor. Potencies for G protein activation for $G\alpha_{i1}$ were previously reported as EC_{50} = 533 ± 91 nM for ATI-2341 and EC_{50} = 0.53 ± 0.19 nM for CXCL12 (Quoyer *et al.*, 2013). These values are lower and show also a bigger shift between the two ligands than the ones measured in this study with 2150 and 9 nM respectively. While no potencies were reported for the cAMP measurements, the published dose response curves showed comparable EC_{50} values and shifts between CXCL12 and ATI-2341 potencies (Janz *et al.*, 2011) to the ones measured in this study. It is also notable that the difference in potencies between CXCL12 and ATI-2341 stays consistent in G protein activation and cAMP inhibition in our studies. The difference is slightly smaller in the internalisation assay. pEC_{50} values are not consistent across assays, potencies measured in G protein activation are 100-fold higher than those measured in cAMP. In general CXCL12 and ATI-2341 reach the same efficacy in all assays apart from the ß-arrestin recruitment. Control pepducins that show no influence on CXCL12 binding in **4.1.2 Displacement of CXCL12-red** showed only very small responses in these functional assays suggesting the importance of the lipid tail and the correct peptide sequence. While the pepducins might not have an influence on the binding pocket of CXCL12 they might still change the conformation of the receptor slightly mediating signalling. Other explanations could be increased expression levels of G proteins or different levels of receptor expression.

β-arrestin recruitment has previously been measured after stimulation with CXCL12 or ATI-2341 (Quoyer *et al.*, 2013). However, only low recruitment by ATI-2341 was observed using 1 µM and measuring for just under 20 min (Quoyer *et al.*, 2013). Our measurements agree with these finding, but when measuring for up to 60 min a slow continuous β-arrestin-2 recruitment by ATI-2341 can be observed. When pre-incubating the cells for 30 min with ATI-2341 before adding CXCL12, the CXCL12 peak reached the same maximum as before with no additional effect of the pepducin. Addition of ATI-2341 and CXCL12 did not change the CXCL12 peak significantly instead of causing an additional effect of CXCL12 and ATI-2341. β-arrestin recruitment is the only tested functional effect in which ATI-2341 behaved differently than CXCL12. The differences in conformational changes observed with the biosensor and oligomer rearrangement might have the biggest effect on the conformation needed for the interaction with β-arrestin. Moreover, ATI-2341 interacts with CXCR4 intracellularly potentially sterically hindering the interaction with β-arrestin.

The internalisation of CXCR4 upon activation with ATI-2341 was observed before on confocal imaging in a qualitative way (Tchernychev *et al.*, 2010) while in flow cytometry only low internalisation was observed (Quoyer *et al.*, 2013). As expected we were able to see the internalisation with a confocal plate reader based assay and could even quantify these effects fitting dose response curves with CXCL12 and ATI-2341 showing the same efficacies. While ATI-2341 shows a slower recruitment of β-arrestin, internalisation of CXCR4 was not impacted suggesting that either the internalisation is mediated β-arrestin independent or the recruitment is sufficient to reach the same amount of internalisation within 1h. It was not possible to investigate the PTX sensitivity of the internalisation as the PTX influenced the shape of the cells too much for image based analysis.

Interestingly, the antagonist AMD3100 has an influence on ATI-2341 activation shifting cAMP and internalisation curves to the right

(pA_2=7.37 ± 0.25 (cAMP); pA_2 = 6.28 ± 0.25 (Internalisation)) with the same potency as the ones of CXCL12 (pA_2=7.01 ± 0.23 (cAMP); pA_2 = 6.23 ± 0.69 (Internalisation)). The pA_2 values obtained in the internalisation and cAMP assay differ from each other. A t-test was performed suggesting that the difference is not significant for CXCL12 ($P > 0.05$), but seems to be significant for ATI-2341 ($P < 0.05$). In the binding assays AMD3100 had no influence on the binding of the pepducin suggesting inhibition of the receptor activation while pepducin is still bound. Previous studies in the group reported pK_b of 6.39 ± 0.53 (n=4) for CXCL12 and 6.31 ± 0.14 (n=7) for ATI-2341 (Goulding *et al.*, 2012).

In the internalisation assay only one concentration was used and therefore no Schild slope was fitted. However, for the cAMP assay Schild slopes not significantly different from another of 0.75 ± 0.05 for CXCL12 (significantly different from 1) and 0.83 ± 0.08 for ATI-2341 (not significantly different from 1) were determined. The Schild slope is a measure of cooperativity between the interaction of agonist and antagonist and a slope smaller than 1 can arise from the non-equilibrium between agonist, antagonist and receptor (agonist is added immediately before the measurement). A Schild slope different from 1 may also indicate a non-competitive antagonism, a drug-disposition mechanism, heterogeneous receptor population or multiple drug properties of the agonist or antagonist (Kenakin, 1993). These values differ from the ones obtained by the GloSensor cAMP assay. The obtained pK_b values are shifted by about 1-log unit between cAMP and internalisation assay. A t-test was performed suggesting that the difference is not significant for CXCL12 ($P > 0.05$), but significant for ATI-2341 ($P < 0.05$). This difference in pK_b might be explained by the different binding modes of AMD3100, CXCL12 and ATI-2341. While AMD3100 is known to bind to a similar site as CXCL12 from the extracellular site of the receptor (Rosenkilde *et al.*, 2004; Xu *et al.*, 2013; Kufareva *et al.*, 2014), ATI-2341 seems to bind intracellularly resulting in two different binding sites for AMD3100 and ATI-2341. Because of this AMD3100 and ATI-2341 are unlikely to

compete directly with each other but rather have opposite effects on the CXCR4 conformation resulting in different functional effects.

In summary, this chapter investigated the functional activation of CXCR4 by ATI-2341 in comparison to CXCL12. As expected from previous publications ATI-2341 acts as an agonist similar to CXCL12 with a 100-fold lower potency in G protein recruitment, cAMP inhibition and internalisation. However, there are some differences in the activation of CXCR4 by the two ligands that have not been observed before. In the previous chapter it was shown, that ATI-2341 and CXCL12 have two distinct binding sites (extracellular vs intracellular) and CXCL12 binds faster to CXCR4 than ATI-2341. Accordingly, measurements with an internal CXCR4 biosensor showed that the activation by ATI-2341 is delayed and slower once CXCR4 and ATI-2341 interact while a response by CXCL12 is fast and immediate. Moreover, the change in BRET caused in oligomers by the two ligands is opposite to each other with CXCL12 showing an increase in BRET and ATI-2341 showing a decrease. Finally, the recruitment of β-arrestin by ATI-2341 is slow compared to a rapid increase caused by CXCL12.

ATI-2341 seems to cause similar downstream signalling to CXCL12 at CXCR4. However, the changes in conformation caused by the two ligands are different from each other suggesting that the conformation of CXCR4 in the presence of ATI-2341 is a distinct conformation different from the inactive form stabilized by antagonists and different from the active form caused by CXCL12 binding.

6 Studies to determine the location and mode of action of pepducins

6.1 Introduction

The interactions between a receptor and ligands or other proteins are based on interactions between the receptors amino acids and the amino acids or functional groups of the peptide ligands, proteins or small molecules respectively. By mutation of residues in the receptor or ligand, areas important for interaction or signal transduction can be identified.

There have been multiple mutational studies investigating the residues involved in CXCL12 binding and involved in the functional signal transduction in CXCR4 mediated by CXCL12 (Brelot *et al.*, 2000; Tian *et al.*, 2005; Wescott *et al.*, 2016) (**Figure 6-1**). CXCL12 binding is heavily impacted by mutations at the N-terminal end of the receptor, where the binding takes place, but also mutations throughout the receptor in transmembrane and intracellular regions can impact binding (Wescott *et al.*, 2016). The intracellular loop 3 and the C-terminal tail of CXCR4 are heavily involved in β-arrestin recruitment (Orsini *et al.*, 1999; Cheng *et al.*, 2000) and G protein activation (Wescott *et al.*, 2016) and therefore mutations in these areas have an impact on signalling.

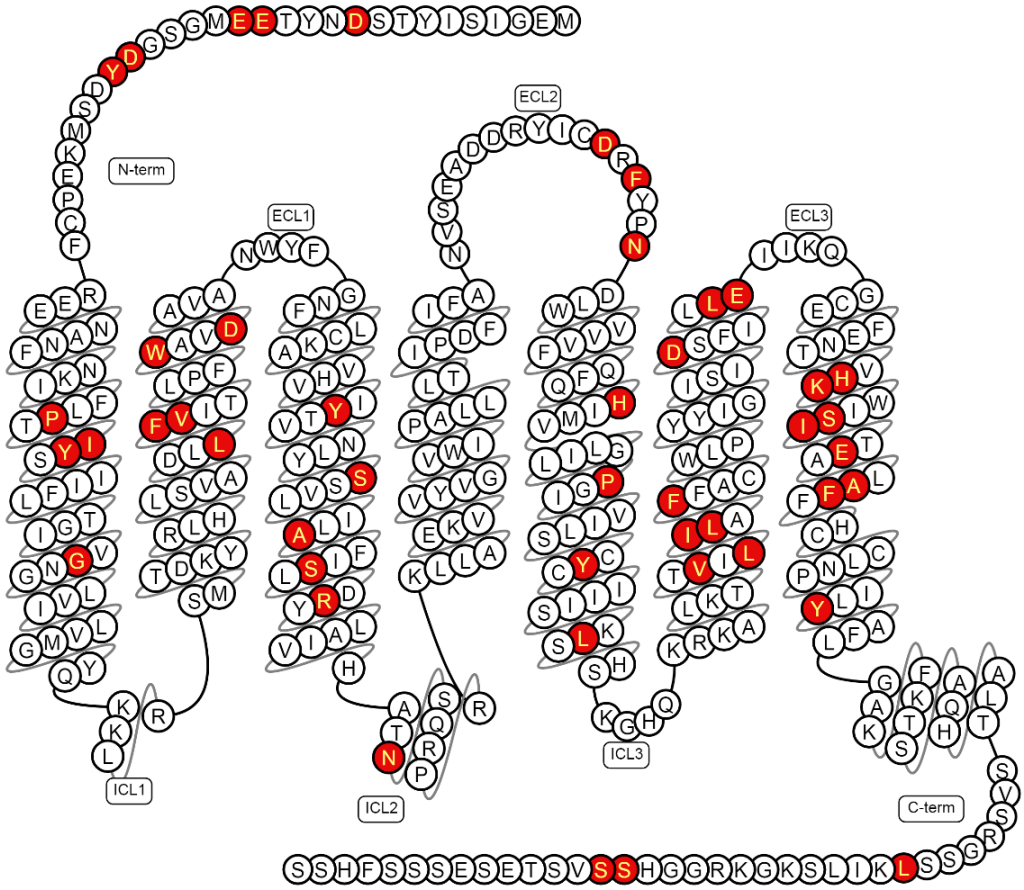

Figure 6-1: Key residues of CXCR4-CXCL12 interaction. Schematic representation of the amino acid sequence of CXCR4 adapted from GPCRdb (Horn et al., 2003) with marked key residues important for CXCL12 interaction and signal transduction identified in (Brelot et al., 2000; Tian et al., 2005; Wescott et al., 2016)

CXCR4 has been reported to form dimers multiple times (Vila-Coro *et al.*, 1999; Babcock *et al.*, 2003; Percherancier *et al.*, 2005; Wang *et al.*, 2006; Wu *et al.*, 2010; Ge *et al.*, 2017) as discussed before in **5.3.1 Oligomerisation of CXCR4 and ACKR3**. In crystal structures, CXCR4 dimerises by association of TM5 and TM6 (Wu *et al.*, 2010). However, mutations in those identified dimer interfaces did not decrease specific BRET signals indicating dimer interaction (Hamatake *et al.*, 2009).

Moreover, CXCR4 has been crystallised with the small molecule IT1t identifying the residues important for the interaction between the receptor and this small molecule (**Figure 6-2**). Some of these residues identified for IT1t binding have also been reported in

mutation studies to cause CXCL12 binding (D97, D187) and are involved in HIV entry (D187, E288) - (see **Figure 1-8** or **Figure 6-1**).

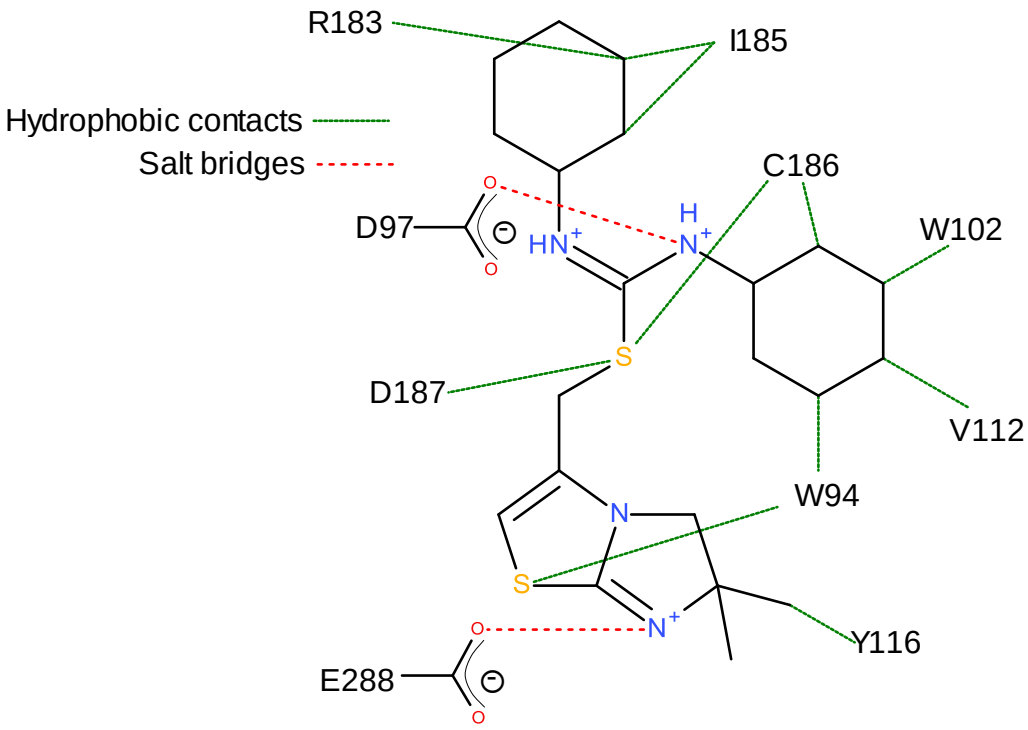

Figure 6-2: CXCR4-IT1t interaction. Schematic representation of selected interactions between CXCR4 and IT1t in the ligand-binding pocket. Hydrophobic contacts marked in green and salt bridges marked in red ; figure adapted from (Wu *et al.*, 2010)

In contrast to these studies looking at binding of CXCL12 and IT1t towards CXCR4, there have only been very few studies regarding the interaction of ATI-2341 and CXCR4. As explained previously two N-terminal truncated CXCR4 mutants, removing amino acids 2 – 21 or 2 – 27 respectively, still interacted with ATI-2341 suggesting a binding site different from CXCL12 (Janz *et al.*, 2011).

A modelling study identified residues important for interaction using three different modelling approaches suggesting interaction between ATI-2341 and ICL1, ICL2, ICL3 and the C-terminal domain of CXCR4 (**Table 6-1**). It can be observed that the residues L69, R70, S71 and M72 of ICL1, R134 of ICL2, A237, L238 and T240 of ICL3 show interactions between ATI-2341 and CXCR4 in all three methods while the other residues showed inconclusive results.

Table 6-1: Interactions between CXCR4 and ATI-2341 identified in modelling, adapted from (Planesas *et al.*, 2015)

	Intracellular Loop 1											
	Y 65	Q 66	K 67	K 68	L 69	R 70	S 71	M 72	T 73	D 74	Y 76	R 77
F				H				H				
HD					H				H			
MD									2H			
	Intracellular Loop 2					**Intracellular Loop 3**						
	I 130	D 133	R 134	R 148	K 149	Q 233	K 234	R 235	K 236	A 237	L 238	K 239
F			H	H					H	H		
HD	H	H	H							H		
MD		H	H	2H					H	H	H	
	Intracellular Loop 3							**C-terminal domain**				
	T 240	T 241	V 242	I 243	L 244	L 246	F 249	L 301	L 302	A 303	F 304	L 305
F	H											
HD	H			H								
MD												

Interactions between ATI-2341 and CXCR4 identified in modelling experiments with FlexPepDock (F), HADDOCK (HD), or MD. Polar interactions in purple boxes and hydrophobic interactions in light green boxes. Side chain hydrogen bonds (H) are indicated in grey letters and backbone hydrogen bonds in black letters.

In this chapter we concentrated on mutating the first internal loop of CXCR4 from which the sequence of ATI-2341 is derived in order to see the impact on the functional activity of ATI-2341 and identify residues important for the interaction and signal transduction between CXCR4 and ATI-2341. Furthermore, ATI-2341 variants were used to identify residues that are important for the interaction within the pepducin.

6.2 Chimeric Receptor studies

One of the initial theories regarding the binding mode of ATI-2341 was that ATI-2341 interacts with the equivalent loop 1 of CXCR4. Because of this, a CXCR4 construct in which the first internal loop was swapped for the sequence of CCR5 in pcDNA3.1 called CXCR4_il1CCR5 was provided by the group of Thomas Sakmar, Rockefeller University, New York (see **3.2. Preparation of Mutations**).

The tagged version of this construct was then characterised in ligand binding and functional assay to determine whether its properties are different from WT CXCR4, prior to the assessment of the activity of ATI-2341 at this receptor.

Initially, it was tested if the chimeric receptor behaves in a similar way to WT CXCR4 regarding the binding of CXCL12-red. The binding was tested in membranes made from NanoLuc-CXCR4_il1CCR5 cells in order to compare the binding affinity of the two receptors. The binding profile showed a saturable increase in BRET ratio with increasing concentrations of CXCL12-red and the fitted equilibrium dissociation constant was similar to that obtained with membranes from NanoLuc-CXCR4 cells (**Figure 6-3**) with a pK_d of 7.78 ± 0.04 (K_d = 17.0 nM, n =4) in comparison to 7.65 ± 0.07 in WT CXCR4 membranes.

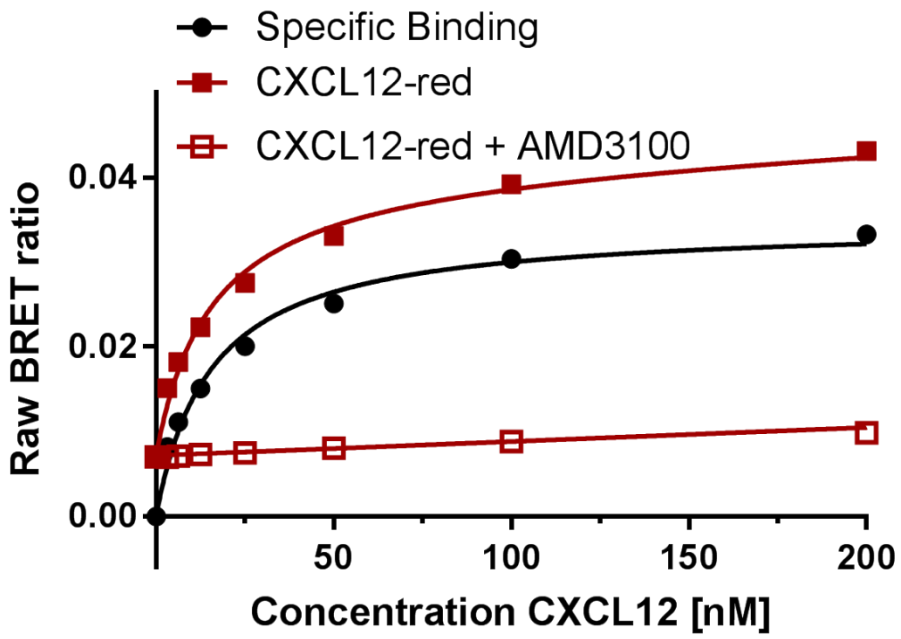

Figure 6-3: Saturation binding of CXCL12-red variants in membranes from HEK293G_NLuc-CXCR4_il1CCR5 cells. Membranes were treated with different concentrations of CXCL12-red (■) or CXCL12-red and 10 µM AMD3100 (□) in a NanoBRET proximity assay, binding as Raw BRET ratio was calculated by dividing the emission of the fluorophore by the emission of the NLuc tag. Specific binding (●) was calculated by subtracting the non-specific binding from the total binding curve. Data are shown as mean ± S.E.M. of one individual experiment performed in triplicate. Similar data were obtained in three further independent experiments.

Next, the displacement of 25 nM CXCL12-red by unlabelled compounds including ATI-2341 was tested in the same NanoLuc-CXCR4_il1CCR5 membranes (**Figure 6-4**). All compounds tested caused a decrease in CXCL12-red binding resulting in a concentration-dependent decrease of BRET ratio. The pK_i values for AMD3100 and IT1t were significantly different in WT CXCR4 and CXCR4_il1CCR5. However, the affinity shifts between the compounds stayed the same as all curves shifted about 0.3 log units to the left in CXCR4_il1CCR5 compared to the WT CXCR4 receptor suggesting that all compounds are impacted in the same way and show higher affinities in the mutated receptor (**Table 6-2**). ATI-2341 is still able to displace CXCL12-red and interact with the mutated receptor.

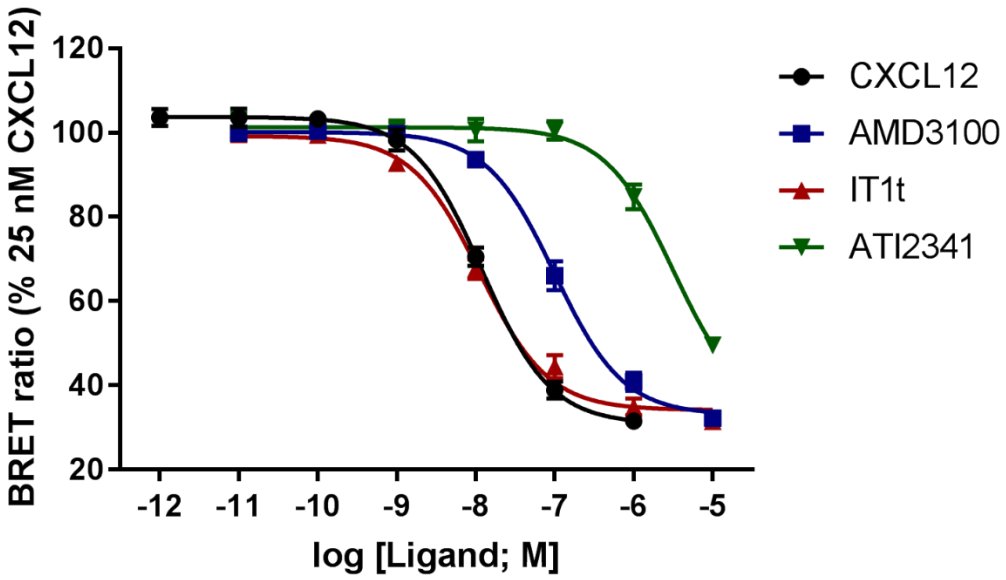

Figure 6-4: Competition binding of CXCL12-red with CXCL12, AMD3100, IT1t and ATI-2341 in membranes from HEK293G_NLuc-CXCR4_il1CCR5 cells. Membranes were treated with 25 nM CXCL12-red and increasing concentrations of CXCL12 (●), AMD3100 (■), IT1t (▲) or ATI-2341 (▼). Change in binding is expressed as a change in the normalized BRET ratio obtained with CXCL12-red alone. Data are shown as mean ± S.E.M. of the combined data from n=4 individual experiments, each performed in triplicate

Table 6-2: pKi values obtained from BRET assay in competition with CXCL12-red in SNAP-CXCR4 or SNAP-CXCR4_il1CCR5 membranes

	pKi (CXCR4) n = 5	**pKi(CXCR4_il1CCR5)** n = 4
CXCL12	7.97 ± 0.07	8.31 ± 0.01
AMD3100	7.00 ± 0.04 (S)	7.38 ± 0.09 (S)
IT1t	8.04 ± 0.01 (S)	8.34 ± 0.07 (S)
ATI-2341	<6	<6

All measurements performed on a PheraStar plate reader; data represented as mean ± S.E.M. from n = 5 or n = 4 independent experiments, respectively; values for AMD3100 and It1t are significantly different from another however all compounds shift consistently 0.3 log units to the left in CXCR4_il1CCR5 membranes

In a last step, the SNAP-CXCR4, CCR5 and SNAP-CXCR4_il1CCR5 cell lines were tested for their ability to inhibit FSK mediated cAMP production in the GloSensor assay (**Figure 6-5**). CCR5 is, like CXCR4,

coupled to G proteins of the $G_{i/o}$ family. ATI-2341 and CXCL12 both inhibited FSK-mediated cAMP production with increasing concentrations in cells expressing CXCR4 as shown previously in **5.5 Inhibition of cAMP production** (**Figure 6-5 A**). pEC_{50} values (**Table 6-3**) of 9.57 ± 0.18 (n=5) for CXCL12 and 7.63 ± 0.27 (n=5) for ATI-2341 were obtained. In contrast, ATI-2341 caused no changes in cAMP levels in cells expressing CCR5, whilst the endogenous ligand, CCL3 (Mip-1α), caused a concentration dependent inhibition of FSK mediated cAMP production with a pEC_{50} of 8.52 ± 0.29 (n=5) and served as a positive control for these cell (**Figure 6-5 B**).

Afterwards, the ability of CXCL12 and ATI-2341 to inhibit FSK mediated cAMP production in the chimeric receptor SNAP-CXCR4_il1CCR5 cells was tested. CXCL12 and ATI-2341 were both able to inhibit the cAMP production with increasing concentration by activating the chimeric receptor (**Figure 6-5 C**). The obtained pEC_{50} values (**Table 6-3**) of 9.02 ± 0.16 (n=5) for CXCL12 and 7.89 ± 0.10 (n=5) for ATI-2341 are not significantly different ($P>0.05$) from those measured in SNAP-CXCR4.

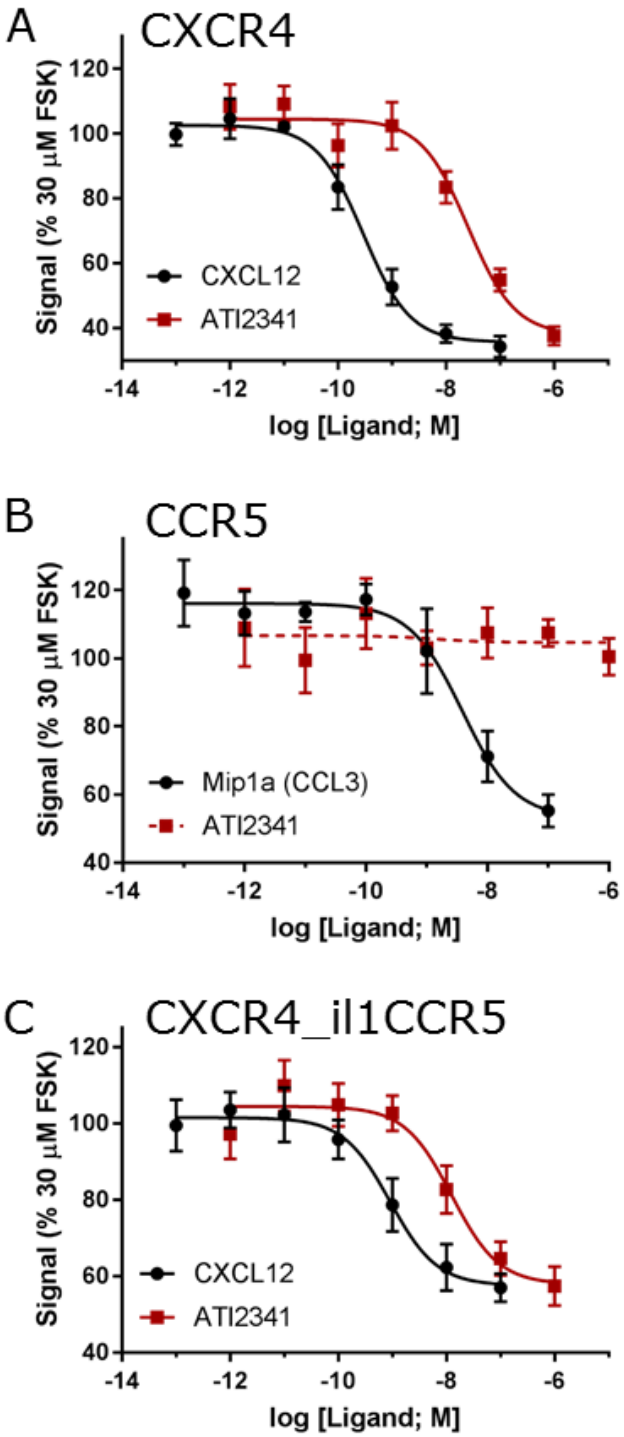

Figure 6-5: **Effect of CXCL12, CCL3 or ATI-2341 on FSK stimulated cAMP formation in HEK293G cells expressing different receptors.** HEK293G cells overexpressing the indicated receptors were stimulated with 30 µM FSK in the presence of CXCL12 (●) or ATI-2341 (■) in a GloSensor assay. Response measured as luminescence of the peak signal analysed from kinetic cAMP curves as described in the Methods section. Data are shown as mean ± S.E.M. of n = 5 independent experiments performed in triplicate in (**A**) HEK293G_SNAP-CXCR4, (**B**) HEK293G_CCR5 or (**C**) HEK293G_SNAP-CXCR4_il1CCR5. Data were normalised to the response to 30 µM FSK. Luminescence was measured on a PheraStar plate reader.

Table 6-3: pEC_{50} and E_{max} values obtained from GloSensor cAMP assay for CXCL12, CCL3 or ATI-2341 in SNAP-CXCR4, SNAP-CXCR4_il1CCR5 or CCR5 cells

		SNAP-CXCR4	SNAP-CXCR4_il1CCR5	CCR5
CXCL12	pEC_{50}	9.57 ± 0.18	9.02 ± 0.16	
	E_{max}	64.7 ± 3.1 %	43.1 ± 4.1 %	
ATI-2341	pEC_{50}	7.63 ± 0.27	7.89 ± 0.10	
	E_{max}	64.1 ± 5.2 %	42.4 ± 4.5 %	
CCL3	pEC_{50}			8.52 ± 0.29
	E_{max}			51.0 ± 5.1%

All data measured on a PheraStar plate reader; data represented as mean ± S.E.M. from n = 5 separate experiments

As a control, a cell line expressing CCR5 with the first internal loop of CXCR4 was created (CCR5_il1CXCR4). However, in the cAMP assay the new cells did not respond to ATI-2341 or CCL3, the positive control (**Figure 6-6**). Because of this, it was unclear if the mutations inhibited CCL3 binding or signalling or if the mutated receptor was not expressed.

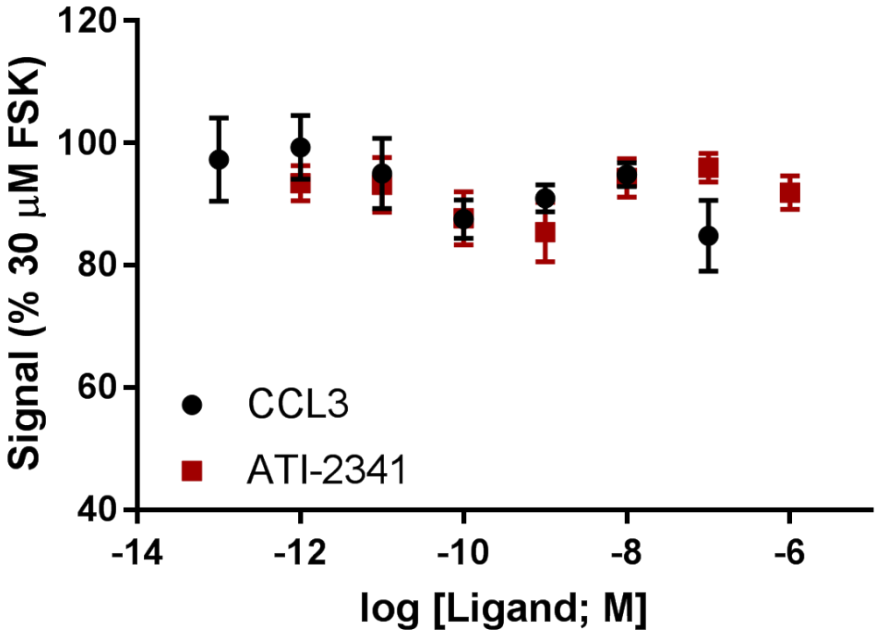

Figure 6-6: Effect of CCL3 or ATI-2341 on FSK stimulated cAMP formation in HEK293G_CCR5-il1CXCR4 cells. HEK293G_SNAP-CCR5_il1CXCR4 cells were stimulated with 30 µM FSK in the presence of CCL3 (●) or ATI-2341 (■) in a GloSensor assay. Response measured as luminescence of the peak signal analysed from kinetic cAMP curves as described in the Methods section. Data are shown as mean ± S.E.M. of n = 5 independent experiments performed in triplicate. Data were normalised to the response to 30 µM FSK. Luminescence was measured on a PheraStar plate reader.

The change of ICL1 from the CXCR4 to the CCR5 sequence seemed to have no influence on the activation of CXCR4 by ATI-2341. However, CXCR4 and CCR5 share eight amino acids in the first loop that could still be involved in the interaction of CXCR4 and ATI-2341.

The differences in the intracellular loop 1 sequences of CXCR4 and CCR5 can be seen as follows in the one letter amino acid representation of the first internal loop of both receptors with red letters showing a change in amino acid and black letters marking conserved amino acids.

CXCR4-il1: MGYQKKLRSMTDKYRL

CCR5-il1: LINCKRLKSMTDIYLL

Because of this, a series of point mutations was made in which each of those eight shared residues was mutated to an alanine to screen the impact of the conserved receptor amino acids on ATI-2341 function.

The SNAP-tagged single mutant receptors were tested for expression after transient transfection into HEK293G cells on a confocal plate reader by labelling the SNAP-tag with SNAP Surface Alexa Fluor 488 and labelling the cell nucleus with Höchst stain (**Figure 6-7**). It seemed like all mutants, except for the CXCR4 Y76A mutant, express well.

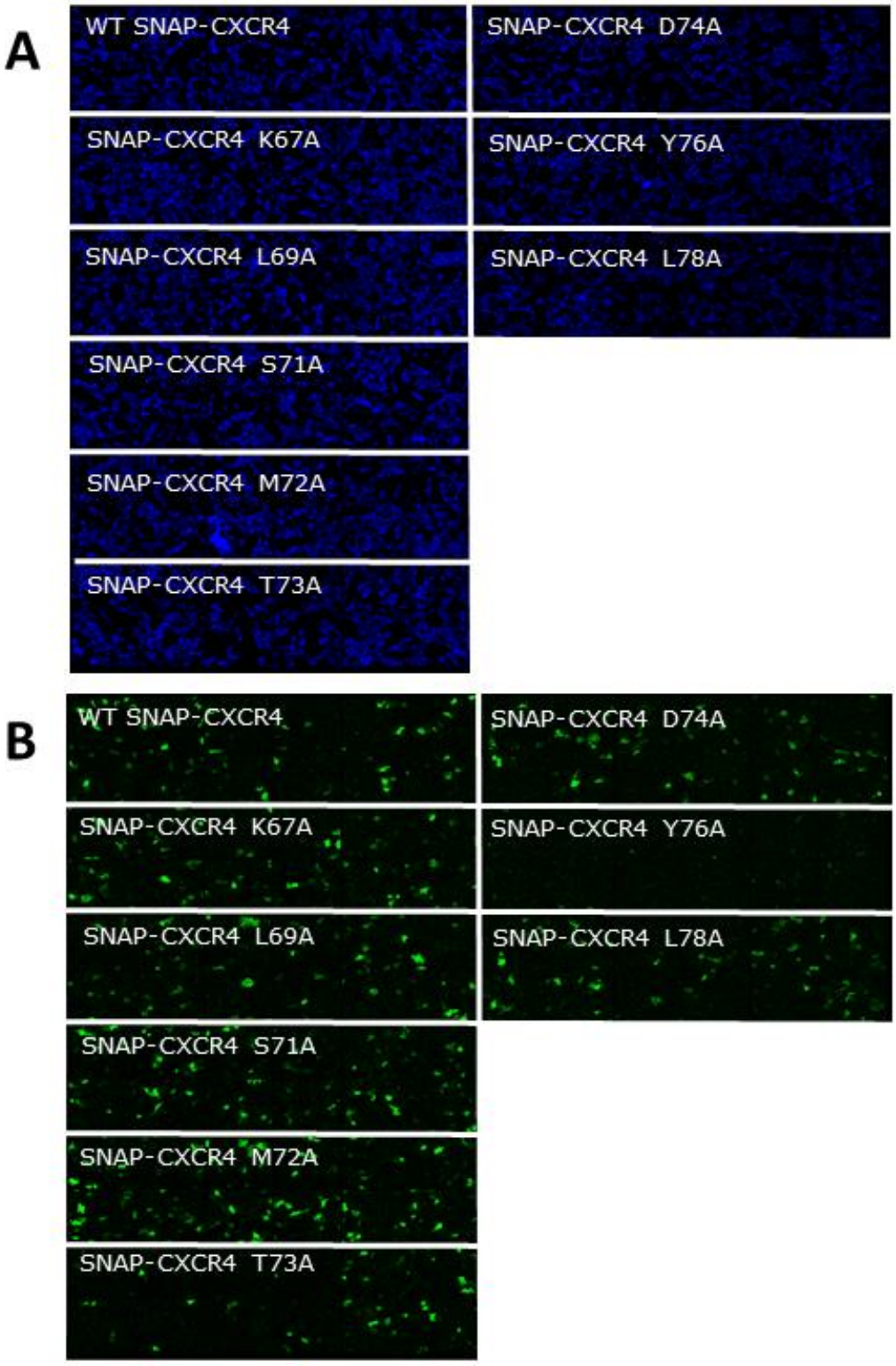

Figure 6-7: Expression control for transiently transfected HEK293G cells. WT CXCR4 and eight alanine point mutants were transfected into HEK293G cells and (**A**) the amount of cells with Höchst stain and (**B**) the amount of expressed receptor with a SNAP 488 label were visualized.

Afterwards, transiently transfected HEK293G cells were screened for their ability to inhibit FSK mediated cAMP production using a single concentration of CXCL12 (0.1 µM) or ATI-2341 (1 µM - **Figure 6-8**). None of the mutants showed a significant difference in inhibition of FSK mediated cAMP production (One-way ANOVA comparing each measurement to the WT measurement of CXCL12 or ATI-2341 respectively with $P<0.05$).

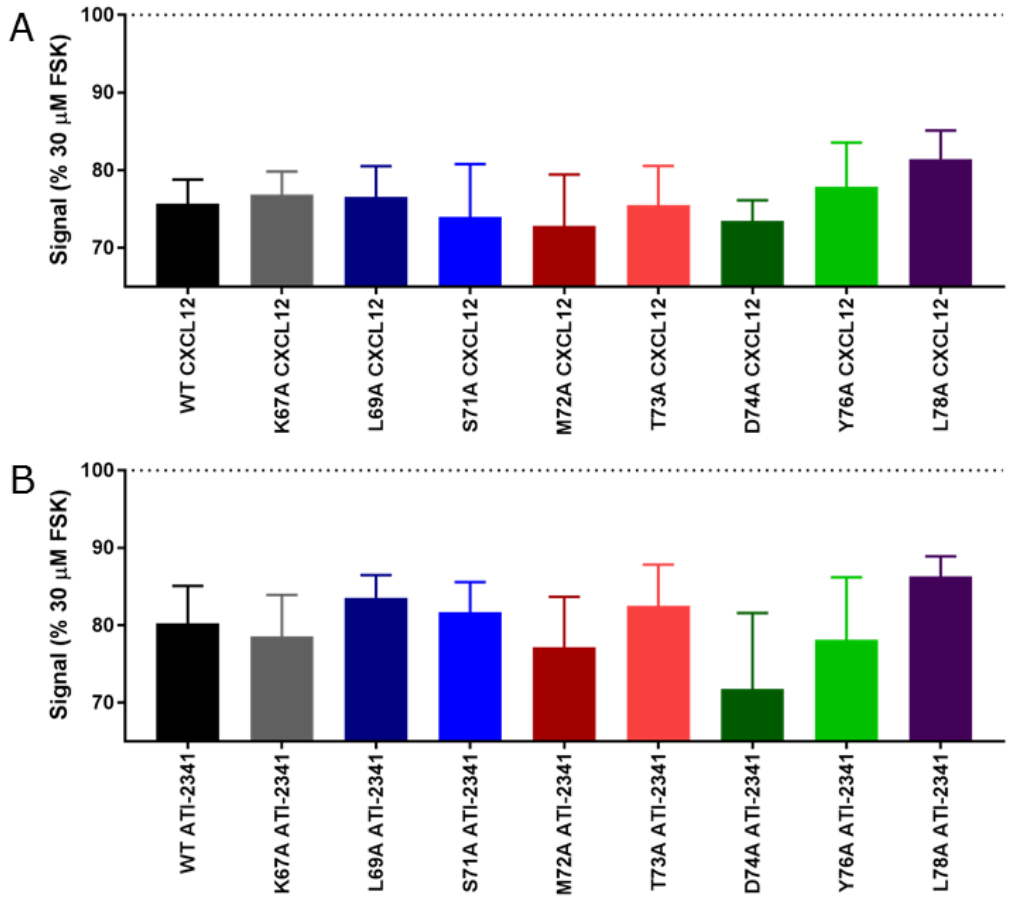

Figure 6-8: Effect of CXCL12 and ATI-2341 on FSK stimulated cAMP formation in CXCR4 mutants. HEK293G cells transiently transfected with CXCR4 mutants were treated with (**A**) 0.1 µM CXCL12 or (**B**) 1 µM ATI-2341 and 30 µM FSK at the same time in a GloSensor assay. Response measured as luminescence of the peak signal analysed from kinetic cAMP curves as described in the methods section. Data are shown ± S.E.M of n=5 (FSK, CXCL12) or n=4 (ATI-2341) individual experiments performed in triplicates. Data were normalized to 30 µM FSK for each construct and 100% marked with a dotted line.

6.3 Pepducin variants

The threonine in ATI-2341 (Pal-MGYQKKLRSM**T**DKYRL-NH_2) was proposed as one of the important residues for binding of the pepducin as it is conserved in the first intracellular loop of many GPCRs, like CXCR4, CCR5 or A_{2A} (**Table 6-4**). Because of this, the threonine was mutated to an alanine and tested in the previously set up assays.

Table 6-4: Sequence alignment of CXCR4 ICL1 and other GPCRs showing the conserved threonine.

Receptor	**Sequence alignment to CXCR4 ICL1**
CXCR4	MGYQKKLRSM**T**DKYRL
CCR5	LINCKRLKSM**T**DIYLL
CXCR1	ILYSRVGRSV**T**DVYLL
Adenosine receptor A_{2a}	VWLNSNLQNV**T**NYFVV
$ß_1$ adrenergic receptor	IAKTPRLQTL**T**NLFIM
$ß_2$ adrenergic receptor	IAKFERLQTV**T**NYFIT
Dopamine receptor D_2	VSREKALQTT**T**NYLIV

First, the pepducin variant ATI-2341 TA was tested for its ability to interfere with CXCL12-red binding to CXCR4 (**Figure 6-9**). ATI-2341 TA caused a decrease in CXCL12-red binding with a lower potency than ATI-2341 (Maximum Displacement 32.1 ± 3.9 % with 30 µM ATI-2341 TA, pK_i < 6). At 10 µM ATI-2341 displaced 41.7 ± 2.2 % of CXCL12-red while ATI-2341TA only displaced 11.9 ± 3.1 %.

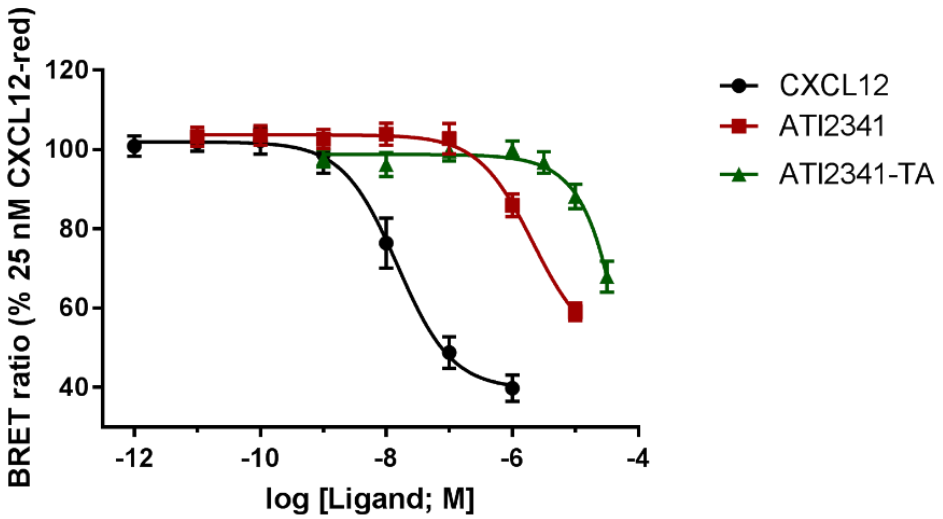

Figure 6-9: Competition binding of CXCL12-red with CXCL12, ATI-2341 and ATI-2341TA in membranes from HEK293G_NLuc-CXCR4 cells. Membranes were treated with 25 nM CXCL12-red and increasing concentrations of CXCL12 (●), ATI-2341 (■) or ATI-2341TA (▲) at the same time. Change in binding is expressed as a change in the normalized BRET ratio. Data are shown as mean ± S.E.M. of the combined data from n=5 individual experiments, each performed in triplicate

In the cAMP GloSensor assay, ATI-2341 TA inhibited FSK mediated cAMP production with increasing concentrations showing a significantly lower potency than ATI-2341 (pEC_{50}(ATI-2341 TA) = 6.70 ± 0.23, n = 5 vs pEC_{50}(ATI-2341) = 7.69 ± 0.08 n=5 performed in parallel on the same plates) (**Figure 6-10 A**).

Finally, ATI-2341 TA was tested in the internalisation assay showing a promotion of CXCR4 internalisation with increasing concentrations similar to ATI-2341. The potency of ATI-2341 TA showed a rightwards shift of more than 10-fold in comparison to ATI-2341. However, the curve does not reach saturation and it is therefore unclear if the compound has the same efficacy as ATI-2341 (**Figure 6-10 B**).

In all three experiments ATI-2341 TA is consistently shifted to lower potencies than ATI-2341 suggesting an important role of the residue in the activation of the receptor by the pepducin.

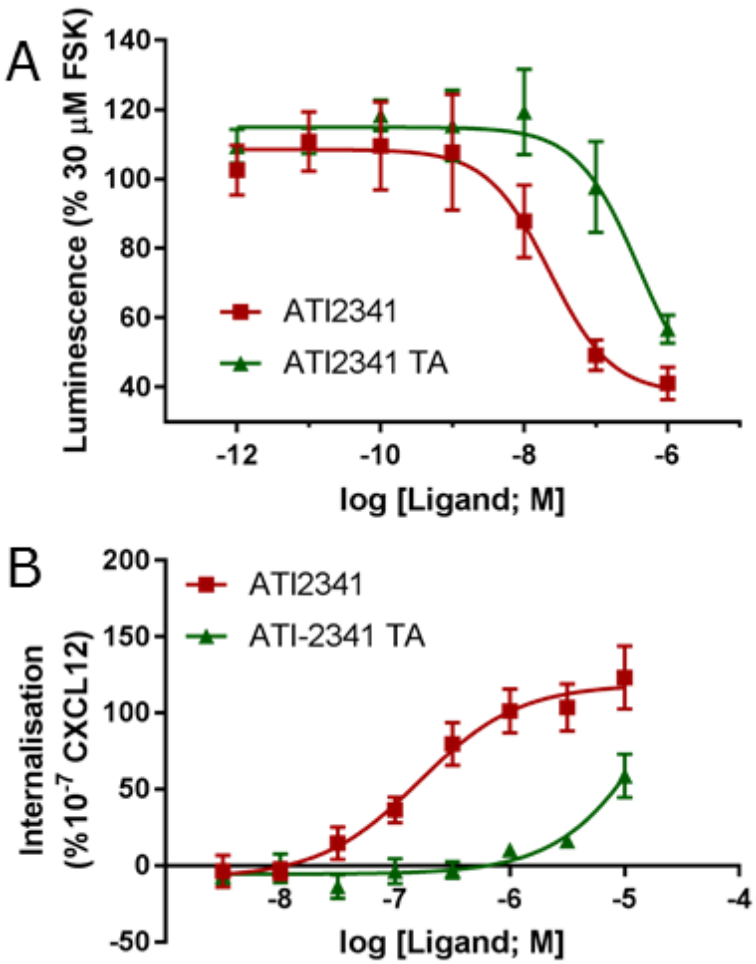

Figure 6-10: Effect of ATI-2341 or ATI-2341TA on FSK stimulated cAMP formation and CXCR4 internalisation. (**A**) HEK293G cells overexpressing CXCR4 were stimulated with 30 µM FSK in the presence of ATI-2341 (■) or ATI-2341TA (▲) in a GloSensor assay. Response measured as luminescence of the peak signal analysed from kinetic cAMP curves as described in the Methods section. Data are shown as mean ± S.E.M. of n=5 independent experiments, each performed with 4 replicates. Data were normalised to 30 µM FSK. Luminescence was measured on a PheraStar plate reader. (**B**) HEK293G_SNAP-CXCR4 cells were treated with increasing concentration of ATI-2341 (■) or ATI-2341TA (▼). Response as increase in brightness of granules colocalising SNAP-label AF488 and AF568-treansferrin. Data are normalised to 100 nM CXCL12. Data are shown as mean ± S.E.M. of n=8 (ATI-2341) or n=4 (ATI-2341TA) independent experiments performed in triplicate.

In order to further test the SAR of the ICL1 pepducins, ATI-2755 a pepducin variant which is the precursor for the fluorescent version ATI-2766 described in the previously mentioned cross-linking experiments (Janz *et al.*, 2011) was tested in the GloSensor and the internalisation assay. ATI-2755 has both methionines changed, one

to an alanine, the other to a glycine (Sequence: GGYQKKLRSA TDKYRL). ATI-2755 shows the same functional behaviour as ATI-2341 in cAMP and internalisation assay as described before (Janz *et al.*, 2011). Increasing concentrations of ATI-2755 cause inhibition of FSK mediated cAMP production with potencies similar to ATI-2341 (**Figure 6-11 A** and **Table 6-5**). Moreover, ATI-2755 promotes with increasing concentrations internalisation of CXCR4 comparable to ATI-2341 (**Figure 6-11 B** and **Table 6-5**). These results suggest no immediate effect of the two methionines on functional activity and binding of the pepducin.

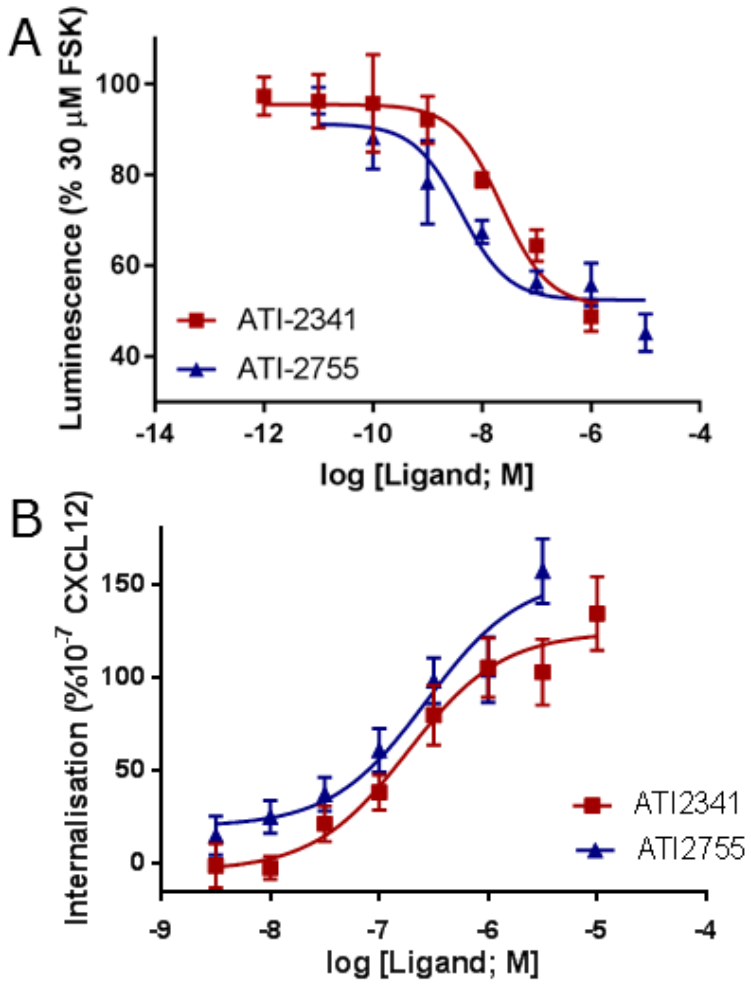

Figure 6-11: Effect of ATI-2755 on FSK stimulated cAMP formation and internalisation of CXCR4. (**A**) HEK293G cells overexpressing CXCR4 were stimulated with 30 µM FSK in the presence of ATI-2341 (■) or ATI-2755 (▲) in a GloSensor assay. Response measured as luminescence of the peak signal analysed from kinetic cAMP curves as described in the Methods section. Data are shown as mean ± S.E.M. of n=5 (ATI-2341) or n=5 (ATI-2755) independent experiments, each performed with three replicates. Data were normalised to 30 µM FSK. Luminescence was measured on an EnVision plate reader. (**B**) HEK293G_SNAP-CXCR4 cells were treated with increasing concentration of ATI-2341 (■) or ATI-2755 (▲). Response as increase in brightness of granules colocalising SNAP-label AF488 and AF568-transferrin. Data were normalised to 100 nM CXCL12. Data are shown as mean ± S.E.M. of n=7 (ATI-2341) or n=5 (ATI-2755) independent experiments performed in triplicate.

Table 6-5: pEC_{50} values obtained from GloSensor cAMP assay and internalisation assay for ATI-2341 or ATI-2755

	pEC_{50} (cAMP)	**Maximal inhibition**	**pEC_{50} (Internalisation)**	**E_{max}**
ATI-2341	8.44 ± 0.60 (n=5)	44.6 ± 3.9 %	6.71 ± 0.14 (n=7)	136.6 ± 17.7 %
ATI-2755	8.65 ± 0.43 (n=5)	47.9 ± 3.4 %	6.60 ± 0.40 (n=5)	154.6 ± 15.7 %

Data represented as mean ± S.E.M. from n separate experiments; cAMP experiments were performed in parallel while Internalisation assays were performed on different plates

6.4 Chapter Summary and Discussion

In this chapter mutations of the first intracellular loop of CXCR4, which is the basis for the ATI-2341 peptide sequence, were studied in different assays to investigate their impact on binding and signalling transduction caused by ATI-2341. Moreover two pepducin variants, ATI-2755 and ATI-2341 TA were tested for their potencies in functional and binding assays in order to identify residues important for the interaction of pepducin and receptor.

Changes in the intracellular loop 1 sequence of CXCR4 seemed to not impact the functional activity of ATI-2341 in a cAMP assay compared to WT CXCR4. A loop swap to the sequence of CCR5 did also not alter the ability of ATI-2341 to inhibit CXCL12-red binding. These results suggest that the interaction between ATI-2341 and CXCR4 is not heavily dependent on an ICL1-pepducin interaction. However there might be a cluster of residues conserved in CCR5 and CXCR4 that impacts the binding of ATI-2341 together as all conserved residues were only tested in single point mutations. Moreover, only one high concentration of CXCL12 and ATI-2341 was used with the eight alanine mutants instead of measuring full concentration curves therefore not controlling for shifts of the EC_{50} values. Based on these experiments it is not possible to conclude an interaction profile of

ATI-2341. However, the interaction of ATI-2341 with ICL1 seems unlikely and the proposed mechanism of the pepducin interacting with the DRY motif of the bottom of TM3 seems like a good proposal for further studies.

Furthermore, pepducin variants were tested in their properties to interact with CXCR4. The two previous chapters showed us that the lipid tail of ATI-2341 is important for binding and signal transduction probably due to its drug delivery properties and that the last three amino acids of the sequence of ATI-2341 have to be included in the sequence either due to key interactions of the pepducin or for correct positioning of the pepducin. ATI-2755 showed a similar behaviour to ATI-2341 suggesting that the two methionines of the sequence are not important for key interactions. The results for ATI-2504 (no lipid), ATI-2339 (missing C-terminal end YRL) and ATI-2755 (no methionine) are in agreement with previous studies where they were used as a control in calcium responses, G protein recruitment and activation assays (Janz *et al.*, 2011; Quoyer *et al.*, 2013). It was also shown that the functionality of ATI-2341 is highly dependent on its sequence as longer and shorter versions of the pepducin showed a loss in potency for mobilizing calcium (Tchernychev *et al.*, 2010).

In all tested assays ATI-2341 TA was consistently shifted to at least 10-fold lower potency (more in the internalisation assay) than ATI-2341 suggesting an important role of the threonine residue in the interaction between the pepducin and receptor. This threonine is conserved throughout a number of class A GPCRs (for example A_{2A}, β_1 or β_2), though 2 of the antagonist pepducins based on intracellular loop 1 do not contain this residue (**Table 6-6**). However the antagonist pepducins based on intracellular loop 1 might follow slightly different interactions. This interesting observation might be a good starting point for further mutations in the receptor.

Table 6-6: Sequences of intracellular loop 1 pepducins with marked conserved threonines in red; all with an palmitic acid at the N terminus except x1/2LCA-i1 with a lithocholate end; the β_2 pepducin is from a big screen with more functional pepducins showing bias

Receptor	Sequence	Pepducin Name
Agonist		
CXCR4	MGYQKKLRSM**T**DKYRL	ATI-2341
β_2	IAKFERLQTV**T**N	ICL1-15
Antagonists		
PAR1	ILKMKVKKAPAV	P1pal-i1-11
PAR4	ATGAPRLPS**T**	P4pal-i1
CXCR1/2	YSRVGRSV**T**D	x1/2LCA-i1
CXCR4	MGYQKKLRSM**T**D	x4pal-i1 or PZ-218
SMO	TFVADWRNSNRY	SMOi1

7 Discussion and Outlook

7.1 Discussion

In this work the interaction between the chemokine receptor CXCR4, which is widely expressed in the body and implicated in inflammation, HIV and cancer, and the intracellular loop 1 pepducin ATI-2341 was studied in detail. Pepducins are synthetic lipidated peptides that have been shown to modulate GPCRs, however their characteristics and mechanisms of activation remained unknown.

The research questions addressed in this study regarded the mode of action of pepducins, in particular the binding and interaction of the pepducin with CXCR4 and the functional responses caused by this interaction. It was tested if the pepducin interacted directly with CXCR4, bound from the extra- or intracellular side of the membrane, influenced binding or signalling of the endogenous extracellular ligand CXCL12, activated downstream signalling of CXCR4 and lastly key residues of the interaction were studied using mutations of the receptor and pepducin.

Summaries of the findings of each results chapter in comparison with literature data can be found in more detail at the end of each individual chapter.

Combining and interpreting all these results together provides insight into the mechanism of action of pepducins and CXCR4 in much more detail than previously known as discussed below.

Does ATI-2341 interact directly with CXCR4?

The direct interaction between the receptor and the pepducin was verified using the BRET ligand-receptor assay in which the pepducin was found in immediate proxiemty to CXCR4. Moreover the experiments with the internal CXCR4 FRET biosensor observing a direct conformational change in the receptor upon addition of ATI-2341 support this finding. The inhibition of cAMP production and G protein recruitment was only measured in cells transfected with CXCR4 and the direct internalisation of labelled SNAP-CXCR4 after incubation with pepducin was observed using confocal imaging.

Does ATI-2341 bind intracellularly towards CXCR4?

The next question addressed was to investigate the possibility of an external or internal binding site for the pepducin. While there have been previous reports indicating an internal binding site for pepducins (Covic *et al.*, 2002; Wielders *et al.*, 2007; Janz *et al.*, 2011), the BRET measurement with an N- and C-terminal tagged receptor supported this hypothesis further as a displaceable BRET signal indicating binding could only be observed with the C-terminal tagged receptor. However, this behaviour was also observed with ACKR3 transfected cells. This would suggest that the intracellular localisation of the pepducin is not specific to the presence of CXCR4 unless the pepducin interacted with the endogenous CXCR4 present in HEK293G cells and was therefore found intracellularly. Furthermore, the 30 second delay observed in the activation of the CXCR4 FRET biosensor in comparison with CXCL12 suggested that there may be mechanisms taking place that delay the activation, for example anchoring of the pepducin lipid into the membrane and flipping of the pepducin into the cells. This kinetic effect was also tested in the BRET based plate assay showing a saturable binding of ATI-2341f within 15 min in saponin treated cells and a displacement of CXCL12-red reaching a plateau also within 15 min in whole cells. Notably, the kinetics measured in plate-based assays are slower than those measured in single cells due to the difference in the diffusion of the compounds and the time required for a detectable and quantifiable fluorescent signal to accumulate. However, in both cases ATI-2341f is slower than CXCL12. Notable is that the timings of ATI-2341f are comparable with the ones of the antagonist SD44 in the BRET assays, but CXCL12-red binding is significantly faster than the other two.

Does ATI-2341 influence CXCL12 at CXCR4?

The next question addressed was whether ATI-2341 influences the binding of CXCL12 or its functional activity. In a BRET proximity assay the fluorescent labelled CXCL12-red was specifically displaced by the

addition of ATI-2341 but not by control pepducins. This suggests an indirect influence of ATI-2341 on the binding pocket of CXCL12-red rather than a direct competition caused by a conformational change of the receptor due to the interaction with ATI-2341. Moreover, ATI-2341 had a similar effect to GTP on CXCL12 binding, suggesting ATI-2341 changes the conformation of CXCR4 into a low affinity conformation. ATI-2341 acted as an agonist with lower potency than CXCL12 in most functional assays and could therefore not be tested for its influence on the CXCL12 response. In the β-arrestin recruitment assay ATI-2341 acted very slowly and was previously reported to not recruit β-arrestin at all. Therefore we added ATI-2341 and CXCL12 at the same time and a non-significant inhibitory effect of ATI-2341 on CXCL12 recruitment could be observed.

Does ATI-2341 mediate downstream signalling of CXCR4?

ATI-2341 causes functional responses in CXCR4. As previously published ATI-2341 causes similar to CXCL12 G protein activation (Quoyer *et al.*, 2013), PTX sensitive inhibition of cAMP production as well as internalisation of the receptor (Tchernychev *et al.*, 2010). Interestingly, AMD3100, a CXCR4 antagonist, directly interfering with binding of CXCL12 also antagonises ATI-2341 functionality in cAMP and internalisation assays while it does not influence the binding of ATI-2341f. In β-arrestin recruitment assays, ATI-2341 shows a different behaviour to CXCL12. While CXCL12 shows a fast increase in recruitment that peaks within 10 min, ATI-2341 shows a slow continuous recruitment of β-arrestin that is still not saturated after 60 min.

While the dimer interface observed for CXCR4 in its crystal structures is between TM5 and TM6 (Wu *et al.*, 2010) it is possible that the intracellular loop 1 pepducin may interfere with dimerisation or oligomerisation. While CXCL12 caused an increase in BRET ratio in dimers, IT1t caused a decrease. Interestingly ATI-2341 also caused

a decrease, suggesting that the changes in oligomers caused by ATI-2341 are more similar to the ones caused by IT1t than CXCL12.

What are the key residues causing the interaction of ATI-2341 and CXCR4?

Lastly, the direct interaction of ATI-2341 and CXCR4 was mapped using mutations in the receptor and the pepducin. The deletion of the lipid tail in the pepducin (ATI-2504) resulted in a loss of function in signalling assays and the ligand did not interfere with CXCL12-red binding. A similar profile was observed upon the deletion of the last three amino acids of ATI-2341 (ATI-2339). ATI-2755 missing both methionines (mutated to one glycine and one alanine) had the same responses as ATI-2341. ATI-2341 TA missing the threonine (mutated to an alanine) showed consistently lower potencies than ATI-2341 indicating the importance of this residue.

The mutations made in the intracellular loop 1 of CXCR4 had no impact on the interaction between pepducin and receptor suggesting a different interaction site or that a cluster of amino acids which were not tested need to be mutated.

Together, these results suggest that ATI-2341 causes a conformational change of the receptor that is different from the active state R* (**Figure 7-1**) caused by CXCL12 but also different from the inactive conformation R stabilised by antagonist as shown below. However, AMD3100 shifted the potencies of CXCL12 and ATI-2341 with the same pA_2 values. This does not necessarily mean that the receptor gets activated in the same way by both, CXCL12 and ATI-2341, as only CXCL12 fulfils the assumption of Schild calculations of direct competition with AMD3100. It might be the case that parts of the receptor that move differently in the case of activation by CXCL12 and ATI-2341, for example those involved in dimerisation, are not impacted by AMD3100.

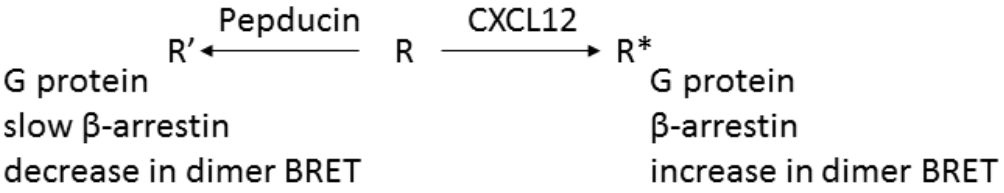

Figure 7-1: Conformational change in CXCR4. Schematic representation of conformational changes in CXCR4 caused by CXCL12 or ATI-2341.

These results give us insight into the mechanism in which the pepducin ATI-2341 interacts with the receptor CXCR4 and thereby represent substantial progress in the elucidation of the interaction of pepducins and GPCRs.

7.2 Outlook

This project focused on the binding mechanism of ATI-2341 to CXCR4 as well as on the differences observed in functional assays between CXCL12 and ATI-2341. It would be very useful to pinpoint the interaction site of ATI-2341 and CXCL12 in more detail for example with more receptor mutations or pepducin variants. The conserved threonine in ICL1 (see Chapter 6) seems to be a good starting point for mutations as well as the modelling efforts made by Planesas *et al*. (2015). Helpful would also be further modelling results for mutations or in a best case scenario structural biology insights. Moreover, there were only small differences in the behaviour of ATI-2341 and CXCL12 in the activation of functional pathways. It would be interesting to see if the slow recruitment of ß-arrestin to CXCR4 by ATI-2341 has any other influences on pathways connected to ß-arrestin. As ATI-2341 and CXCL12 had different effect on the CXCR4 homo-dimers a more in depth study on the effects on dimerisation would be of interest (full dose response curves, effects on hetero-dimers, impact on dimerisation in other techniques).

Moreover, it would be interesting to repeat all results with a different receptor as some of the effects could possibly be only observed with

CXCR4 and ATI-2341. During the process of this thesis we also synthesised potential A_{2A} pepducins that were tested by a master student (Truc Giap) and showed initial promising results. One very interesting fact is also that ATI-2341 becomes an antagonist when deleting the last 4 amino acids of the peptide sequence. Understanding the differences in interaction that cause this change from agonist to antagonist would be interesting as well.

8 References

Adjobo-Hermans MJW, Goedhart J, van Weeren L, Nijmeijer S, Manders EMM, Offermanns S, and Gadella TWJ (2011) Real-time visualization of heterotrimeric G protein Gq activation in living cells. *BMC Biol* **9**:32.

Adlere I, Sun S, Zarca A, Roumen L, Gozelle M, Viciano Perpiñá C, Caspar B, Arimont M, Bebelman JP, Briddon SJ, Hoffmann C, Hill SJ, Smit MJ, Vischer HF, Wijtmans M, de Graaf C, de Esch IJP, and Leurs R (2019) Structure-based exploration and pharmacological evaluation of N-substituted piperidin-4-yl-methanamine CXCR4 chemokine receptor antagonists. *Eur J Med Chem* **162**:631–649.

Arimont M, Sun S, Leurs R, Smit M, Esch IJP De, and Graaf C De (2017) Structural Analysis of Chemokine Receptor – Ligand Interactions. *J Med Chem* **60**:4735–4779.

Arunlakshana O, and Schild HO (1959) Some Quantitative Uses of Drug Antagonists. *Br J Pharmacol Chemother* **14**:48–58.

Azzi M, Charest PG, Angers S, Rousseau G, Kohout T, Bouvier M, and Pineyro G (2003) β-Arrestin-mediated activation of MAPK by inverse agonists reveals distinct active conformations for G protein-coupled receptors. *PNAS* **100**:11406–11411.

Babcock GJ, Farzan M, and Sodroski J (2003) Ligand-Independent Dimerization of CXCR4, a Principal HIV-1 Coreceptor. *J Biol Chem* **278**:3378–3385.

Bachelerie F, Ben-Baruch A, Burkhardt AM, Combadiere C, Farber JM, Graham GJ, Horuk R, Sparre-Ulrich AH, Locati M, Luster AD, Mantovani A, Matsushima K, Murphy PM, Nibbs R, Nomiyama H, Power CA, Proudfoot AEI, Rosenkilde MM, Rot A, Sozzani S, Thelen M, Yoshie O, and Zlotnik A (2014) International Union of Basic and Clinical Pharmacology. LXXXIX. Update on the Extended Family of Chemokine Receptors and Introducing a New Nomenclature for Atypical Chemokine Receptors. *Pharmacol Rev* **66**:1–79.

Baker JG, and Hill SJ (2007) A comparison of the antagonist affinities for the Gi- and Gs-coupled states of the human adenosine A1-receptor. *J Pharmacol Exp Ther* **320**:218–228.

Balabanian K, Lagane B, Infantino S, Chow KYC, Harriague J, Moepps B, Arenzana-Seisdedos F, Thelen M, and Bachelerie F (2005) The chemokine SDF-1/CXCL12 binds to and signals through the orphan receptor RDC1 in T lymphocytes. *J Biol Chem* **280**:35760–35766.

Balkwill F (2004a) Cancer and the chemokine network. *Nat Rev Cancer* **4**:540–550.

Balkwill F (2004b) The significance of cancer cell expression of the chemokine receptor CXCR4. *Semin Cancer Biol* **14**:171–179.

Balkwill FR (2012) The chemokine system and cancer. *J Pathol*

226:148–157.

Benredjem B, Girard M, Rhainds D, St-Onge G, and Heveker N (2017) Mutational analysis of atypical chemokine receptor 3 (ACKR3/CXCR7) interaction with its chemokine ligands CXCL11 and CXCL12. *J Biol Chem* **292**:31–42.

Berger EA, Murphy PM, and Farber JM (1999) CHEMOKINE RECEPTORS AS HIV-1 CORECEPTORS: Roles in Viral Entry, Tropism, and Disease. *Annu Rev Immunol* **17**:657–700.

Binkowski BF, Butler BL, Stecha PF, Eggers CT, Otto P, Zimmerman K, Vidugiris G, Wood MG, Encell LP, Fan F, and Wood K V. (2011) A luminescent biosensor with increased dynamic range for intracellular cAMP. *ACS Chem Biol* **6**:1193–1197.

Bjarnadóttir TK, Gloriam DE, Hellstrand SH, Kristiansson H, Fredriksson R, and Schiöth HB (2006) Comprehensive repertoire and phylogenetic analysis of the G protein-coupled receptors in human and mouse. *Genomics* **88**:263–273.

Blanpain C, Doranz BJ, Bondue A, Govaerts C, De Leener A, Vassart G, Doms RW, Proudfoot A, and Parmentier M (2003) The core domain of chemokines binds CCR5 extracellular domains while their amino terminus interacts with the transmembrane helix bundle. *J Biol Chem* **278**:5179–5187.

Blanpain C, Lee B, Vakili J, Doranz BJ, Govaerts C, Migeotte I, Sharron M, Dupriez V, Vassart G, Doms RW, and Parmentier M (1999) Extracellular cysteines of CCR5 are required for chemokine binding, but dispensable for HIV-1 coreceptor activity. *J Biol Chem* **274**:18902–18908.

Bleul CC, Farzant M, Choet H, Parolint C, Clark-lewis I, Sodroskitll J, and Springer TA (1996) The lymphocyte chemoattractant SDF-1 is a ligand for LESTR/fusin and blocks HIV-1 entry. *Nature* **382**:695–698.

Bleul CC, Wu L, Hoxie JA, Springer TA, and Mackay CR (1997) The HIV coreceptors CXCR4 and CCR5 are differentially expressed and regulated on human T lymphocytes. *PNAS* **94**:1925–1930.

Booth V, Clark-Lewis I, and Sykes BD (2004) NMR structure of CXCR3 binding chemokine CXCL11 (ITAC). *Protein Sci* **13**:2022–2028.

Bourne HR, Sanders DA, and Mccormick F (1990) The GTPase superfamily : a conserved switch for diverse cell functions. *Nature* **348**:125–131.

Bray A, Johnson H, Raff L, and Walter R (2010) *Essential Cell Biology*, 3rd ed., Garland Science.

Brelot A, and Chakrabarti LA (2018) CCR5 Revisited: How Mechanisms of HIV Entry Govern AIDS Pathogenesis. *J Mol Biol* **430**:2557–2589.

Brelot A, Heveker N, Montes M, and Alizon M (2000) Identification of

residues of CXCR4 critical for human immunodeficiency virus coreceptor and chemokine receptor. *J Biol Chem* **275**:23736–23744.

Burg JS, Ingram JR, Venkatakrishnan AJ, Jude KM, Dukkipati A, Feinberg EN, Angelini A, Waghray D, Dror RO, Ploegh HL, and Garcia KC (2015) Structural basis for chemokine recognition and activation of a viral G protein – coupled receptor. *Science* **347**:1113–1118.

Burns JM, Summers BC, Wang Y, Melikian A, Berahovich R, Miao Z, Penfold MET, Sunshine MJ, Littman DR, Kuo CJ, Wei K, McMaster BE, Wright K, Howard MC, and Schall TJ (2006) A novel chemokine receptor for SDF-1 and I-TAC involved in cell survival, cell adhesion, and tumor development. *J Exp Med* **203**:2201–2213.

Busillo JM, and Benovic JL (2007) Regulation of CXCR4 signaling. *Biochim Biophys Acta - Biomembr* **1768**:952–963.

Canals M, Scholten DJ, de Munnik S, Han MKL, Smit MJ, and Leurs R (2012) Ubiquitination of CXCR7 controls receptor trafficking. *PLoS One* **7**:1–13.

Carlson KE, Mcmurry TJ, and Hunt SW (2012) Pepducins : lipopeptide allosteric modulators of GPCR signaling. *Drug Discov Today Technol* **9**:e33–e39.

Carr R, Du Y, Quoyer J, Panettieri RA, Janz JM, Bouvier M, Kobilka BK, and Benovic JL (2014) Development and characterization of pepducins as Gs-biased allosteric agonists. *J Biol Chem* **289**:35668–35684.

Castellino F, Huang AY, Altan-Bonnet G, Stoll S, Scheinecker C, and Germain RN (2006) Chemokines enhance immunity by guiding naive CD8+T cells to sites of CD4+T cell-dendritic cell interaction. *Nature* **440**:890–895.

Chaturvedi M, Schilling J, Beautrait A, Bouvier M, Benovic JL, and Shukla AK (2018) Emerging Paradigm of Intracellular Targeting of G Protein-Coupled Receptors. *Trends Biochem Sci* **43**:533–546.

Cheng ZJ, Zhao J, Sun Y, Hu W, Wu YL, Cen B, Wu GX, and Pei G (2000) β-arrestin differentially regulates the chemokine receptor CXCR4-mediated signaling and receptor internalization, and this implicates multiple interaction sites between β-arrestin and CXCR4. *J Biol Chem* **275**:2479–2485.

Chin B, Aubel D, and Fussenegger M (2013) An overview of the diverse roles of G-protein coupled receptors (GPCRs) in the pathophysiology of various human diseases. *Biotechnol Adv* **31**:1676–1694.

Chow MT, and Luster AD (2014) Chemokines in Cancer. *Cancer Immunol Res* **2**:1125–1131.

Christopoulos A, and Kenakin T (2002) G protein-coupled receptor allosterism and complexing. *Pharmacol Rev* **54**:323–374.

Cohen FR, Lazareno S, and Birdsall NJM (1996) The effects of saponin on the binding and functional properties of the human adenosine A1receptor. *Br J Pharmacol* **117**:1521–1529.

Cole NB (2013) Site-Specific Protein Labeling with SNAP-Tags Nelson. *Curr Protoc Protein Sci* **73**:30.1.1-30.1.16.

Cottet M, Faklaris O, Falco A, Trinquet E, Pin J, and Mouillac B (2013) Fluorescent ligands to investigate GPCR binding properties and oligomerization. *Biochem Soc Trans* **41**:148–153.

Covic L, Gresser AL, Talavera J, Swift S, and Kuliopulos A (2002) Activation and inhibition of G protein-coupled receptors by cell-penetrating membrane-tethered peptides. *PNAS* **99**:643–648.

Creveling CR, McNeal ET, McCulloh DH, and Daly JW (1980) Membrane Potentials in Cell-free Preparations from Guinea Pig Cerebral Cortex: Effect of Depolarizing Agents and Cyclic Nucleotides. *J Neurochem* **35**:922–932.

Crump MP, Gong JH, Loetscher P, Rajarathnam K, Amara a, Arenzana-Seisdedos F, Virelizier JL, Baggiolini M, Sykes BD, and Clark-Lewis I (1997) Solution structure and basis for functional activity of stromal cell-derived factor-1; dissociation of CXCR4 activation from binding and inhibition of HIV-1. *EMBO J* **16**:6996–7007.

Czaplewski LG, Mckeating J, Craven CJ, Higgins LD, Appay V, Brown A, Dudgeon T, Howard LA, Meyers T, Owen J, Palan SR, Tan P, Wilson G, Woods NR, Heyworth CM, Lord BI, Brotherton D, Christison R, Craig S, Cribbes S, Edwards RM, Evans SJ, Gilbert R, Morgan P, Randle E, Schofield N, Varley PG, Fisher J, Waltho JP, and Hunter MG (1999) Identification of Amino Acid Residues Critical for Aggregation of Human CC Chemokines Macrophage Inflammatory Protein (MIP)-1a , MIP-1b , and RANTES. *J Biol Chem* **274**:16077–16084.

Dar A, Goichberg P, Shinder V, Kalinkovich A, Kollet O, Netzer N, Margalit R, Zsak M, Nagler A, Hardan I, Resnick I, Rot A, and Lapidot T (2005) Chemokine receptor CXCR4-dependent internalization and resecretion of functional chemokine SDF-1 by bone marrow endothelial and stromal cells. *Nat Immunol* **6**:1038–1046.

Davis BCB, Dikic I, Unutmaz D, Hill CM, Arthos J, Siani M a, Thompson D a, Schlessinger J, and Littman DR (1997) Signal Transduction Due to HIV-1 Envelope Interactions with Chemokine Receptors CXCR4 or CCR5. *Cell* **186**:1793–1798.

Dealwis C, Fernandez EJ, Thompson DA, Simon RJ, Siani MA, and Lolis E (1998) Crystal structure of chemically synthesized [N33A] stromal cell-derived factor 1alpha, a potent ligand for the HIV-1 "fusin" coreceptor. *PNAS* **95**:6941–6946.

Décaillot FM, Kazmi MA, Lin Y, Ray-Saha S, Sakmar TP, and Sachdev P (2011) CXCR7/CXCR4 heterodimer constitutively recruits β-arrestin to enhance cell migration. *J Biol Chem* **286**:32188–32197.

Decker T, and Lohmann-Matthes ML (1988) A quick and simple method for the quantitation of lactate dehydrogenase release in measurements of cellular cytotoxicity and tumor necrosis factor (TNF) activity. *J Immunol Methods* **15**:61–69.

Del Corno M, Liu Q, Schols D, Clercq E De, Gessani S, Freedman BD, and Collman RG (2011) toxin − insensitive chemokine receptor signaling HIV-1 gp120 and chemokine activation of Pyk2 and mitogen-activated protein kinases in primary macrophages mediated by calcium-dependent , pertussis toxin – insensitive chemokine receptor signaling. *Blood* **98**:2909–2916.

Dimond P, Carlson K, Bouvier M, Gerard C, Xu L, Covic L, Agarwal A, Ernst OP, Janz JM, Schwartz TW, Gardella TJ, Milligan G, Kuliopulos A, Sakmar TP, and Hunt SW (2011) G protein-coupled receptor modulation with pepducins: Moving closer to the clinic. *Ann N Y Acad Sci* **1226**:34–49.

Dragic T, Litwin V, Allaway GP, Martin SR, Huang Y, Nagashima KA, Cayanan C, Maddon PJ, Koup RA, Moore JP, and Paxton WA (1996) HIV-1 entry into CD4+ cells is mediated by the chemokine receptor CC-CKR-5. *Nature* **381**:667–673.

Drury LJ, Ziarek JJ, Gravel S, Veldkamp CT, Takekoshi T, Hwang ST, Heveker N, Volkman BF, and Dwinell MB (2011) Monomeric and dimeric CXCL12 inhibit metastasis through distinct CXCR4 interactions and signaling pathways. *PNAS* **108**:17655–17660.

Dunham TD, Farrens DL, and Science HG (1999) Conformational Changes in Rhodopsin. *J Biol Chem* **274**:1683–1690.

Ettre LS (1993) Nomenclature for chromatography (IUPAC Recommendations 1993). *Pure Appl Chem* **65**:819–872.

Farrens DL, Altenbach C, Yang K, Hubbell WL, and Khoranat HG (1996) Requirement of Rigid-Body Motion of Transmembrane Helices for Light Activation of Rhodopsin. *Science* **274**:768–770.

Farzan M, Choe H, Vaca L, Martin K, Sun Y, Desjardins E, Ruffing N, Wu L, Wyatt R, Gerard N, Gerard C, and Sodroski J (1998) A tyrosine-rich region in the N terminus of CCR5 is important for human immunodeficiency virus type 1 entry and mediates an association between gp120 and CCR5. *J Virol* **72**:1160–1164.

Fätkenheuer G, Pozniak AL, Johnson MA, Plettenberg A, Staszewski S, Hoepelman AIM, Saag MS, Goebel FD, Rockstroh JK, Dezube BJ, Jenkins TM, Medhurst C, Sullivan JF, Ridgway C, Abel S, James IT, Youle M, and Van Der Ryst E (2005) Efficacy of short-term monotherapy with maraviroc, a new CCR5 antagonist, in patients infected with HIV-1. *Nat Med* **11**:1170–1172.

Felce JH, Latty SL, Knox RG, Lee SF, Klenerman D, Davis SJ, Felce JH, Latty SL, Knox RG, Mattick SR, Lui Y, Lee SF, Klenerman D, and Davis SJ (2017) Receptor Quaternary Organization Explains G Protein-Coupled Receptor Family Structure Article Receptor Quaternary Organization Explains G Protein-Coupled Receptor Family Structure. *CellReports* **20**:2654–2665.

Feng Y, Broder CC, Kennedy PE, and Berger EA (1996) HIV-1 entry cofactor: functional cDNA cloning of a seven-transmembrane. *Science* **272**:872–877.

Fernandez EJ, and Lolis E (2002) Structure , Function , and Inhibition of Chemokines. *Annu Rev Pharmacol Toxicol* **42**:469–499.

Fong AM, Premont RT, Richardson RM, Yu Y-RA, Lefkowitz RJ, and Patel DD (2002) Defective lymphocyte chemotaxis in β-arrestin2- and GRK6-deficient mice. *PNAS* **99**:7478–83.

Foxman EF, Campbell JJ, and Butcher EC (1997) Multistep Navigation and the Combinatorial Control of Leukocyte Chemotaxis. *J Cell Biol* **139**:1349–1360.

Fredrikson R, Lagerström MC, Lundin L, and Schiöth HB (2003) The G-Protein-Coupled Receptors in the Human Genome Form Five Main Families . Phylogenetic Analysis , Paralogon Groups , and Fingerprints. *Mol Pharmacol* **63**:1256–1272.

Furusato B, Mohamed A, Uhlén M, and Rhim JS (2010) CXCR4 and cancer. *Pathol Int* **60**:497–505.

Gaertner H, Cerini F, Escola JM, Kuenzi G, Melotti A, Offord R, Rossitto-Borlat I, Nedellec R, Salkowitz J, Gorochov G, Mosier D, and Hartley O (2008) Highly potent, fully recombinant anti-HIV chemokines: reengineering a low-cost microbicide. *PNAS* **105**:17706–17711.

Gainetdinov RR, Premont RT, Bohn LM, Lefkowitz RJ, and Caron MG (2004) Desensitization of G Protein–Coupled Receptors and Neuronal Functions. *Annu Rev Neurosci* **27**:107–144.

Garcia-Perez J, Rueda P, Alcami J, Rognan D, Arenzana-Seisdedos F, Lagane B, and Kellenberger E (2011) Allosteric model of maraviroc binding to CC Chemokine Receptor 5 (CCR5). *J Biol Chem* **286**:33409–33421.

Garcia-Perez J, Rueda P, Staropoli I, Kellenberger E, Alcami J, Arenzana-Seisdedos F, and Lagane B (2011) New insights into the mechanisms whereby low molecular weight CCR5 ligands inhibit HIV-1 infection. *J Biol Chem* **286**:4978–4990.

Ge B, Lao J, Li J, Chen Y, Song Y, and Huang F (2017) Single-molecule imaging reveals dimerization / oligomerization of CXCR4 on plasma membrane closely related to its function. *Sci Rep* **1**:1–9, Springer US.

Gether (2000) Uncovering molecular mechanisms involved in activation of G protein-coupled receptors. *Endocr Rev* **21**:90–

113.

Goedhart J, van Weeren L, Adjobo-Hermans MJW, Elzenaar I, Hink MA, and Gadella TWJ (2011) Quantitative Co-expression of proteins at the single cell level - application to a multimeric FRET sensor. *PLoS One* **6**:1–8.

Goulding J, May LT, and Hill SJ (2018) Characterisation of endogenous A2A and A2B receptor-mediated cyclic AMP responses in HEK 293 cells using the GloSensor™ biosensor: Evidence for an allosteric mechanism of action for the A2B-selective antagonist PSB 603. *Biochem Pharmacol* **147**:55–66.

Goulding J, Stoddart LA, Carlson KE, Hunt S, and Hill SJ (2012) Characterisation of the interaction between the pepducin ATI 2341 and CXCR4 in HEK293 cells stably expressing a SNAP tagged receptor and the Glosensor, in *Proceeding of the British Pharmacological Society*.

Granelli-Piperno A (1996) Efficient Interaction of HIV-1 with Purified Dendritic Cells via Multiple Chemokine Coreceptors. *J Exp Med* **184**:2433–2438.

Guo W, Urizar E, Kralikova M, Mobarec JC, Shi L, Filizola M, and Javitch JA (2008) Dopamine D2 receptors form higher order oligomers at physiological expression levels. *EMBO J* **27**:2293–2304.

Gustavsson M, Wang L, Gils N Van, Stephens BS, Zhang P, Schall TJ, Yang S, Abagyan R, Chance MR, Kufareva I, and Handel TM (2017) Structural basis of ligand interaction with atypical chemokine receptor 3. *Nat Commun* **8**:1–14.

Haider RS, Godbole A, and Hoffmann C (2019) To sense or not to sense—new insights from GPCR-based and arrestin-based biosensors. *Curr Opin Cell Biol* **57**:16–24.

Hall MP, Unch J, Binkowski BF, Valley MP, Butler BL, Wood MG, Otto P, Zimmerman K, Vidugiris G, MacHleidt T, Robers MB, Benink HA, Eggers CT, Slater MR, Meisenheimer PL, Klaubert DH, Fan F, Encell LP, and Wood K V. (2012) Engineered luciferase reporter from a deep sea shrimp utilizing a novel imidazopyrazinone substrate. *ACS Chem Biol* **7**:1848–1857.

Hamatake M, Aoki T, Futahashi Y, Urano E, Yamamoto N, and Komano J (2009) Ligand-independent higher-order multimerization of CXCR4, a G-protein-coupled chemokine receptor involved in targeted metastasis. *Cancer Sci* **100**:95–102.

Hao M, Zheng J, Hou K, Wang J, Chen X, Lu X, Bo J, Xu C, Shen K, and Wang J (2012) Role of chemokine receptor CXCR7 in bladder cancer progression. *Biochem Pharmacol* **84**:204–214.

Hargreaves AC, Lummis SCR, and Taylor CW (1994) Ca2+ Permeability of Cloned and Native 5-Hydroxytryptamine Type 3 Receptors. *Mol Cancer Ther* **46**:1120–1128.

Hattermann K, Held-Feindt J, Lucius R, Müerköster SS, Penfold MET, Schall TJ, and Mentlein R (2010) The chemokine receptor CXCR7 is highly expressed in human glioma cells and mediates antiapoptotic effects. *Cancer Res* **70**:3299–3308.

He J, Chen Y, Farzan M, Choe H, Ohagen A, Gartner S, Busciglo J, Yang X, Hofmann W, Newman W, Mackay CR, Sodroskl J, and Gabuzda D (1997) CCR3 and CCR5 are co-receptors for HIV-1 infection of microglia. *Nature* **385**:645–649.

Hendrickson WA, Kwong PD, Wyatt R, Robinson J, Sweet RW, and Sodroski J (1998) Structure of an HIV gp120 envelope glycoprotein in complex with the CD4 receptor and a neutralizing human antibody. *Nature* **393**:648–659.

Hernandez PA, Gorlin RJ, Lukens JN, Taniuchi S, Bohinjec J, Francois F, Klotman ME, and Diaz GA (2003) Mutations in the chemokine receptor gene CXCR4 are associated with WHIM syndrome, a combined immunodeficiency disease. *Nat Genet* **34**:70–74.

Hirota K, and Semenza GL (2006) Regulation of angiogenesis by hypoxia-inducible factor 1. *Crit Rev Oncol Hematol* **59**:15–26.

Hoffmann C, Gaietta G, Bünemann M, Adams SR, Oberdorff-Maass S, Behr B, Vilardaga JP, Tsien RY, Ellisman MH, and Lohse MJ (2005) A FlAsH-based FRET approach to determine G protein-coupled receptor activation in living cells. *Nat Methods* **2**:171–176.

Hoffmann F, Müller W, Schütz D, Penfold ME, Wong YH, Schulz S, and Stumm R (2012) Rapid uptake and degradation of CXCL12 depend on CXCR7 carboxyl-terminal serine/threonine residues. *J Biol Chem* **287**:28362–28377.

Horn F, Bettler E, Oliveira L, Campagne F, Cohen FE, and Vriend G (2003) GPCRDB information system for G protein-coupled receptors. *Nucleic Acids Res* **31**:294–297.

Howard OMZ, Shirakawa AK, Turpin JA, Maynard A, Tobin GJ, Carrington M, Oppenheim JJ, and Dean M (1999) Naturally occurring CCR5 extracellular and transmembrane domain variants affect HIV-1 co-receptor and ligand binding function. *J Biol Chem* **274**:16228–16234.

Insel PA, Wilderman A, Zambon AC, Snead AN, Murray F, Aroonsakool N, Mcdonald DS, Zhou S, Mccann T, Zhang L, Sriram K, Chinn AM, Michkov A V, Lynch RM, Overland AC, Corriden R, and I DPPA (2015) MINIREVIEW — 50 th ANNIVERSARY SPECIAL ISSUE G Protein – Coupled Receptor (GPCR) Expression in Native Cells : " Novel " endoGPCRs as Physiologic Regulators and Therapeutic Targets. *Mol Pharmacol* **88**:181–187.

International Agency for Research on Cancer (2018) *Press Release 263, Latest global cancer data*.

Janz JM, Ren Y, Looby R, Kazmi M a., Sachdev P, Grunbeck A, Haggis L, Chinnapen D, Lin AY, Seibert C, McMurry T, Carlson KE, Muir

TW, Hunt S, and Sakmar TP (2011) Direct interaction between an allosteric agonist pepducin and the chemokine receptor CXCR4. *J Am Chem Soc* **133**:15878–15881.

Jaradat DMM (2018) Thirteen decades of peptide synthesis: key developments in solid phase peptide synthesis and amide bond formation utilized in peptide ligation. *Amino Acids* **50**:39–68.

Jensen JB, Lyssand JS, Hague C, and Hille B (2009) Fluorescence changes reveal kinetic steps of muscarinic receptor–mediated modulation of phosphoinositides and Kv7.2/7.3 K^+ channels. *J Gen Physiol* **133**:347–359.

Ji TH, Grossmann M, and Ji I (1998) Minireview: G Protein-Coupled Receptors - I. Diversity of Receptor-Ligand Interactions. *J Biol Chem* **273**:17299–17302.

Jin H, Shen X, Baggett BR, Kong X, and LiWang PJ (2007) The human CC chemokine MIP-1beta dimer is not competent to bind to the CCR5 receptor. *J Biol Chem* **282**:27976–27983.

Jones KA, Borowsky B, Tamm JA, Craig DA, Durkin MM, Dai M, Yao W, Johnson M, Gunwaldsen C, Huang L, Tang C, Shen Q, Salon JA, Morse K, Laz T, Smith KE, Nagarathnam D, Noble SA, Branchek TA, and Gerald C (1998) GABAB receptors function as a heteromeric assembly of the subunits GABABR1 and GABABR2. *Nature* **396**:674–678.

Jones KL, Maguire JJ, and Davenport AP (2011) Chemokine receptor CCR5: From AIDS to atherosclerosis. *Br J Pharmacol* **162**:1453–1469.

Kalatskaya I, Berchiche YA, Gravel S, Limberg BJ, Rosenbaum JS, and Heveker N (2009) AMD3100 Is a CXCR7 Ligand with Allosteric Agonist Properties. *Mol Pharmacol* **75**:1240–1247.

Kaneider NC, Agarwal A, Leger AJ, and Kuliopulos A (2005) Reversing systemic inflammatory response syndrome with chemokine receptor pepducins. *Nat Med* **11**:661–665.

Kato M, Kitayama J, Kazama S, and Nagawa H (2003) Expression pattern of CXC chemokine receptor-4 is correlated with lymph node metastasis in human invasive ductal carcinoma. *Breast cancer Res* **5**.

Kauk M, and Hoffmann C (2018) Intramolecular and Intermolecular FRET Sensors for GPCRs – Monitoring Conformational Changes and Beyond. *Trends Pharmacol Sci* **39**:123–135.

Kaupmann K, Malitschek B, Heid J, Froestl W, Beck P, Mosbacher J, Bischoff S, Kulik A, Shigemoto R, Karschin A, and Bettler B (1998) GABAB-receptor subtypes assemble into functional heteromeric complexes. *Nature* **396**:683–687.

Kenakin T (2014) *A Pharmacology primer*, 4th ed., Elsevier Science Publishing Co Inc , Academic Press Inc.

Kenakin T (1993) *Pharmacologic Analysis of Drug-Receptor Interaction*, 2nd ed., Raven Press, New York.

Kenakin T (2015) The mass action equation in pharmacology. *Br J Clin Pharmacol* **81**:41–51.

Keppler A, Pick H, Arrivoli C, Vogel H, and Johnsson K (2004) Labeling of fusion proteins with synthetic fluorophores in live cells. *PNAS* **101**:9955–9959.

Khan IA, Thomas SY, Moretto MM, Lee FS, Islam SA, Combe C, Schwartzman JD, and Luster AD (2006) CCR5 is essential for NK cell trafficking and host survival following Toxoplasma gondii infection. *PLoS Pathog* **2**:0484–0500.

Kilpatrick LE, Briddon SJ, and Holliday ND (2012) Fluorescence correlation spectroscopy, combined with bimolecular fluorescence complementation , reveals the effects of β-arrestin complexes and endocytic targeting on the membrane mobility of neuropeptide Y receptors . BBA Molecular on the membrane mobili. *BBA - Mol Cell Res* **1823**:1068–1081.

Kleemann P, Papa D, Vigil-Cruz S, and Seifert R (2008) Functional reconstitution of the human chemokine receptor CXCR4 with G(i)/G (o)-proteins in Sf9 insect cells. *Naunyn Schmiedebergs Arch Pharmacol* **378**:261–74.

Kobilka BK (2007) G protein coupled receptor structure and activation. *Biochim Biophys Acta* **1768**:794–807.

Korzeniewski C, and Callewaert DM (1983) An enzyme-release assay for natural cytoxicity. *J Immunol Methods* **64**:313–320.

Kozak M (1987) At least six nucleotides preceding the AUG initiator codon enhance translation in mammalian cells. *J Mol Biol* **196**:947–950.

Kozak M (1986) Point mutations define a sequence flanking the AUG initiator codon that modulates translation by eukaryotic ribosomes. *Cell* **44**:283–292.

Krebs A, Villa C, Edwards PC, and Schertler GFX (1998) Characterisation of an Improved Two-dimensional p 22 1 2 1 Crystal from Bovine Rhodopsin. *J Mol Biol* **282**:991–1003.

Kroeze WK, Douglas J, and Roth BL (2003) G-protein-coupled receptors at a glance. *J Cell Sci* **116**:4867–4869.

Krupnick JG, and Benovic JL (1998) THE ROLE OF RECEPTOR KINASES AND ARRESTINS IN G PROTEIN – COUPLED RECEPTOR REGULATION. *Annu Rev Pharmacol Toxicol* **38**:289–319.

Kufareva I, Gustavsson M, Zheng Y, Stephens BS, and Handel TM (2017) What Do Structures Tell Us About Chemokine Receptor Function and Antagonism ? *Annu Rev Biophys* **46**:175–200.

Kufareva I, Stephens BS, Holden LG, Qin L, Zhao C, Kawamura T,

Abagyan R, and Handel TM (2014) Stoichiometry and geometry of the CXC chemokine receptor 4 complex with CXC ligand 12: molecular modeling and experimental validation. *PNAS* **111**:E5363–E5372.

Kuliopulos A, and Covic L (2003) Blocking receptors on the inside: Pepducin-based intervention of PAR signaling and thrombosis. *Life Sci* **74**:255–262.

Kumar A, Kremer KN, Dominguez D, Tadi M, and Hedin KE (2011) G 13 and Rho Mediate Endosomal Trafficking of CXCR4 into Rab11+ Vesicles upon Stromal Cell-Derived Factor-1 Stimulation. *J Immunol* **186**:951–958.

Langel U (2011) *Cell-Penetrating Peptides Methods and Protocols*, Springer Protocols.

Lappano R, and Maggiolini M (2012) GPCRs and cancer. *Acta Pharmacol Sin* **33**:351–362.

Laurence JS, Blanpain C, Burgner JW, Parmentier M, and LiWang PJ (2000) CC chemokine MIP-1 beta can function as a monomer and depends on Phe13 for receptor binding. *Biochemistry* **39**:3401–3409.

Lee JW, Hoshino A, Inoue K, Saitou T, Uehara S, Kobayashi Y, Ueha S, Matsushima K, Yamaguchi A, Imai Y, and Iimura T (2017) The HIV co-receptor CCR5 regulates osteoclast function. *Nat Commun* **8**: 2226.

Lee KB, Pals-rylaarsdam R, Benovic JL, and Hosey MM (1998) Arrestin-independent Internalization of the m1, m3 and m4 Subtypes of Muscarinic Cholinergic Receptors. *J Biol Chem* **273**:12967–12972.

Lefkowitz RJ (1998) G Protein-coupled Receptors III. New roles for receptor kinases and b-arresins in receptor signaling and desentization. *J Biol Chem* **273**:18677–18680.

Levoye A, Balabanian K, Baleux F, Bachelerie F, and Lagane B (2009) CXCR7 heterodimerizes with CXCR4 and regulates CXCL12-mediated G protein signaling. *Blood* **113**:6085–6093.

Libert F, Parmentier M, Lefort A, Dumont J, and Vassart G (1990) Complete nucleotide sequence of a putative G protein coupled receptor: RDC1. *Nucleic Acids Res* **18**:1917.

Lin SW, and Sakmar TP (1996) Specific Tryptophan UV-Absorbance Changes Are Probes of the Transition of Rhodopsin to Its Active State †. *Biochemistry* **2**:11149–11159.

Liu Q-H, Williams DA, McManus C, Baribaud F, Doms RW, Schols D, De Clercq E, Kotlikoff MI, Collman RG, and Freedman BD (2000) HIV-1 gp120 and chemokines activate ion channels in primary macrophages through CCR5 and CXCR4 stimulation. *PNAS* **97**:4832–4837.

Liu X, Ahn S, Kahsai AW, Meng KC, Latorraca NR, Pani B, Venkatakrishnan AJ, Masoudi A, Weis WI, Dror RO, Chen X, Lefkowitz RJ, and Kobilka BK (2017) Mechanism of intracellular allosteric β 2 AR antagonist revealed by X-ray crystal structure. *Nature* **548**:480–484.

Lohse MJ, Hein P, Hoffmann C, Nikolaev VO, Vilardaga JP, and Buenemann M (2008) Kinetics of G-protein-coupled receptor signals in intact cells. *Br J Pharmacol* **153**:125–132.

Lohse MJ, Nuber S, and Hoffmann C (2012) Fluorescence / Bioluminescence Resonance Energy Transfer Techniques to Study G-Protein-Coupled Receptor Activation and Signaling. *Pharmacol Rev* **64**:299–336.

Loos T, Mortier A, Gouwy M, Ronsse I, Put W, Lenaerts J, Damme J Van, and Proost P (2008) Citrullination of CXCL10 and CXCL11 by peptidylarginine deiminase : a naturally occurring posttranslational modification of chemokines and new dimension of immunoregulation. *Blood* **112**:2648–2657.

Luker KE, Steele JM, Mihalko LA, Ray P, and Luker GD (2010) Constitutive and Chemokine-dependent Internalization and Recycling of CXCR7 in Breast Cancer Cells to Degrade Chemokine Ligands. *Oncogene* **29**:4599–4610.

Luttrell LM, and Lefkowitz RJ (2002) The role of β - arrestins in the termination and transduction of G-protein-coupled receptor signals. *J Cell Sci* **115**:455–465.

Luttrell LM, Wang J, Plouffe B, Smith JS, Yamani L, Kaur S, Jean-Charles P-Y, Gauthier C, Lee M, Pani B, Kim J, Ahn S, Rajagopal S, Reiter E, Bouvier M, Shenoy SK, Laporte SA, Rockman HA, and Lefkowitz RJ (2018) Manifold roles of β-arrestins in GPCR signaling elucidated with siRNA and CRISPR/Cas9. *Sci Signal* **11**:eaat7650.

Ma L, and Pei G (2007) β-arrestin signaling and regulation of transcription. *J Cell Sci* **120**:213–218.

Machleidt T, Woodroofe CC, Schwinn MK, Méndez J, Robers MB, Zimmerman K, Otto P, Daniels DL, Kirkland TA, and Wood K V. (2015) NanoBRET-A Novel BRET Platform for the Analysis of Protein-Protein Interactions. *ACS Chem Biol* **10**:1797–1804.

Magalhaes AC, Dunn H, and Ferguson SSG (2012) Regulation of GPCR activity, trafficking and localization by GPCR-interacting proteins. *Br J Pharmacol* **165**:1717–1736.

Maksym RB, Tarnowski M, Grymula K, Tarnowska J, Wysoczynski M, Liu R, Czerny B, Ratajczak J, Kucia M, and Ratajczak MZ (2009) The role of stromal-derived factor-1 - CXCR7 axis in development and cancer. *Eur J Pharmacol* **625**:31–40.

Mañes S, Del Real G, Lacalle RA, Lucas P, Gómez-Moutón C, Sánchez-Palomino S, Delgado R, Alcamí J, Mira E, and Martínez-A C (2000)

Membrane raft microdomains mediate lateral assemblies required for HIV-1 infection. *EMBO Rep* **1**:190–196.

Marchese A, Chen C, Kim YM, and Benovic JL (2003) The ins and outs of G protein-coupled receptor trafficking. *Trends Biochem Sci* **28**:369–376.

McMurry TJ, Kuliopulos A, Covic L, and Tchernychev B (2015) CXCR4 Receptor Compounds, Patent US 9,096,646 B2.

Menten P, Struyf S, Schutyser E, Wuyts A, De Clercq E, Schols D, Proost P, and Van Damme J (1999) The LD78β isoform of MIP-1α is the most potent CCR5 agonist and HIV-1–inhibiting chemokine. *J Clin Invest* **104**:R1–R5.

Merrifield RB (1963) Solid Phase Peptide Synthesis. I. The Synthesis of Tetrapeptide. *J Am Chem Soc* **85**:2149.

Middleton RJ, and Kellam B (2005) Fluorophore-tagged GPCR ligands. *Curr Opin Chem Biol* **9**:517–525.

Molnar I, and Horvath C (1976) Reverse phase chromatography of polar biological substances: separation of catechol compounds by high performance liquid chromatography. *Clin Chem* **22**:1497–1502.

Monteclaro FS, and Charo IF (1996) The amino-terminal extracellular domain of the MCP-1 receptor, but not the RANTES/MIP-1α receptor, confers chemokine selectivity. Evidence for a two-step mechanism for MCP-1 receptor activation. *J Biol Chem* **271**:19084–19092.

Moy RH, Huffman AP, Richman LP, Crisalli L, Wang XK, Hoxie JA, Mick R, Emerson SG, Zhang Y, Vonderheide RH, Porter DL, and Reshef R (2017) Clinical and immunologic impact of CCR5 blockade in graft-versus-host disease prophylaxis. *Blood* **129**:906–916.

Mueller A, Mahmoud NG, and Strange PG (2006) Diverse signalling by different chemokines through the chemokine receptor CCR5. *Biochem Pharmacol* **72**:739–748.

Mueller A, and Strange PG (2004) CCL3, acting via the chemokine receptor CCR5, leads to independent activation of Janus kinase 2 (JAK2) and Giproteins. *FEBS Lett* **570**:126–132.

Mülhardt C (2009) *Der Experimentator Molekularbiologie/Genomics (The Experimenter Molecular Biology/Genomics)*, Spektrum.

Müller A, Homey B, Soto H, Ge N, Catron D, Buchanan ME, McClanahan T, Murphy E, Yuan W, Wagner SN, Barrera JL, Mohar a, Verástegui E, and Zlotnik a (2001) Involvement of chemokine receptors in breast cancer metastasis. *Nature* **410**:50–56.

Muñoz LM, Holgado BL, Martínez-A C, Rodríguez-Frade JM, and Mellado M (2012) Chemokine receptor oligomerization: A further step toward chemokine function. *Immunol Lett* **145**:23–29.

Murphy PM, Baggiolini M, Charo IF, Hébert C a, Horuk R, Matsushima K, Miller LH, Oppenheim JJ, and Power C a (2000) International union of pharmacology. XXII. Nomenclature for chemokine receptors. *Pharmacol Rev* **52**:145–176.

Nagai T, Ibata K, Park ES, Kubota M, and Mikoshiba K (2002) A variant of yellow fluorescent protein with fast and efficient maturation for cell-biological applications. *Nat Biotechnol* **20**:1585–1588.

Nagarsheth N, Wicha MS, and Zou W (2017) Chemokines in the cancer microenvironment and their relevance in cancer immunotherapy. *Nat Publ Gr* **17**:559–572.

Nasser MW, Raghuwanshi SK, Grant DJ, Jala VR, Rajarathnam K, and Richardson RM (2009) Differential Activation and Regulation of CXCR1 and CXCR2 by CXCL8 Monomer and Dimer. *J Immunol* **183**:3425–3432.

Naumann U, Cameroni E, Pruenster M, Mahabaleshwar H, Raz E, Zerwes HG, Rot A, and Thelen M (2010) CXCR7 functions as a scavenger for CXCL12 and CXCL11. *PLoS One* **5**:1–11.

Nelson PJ, Krensky AM, and Poliklinik M (2001) Chemokines, Chemokine Receptors, and Allograft Rejection. *Immunity* **14**:377–386.

Nesmelova I V., Sham Y, Dudek AZ, Van Eijk LI, Wu G, Slungaard A, Mortari F, Griffioen AW, and Mayo KH (2005) Platelet factor 4 and interleukin-8 CXC chemokine heterodimer formation modulates function at the quaternary structural level. *J Biol Chem* **280**:4948–4958.

Nobles M, Benians A, and Tinker A (2005) Heterotrimeric G proteins precouple with G protein-coupled receptors in living cells. *PNAS* **102**:18706–18711.

O'Callaghan K, Kuliopulos A, and Covic L (2012) Turning receptors on and off with intracellular pepducins: New insights into G-protein-coupled receptor drug development. *J Biol Chem* **287**:12787–12796.

O'Callaghan K, Lee L, Nguyen N, Hsieh MY, Kaneider NC, Klein AK, Sprague K, Van Etten R a., Kuliopulos A, and Covic L (2012) Targeting CXCR4 with cell-penetrating pepducins in lymphoma and lymphocytic leukemia. *Blood* **119**:1717–1725.

Oberlin E, Amara A, Bachelerie F, Bessia C, Virelizier JL, Arenzana-Seisdedos F, Schwartz O, Heard JM, Clark-Lewis I, Legler DF, Loetscher M, Baggiolini M, and Moser B (1996) The CXC chemokine, stromal cell derived factor 1 (SDF-1), is the ligand for LESTR/fusin and prevents infection by lymphocyte-tropic HIV-1 syncytium-inducing strains. *Nature* **382**:833–835.

Ödemis V, Lipfert J, Kraft R, Hajek P, Abraham G, Hattermann K, Mentlein R, and Engele J (2012) The presumed atypical chemokine receptor CXCR7 signals through Gi/oproteins in

primary rodent astrocytes and human glioma cells. *Glia* **60**:372–381.

Okada T, Sugihara M, Bondar AN, Elstner M, Entel P, and Buss V (2004) The retinal conformation and its environment in rhodopsin in light of a new 2.2 Å crystal structure. *J Mol Biol* **342**:571–583.

Oppermann M (2004) Chemokine receptor CCR5: Insights into structure, function, and regulation. *Cell Signal* **16**:1201–1210.

Orsini M, Parent J, Mundell S, and Benovic J (1999) Trafficking of the HIV coreceptor CXCR4. *J Biol Chem* **274**:31076–31086.

Oswald C, Rappas M, Kean J, Doré AS, Errey JC, Bennett K, Deflorian F, Christopher JA, Jazayeri A, Mason JS, Congreve M, Cooke RM, and Marshall FH (2016) Intracellular allosteric antagonism of the CCR9 receptor. *Nature* **540**:462–465.

Palczewski K, Kumasaka T, Hori T, Behnke CA, Motoshima H, Fox BA, Trong I Le, Teller DC, Okada T, Stenkamp RE, Yamamoto M, and Miyano M (2000) Crystal Structure of Rhodopsin : A G Protein – Coupled Receptor. *Science* **289**:739–745.

Payne AS, and Cornelius LA (2002) The role of chemokines in melanoma tumor growth and metastasis. *J Invest Dermatol* **118**:915–922.

Percherancier Y, Berchiche YA, Slight I, Volkmer-Engert R, Tamamura H, Fujii N, Bouvier M, and Heveker N (2005) Bioluminescence resonance energy transfer reveals ligand-induced conformational changes in CXCR4 homo- and heterodimers. *J Biol Chem* **280**:9895–9903.

Petersen J, Wright SC, Rodríguez D, Matricon P, Lahav N, Vromen A, Friedler A, Strömqvist J, Wennmalm S, Carlsson J, and Schulte G (2017) Agonist-induced dimer dissociation as a macromolecular step in G protein-coupled receptor signaling. *Nat Commun* **8**:226–241.

Pfleger KDG, and Eidne KA (2006) Illuminating insights into protein-protein interactions using bioluminescence resonance energy transfer (BRET). *Nat Methods* **3**:165–174.

Planesas JM, Pérez-Nueno VI, Borrell JI, and Teixidó J (2015) Studying the binding interactions of allosteric agonists and antagonists of the CXCR4 receptor. *J Mol Graph Model* **60**:1–14.

Proudfoot AE, Handel TM, Johnson Z, Lau EK, LiWang P, Clark-Lewis I, Borlat F, Wells TN, and Kosco-Vilbois MH (2003) Glycosaminoglycan binding and oligomerization are essential for the in vivo activity of certain chemokines. *PNAS* **100**:1885–1890.

Qin L, Kufareva I, Holden LG, Wang C, Zheng Y, Zhao C, Fenalti G, Wu H, Han GW, Cherezov V, Abagyan R, Stevens RC, and Handel TM (2015) Structural biology. Crystal structure of the chemokine receptor CXCR4 in complex with a viral chemokine. *Science* **347**:1117–1122.

Quoyer J, Janz JM, Luo J, Ren Y, Armando S, Lukashova V, Benovic JL, Carlson KE, Hunt SW, and Bouvier M (2013) Pepducin targeting the C-X-C chemokine receptor type 4 acts as a biased agonist favoring activation of the inhibitory G protein. *PNAS* **110**:E5088–E5097.

Rajagopal S, Kim J, Ahn S, Craig S, Lam CM, Gerard NP, Gerard C, and Lefkowitz RJ (2010) β-arrestin- but not G protein-mediated signaling by the "decoy" receptor CXCR7. *PNAS* **107**:628–632.

Rapp C, Snow S, Laufer T, and McClendon CL (2013) The role of tyrosine sulfation in the dimerization of the CXCR4:SDF-1 complex. *Protein Sci* **22**:1025–1036.

Rasmussen SGF, Choi H, Rosenbaum DM, Kobilka TS, Thian FS, Edwards PC, Burghammer M, Ratnala VRP, Sanishvili R, Fischetti RF, Schertler GFX, Weis WI, and Kobilka BK (2007) Crystal structure of the human b2 adrenergic G-protein-coupled receptor. *Nature* **450**:383–388.

Ray P, Mihalko LA, Coggins NL, Moudgil P, Ehrlich A, Luker KE, and Luker GD (2012) Carboxy-terminus of CXCR7 regulates receptor localization and function. *Int J Biochem Cell Biol* **44**:669–678.

Reiter E, and Lefkowitz RJ (2006) GRKs and β-arrestins: roles in receptor silencing, trafficking and signaling. *Trends Endocrinol Metab* **17**:159–165.

Rink H (1987) Solid-phase synthesis of protected peptide fragments using a trialkoxy-diphenyl-methylester resin. *Tetrahedron Lett* **28**:3787–3790.

Rodríguez-Frade JM, Mellado M, and Martínez-A C (2001) Chemokine receptor dimerization: Two are better than one. *Trends Immunol* **22**:612–617.

Rodriguez-Frade JM, Vila-Coro AJ, Martin de Ana A, Albar JP, Martinez-A. C, and Mellado M (1999) The chemokine monocyte chemoattractant protein-1 induces functional responses through dimerization of its receptor CCR2. *PNAS* **96**:3628–3633.

Rosenbaum DM, Rasmussen SGF, and Kobilka BK (2009) The structure and function of G-protein-coupled receptors. *Nature* **459**:356–363.

Rosenkilde MM, Gerlach LO, Jakobsen JS, Skerlj RT, Bridger GJ, and Schwartz TW (2004) Molecular mechanism of AMD3100 antagonism in the CXCR4 receptor: Transfer of binding site to the CXCR3 receptor. *J Biol Chem* **279**:3033–3041.

Rossi D, and Zlotnik A (2002) The Biology of Chemokines and their Receptors. *Annu Rev Entomol* **47**:917–949.

Rozenfeld R, and Devi LA (2010) Receptor heteromerization and drug discovery. *Trends Pharmacol Sci* **31**:124–130, Elsevier Ltd.

Sakyiamah MM, Nomura W, Kobayakawa T, and Tamamura H (2019)

Development of a NanoBRET-Based Sensitive Screening Method for CXCR4 Ligands. *Bioconjug Chem* **30**:1442–1450.

Santos R, Ursu O, Gaulton A, Bento AP, Donadi RS, Bologa CG, Karlsson A, Al-lazikani B, Hersey A, Oprea TI, and Overington JP (2016) A comprehensive map of molecular drug targets. *Nat Rev Drug Discov* **16**:19–34.

Schertler GFX, Villa C, and Henderson R (1993) Projection structure of rhodopsin. *Nature* **362**:770–772.

Schindelin J, Arganda-Carreras I, Frise E, Kaynig V, Longair M, Pietzsch T, Preibisch S, Rueden C, Saalfeld S, Schmid B, Tinevez JY, White DJ, Hartenstein V, Eliceiri K, Tomancak P, and Cardona A (2012) Fiji: An open-source platform for biological-image analysis. *Nat Methods* **9**:676–682.

Schwehm C, Kellam B, Garces AE, Hill SJ, Kindon ND, Bradshaw TD, Li J, Macdonald SJF, Rowedder JE, Stoddart LA, and Stocks MJ (2017) Design and Elaboration of a Tractable Tricyclic Scaffold To Synthesize Druglike Inhibitors of Dipeptidyl Peptidase-4 (DPP-4), Antagonists of the C-C Chemokine Receptor Type 5 (CCR5), and Highly Potent and Selective Phosphoinositol-3 Kinase δ (PI3Kδ) Inhib. *J Med Chem* **60**:1534–1554.

Seki E, De Minicis S, Gwak GY, Kluwe J, Inokuchi S, Bursill CA, Llovet JM, Brenner DA, and Schwabe RF (2009) CCR1 and CCR5 promote hepatic fibrosis in mice. *J Clin Invest* **119**:1858–1870.

Shenoy SK, Drake MT, Nelson CD, Houtz DA, Xiao K, Madabushi S, Reiter E, Premont RT, Lichtarge O, and Lefkowitz RJ (2006) β-Arrestin-dependent, G Protein-independent ERK1/2 Activation by the β2 Adrenergic Receptor. *J Biol Chem* **281**:1261–1273.

Simon MI, Strathmann MP, and Gautam N (1990) Diversity of G Proteins in Signal Transduction. *Nature* **252**:802–808.

Soede RD, Zeelenberg IS, Wijnands YM, Kamp M, and Roos E (2001) Stromal cell-derived factor-1-induced LFA-1 activation during in vivo migration of T cell hybridoma cells requires Gq/11, RhoA, and myosin, as well as Gi and Cdc42. *J Immunol* **166**:4293–4301.

Sorce S, Myburgh R, and Krause KH (2011) The chemokine receptor CCR5 in the central nervous system. *Prog Neurobiol* **93**:297–311.

Springael JY, Urizar E, and Parmentier M (2005) Dimerization of chemokine receptors and its functional consequences. *Cytokine Growth Factor Rev* **16**:611–623.

Srikun D, Albers AE, Nam CI, Iavarone AT, and Chang CJ (2010) Organelle-Targetable Fluorescent Probes for Imaging Hydrogen Peroxide in Living Cells via SNAP-Tag Protein Labeling. *J Am Chem Soc* **132**:4455–4465.

Standfuss J, Edwards PC, Antona AD, Fransen M, Xie G, Oprian DD, and Schertler GFX (2011) The structural basis of agonist-induced

activation in constitutively active rhodopsin. *Nature* **471**:656–661.

Stewart BW, and Wild CP (2014) *World Cancer Report 2014*, International Agency for Research on Cancer.

Stoddart LA, Briddon SJ, and Hill SJ (2013) Fluorescent ligands for G protein-coupled receptors: illuminating receptor–ligand interactions for drug discovery. *Future Med Chem* **5**:1367–1369.

Stoddart LA, Johnstone EKM, Wheal AJ, Goulding J, Robers MB, Machleidt T, Wood K V, Hill SJ, and Pfleger KDG (2015) Application of BRET to monitor ligand binding to GPCRs. *Nat Methods* **12**:661–663.

Stone MJ, Hayward JA, Huang C, Huma ZE, and Sanchez J (2017) Mechanisms of Regulation of the Chemokine-Receptor Network. *Int J Mol Sci* **18**:342–375.

Strader CD, Ming Fong T, Tota MR, and Underwood D (1994) Structure and Function of G Protein-coupled Receptors. *Annu Rev Biochem* **63**:101–132.

Stráner P, Taricska N, Szabó M, K. Tóth G, and Perczel A (2016) Bacterial expression and/or solid phase peptide synthesis of 20-40 amino acid long polypeptides and miniproteins, the case study of Class B GPCR ligands. *Curr Protein Pept Sci* **17**:147–155.

Struyf S, Noppen S, Loos T, Gouwy M, Verbeke H, Huskens D, Luangsay S, Parmentier M, Geboes K, Schols D, Damme J Van, Proost P, Cxcr A, Struyf S, Noppen S, Loos T, Mortier A, Gouwy M, Verbeke H, Huskens D, Luangsay S, Parmentier M, Geboes K, Schols D, Damme J Van, and Proost P (2009) Citrullination of CXCL12 Differentially Reduces CXCR4 and CXCR7 Binding with Loss of Inflammatory and Anti-HIV-1 Activity via CXCR4. *J Immunol* **182**:666–674.

Stryer L (1978) Fluorescence Energy Transfer as a Spectroscopic Ruler. *Annu Rev Biochem* **47**:819–846.

Sun X, Cheng G, Hao M, Zheng J, Zhou X, Zhang J, Taichman RS, Pienta KJ, and Wang J (2010) CXCL12 / CXCR4 / CXCR7 chemokine axis and cancer progression. *Cancer Metastasis Rev* **29**:709–722.

Sun Y, Cheng Z, Ma L, and Pei G (2002) β-Arrestin2 Is Critically Involved in CXCR4-mediated Chemotaxis, and This Is Mediated by Its Enhancement of p38 MAPK Activation. *J Biol Chem* **277**:49212–49219.

Syrovatkina V, Alegre KO, Dey R, and Huang XY (2016) Regulation, Signaling, and Physiological Functions of G-Proteins. *J Mol Biol* **428**:3850–3868.

Tachibana K, Hirota S, Iizasa H, Yoshida H, Kawabata K, Kataoka Y, Kitamura Y, Matsushima K, Yoshida N, Nishikawa SI, Kishimoto T, and Nagasawa T (1998) The chemokine receptor CXCR4 is

essential for vascularization of the gastrointestinal tract. *Nature* **393**:591–594.

Tan JHY, Canals M, Ludeman JP, Wedderburn J, Boston C, Butler SJ, Carrick AM, Parody TR, Taleski D, Christopoulos A, Payne RJ, and Stone MJ (2012) Design and receptor interactions of obligate dimeric mutant of chemokine monocyte chemoattractant protein-1 (MCP-1). *J Biol Chem* **287**:14692–14702.

Tan Q, Zhu Y, Li J, Chen Z, Han GW, Kufareva I, Li T, Ma L, Fenalti G, Li J, Zhang W, Xie X, Yang H, Jiang H, Cherezov V, Liu H, Stevens RC, Zhao Q, and Wu B (2013) Structure of the CCR5 Chemokine Receptor-HIV Entry Inhibitor Maraviroc Complex. *Science* **341**:1387–1390.

Tan W, Martin D, and Gutkind JS (2006) The Gα13-Rho signaling axis is required for SDF-1-induced migration through CXCR. *J Biol Chem* **281**:39542–39549.

Tchernychev B, Ren Y, Sachdev P, Janz JM, Haggis L, O'Shea A, McBride E, Looby R, Deng Q, McMurry T, Kazmi M a, Sakmar TP, Hunt S, and Carlson KE (2010) Discovery of a CXCR4 agonist pepducin that mobilizes bone marrow hematopoietic cells. *PNAS* **107**:22255–22259.

Teixidó J, Martínez-Moreno M, Díaz-Martínez M, and Sevilla-Movilla S (2018) The good and bad faces of the CXCR4 chemokine receptor. *Int J Biochem Cell Biol* **95**:121–131.

Terpe K (2006) Overview of bacterial expression systems for heterologous protein production: From molecular and biochemical fundamentals to commercial systems. *Appl Microbiol Biotechnol* **72**:211–222.

Terrillon S, and Bouvier M (2004) Roles of G-protein-coupled receptor dimerization. *EMBO Rep* **5**:30–34.

Tian S, Choi W-T, Liu D, and Pesavento J (2005) Distinct Functional Sites for Human Immunodeficiency Virus Type 1 and Stromal Cell-Derived Factor 1α on CXCR4 Transmembrane Helical Domains. *J Virol* **79**:12667–12673.

Torossian F, Anginot A, Chabanon A, Clay D, Guerton B, Desterke C, Boutin L, Marullo S, Scott MGH, Lataillade JJ, and Le Bousse-Kerdilès MC (2014) CXCR7 participates in CXCL12-induced CD34+ cell cycling through b-arrestin-dependent Akt activation. *Blood* **123**:191–202.

Uhlén M, Fagerberg L, Hallström BM, Lindskog C, Oksvold P, Mardinoglu A, Sivertsson Å, Kampf C, Sjöstedt E, Asplund A, Olsson I, Edlund K, Lundberg E, Navani S, Szigyarto CA, Odeberg J, Djureinovic D, Takanen JO, Hober S, Alm T, Edqvist P, Berling H, Tegel H, Mulder J, Rockberg J, Nilsson P, Schwenk JM, Hamsten M, Feilitzen K Von, Forsberg M, Persson L, Johansson F, Zwahlen M, Heijne G Von, Nielsen J, and Pontén F (2015) Tissue-based map of the human proteome. *Science* **347**:1260419-1–9.

Ulvmar MH, Hub E, and Rot A (2011) Atypical Chemokine Receptors. *Exp Cell Res* **317**:556–568.

Van Unen J, Stumpf AD, Schmid B, Reinhard NR, Hordijk LP, Hoffmann C, Gadella TWJ, and Goedhart J (2016) A New Generation of FRET Sensors for Robust Measurement of G α i1 , G α i2 and G α i3 Activation Kinetics in Single Cells. *PLoS One* **11**:e0146789.

Venkatakrishnan AJ, Deupi X, Lebon G, Tate CG, Schertler GF, and Babu MM (2013) Molecular signatures of G-protein-coupled receptors. *Nature* **494**:185–194.

Vila-Coro AJ, Rodríguez-Frade JM, Martín De Ana A, Moreno-Ortíz MC, Martínez-A C, and Mellado M (1999) The Chemokine SDF-1alpha Triggers CXCR4 Receptor Dimerization and Activates the JAK/STAT Pathway. *FASEB J* **13**:1699–1710.

Viola A, and Luster AD (2008) Chemokines and Their Receptors: Drug Targets in Immunity and Inflammation. *Annu Rev Pharmacol Toxicol* **48**:171–197.

Wang J, He L, Combs CA, Roderiquez G, and Norcross MA (2006) Dimerization of CXCR4 in living malignant cells : control of cell migration by a synthetic peptide that reduces homologous CXCR4 interactions. *Mol Cancer Ther* **5**:2474–2484.

Wang X, Sharp JS, Handel TM, and Prestegard JH (2013) Chemokine oligomerization in cell signaling and migration. *Prog Mol Biol Transl Sci* **117**:531–578.

Wescott MP, Kufareva I, Paes C, Goodman JR, Thaker Y, Puffer BA, Berdougo E, Rucker JB, Handel TM, and Doranz BJ (2016) Signal transmission through the CXC chemokine receptor 4 (CXCR4) transmembrane helices. *PNAS* **113**:9928–9933.

White CW, Vanyai HK, See HB, Johnstone EKM, and Pfleger KDG (2017) Using nanoBRET and CRISPR/Cas9 to monitor proximity to a genome-edited protein in real-time. *Sci Rep* **7**:1–14.

Wielders SJH, Bennaghmouch A, Reutelingsperger CPM, and Bevers EM (2007) Anticoagulant and antithrombotic properties of intracellular protease-activated receptor antagonists. *J Thromb Haemost* **5**:571–576.

Wilcox T, and Hirshkowitz A (2005) The HIV-1 coat protein gp120 regulates CXCR4-mediated signaling in neural progenitor cells. *J Neuroimmunol* **160**:68–76.

Wnorowski A, and Jozwiak K (2014) Homo- and hetero-oligomerization of β 2 -adrenergic receptor in receptor traf fi cking , signaling pathways and receptor pharmacology. *Cell Signal* **26**:2259–2265.

Wood K, Fan F, Binkowski BF, Butler BL, Stecha PF, and Lewis MK (2008) Novel Genetically Encoded Biosensors Using Firefly Luciferase. *ACS Chem Biol* **3**:346–351.

Wootten D, Christopoulos A, and Sexton PM (2013) Emerging paradigms in GPCR allostery: implications for drug discovery. *Nat Rev Drug Discov* **12**:630–44.

Wu B, Chien EYT, Mol CD, Fenalti G, Liu W, Katritch V, Abagyan R, Brooun A, Wells P, Bi FC, Hamel DJ, Kuhn P, Handel TM, Cherezov V, and Stevens RC (2010) Structures of the CXCR4 Chemokine. *Science* **330**:1066–1071.

Xu L, Li Y, Sun H, Li D, and Hou T (2013) Structural basis of the interactions between CXCR4 and CXCL12/SDF-1 revealed by theoretical approaches. *Mol Biosyst* **9**:2107–2117.

Zaitseva M, Blauvelr A, Lee S, Lapham CK, Klaus-kovtljn V, Mostowski H, Manischewitz ODY, and Golding H (1997) Expression and function of CCR5 and CXCR4 on human Langerhans cells and macrophages: Implications for HIV primary infection. *Nat Med* **3**:1369–1375.

Zheng Y, Han GW, Abagyan R, Wu B, Stevens RC, Cherezov V, Kufareva I, and Handel TM (2017) Structure of CC Chemokine Receptor 5 with a Potent Chemokine Antagonist Reveals Mechanisms of Chemokine Recognition and Molecular Mimicry by HIV. *Immunity* **46**:1005–1017.e5.

Zheng Y, Qin L, Zacarías NVO, De Vries H, Han GW, Gustavsson M, Dabros M, Zhao C, Cherney RJ, Carter P, Stamos D, Abagyan R, Cherezov V, Stevens RC, Ijzerman AP, Heitman LH, Tebben A, Kufareva I, and Handel TM (2016) Structure of CC chemokine receptor 2 with orthosteric and allosteric antagonists. *Nature* **540**:458–461.

Zhou N, Luo Z, Hall JW, Luo J, Han X, and Huang Z (2000) Molecular modeling and site-directed mutagenesis of CCR5 reveal residues critical for chemokine binding and signal transduction. *Eur J Immunol* **30**:164–173.

Zlotnik A, Burkhardt AM, and Homey B (2011) Homeostatic chemokine receptors and organ-specific metastasis. *Nat Rev Immunol* **11**:597–606.

Zlotnik A, and Yoshie O (2012) The Chemokine Superfamily Revisited. *Immunity* **36**:705–716.

Zlotnik A, Yoshie O, and Nomiyama H (2006) The chemokine and chemokine receptor superfamilies and their molecular evolution. *Genome Biol* **7**:243.1-243.11.

Zou Y-R, Kottmann AH, Kuroda M, Taniuchi I, and Littman DR (1998) Function of the chemokine receptor CXCR4 in haematopoiesis and in cerebellar development. *Nature* **393**:595–599.

Zwier JM, Roux T, Cottet M, Durroux T, Douzon S, Bdioui S, Gregor N, Bourrier E, Oueslati N, Nicolas L, Tinel N, Boisseau C, Yverneau P, Charrier-savournin F, Fink M, and Trinquet E (2010) A Fluorescent Ligand-Binding Alternative Using Tag-lite ®

Technology. *J Biomol Screen* **15**:1248–1259.

9 Appendix

9.1 Appendix for Chapter 2

Suppliers for used consumables

Compounds

AMD3100	Sigma Aldrich, Gillingham, UK
ATI-2339	Anchor Therapeutics, Cambridge, USA
ATI-2341	Anchor Therapeutics, Cambridge, USA in cooperation with ALMAC, Edinburgh
ATI-2341f	in cooperation with ALMAC, Edinburgh, UK
ATI-2341TA	in cooperation with ALMAC, Edinburgh, UK
ATI-2346	Anchor Therapeutics, Cambridge, USA
ATI-2504	Anchor Therapeutics, Cambridge, USA
ATI-2755	Anchor Therapeutics, Cambridge, USA
CCL3	PeproTech, London, UK
CXCL12	PeproTech, London, UK
CXCL12-green	ALMAC, Edinburgh, UK or Cisbio, Codolet, France
CXCL12-red	ALMAC, Edinburgh, UK or Cisbio, Codolet, France
Forskolin	Tocris bioscience, Bristol, UK
GTP	Sigma Aldrich, Gillingham, UK
IT1t	Torcis bioscience, Bristol, UK
SD44	Sebastian Dekkers, University of Nottingham
SD42	Sebastian Dekkers, University of Nottingham

Buffers

HBSS 1x Buffer		all Sigma Aldrich	
	0.22 g/l Sodium Pyruvate	2	mM
	8.46 g/l NaCl	145	mM
	1.8 g/l D-Glucose	10	mM
	0.372 g/l KCl	5	mM
	0.264 g/l $MgSO_4 \cdot 7\ H_2O$	1	mM
	2.384 g/l HEPES	10	mM
	0.191 g/l $CaCl_2 \cdot 2\ H_2O$	1.3	mM
	0.126 g/l $NaHCO_3$	1.5	mM

TBE 10x Buffer		all Sigma Aldrich	
	61.8 g/l Boric Acid	1	M
	121.1 g/l Tris base	1	M
	7.4 g/l EDTA	25	mM

DNA

WT CXCR4	Martine Smit, Vrije Universiteit, Amsterdam, The Netherlands
WT CXCR7	Martine Smit, Vrije Universiteit Amsterdam, The Netherlands
CXCR4_CCR5il1	Thomas Sakmar, The Rockefeller University, New York, USA
Primers	Sigma Aldrich Gilingham, UK

Molecular Biology

1kb DNA ladder	Promega, Southampton, UK
Agarose	Sigma Aldrich Gilingham, UK
Ampicilin	Sigma Aldrich, Gillingham, UK
dNTPs	Promega, Southampton, UK
ethidium bromide	Sigma Aldrich Gilingham, UK
LB Agar	Sigma Aldrich, Gillingham, UK
LB Broth	Sigma Aldrich, Gillingham, UK
Maxiprep Kit	Promega, Southampton, UK
Miniprep Kit	Promega, Southampton, UK
One Shot® TOP10 Chemically Competent *E. coli* cells	Invitrogen, Waltham, USA
Petri Dishes	Torcis bioscience, Bristol, UK
Restriction Enzymes	Promega, Southampton, UK
T4 Ligase	Promega, Southampton, UK
	NEB, Ipswich, MA, USA
TA Cloning Kit	Invitrogen, Waltham, USA
PCR mashine	Eppendorf, Stevenage, UK

PCR tubes	Eppendorf, Stevenage, UK

Cell Culture

Culture Flasks	Fischer Scientific, Loughborough, UK
DMEM D-6249	Sigma Aldrich, Gilingham, UK
FCS	Sigma Aldrich, Gilingham, UK
0.2 µm Filters	Merck, Darmstadt, Germany
HEK293G	Promega, Southampton, UK
PBS	Sigma Aldrich, Gilingham, UK
Pipettes	Fischer Scientific, Loughborough, UK
Syringes	Fischer Scientific, Loughborough, UK

Assays

96-well plates white	Greiner Bio-One, Stonehouse, UK
96-well plates black	Greiner Bio-One, Stonehouse, UK
96-well plates clear	Greiner Bio-One, Stonehouse, UK
Furimazine	Promega, Southampton, UK
GloSensor reagent	Promega, Southampton, UK
Höchst stain (33342)	Molecular Probes, Eugene, Oregon, USA
LDH assay kit	Thermo Scientific
SNAP Alexa Fluor 488	NEB, Ipswich, MA, USA
Transferrin568	Invitrogen, Waltham, USA

Imaging

8-well chamber	Sigma Aldrich, Gillingham, UK
MaTek dishes	Ashland, MA, USA

9.2 Appendix for Chapter 3

Pepducin quality control

ATI-2341:

Project Name: Jan 2017

Sample Name: 3119P01 Final

Sample Set Name: 19 January 2017

Vial 8

Date Acquired: 19/01/2017 17:18:14 GMT

Injection Volume: 50.00 uL

Processing Method: General

Column Number:

Date Processed: 20/01/2017 09:00:51 GMT

Run Time: 46.00 Minutes

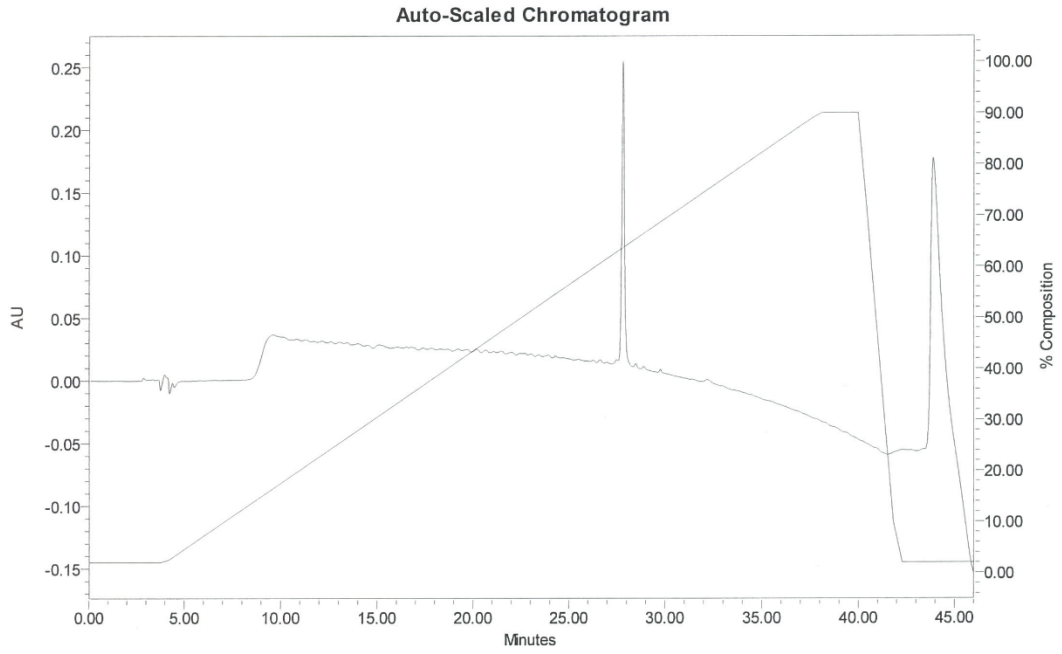

Peak Results

	Name	RT	Relative RT (min)	Height	Area	% Area
1		27.506		3636	34038	1.44
2		27.819		242011	2330744	98.56

Analysis Info

Analysis Name	D:\Data\almac\Birgit\3119P01 Final_23_01_69209.d	Acquisition Date	1/20/2017 9:47:48 AM
Method	60v_gsm_lc_400_1900.m	Operator	Bruker Customer
Sample Name	3119P01 Final	Instrument	micrOTOF
Comment			

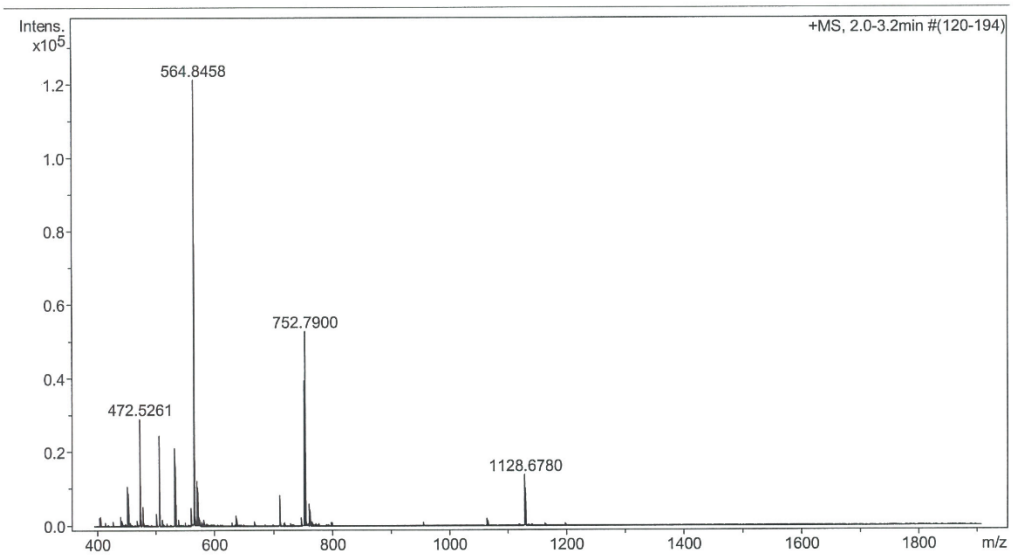

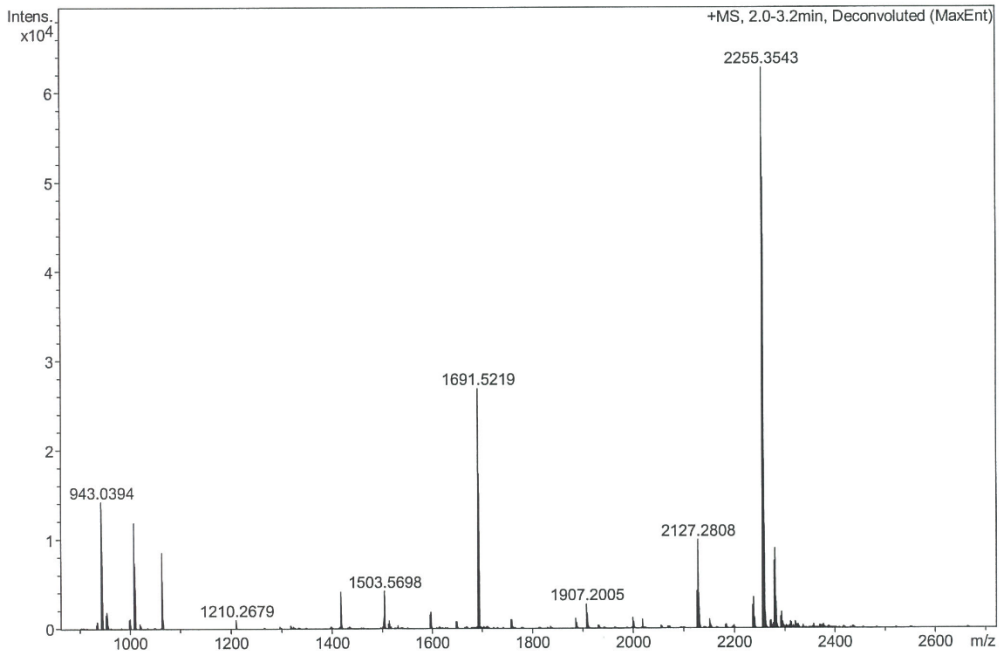

ATI-2341f

Project Name: Jan 2017

Sample Name: 3119P02 13-16

Vial 2

Injection Volume: 50.00 uL

Column Number:

Run Time: 46.00 Minutes

Sample Set Name: 30Jan2017

Date Acquired: 30/01/2017 13:27:23 GMT

Processing Method: General

Date Processed: 30/01/2017 14:14:18 GMT

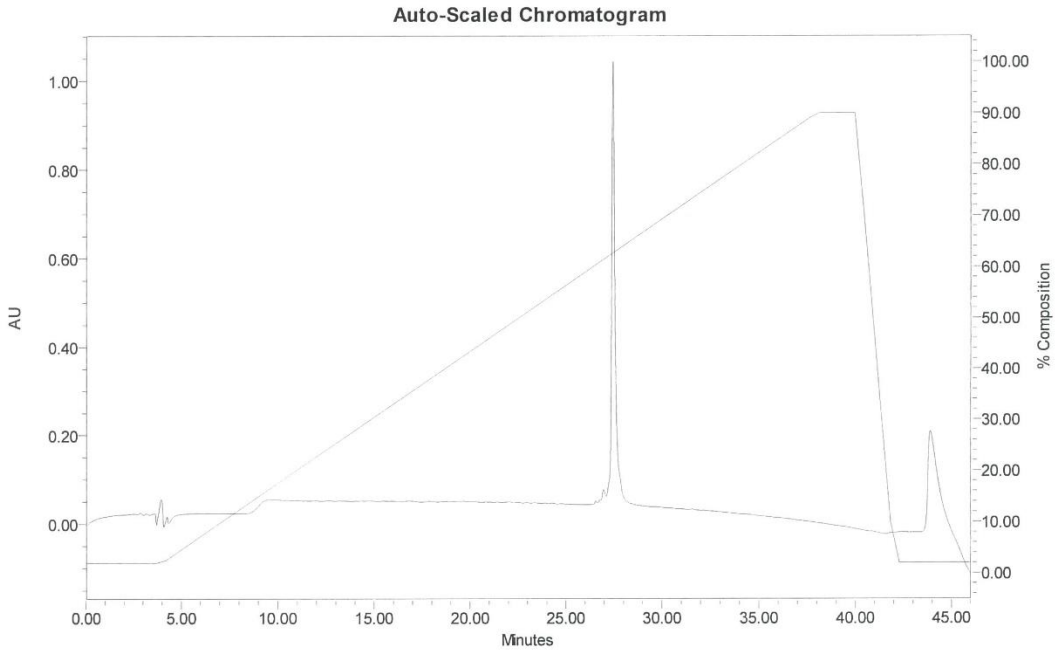

Peak Results

	Name	RT	Relative RT (min)	Height	Area	% Area
1		26.563		5205	33041	0.25
2		26.788		9155	59811	0.45
3		26.965		31161	336693	2.53
4		27.445		999627	12883587	96.77

Analysis Info

Analysis Name	D:\Data\almac\Birgit\3119P02 Final_33_01_69496.d	Acquisition Date	1/31/2017 2:59:28 PM
Method	60v_gsm_lc_400_1900.m	Operator	Bruker Customer
Sample Name	3119P02 Final	Instrument	micrOTOF
Comment			

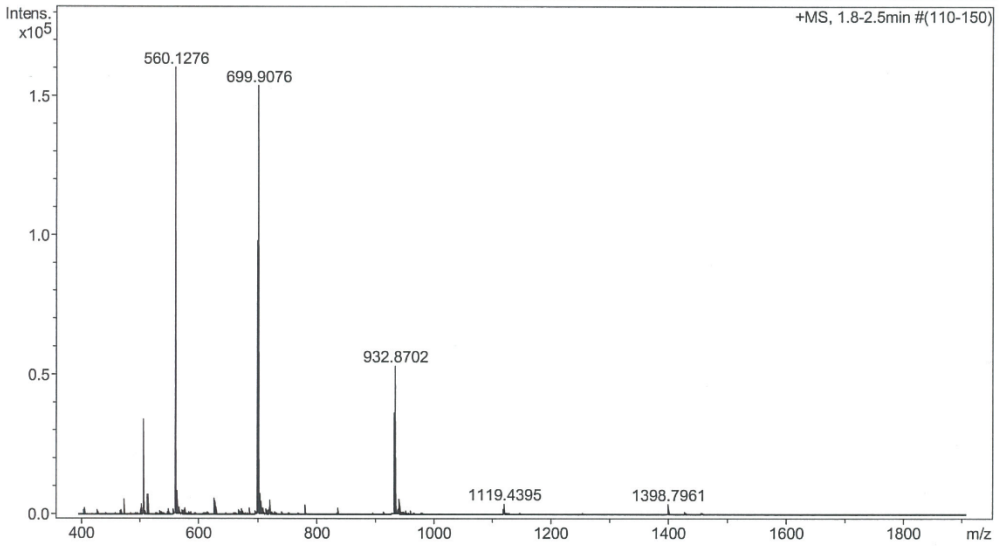

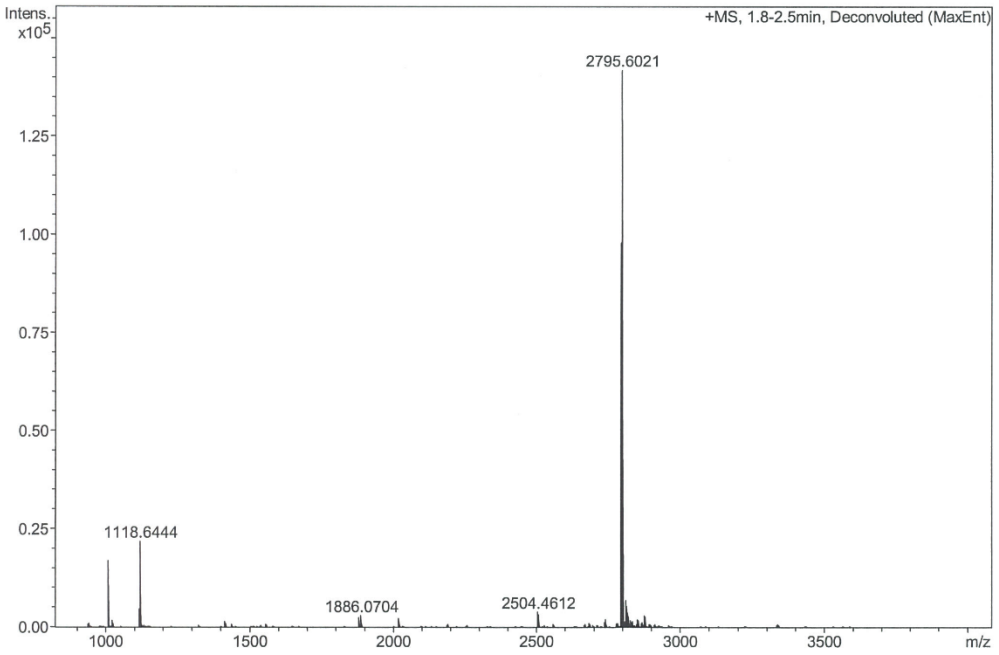

ATI-2341 TA

Project Name: Jan 2017

Sample Name: 3119P03 Final

Vial 9

Injection Volume: 50.00 uL

Column Number:

Run Time: 46.00 Minutes

Sample Set Name: 19 January 2017

Date Acquired: 19/01/2017 18:05:22 GMT

Processing Method: General

Date Processed: 20/01/2017 09:05:14 GMT

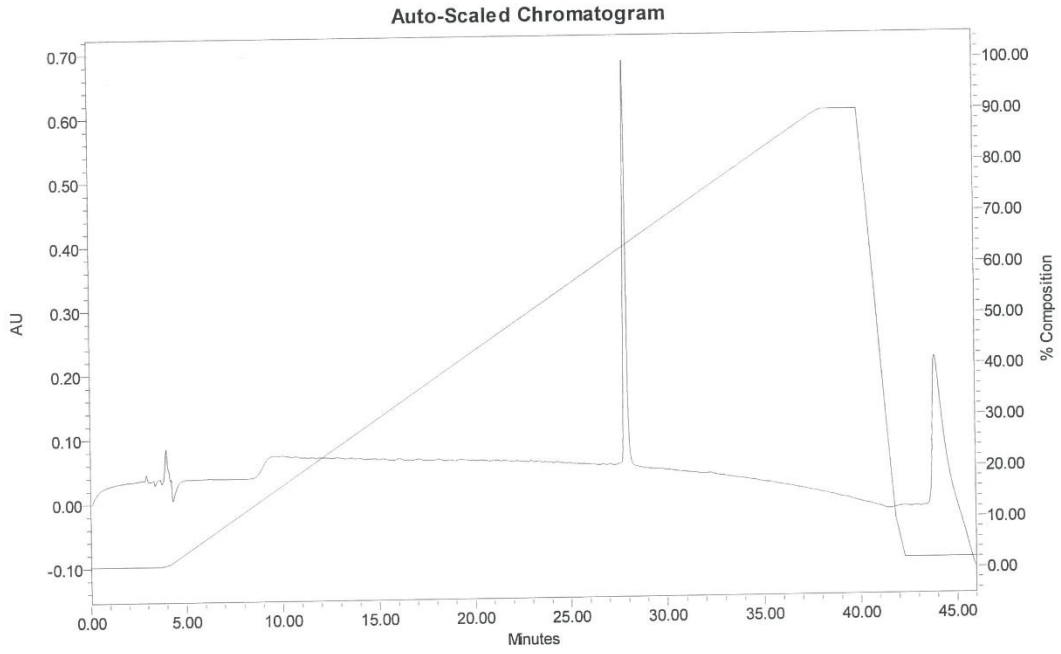

Peak Results

	Name	RT	Relative RT (min)	Height	Area	% Area
1		27.650		3543	30940	0.48
2		27.877		639867	6410538	99.52

Analysis Info

Analysis Name	D:\Data\almac\Birgit\3119P03 Final_25_01_69206.d	Acquisition Date	1/20/2017 9:28:23 AM
Method	60v_gsm_lc_400_1900.m	Operator	Bruker Customer
Sample Name	3119P03 Final	Instrument	micrOTOF
Comment			

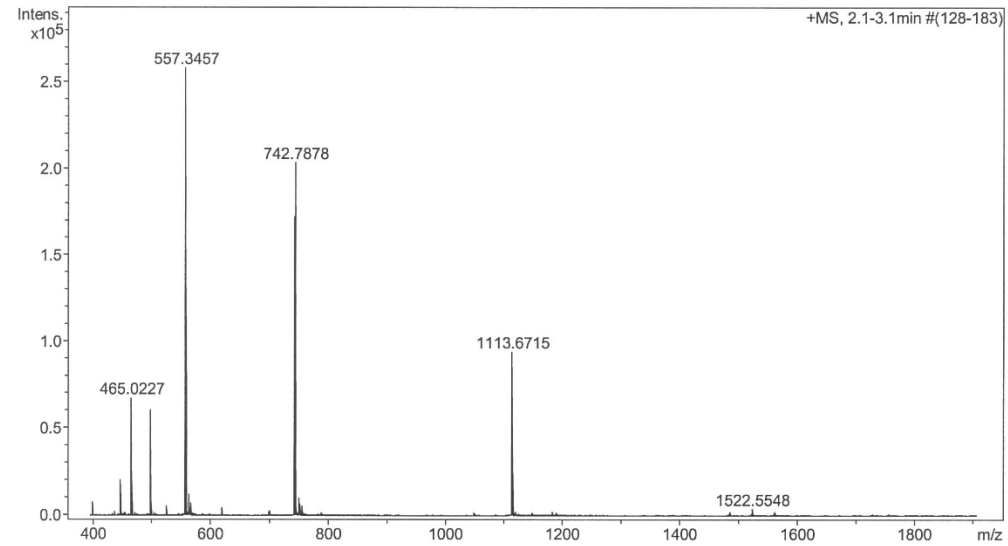

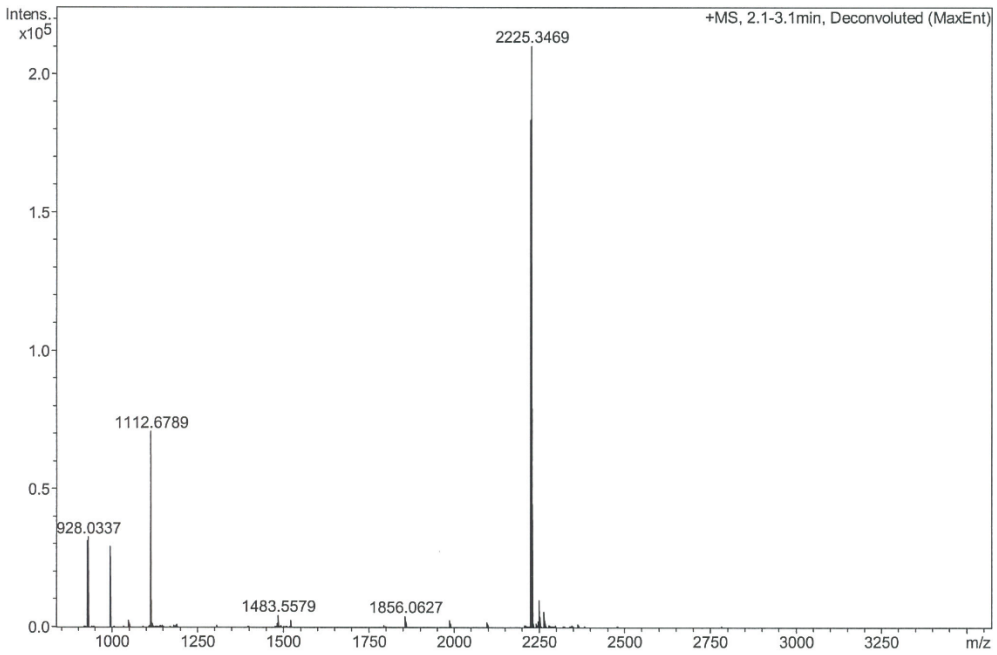

9.3 Appendix for Chapter 4

Ligand depletion

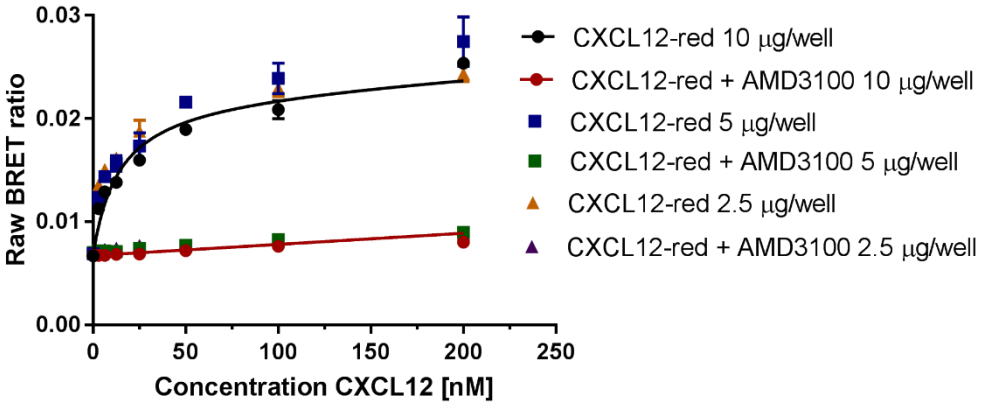

Figure 9-1: Saturation binding of CXCL12-red to different concentrations of membranes from HEK293G cells stably expressing NanoLuc-CXCR4 in the presence and absence of 10 µM AMD3100, n = 2

Membrane concentration [µg/well]	K_d n =1 [nM]	K_d n=2 [nM]
2,500	6.49 ± 0.88	38.82 ± 6.22
5,000	12.06 ± 2.45	34.09 ± 4.95
10,000	13.87 ± 2.47	34.46 ± 4.87

9.4 Appendix for Chapter 5

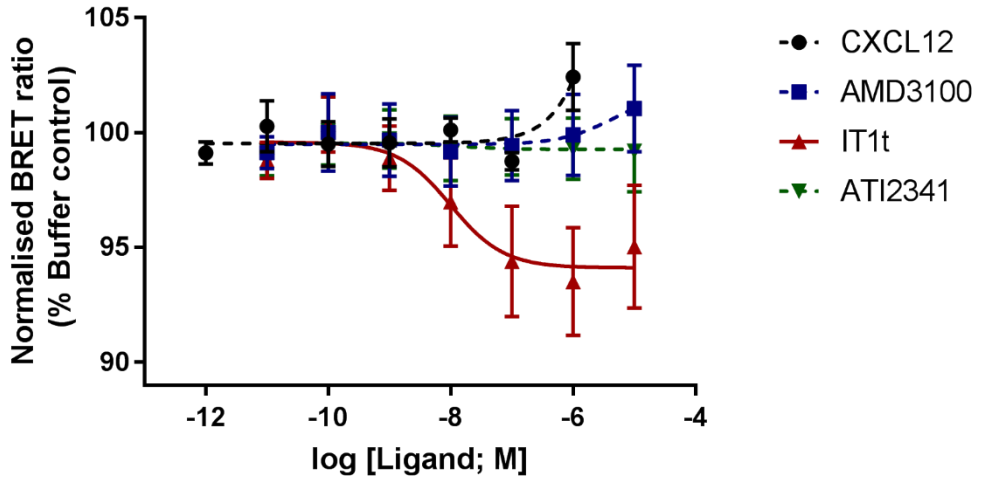

Figure 9-2: Influence of addition of compounds on CXCR4 oligomers. Change in oligomers as change in Raw BRET Ratio. HEK293G cells transfected with 25 ng/well SNAP-CXCR4 and 50 ng/well NanoLuc-CXCR4 in an endpoint BRET assay with subtracted HBSS, showing pooled data of 1 µM CXCL12, 10 µM IT1t, 10 µM AMD3100, 10 µM ATI-2341. Data are background subtracted (HBSS alone) and shown as mean ± S.E.M. of n=6 individual experiments performed in triplicate.

Acknowledgements

Before thanking anyone by name, I would like to thank every single person who played a big or small part in getting this thesis together, no matter in what way (actually helping with science or keeping me happy). And anyone who is not named below should remember they were mentioned first - right here.

I would like to thank my supervisors Steve Hill and Steve Briddon who have been amazing throughout the past years and I felt very lucky in having two helpful supervisors with open doors. Also, a massive thank you to Leigh and Joëlle who have been there to supervise me in the lab and answered all the questions I had no matter how simple they might seem.

Thank you to Nick and Graham who had lots of work reading this thesis, writing reports and examining me and were still lovely and asked not too bad questions – it's Höchst.

Thanks to Carl, who also worked on CXCR4 and exchanging data points was always very helpful. Also a big thanks to Truc, who spent some time after I finished my lab work with screening A_{2A} pepducins that were synthesised at ALMAC which might be a start for more pepducin work. Also, thanks to Sebastian who was my fellow ONCORNET student in Nottingham and who synthesised some fluorescent small molecules for CXCR4.

A big thank you to June and Marleen who keep the lab running and take a lot of work from all of us by making sure that things are autoclaved, washed and consumable stocks are filled.

I would like to give a big shout out to the science family in the Cell Signalling labs in general as they make coming to work so much more fun and I hope this lab dynamic never changes. I have so many happy memories from this bunch and couldn't have done it without you! Thanks for entertaining me, being my friends and answering stupid questions to Quynh, Chloe, Laura H, Laura K, Desi, Nicki, Mark, Nick, Diana, Rachel, Lisa, Liz and everyone else!

This project was part of an EU funded Marie Curie ITN “ONCORNET” and I would like to thank the funding body of the EU to give us students such a great opportunity but also all the great scientists involved in making this happen for us students. We met every 6 months in one of the labs and had good discussions, food and fun. Thank you to everyone in ONCORNET.

Parts of this thesis were performed at the ONCORNET partners ALMAC in Edinburgh and in Carsten Hoffmann’s lab in Würzburg. Therefore, a special thanks to the ALMAC team especially Colin, Jenny and Gillian and to Carsten and Cristina, who was very patient with me and also kept me entertained in Würzburg.

Lastly, I would also like to thank the people back home in Germany (especially Frankfurt) who kept me entertained over so many visits and were there for discussing any personal crisis and taking me away from all the science chatter.